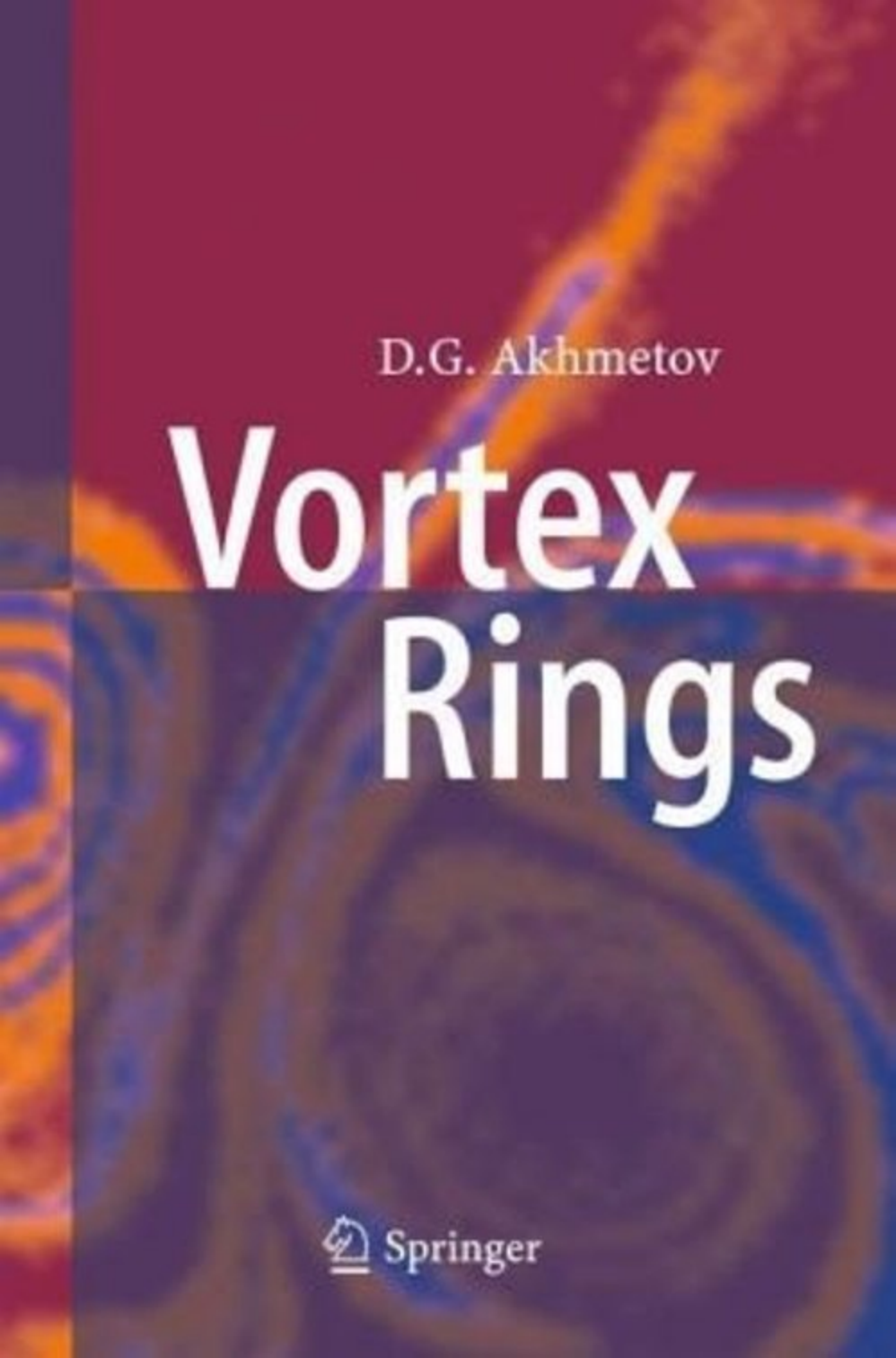
D.G. Akhmetov
Vortex Rings
Springer

Vortex Rings

D.G. Akhmetov

Vortex Rings

Springer

D.G. Akhmetov
Lavrentiev Institute of Hydrodynamics
15 Lavrentiev prosp.
Novosibirsk, 630090
Russia
E-mail: akhmetov@hydro.nsc.ru

ISBN 978-3-642-05015-2 e-ISBN 978-3-642-05016-9

DOI 10.1007/978-3-642-05016-9

Library of Congress Control Number: 2009937143

Typesetting: Data supplied by the authors

Production & Cover Design: Scientific Publishing Services Pvt. Ltd., Chennai, India

Printed in acid-free paper

9 8 7 6 5 4 3 2 1

springer.com

Abstract

Vortex Rings

Akhmetov D.G.

This monograph includes results of research into the regularities of formation and motion of one of the most interesting types of liquid and gas vortex motions — vortex rings. In early period the concept of vortex rings was based only on results of theoretical studies within the frames of the ideal liquid model and on qualitative observations of vortex ring motion. The emphasis in this book is placed on the description of recent results of experimental investigations of structure, formation laws and motion of real vortex rings. A model of vortex ring formation is presented and formulas are obtained for calculation of parameters of a broad family of vortex rings forming during outflow of submerged jets. A theoretical model has been first proposed for the motion and evolution of turbulent vortex rings in an unbounded medium are outlined. A radically new method is developed for the practical application of vortex rings for solving an important technological problem, extinguishing powerful fires on damaged gushing gas and oil wells.

This book is intended for researchers and engineers interested in vortex flows and their applications as well as for lecturers, students and postgraduate students of fluid mechanics.

Contents

Nomenclature

$\mathbf{A}$	vector potential
a	radius of a vortex core
c_p	specific heat of a gas
d_0	exit diameter of a jet
D_F	plume diameter
D_V	vortex ring diameter
E, K	complete elliptic integrals
$\mathbf{F}$	vector of volume (body) forces
F	energy dissipation in a volume of fluid
H	value of Bernoulli's integral
h, l	lengths of semi-axes of vortex ring atmosphere
$J = P/\rho$	kinematic impulse
k, λ	modulus of elliptic integrals
L	jet length
l_c	nozzle length
$\mathbf{P}$	vortex impulse
q, Q	gas flowrate
R	radius of a vortex ring
R_0	nozzle radius
T	kinetic energy
p	pressure
T	duration of jet outflow
t	current time
$\mathbf{u}$	velocity vector
u, v	velocity components
u_0	translational velocity of a vortex ring
u_f	local velocity of a jet
U	potential of volume (body) forces
U, V	magnitudes of output signals of hot-wire anemometers
V_0	jet outflow velocity
w_t	turbulent burning velocity
w	absolute value of velocity
W	calorific value of gas
z, r	cylindrical coordinates

Greek Symbols

α	divergence angle of a vortex ring
Γ	circulation
γ	circulation around a core of a vortex
ΔT	temperature difference
ε	parameter of smallness of a vortex cross-section
ζ, σ	cylindrical coordinates
θ	angle between a velocity vector and an axis of symmetry
λ	length of a jet tail
λ_t	turbulent viscosity coefficient
μ, ν	dynamic and kinematic viscosity coefficients
$\Pi_1,\ldots, \Pi_5$, Φ_z, Φ_r	dimensionless parameters
ρ	density of a medium
Φ	energy dissipation
φ	angle between a velocity vector and an anemometer wire
ψ	stream function
ω, Ω	vorticity (rot **u**)

Introduction

Vortex flow is one of the fundamental types of fluid and gas motion. These flows are the most spectacular in the form of concentrated vortices, characterized by the localization of vorticity (curl of velocity) in bounded regions of a space, beyond which the vorticity is either absent or rapidly falls down to zero.

Concentrated vortices are often observed in nature, exemplified by atmospheric cyclones, whirlwinds and tornados, oceanic vortices, whirlpools on a water surface, and ring vortices caused by explosive outburst of volcanoes. In technical devices concentrated vortices form when flow separates from sharp edges of flying vehicles and ships. Among these are vortices flowing off the ends of airplane wings, and intentionally generated vortices for intensification of burning in combustion chambers, vortices in cyclonic devices used for mixing or separation of impurities in fluids and gases. One such remarkable and frequent type of concentrated vortices is a vortex ring which constitutes a vortex tube closed into a toroidal ring moving in a surrounding fluid like an isolated body out of contact with solid boundaries of the flow region if such boundaries exist.

Formation and motion of vortex rings are important part of the dynamics of a continuum medium and have been studied for more than a century. These investigations promoted elucidation of many general mechanisms of vortex motions of a fluid and a gas, and recently provided a basis for developing high efficiency operating procedures, such as a new method of extinguishing heavy fires on emergency spouting gas-oil wells by means of air vortex rings. Originally vortex rings sparked interest because of simplicity of their generation and observation, and due to approximately steady character of fluid motion relative to the vortex ring. Vortex rings intrigued many famous researchers in mechanics and physics (Helmholtz 1858; Kelvin 1867a,b; Reynolds 1876; Thomson and Newall 1885; Prandtl and Tietjens 1934; Joukowski 1937; Lamb 1932; Prandtl 1949; Taylor 1953; Sommerfeld 1950; Feynman et al. 1964; Kirchhoff 1962; Batchelor 1967). Their investigations resulted in the development of mathematical models for vortex rings in the framework of an ideal (inviscid) fluid, and formulas were obtained for determination of the fundamental vortex ring properties: impulse, energy, translational velocity, and streamline structure.

For a long time the concepts of vortex rings were based only on these theoretical results. Though numerous, experimental studies of that time mostly qualitatively described observations of vortex ring motion, measurement results, and estimation of several external characteristics, namely, translational velocity and geometric parameters, which were determined by visualization of the flow (Banerji and Barave 1931; Magarvey and MacLatchy 1964; Didden 1979). Until

recently, there were almost no studies of the internal structure, mechanisms of formation of real vortex rings, and the dependence of vortex ring characteristics on the conditions of their formation. Theoretical methods and sufficiently full experimental data on motion and evolution of a vortex ring in an unbounded viscous medium after the completion of its formation did not exist, either.

As far back as the 1960s, Academician M.A. Lavrentyev, the founder of the Siberian Branch of the USSR Academy of Sciences, drew attention to the urgency of studying the structure, formation and motion of vortex rings and to the necessity of searching for fields of practical use of vortex rings. The investigations on vortex rings conducted at the Institute of Hydrodynamics of the Siberian Branch of the USSR (now Russian) Academy of Sciences in the ensuing years enabled a clear understanding of the structure of real vortex rings as well as of the regularities of their formation and motion (Akhmetov and Kisarov 1966; Lugovtsov et al. 1969; Lugovtsov 1970, 1974, 1976a,b, 1979; Lugovtsov B.A. and Lugovtsov A.A. 1971; Tarasov 1973, 1975a,b; Vladimirov 1973, 1977, 1979; Sennitskii 1973, 1975a,b, 1980, 1981; Vladimirov and Rybak 1976, 1978; Vladimirov and Tarasov 1979a,b, 1980; Vladimirov et al. 1980; Akhmetov et al. 1980a,b, 1981; Akhmetov and Tarasov 1983, 1986; Akhmetov et al. 1999; Akhmetov 2001; Akhmetov and Lugovtsov 2002; Akhmetov 2007). Based on this research, subsequently a novel high-efficiency technique was developed for extinguishing heavy fires on emergency spouting gas-oil wells by means of air vortex rings. The present monograph is devoted to the systematic treatment of the methods and results of these investigations.

The first chapter reports qualitative data on the structure of vortex rings. The known theoretical models of vortex rings are depicted, the fundamental characteristics of vortex rings are defined, and some formulas used for presenting results are given in following chapters. This introductive chapter is a kind of synopsis; it seemed excessive to present in more detail the early theoretical studies of vortex rings made within the framework of an ideal fluid, because this aspect of the problem was comprehensively outlined in the classic books on fluid mechanics by Lamb (1932) and Batchelor (1967), in original papers which are cited in this monograph, and in the recently published books by Saffman (1992) and Alekseenko, Kuibin, and Okulov (2007).

The second chapter reports results of the first experimental investigation of the hydrodynamic structure of one specific realization of an air vortex ring (Akhmetov and Kisarov 1966). A procedure of determination of an axisymmetric velocity field of a vortex ring using hot-wire anemometers is described. The resulting distributions of velocity, stream function and vorticity are presented. The basic kinematic and dynamic properties of a vortex ring are determined. Dissipation of energy of a vortex ring is found and compared with the power needed for the motion of a streamlined body with the same volume as that of the fluid moving together with the vortex ring. Some results of the experimental studies of vortex ring structure performed later by other researchers are presented as well.

The results of the experimental investigation (Akhmetov 2001) of the features of a whole family of vortex rings being formed during the impulsive outflow of a

jet from a circular nozzle as functions of the criteria that determine the process of formation of a vortex ring, are outlined in the third chapter.

In the fourth chapter the process of vortex ring formation is considered, and a model of its generation based on conservation laws is proposed (Akhmetov, 2001). Formulas for estimating the fundamental parameters of the vortex ring are derived. The results are compared with the experimental data of the third chapter.

The fifth chapter outlines the basics of the theoretical model proposed by B.A. Lugovtsov to describe motion of turbulent vortex rings in an unbounded medium (Lugovtsov et al. 1969; Lugovtsov 1970, 1974, 1976a,b; Vladimirov et al. 1980). The problem is formulated, and the formulas describing motion and time evolution of the main parameters of the turbulent vortex rings are presented. A set of equations for finding the structure of such vortices, and some results of the analysis and numerical solution of these equations are reported.

The sixth chapter describes a radically new method of the practical use of vortex rings for solving an important technological problem, namely extinguishing heavy fires on gas-oil gushers (Akhmetov et al. 1980a,b, 1981; Akhmetov and Tarasov 1983; Akhmetov et al. 1999; Akhmetov and Lugovtsov 2002). Burning gas-oil spouts are characterized and conditions of flame stabilization and blowout from a jet are presented. Procedure for estimating flow rate of burning underexpanded gas jets over the height of the plume are developed. A mechanism of extinguishing a diffusive plume by a vortex ring is explained, experimental results and principles of calculation of fire extinguishing agents are given. The first application of a vortex ring to extinguish a real fire on a powerful gas spout in Uzbekistan is described.

The results reported in Chapters 2–4 are based on the works of the author, and Chapter 5 contains the results obtained by B.A. Lugovtsov with coworkers. Experimental data confirming the theoretical laws of motion of the turbulent vortex ring were obtained mainly by V.F. Tarasov. The method of fire-extinguishing of gas and oil spouts by vortex rings described in Chapter 6 has been developed by a group of authors, but a considerable part of ideas and results obtained while elaborating this practical application of vortex rings belongs to the author of this book.

I would like to thank V.V. Mitrofanov who has proposed to present the results of investigations on vortex rings in the form of a monograph, and T.D. Akhmetov for some numerical calculations.

1 Theoretical Models of Vortex Rings

1.1 Vortex Rings

Systematic scientific studies of vortex rings have been performed since the middle of the 19th century. Originally they were stimulated by the work of Helmholtz, who founded the theory of vortex motions of fluids and also carried out a series of experimental observations of vortex ring motion (Helmholtz 1858). Experiments with the motion of air vortex rings colored with smoke and vortex rings in fluids visualized with dye showed that a vortex ring is a toroidal volume of vortical fluid moving in a surrounding medium at an approximately constant translational speed perpendicular to the ring plane (Fig. 1.1). The fluid motion is axisymmetric, and the vector of vorticity (rotor of velocity $\boldsymbol{\omega} = \mathrm{rot}\,\mathbf{u}$) in the torus is directed along the circles concentric with the circular axis of the torus. A certain volume of the fluid which embraces the ring and looks like an ellipsoid flattened along the direction of motion is moving together with the toroidal vortex ring. This enclosed volume of the fluid is called vortex atmosphere. Inside the vortex atmosphere the fluid is circulating along the closed streamlines encompassing the toroidal core of the vortex. Motion of the fluid surrounding the vortex atmosphere resembles a pattern of flow without separation past a corresponding solid body (Fig. 1.2). This qualitative picture of the flow structure around a vortex ring was described by Reynolds back in 1876 (Reynolds 1876). Later for a long period of time studies of vortex rings were mostly developed theoretically within the framework of an inviscid (ideal) fluid. Information concerning the results of the theoretical investigations and some experimental data on vortex ring dynamics can be found in the books by Villat (1930), Lamb (1932), Milne-Thomson (1938), Batchelor (1967), Saffman (1992), Alekseenko et al. (2007), and in the original papers by Banerji and Barave (1931), Magarvey and MacLatchy (1964), Didden (1979), Weigand and Gharib (1997), and Sullivan et al. (2008). A large number of more recent studies of vortex rings was reviewed by Shariff and Leonard (1992). A long list of papers on vortex motions in general and particularly on vortex ring dynamics for the period 1975–1987 is found in the bibliography by Akhmetov et al. (1988). Basic theoretical models of vortex rings and present-day results will be discussed with the corresponding references throughout the book.

According to formation methods and characteristics of motion in an unbounded medium, vortex rings are divided into two classes. These are so-called buoyant vortex rings that form when a compact volume of a light fluid or gas starts buoying in a medium of larger density by the force of gravity, and pulse vortex rings

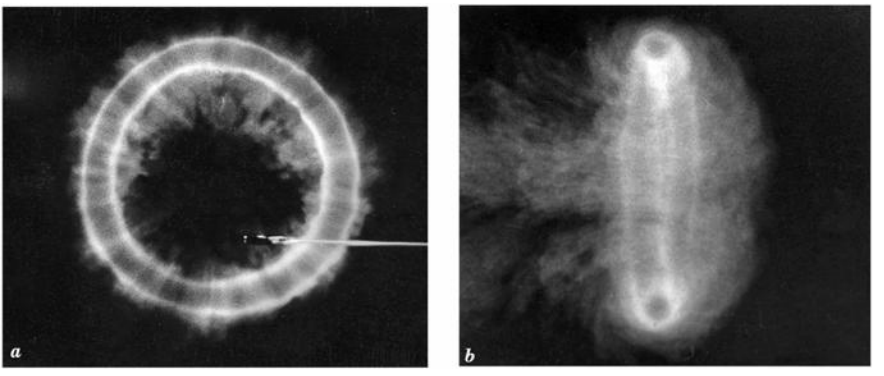

Fig. 1.1. A vortex ring. (*a*) front view; (*b*) side view

that originate when a certain compact part of a fluid is impulsively given a certain momentum. Obviously the motion of buoyant vortex rings is accompanied with the growth of the vortex momentum as a consequence of Archimedes' buoyancy forces. The best known example of buoyant vortex rings is a mushroom cloud of a hot gas produced by nuclear explosion rising in atmosphere. This class of vortex rings also includes thermals in atmosphere which emerge when a localized area of the ground surface is heated rapidly enough. Theoretical and experimental studies of buoyant vortex rings and thermals were performed by Turner (1957, 1963), Onufriev (1967), Gostintsev et al. (1986), Scorer (1978), Zaslavsky (1983), and Zaslavsky and Yur'ev (1983), but analysis of these works is beyond the scope of this book and therefore omitted. This monograph deals mainly with impulsive vortex rings.

Impulsive vortex rings can be generated by various means. One of them is that a circular disk in a fluid is suddenly moved normal to the disk surface and then pulled out of the fluid. Such method of vortex ring formation was described by Helmholtz back in 1858 (Helmholtz 1858). Parameters of the vortex rings generated in so doing were obtained by Taylor (1953). Such vortex rings (more precisely, half-rings), which originate when a tea-spoon is rapidly moved over the surface of coffee in a cup, were also observed by Klein (1910), Anton (1939), and Betz (1950), who carried out experiments to understand the mechanism of origination of the vortical regions in an ideal fluid.

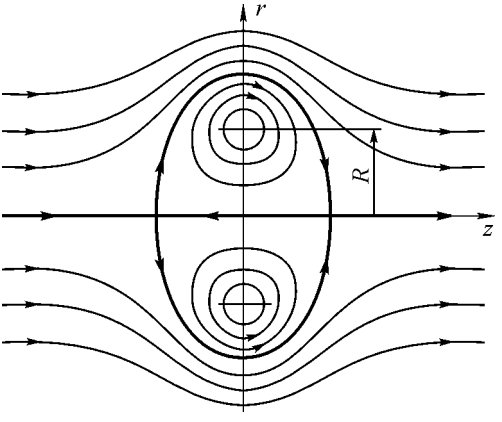

Fig. 1.2. Streamline pattern of a vortex ring in cylindrical coordinates (z, r). R is the vortex ring radius

However vortex rings are more often generated by impulsive pushing a portion of a fluid from a circular orifice in a plane wall or from an open end of a

circular tube, as this is an easier procedure providing controllable formation conditions. In this case the formation of a vortex ring is finished at a distance of several exit diameters, and then the ring moves along the orifice axis in an unbounded medium almost regardless of the device which generated it, and travels a distance over a hundred of orifice diameters until decay.

Remarkable photographs of various stages of vortex ring formation and motion obtained using flow visualization are presented in the works by Didden (1979), Magarvey and MacLatchy (1964), and in the "An Album of Fluid Motion" by Van Dyke (1982).

Self-consistent motion of the formed vortex ring proceeds under the action of viscosity, but the impulse of the vortex is conserved in the viscous medium as well (Lugovtsov et al. 1969; Lugovtsov 1970, 1974, 1976a,b; Lugovtsov and Lugovtsov 1971; Vladimirov et al. 1980; Alekseenko et al. 2007). It is more convenient to consider this stage of ring motion separately. B.A. Lugovtsov was the first to suggest a theoretical model of turbulent vortex ring motion and evolution based on the condition of vortex impulse conservation (Lugovtsov et al. 1969; Lugovtsov 1970, 1974, 1976a,b, 1979; Lugovtsov and Lugovtsov 1971). According to this model, the vortex ring structure at large Reynolds numbers occurs to be self-similar regardless of the generation method. Statement of the problem of turbulent vortex ring motion and the obtained results will be discussed in more detail in Chapter 5. The current status of research on vortex ring vibrations and of the problems of turbulence origination in a vortex ring is given in the review by Kop'ev and Chernyshev (2000).

1.2 Equations of Motion. Vorticity, Circulation, and Stream Function

The Euler equations representing conservation of mass and rate of change of momentum under the action of volume forces **F** form the basis for the theoretical description of motion of an ideal fluid:

$$\frac{d\rho}{dt} = \frac{\partial \rho}{\partial t} + \mathbf{u} \cdot \nabla \rho + \rho \nabla \cdot \mathbf{u} = 0,$$

$$\frac{d\mathbf{u}}{dt} = \frac{\partial \mathbf{u}}{\partial t} + (\mathbf{u} \cdot \nabla)\mathbf{u} = -\frac{1}{\rho}\nabla p + \mathbf{F},$$

where t is the time, **u** is the velocity vector, ρ is the density, p is the pressure, **F** is the vector of the body force per unit mass, and ∇ is Hamilton's operator (nabla). The equation of impulses (the second one) can be rearranged using the vector identity $(\mathbf{u} \cdot \nabla)\mathbf{u} = \nabla(u^2/2) + \mathrm{rot}\mathbf{u} \times \mathbf{u}$ to the form

$$\frac{\partial \mathbf{u}}{\partial t} + \nabla\left(\frac{u^2}{2}\right) + \mathrm{rot}\,\mathbf{u} \times \mathbf{u} = -\frac{1}{\rho}\nabla p + \mathbf{F},$$

which is known as the equation of motion in Lamb's form. Here $\mathrm{rot}\,\mathbf{u} = \boldsymbol{\omega}$ is the vorticity vector, which is the fundamental characteristic of vortex motions of the fluid.

From this point on we will consider vortex motions of a uniform incompressible fluid in which the volume forces **F**, if any, are conservative with the potential *U*, i.e. $\mathbf{F} = -\nabla U$. Under these conditions ρ = const, and the equations of motion take the form

$$\nabla \cdot \mathbf{u} = 0, \tag{1.1}$$

$$\frac{\partial \mathbf{u}}{\partial t} + \boldsymbol{\omega} \times \mathbf{u} = -\nabla H, \tag{1.2}$$

where $H = u^2/2 + p/\rho + U$ is the Bernoulli integral that remains constant along any certain streamline for steady flow of the fluid (that is, for $\partial \mathbf{u}/\partial t = 0$). Note that a streamline is a line whose tangent is everywhere parallel to velocity. Streamlines in the Cartesian coordinates are defined by the equations

$$\frac{dx}{u_x} = \frac{dy}{u_y} = \frac{dz}{u_z},$$

where u_x, u_y, u_z are the corresponding velocity vector **u** components. In the same manner vortex lines can be defined

$$\frac{dx}{\omega_x} = \frac{dy}{\omega_y} = \frac{dz}{\omega_z},$$

where $\omega_x, \omega_y, \omega_z$ are the components of the vorticity vector **ω**. Applying the rot (rotor) operator to (1.2), one may arrive at the equation of vorticity evolution originally obtained by Helmholtz (1858)

$$\frac{\partial \boldsymbol{\omega}}{\partial t} + (\mathbf{u} \cdot \nabla)\boldsymbol{\omega} = (\boldsymbol{\omega} \cdot \nabla)\mathbf{u} \quad \text{or} \quad \frac{d\boldsymbol{\omega}}{dt} = (\boldsymbol{\omega} \cdot \nabla)\mathbf{u}, \tag{1.3}$$

which is notable for the absence of pressure. The Helmholtz equation implies that the vortex tubes move together with the fluid and have constant intensity (Kochin et al. 1964; Batchelor 1967).

Since vortex rings are axisymmetric, it is convenient to study the flow inside them in cylindrical coordinates *z*, *r*, *θ*, where *z* is the axial coordinate measured along the symmetry axis which passes through the center of the ring normal to its plane, and *r*, *θ* are the radial and azimuthal coordinates, respectively. In this coordinate system the velocity field of a vortex ring has two velocity components, namely the axial one *u* and the radial *v*, and the ring vorticity has only a single azimuthal component $\omega_\theta = |\boldsymbol{\omega}| = \omega$. Since in the case of axisymmetric flow without swirl $\boldsymbol{\omega} = \omega\boldsymbol{\kappa}$, where **κ** is a unit vector in the azimuthal direction, and

$d\boldsymbol{\omega}/dt = \boldsymbol{\kappa}\, d\omega/dt$, $(\boldsymbol{\omega}\cdot\nabla)\mathbf{u} = \boldsymbol{\kappa}\,\omega v/r$, continuity equation (1.1) and equation of motion (Helmholtz equation) (1.3) in cylindrical coordinates can be written in a scalar form:

$$\nabla\cdot\mathbf{u} = \frac{\partial u}{\partial z} + \frac{1}{r}\frac{\partial (rv)}{\partial r} = 0, \tag{1.4}$$

$$\frac{d\omega}{dt} = \frac{v\omega}{r}. \tag{1.5}$$

The value of vorticity is defined by the velocity components

$$\omega = \frac{\partial v}{\partial z} - \frac{\partial u}{\partial r}. \tag{1.6}$$

The continuity equation (1.4) implies that there exists a stream function ψ which is related to the velocity components u and v by the flowing relations

$$u = \frac{1}{r}\frac{\partial \psi}{\partial r}, \quad v = -\frac{1}{r}\frac{\partial \psi}{\partial z}. \tag{1.7}$$

In steady case (for $\partial\omega/\partial t = 0$) equation (1.5) can be recast in the form $d(\omega/r)/dt = 0$. It follows that in steady axisymmetric flow the quantity ω/r is constant along a streamline and depends only on the value of the stream function ψ. Hence the condition for steadiness of axisymmetric vortex flows can be written in the form

$$\omega/r = f(\psi), \tag{1.8}$$

where f is an arbitrary function of ψ.

1.3 Vorticity Distribution and Velocity Field of a Vortex Ring

Velocity field of a vortex ring can be found from the given (or known) distribution of vorticity $\boldsymbol{\omega} = \mathrm{rot}\,\mathbf{u} = \nabla\times\mathbf{u}$ in the ring. From books on vector analysis and hydrodynamics (Lamb 1932; Kochin et al. 1964; Kochin 1965; Batchelor 1967) it is known that the problem of finding a vector $\mathbf{u}$ satisfying the conditions $\mathrm{div}\,\mathbf{u} = 0$, $\nabla\times\mathbf{u} = \boldsymbol{\omega}$, is reduced by introducing a vector potential $\mathbf{A}$ via $\mathbf{u} = \nabla\times\mathbf{A}$ (i.e. $\boldsymbol{\omega} = \nabla\times(\nabla\times\mathbf{A})$) to the solution of a vector Poisson's equation $\Delta\mathbf{A} = -\boldsymbol{\omega}$, where Δ is the Laplace operator. Solution of this equation is given by the integral over the volume V, occupied by the vortical fluid,

$$\mathbf{A}(x,y,z) = \frac{1}{4\pi}\int_V \frac{\boldsymbol{\omega}(\xi,\eta,\zeta)\,dV}{s}, \tag{1.9}$$

where $s = \left((x-\xi)^2 + (y-\eta)^2 + (z-\zeta)^2\right)^{1/2}$ is the distance between the observation point (x, y, z) and a moving integration point (ξ, η, ζ) in the region *V*, where the distribution $\boldsymbol{\omega}$ is given. This solution is unique if the vector **u** is continuous over the whole space and vanishes at infinity. Calculations simplify when they are performed in cylindrical coordinates (Fig. 1.3) with the *z*-axis coinciding with the ring axis of symmetry. In this system the vorticity vector $\boldsymbol{\omega}$ has only the azimuthal component equal to the absolute value of $\boldsymbol{\omega}$. Evidently the direction of the vector potential **A** coincides with the direction of $\boldsymbol{\omega}$, and equation (1.9) for determining **A** becomes scalar. As can be seen from Fig. 1.3, in cylindrical coordinates $x = r\cos\theta, \quad y = r\sin\theta, \quad \xi = \sigma\cos\alpha, \quad \eta = \sigma\sin\alpha, \quad dV = \sigma d\alpha d\sigma d\zeta,$ $\omega = \omega(\zeta, \sigma),$ and the vorticity components are $\omega_x = -\omega\sin\alpha, \ \omega_y = \omega\cos\alpha.$ The components of the vector potential **A** are

$$A_x = -\int_{\Sigma}\int_{0}^{2\pi} \frac{\omega\sin\alpha}{s} d\alpha\, \sigma\, d\sigma\, d\zeta, \quad A_y = \int_{\Sigma}\int_{0}^{2\pi} \frac{\omega\cos\alpha}{s} d\alpha\, \sigma\, d\sigma\, d\zeta, \quad A_z = 0,$$

where Σ is the cross-section area of the ring. It is sufficient to find distribution of *A* in one of the planes θ = const, passing through the symmetry axis *Oz*, because an axisymmetric field is the same in any of these planes. For convenience, we assume that $\theta = 0$, since in this case $A_y = A_\theta = A$ and therefore,

$$A_\theta = A = \frac{1}{4\pi}\int_{\Sigma} \omega(\sigma, \zeta) \int_{0}^{2\pi} \frac{\cos\alpha\, d\alpha}{\left(r^2 + \sigma^2 - 2r\sigma\cos\alpha + (z-\zeta)^2\right)^{1/2}} \sigma\, d\sigma\, d\zeta. \qquad (1.10)$$

Knowing *A*, one can find the velocity components. Since $\mathbf{u} = \mathrm{rot}\mathbf{A}$, where $\mathbf{A}(0,0,A)$, $u = r^{-1}\partial(rA)/\partial r, \quad v = -\partial A/\partial z.$ Then together with (1.7) it implies $\psi = rA$, that is formula (1.10) immediately determines the stream function of the

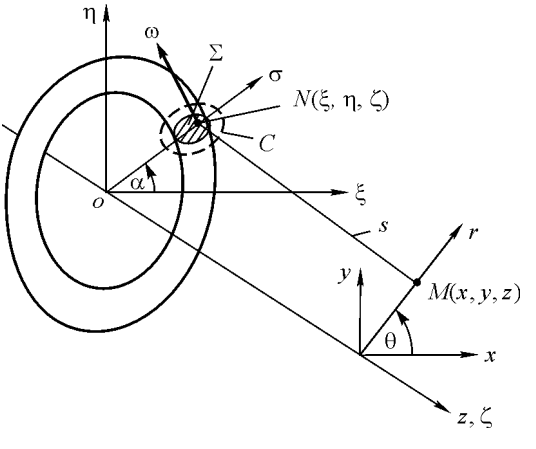

Fig. 1.3. A vortex ring in the cylindrical coordinate system

vortex ring. The integral over the angle α in (1.10) is expressed in terms of the complete elliptic integrals of the first and second kind, K and E:

$$I = \int_0^{2\pi} \frac{\cos\alpha\, d\alpha}{\left(r^2+\sigma^2-2r\sigma\cos\alpha+(z-\zeta)^2\right)^{1/2}} = \frac{2}{(r\sigma)^{1/2}}\left[\left(\frac{2}{k}-k\right)K(k)-\frac{2}{k}E(k)\right], \quad (1.11)$$

where $k = \left[4r\sigma \Big/ \left((z-\zeta)^2+(r+\sigma)^2\right)\right]^{1/2}$ is the modulus of the elliptic integrals.

Then $A = (4\pi)^{-1}\int_\Sigma \omega(\zeta,\sigma) I(z-\zeta, r, \sigma)\,\sigma\, d\zeta\, d\sigma$, and the stream function is now determined by

$$\psi = \frac{r^{1/2}}{2\pi}\int_\Sigma \sigma^{1/2}\left[\left(\frac{2}{k}-k\right)K(k)-\frac{2}{k}E(k)\right]\omega(\zeta,\sigma)\, d\zeta\, d\sigma. \quad (1.12)$$

In some cases it is more convenient to use an alternative, more symmetric form of integral (1.11). It is known (Lamb 1932; Kochin et al. 1964) that with the following notation

$$r_1^2 = (z-\zeta)^2+(r-\sigma)^2, \quad r_2^2 = (z-\zeta)^2+(r+\sigma)^2, \quad \lambda = (r_2-r_1)\big/(r_2+r_1) \quad (1.13)$$

$$I = \int_0^{2\pi} \frac{\cos\alpha\, d\alpha}{\left(r^2+\sigma^2-2r\sigma\cos\alpha+(z-\zeta)^2\right)^{1/2}} = \frac{8}{r_2-r_1}\,[K(\lambda)-E(\lambda)] =$$

$$= \frac{2(r_2+r_1)}{r\sigma}\,[K(\lambda)-E(\lambda)],$$

hence,

$$\psi = \frac{1}{2\pi}\int_\Sigma (r_2+r_1)[K(\lambda)-E(\lambda)]\,\omega(\zeta,\sigma)\, d\zeta\, d\sigma. \quad (1.14)$$

1.4 Integral Characteristics of a Vortex Ring

Besides the velocity field, several integral parameters are also important for characterization of vortex rings, namely the intensity or the total circulation of a vortex ring, the impulse and the kinetic energy. Circulation Γ is defined as a contour integral of the velocity u over the length of the curve. By Stokes's theorem (Kochin et al. 1964), the circulation Γ around a closed contour C is equal to the flux of vorticity $\boldsymbol{\omega}$ through an arbitrary surface Σ, bounded by this contour, $\Gamma = \oint_C \mathbf{u}\cdot d\mathbf{l} = \iint_\Sigma \boldsymbol{\omega}\cdot d\boldsymbol{\Sigma}$. Hence, the circulation around a contour bounding a transverse cross-section of a vortex ring (see Fig. 1.3)

$$\Gamma = \iint_\Sigma \omega(\zeta,\sigma)\, d\zeta\, d\sigma, \quad (1.15)$$

characterizes the intensity of a vortex ring. Circulation around a closed fluid contour in an ideal incompressible fluid in case when volume forces acting on the fluid are conservative is an integral of motion, i.e. it does not change in time. Though in a viscous fluid the law of circulation conservation does not hold, the concept of circulation is useful for estimating instantaneous intensity of vortex rings in real media as well.

Another important characteristic is the impulse of the vortex **P**. Common definition of momentum as a product of density ρ by a volume integral of velocity $\mathbf{K} = \rho \int_V \mathbf{u}\, dV$ fails for the majority of flows of an ideal incompressible fluid at rest at infinity, because **K** exists only when the velocity field **u**(*r*,*t*) satisfies the condition $r^3 |\mathbf{u}(r,t)| \to 0$ as $r = |\boldsymbol{r}| \to \infty$. It can be shown that in this case **K** = 0. As for flows with point-source or dipole asymptotics, among which are the flows due to the motion of solid bodies and vortex rings in an unbounded medium, **K** simply does not exist. Therefore, Lamb (1932) introduced the concept of the vortex impulse **P**, which as well as **K**, has the dimension of momentum and is interpreted as the impulse of external forces that must be applied to a limited portion of flow in order to generate the observed fluid motion from rest. The vortex impulse is defined by an integral of vector product of the radius vector **r** by the vorticity $\boldsymbol{\omega}$ over the volume *V* including all vortices

$$\mathbf{P} = \frac{1}{2}\rho \int_V \mathbf{r} \times \boldsymbol{\omega}\, dV. \tag{1.16}$$

This integral converges under weaker requirements to a flow asymptotic, i.e. at $|\boldsymbol{\omega}| \sim \text{const} \cdot |\mathbf{r}|^{-4}$, as $|\mathbf{r}| \to \infty$. This condition usually holds for flows like vortex rings, since $\boldsymbol{\omega}$ is localized within a finite volume of a vortex ring. Vortex impulse is notable for conservation (invariance) of **P** in time not only in an ideal, but also in a viscous incompressible fluid. Proof of this statement can be found in the papers (Lugovtsov et al. 1969; Lugovtsov 1970, 1974, 1976a,b, 1979; Lugovtsov and Lugovtsov 1971; Vladimirov et al. 1980) and in the book by Alekseenko et al. (2007).

It follows from (1.16) that the value of the impulse of a vortex ring in cylindrical coordinates (z, r, θ) with the radius vector of the integration point $\mathbf{r} = \mathbf{r}(\zeta, \sigma, \theta)$ and vorticity $\boldsymbol{\omega} = \boldsymbol{\omega}(0,0,\omega)$ is

$$P = |\mathbf{P}| = \pi\rho \iint_\Sigma \omega(\zeta, \sigma)\, \sigma^2\, d\sigma\, d\zeta, \tag{1.17}$$

and **P** is directed along the axis of symmetry *Oz*. Vladimirov (1977, 1979) substantially broadened Lamb's definition by extending the concept of vortex impulse to the flows that are confined by internal and external boundaries. He showed that if a closed surface ∂A containing all vortices, with $\boldsymbol{\omega} = 0$ outside of it, exists in a fluid, then the vortex impulse of the flow can be represented as a sum of the momentum of this volume of the fluid *V* itself and its virtual momentum

$$\mathbf{P} = \frac{1}{2}\rho\int(\mathbf{r}\times\boldsymbol{\omega})\,dV = \rho\int_V \mathbf{u}\,dV + \frac{1}{2}\rho\int_{\partial A}\mathbf{r}\times(\mathbf{n}\times\mathbf{u})\,d\Sigma = \rho\int_V \mathbf{u}\,dV + \rho\int_{\partial A}\mathbf{n}\varphi\,d\Sigma, \quad (1.18)$$

where φ is the velocity potential outside the volume V containing all vortices, and $\mathbf{n}$ is the outward unit normal to ∂A. Here the second term in the right-hand side (integral over the surface ∂A) is the virtual momentum of the body bounded by the surface ∂A (Lamb 1932; Kochin et al. 1964). Such form of the vortex impulse is in many cases very useful. Particularly, it follows from (1.18) that if V is chosen to be a vortex ring atmosphere moving together with the vortex (see Fig. 1.2), the ring impulse will be equal to the sum of the vortex atmosphere momentum and the virtual momentum of the latter. Since the vortex ring is translated with velocity $\mathbf{u}_0$, $\mathbf{P} = m(1+\mu)\mathbf{u}_0$, where m is the mass of the fluid inside the vortex atmosphere, and μ is the virtual-mass coefficient of the vortex atmosphere (Kochin et al. 1964; Batchelor 1967).

The kinetic energy of the flow is given by the integral $T = (\rho/2)\int\mathbf{u}\cdot\mathbf{u}\,dV = (\rho/2)\int\mathbf{u}(\nabla\times\mathbf{A})\,dV$ over the whole volume V of an unbounded medium which is occupied by the fluid. Assuming the vector identity $\nabla\cdot(\mathbf{a}\times\mathbf{b}) = \mathbf{b}(\nabla\times\mathbf{a}) - \mathbf{a}(\nabla\times\mathbf{b})$ this expression can be recast to the form $T = (\rho/2)\int_V[\mathbf{A}(\nabla\times\mathbf{u}) - \nabla\cdot(\mathbf{u}\times\mathbf{A})]\,dV$. The last term in the form of a divergence turns to a surface integral, which is zero in an unbounded fluid, hence $T = (\rho/2)\int\mathbf{A}\cdot\boldsymbol{\omega}\,dV$. Since outside of the vortex ring $\boldsymbol{\omega} = 0$, the region of integration reduces to the volume of the ring. Thus, assuming that in cylindrical coordinates $\boldsymbol{\omega} = \boldsymbol{\omega}(0,0,\omega)$, $\mathbf{A} = \mathbf{A}(0,0,A)$, and $A = \psi/r$, the kinetic energy of the vortex ring takes the form

$$T = \frac{1}{2}\rho\int_\Sigma \frac{\psi}{r}\omega\,dr\,r\,d\theta\,dz = \pi\rho\iint_\Sigma \psi\,\omega\,dr\,dz, \quad (1.19)$$

where Σ is the cross-section of the ring. In theoretical calculations of vortex ring parameters an alternative expression for the kinetic energy given in Lamb's book (1932) might be useful

$$T = \rho\int\mathbf{u}\cdot(\mathbf{r}\times\boldsymbol{\omega})\,dV = 2\pi\rho\iint_\Sigma \omega\sigma(\zeta u - rv)\,d\zeta\,d\sigma. \quad (1.20)$$

It can be obtained using the vector identity

$$\frac{1}{2}u^2 - \mathbf{u}\cdot(\mathbf{r}\times\boldsymbol{\omega}) = \nabla\cdot\left[\frac{1}{2}u^2\mathbf{r} - \mathbf{u}(\mathbf{r}\cdot\mathbf{u})\right].$$

When this relation is integrated over the volume, the right-hand side reduces to the surface integral which turns to zero, as $|\mathbf{r}| \to \infty$. Equations (1.12)–(1.20) are of general nature for axisymmetric vortex rings with arbitrary distribution of vorticity,

and the precise structure of a vortex ring is found once the vorticity distribution $\omega(\zeta,\rho)$ is specified.

1.5 Circular Line Vortex of Zero Cross-Section

A circular line vortex of zero cross-section provides the simplest theoretical model of a vortex ring that reveals some features of the flow near the ring. Let the line coordinates be $\zeta = \zeta_0$, $\sigma = R$, i.e. the line be a circumference of radius R (Fig. 1.4). Circulation around the line will be considered finite despite zero thickness of the line. It is possible if the vorticity of the line goes to infinity, i.e. the vorticity is represented by Dirac delta-functions $\omega = \Gamma_0 \delta(\zeta - \zeta_0)\,\delta(\sigma - R)$. Then the circulation of the line is $\Gamma = \int_\Sigma \omega(\zeta,\sigma)\,d\zeta\,d\sigma = \Gamma_0$, and the stream function (1.14) of the flow induced by the circular line vortex becomes

$$\psi = \frac{\Gamma_0}{2\pi}(r_2 + r_1)[K(\lambda) - E(\lambda)]. \tag{1.21}$$

This formula originally obtained by Maxwell (1954) allows plotting streamlines of the flow. The shape of the streamlines of a circular line vortex in the plane z,O,r for equidistant values of ψ depicted in the books by Lamb (1932) and Batchelor (1967) is shown in Fig. 1.5. One can see that near the line the fluid moves along the closed streamlines, encircling the line. It can be noted here that the circular

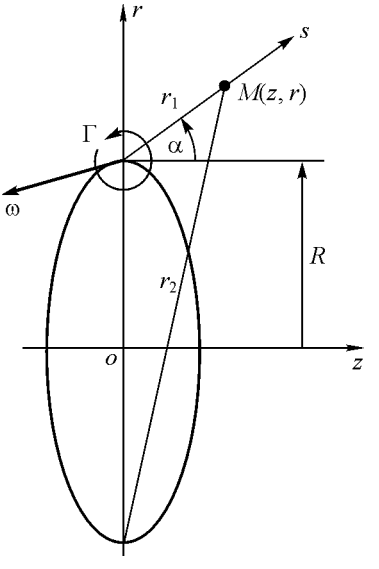

Fig. 1.4. A circular vortex line of zero cross-section

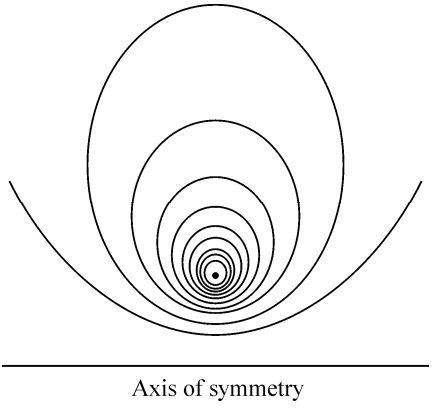

Fig. 1.5. Streamlines of a circular vortex line in fluid at rest at infinity (Batchelor 1967)

line vortex has an electromagnetic analog. If one considers a circular conductor with a steady current proportional to Γ_0 instead of a line vortex, then formula (1.21) with coefficients corresponding to this problem can be used to find a magnetic field induced by this current. These formulas in electromagnetic theory describe the known Biot-Savart law.

It is of interest to estimate the velocity field in the vicinity of the line vortex. Let the coordinates of the line vortex be $\zeta = 0$, $\sigma = R$. Consider a flow in polar coordinates s, α with the origin at the intersection of a meridional plane by the line (see Fig. 1.4). Then coordinates of the point $M(z,r)$, where velocity is determined, are written as $z = s\cos\alpha$, $r = R + s\sin\alpha$. When $s/R \ll 1$, the modulus of the elliptic integrals λ in (1.21) is close to unity, and hence in the vicinity of the line the following asymptotic forms of these integrals are valid (Dwight 1961; Gradshtein and Ryzhik 1965)

$$K(\lambda) = \ln\frac{4}{\lambda'} + \frac{1}{4}\left(\ln\frac{4}{\lambda'} - 1\right)\lambda'^2, \quad E(\lambda) \approx 1 + \frac{1}{2}\left(\ln\frac{4}{\lambda'} - \frac{1}{2}\right)\lambda'^2,$$

where $\lambda'^2 = 1 - \lambda^2 = 4r_1 r_2 / (r_2 + r_1)^2$, $r_1^2 = z^2 + (r-R)^2 = s^2$, λ' is the complementary modulus of the integrals K and E, and $r_2^2 = z^2 + (r+R)^2 \approx 4R^2\left[1 + sR^{-1}(1+\sin\alpha)\right]$.

In this approximation expression (1.21) for a stream function takes the form

$$\psi \approx \frac{\Gamma_0 R}{2\pi}\left[\ln\frac{8R}{s} - 2 + \frac{s}{2R}\sin\alpha\left(\ln\frac{8R}{s} - 1\right) + O\left(\frac{s^2}{R^2}\ln\frac{8R}{s}\right)\right].$$

This yields the velocity components near the line vortex:

$$u = \frac{1}{r}\frac{\partial\psi}{\partial r} = \frac{\Gamma_0}{2\pi}\left[-\frac{1}{s}\sin\alpha + \frac{1}{2R}\ln\frac{8R}{s} - \frac{1}{2R}\cos^2\alpha + O\left(\frac{s}{R}\ln\frac{R}{s}\right)\right],$$

$$v = -\frac{1}{r}\frac{\partial\psi}{\partial z} = \frac{\Gamma_0}{2\pi}\left[\frac{1}{s}\cos\alpha - \frac{\sin\alpha\cos\alpha}{2R} + O\left(\frac{s}{R}\ln\frac{R}{s}\right)\right].$$

The first terms in these expressions correspond to the rotational motion of the fluid around the line vortex. The second term with the logarithmic singularity in the expression for the axial velocity u means that the line vortex moves in the direction normal to the plane of the circle with an infinite speed. It can be shown that the kinetic energy of fluid motion induced by a circular line vortex is also infinite, and the vortex impulse according to (1.17) has the finite value $P = \pi\rho R^2\Gamma$. The fact that the velocity of the rotational motion near the line vortex and the translational velocity of the line itself go to infinity, is unacceptable from the physical point of view. Clearly, the singular behavior of the rotational velocity near the line and of the energy of a circular line vortex are due to zero thickness of the line, and the fact that the translational velocity tends to infinity is due to finite curvature of the line as it is shown in hydrodynamic textbooks (for instance, Batchelor (1967)). These drawbacks disappear when a mathematical model for a vortex ring of finite cross-section is considered.

1.6 Vortex Ring with Finite Cross-Section (Lamb's Model)

A model of a vortex ring whose cross-section has the form of a circle of radius a, and moreover the ratio of a to the ring radius R is small $a/R \ll 1$, and the vorticity inside the circle is constant, was presented in Lamb's book (1932). A stream function ψ in this case can be found from (1.14). When $a/R \ll 1$, inside and close to the cross-section of the ring, according to (1.13), $r_1/r_2 \ll 1$, $r_2 \approx 2R$ and $\lambda \approx 1$, hence the approximate forms of the elliptic integrals can be used $K(\lambda) \approx (1/2)\ln 16/\lambda'^2$, $E(\lambda) \approx 1$, where $\lambda'^2 = 1-\lambda^2 = 4r_2 r_1/(r_2+r_1)^2 \approx 4r_1/R$. Then for $\omega = \text{const}$ formula (1.14) for the stream function takes the form

$$\psi = \frac{R\omega}{2\pi}\iint\left(\ln\frac{8R}{r_1}-2\right)d\zeta\, d\sigma,$$

where $r_1 = [(z-\zeta)^2-(r-\sigma)^2]^{1/2}$ according to (1.13). It is convenient to calculate ψ in polar coordinates s, θ with the origin at the center of a circular cross-section of the ring (Fig. 1.6). Using relations between Cartesian and polar coordinates, $z = \zeta_0 + s\cos\theta$, $r = R + s\sin\theta$, $\zeta = \zeta_0 + s'\cos\theta'$, $\sigma = R + s'\sin\theta'$, we have $d\zeta\, d\sigma = s'd\theta' ds'$, $r_1 = [s^2+s'^2-2s\,s'\cos(\theta-\theta')]^{1/2}$, and hence, $\psi = (\omega R/2\pi)\int_0^a\int_0^{2\pi}\left(\ln 8R/r_1 - 2\right)d\theta' s' ds'$. The definite integral of the function $\ln r_1$ over angle θ' is known (Gradshtein and Ryzhik 1965):

$$\int_0^{2\pi}\ln\left[s^2+s'^2-2ss'\cos(\theta-\theta')\right]^{1/2}d\theta' = \begin{cases} 2\pi\ln s & \text{at} \quad s'<s \\ 2\pi\ln s' & \text{at} \quad s'>s \end{cases}.$$

Thus for the points within the cross-section of the ring

$$\psi = \omega R\int_0^a(\ln 8R-2)s'ds' - \left(\int_0^s \ln s\, s'ds' + \int_s^a \ln s' s'ds'\right) = \frac{\omega R a^2}{2}\left(\ln\frac{8R}{a}-\frac{3}{2}-\frac{1}{2}\frac{s^2}{a^2}\right).$$

Now we can find circulation, impulse, and energy of the vortex ring using (1.15), (1.17), (1.19). Considering that $\sigma \approx R$, when $a/R \ll 1$, we have:

$$\Gamma = \iint \omega\, d\zeta\, d\sigma = \int_0^a\int_0^{2\pi}\omega\, s'ds'd\theta' = \pi\omega a^2, \tag{1.22}$$

$$P = \pi\rho\iint\omega\sigma^2 d\zeta\, d\sigma = \pi\rho R^2\Gamma, \tag{1.23}$$

$$T = \pi\rho\iint\omega\psi\, d\zeta\, d\sigma = \pi\rho\iint\omega\psi\, s'ds'd\theta' = \frac{1}{2}\rho\Gamma^2 R\left(\ln\frac{8R}{a}-\frac{7}{4}\right). \tag{1.24}$$

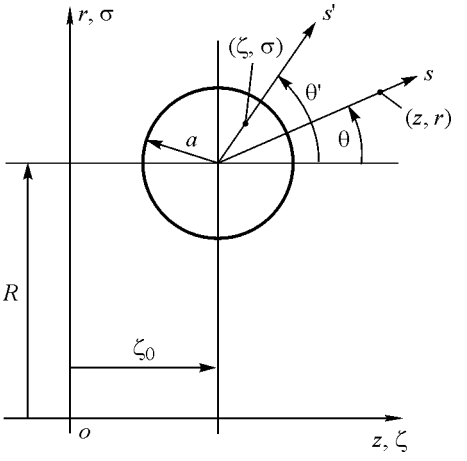

Fig. 1.6. Cross-section of a vortex in polar coordinates

The translational velocity of the vortex ring can be found following the procedure used by Lamb (1932). Let us define coordinates of the center of vorticity by the formulas

$$\zeta_0 = \frac{\iint \omega\zeta\sigma^2 d\zeta d\sigma}{\iint \omega\sigma^2 d\zeta d\sigma} = \frac{\iint \omega\zeta\sigma^2 d\zeta d\sigma}{P/\pi\rho}, \quad R^2 = \frac{\iint \omega\sigma^2 d\zeta d\sigma}{\iint \omega\, d\zeta d\sigma} = \frac{P}{\pi\rho\Gamma},$$

where integration is taken over the cross-section of the ring. Obviously the average radius of the ring R does not depend on time, since P and Γ are invariants of the motion. The translational velocity u_0 of the vortex ring can be deduced by taking the time derivative of ζ_0,

$$u_0 = \frac{d\zeta_0}{dt} = \frac{\pi\rho}{P}\iint \omega\left(\frac{d\zeta}{dt}\sigma^2 + 2\zeta\sigma\frac{d\sigma}{dt}\right)d\Sigma = \frac{\pi\rho}{P}\iint \omega(u\sigma^2 + 2\zeta\sigma v)\,d\Sigma =$$

$$= \frac{\pi\rho}{P}\left[\iint \omega\sigma(\sigma u - \zeta v)\,d\Sigma + 3\iint \omega\sigma\zeta v\,d\Sigma\right]. \qquad (1.25)$$

Here $\iint \omega\sigma(\sigma u - \zeta v)\,d\Sigma = T/2\pi\rho$ as inferred from (1.20). The last integral in (1.25), taking into account that $\iint \omega\sigma v\,d\Sigma = (1/2)\,d\left(\iint \omega\sigma^2 d\Sigma\right)\Big/dt = 0$ (due to the constancy of R^2) and that within the cross-section of the ring $v = \omega(\zeta - \zeta_0)/2$, can be transformed into

$$\iint \omega\sigma\zeta v\,d\Sigma = \iint \omega\sigma(\zeta - \zeta_0)v\,d\Sigma = \frac{1}{2}\iint \omega^2\sigma(\zeta - \zeta_0)^2 d\zeta d\sigma.$$

Using polar coordinates introduced above with the origin at $\zeta = \zeta_0$, $\sigma = R$, one can show that $(1/2)\iint \omega^2 \sigma (\zeta - \zeta_0)^2 \, d\zeta \, d\sigma = R\Gamma^2/8\pi$. Substitution of this expression together with (1.23) and (1.24) for the impulse and the kinetic energy into (1.25) yields

$$u_0 = \frac{\Gamma}{4\pi R}\left(\ln\frac{8R}{a} - \frac{1}{4}\right). \tag{1.26}$$

This formula was originally obtained by Kelvin in 1867 (Kelvin 1867).

One may also find the velocity distribution $u_*(z,0)$ on the axis of symmetry $r = 0$ of a vortex ring. The stream function is found from (1.14). In this case the modulus of the elliptic integrals in (1.14) $\lambda = (r_2 - r_1)/(r_2 + r_1) \to 0$ and the integrals themselves are approximated (Dwight 1961; Gradshtein and Ryzhik 1965) by the formulas

$$K(\lambda) \approx \frac{\pi}{2}\left(1 + \frac{\lambda^2}{4}\right), \quad E(\lambda) \approx \frac{\pi}{2}\left(1 - \frac{\lambda^2}{4}\right), \quad K(\lambda) - E(\lambda) = \frac{\pi}{4}\lambda^2.$$

Recalling that $\varepsilon = a/R \ll 1$, let us neglect variations in ζ and σ in the cross-section of the vortex core and assume $\zeta = 0$, $\sigma = R$ Then equations (1.13) imply

$$r_1^2 \approx z^2 + (r - R)^2 = (R^2 + z^2)\left(1 - \frac{2}{1 + z^2/R^2}\frac{r}{R}\right),$$

$$r_2^2 \approx z^2 + (r + R)^2 = (R^2 + z^2)\left(1 + \frac{2}{1 + z^2/R^2}\frac{r}{R}\right),$$

$$r_2 + r_1 \approx 2\left(R^2 + z^2\right)^{1/2}, \quad \lambda \approx \frac{rR}{R^2 + z^2}, \quad K(\lambda) - E(\lambda) = \frac{\pi}{4}\lambda^2 \approx \frac{\pi}{4}\frac{r^2R^2}{(R^2 + z^2)^2}.$$

Upon insertion of these expressions into (1.14) we obtain the stream function

$$\psi = \frac{1}{2\pi}\iint_{\Sigma}(r_2 + r_1)[K(\lambda) - E(\lambda)]\,\omega \, d\Sigma = \frac{\Gamma}{4}\frac{r^2R^2}{(z^2 + R^2)^{3/2}}.$$

Now the velocity distribution along the symmetry axis can be calculated $u_*(z,0) = r^{-1}\partial\psi/\partial r \approx (\Gamma/2)R^2(z^2 + R^2)^{-3/2}$. Hence, the velocity in the ring center (at $r = z = 0$) is $u_{*0} = u_*(0,0) = \Gamma/2R$.

Theoretically, the speed of a vortex ring u_0 depending on the value of the parameter $\varepsilon = a/R$ might be both greater and smaller than the speed u_{*0} at the center of the ring. It determines the shape of a ring atmosphere, i.e. the volume of fluid transported together with a vortex ring (see Fig. 1.2). The shape of the atmosphere can be obtained by plotting streamlines in a coordinated system moving with the

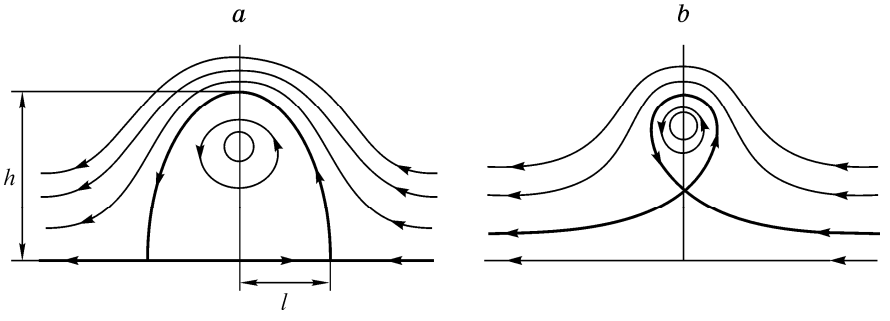

Fig. 1.7. Different streamline patterns of vortex rings: (*a*) fat ring, ε > 1/86; (*b*) thin ring, ε < 1/86

vortex ring. The stream function ψ_0 in such a system is defined as $\psi_0 = \psi - u_0 r^2/2$, where ψ is the stream function in a fluid fixed coordinate system, in which the velocity at infinity vanishes, given by equivalent formulas (1.12) or (1.14). When $u_0 < u_{*0}$, then two flow stagnation points exist on the streamline $\psi_0 = 0$, coinciding with the *z*-axis, at which this streamline branches and forms an oval shaped contour bounding the vortex atmosphere (Fig. 1.7*a*). Coordinates of the stagnation points at the *z*-axis are obtained by solving the equation $u_0 - u_*(z,\ 0) = 0$ with respect to *z*:

$$z_{1,2} = \pm R\left[\left(\frac{2\pi}{A(\varepsilon)}\right)^{2/3} - 1\right]^{1/2}, \qquad (1.27)$$

where $\varepsilon = a/R$ and $A(\varepsilon) = \ln(8/\varepsilon) - 1/4$ as it follows from expression (1.26) for the translational speed of the vortex ring. Hence the branching points of the streamline ψ_0 are located at the *z*-axis on both sides of the center ($r = z = 0$) of the vortex ring at equal distances $l = |z_1| = |z_2|$. The value *l* determines the length of the longitudinal semi-axis of the vortex atmosphere. Dependence of *l*/*R* on the parameter $\varepsilon = a/R$, obtained using (1.27) is shown in Fig. 1.8. It should be noted that theoretically another, non-oval, shape of a vortex atmosphere is also possible. When $u_0 = u_{*0}$, the stagnation points at the *z*-axis merge at one point $(z_1 = z_2 = 0)$, which corresponds to the value ε = 1/86. At smaller values of ε, i.e. when $u_0 > u_{*0} = \Gamma/2R$ this point moves radially from the axis of symmetry, and the vortex atmosphere takes the shape of a torus with fluid flowing through the ring center (Fig. 1.7*b*). In experiments, vortex rings with oval shaped atmosphere are usually observed, which is probably either due to complexity of generating rather thin vortex rings with toroidal atmosphere in laboratory conditions or to the instability of such rings.

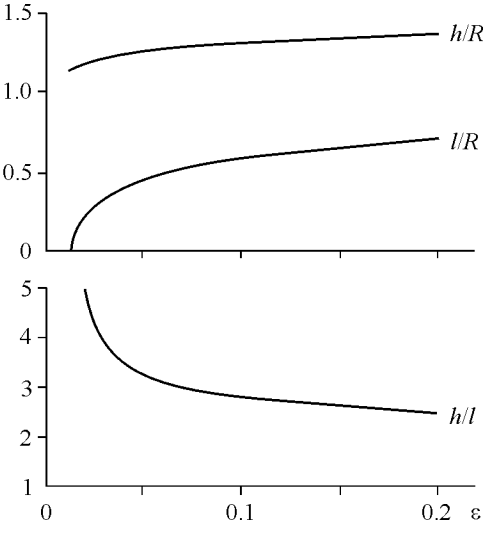

Fig. 1.8. Dimensions of vortex atmosphere semiaxes versus parameter ε

One may also estimate the length of a transverse semi-axis $r = h$ of the vortex atmosphere (see Fig. 1.7*a*), i.e. the distances to the point where the *r*-axis intersects the streamline $\psi_0 = 0$ in the coordinate system moving with the vortex ring. This value of *r* is found from the equation

$$\psi_0 = -u_0 r^2/2 + \psi(r) = 0, \tag{1.28}$$

where, as before, ψ is the stream function in the coordinate system, in which the fluid at infinity is at rest. Let us find ψ using (1.12). The modulus of the elliptic integrals *K* and *E*, required for calculation of ψ, in this case is $k^2 = 4r\sigma/\left((z-\zeta)^2 + (r+R)^2\right)$. Under the assumption that $\varepsilon = a/R \ll 1$, we neglect variations in ζ and σ within the cross-section of a vortex core and take $\zeta \approx 0$, $\sigma \approx \sigma_0 = R$. Then $k \approx 2(rR)^{1/2}/(r+R)$. From subsequent calculation it is clear that $R < h \le 1.5R$. In this case $k \ge 0.98$, i.e. the modulus of the elliptic integrals *K* and *E* is close to unity. Then approximately $K \approx \ln 4/k'$, $E \approx 1$, where

$$k' = \left(1-k^2\right)^{1/2} = \frac{r-R}{r+R} \quad \text{and} \quad \psi \approx \frac{\Gamma}{2\pi}\left[\frac{r^2+R^2}{r+R}\ln\frac{4(r+R)}{r-R} - (r+R)\right].$$

Substituting expressions for ψ and u_0 from (1.26) into (1.28), we obtain the equation for the value $r = h$, corresponding to the point of intersection with the streamline $\psi_0 = 0$,

$$\psi_0(0,r) = -\frac{u_0 r^2}{2} + \psi(0,r) = \frac{\Gamma}{2\pi}\left[-A(\varepsilon)\frac{r^2}{4R} + \frac{r^2+R^2}{r+R}\ln\frac{4(r+R)}{r-R} - (r+R)\right] = 0.$$

By introducing the dimensionless variable $y = r/R$, this equation for the length of the transverse semi-axis of a vortex atmosphere $r = h$ is written as

$$y^2 - \frac{4}{A(\varepsilon)}\left[\frac{y^2+1}{y+1}\ \ln\frac{4(y+1)}{y-1} - (1+y)\right] = 0.$$

The solution h/R and the ratio of vortex atmosphere semi-axes h/l as functions of the parameter ε are shown in Fig. 1.8.

Thus, the model of a thin cored vortex ring of finite cross-section provides finite values of the translational speed and the kinetic energy of a vortex. However it is necessary to keep in mind that this model was derived under quite arbitrary assumptions that a core cross-section is circular, and that vorticity is constant over the cross-section of the ring. Within the framework of an ideal fluid there exist models of a vortex ring obtained without these constraints, based only on the condition that fluid motion in the coordinated system moving with a vortex ring should be steady.

1.7 Hill's Spherical Vortex

As it was shown earlier (1.8), axisymmetric vortex fluid flows are steady if the ratio ω/r remains constant along each streamline. That is, this ratio depends only on the value of a stream function ψ. Hence $\omega/r = f(\psi)$, where f is an arbitrary function of ψ. According to (1.6) and (1.7) vorticity is expressed in terms of a stream function as $\omega = -\frac{1}{r}\left(\frac{\partial^2\psi}{\partial z^2} + \frac{\partial^2\psi}{\partial r^2} - \frac{1}{r}\frac{\partial\psi}{\partial r}\right)$, which together with the condition of flow steadiness (1.8) yields an equation for determining ψ

$$\frac{\partial^2\psi}{\partial z^2} + \frac{\partial^2\psi}{\partial r^2} - \frac{1}{r}\frac{\partial\psi}{\partial r} = -r^2 f(\psi). \tag{1.29}$$

A similar equation is encountered also in plasma physics when plasma equilibrium in toroidal magnetic fields is considered, and it is known there as the Grad-Shafranov equation (Shafranov 1967). This analogy is evidently caused by a similarity between steady equations of motion of an inviscid fluid $\boldsymbol{\omega}\times\mathbf{u} = -\nabla H$, $\boldsymbol{\omega} = \nabla\times\mathbf{u}$ and equations of magnetostatic equilibrium in a perfectly conducting fluid $\mathbf{j}\times\mathbf{B} = -\nabla p$, $\mathbf{j} = \nabla\times\mathbf{B}$, where H is the above-specified Bernoulli integral (1.2) of steady equations of fluid motion which is constant along a streamline, p is the pressure, $\mathbf{j}$ is the electric current density, and $\mathbf{B}$ is the vector of magnetic field intensity.

Although within the framework of an ideal fluid there are no conditions for determining a function $f(\psi)$, there exists one exact solution to equation (1.29), which is obtained under the assumption that $\omega/r = f(\psi) = A = \text{const}$ inside a sphere of radius a. This solution is known as Hill's spherical vortex (Hill 1894; Lamb 1932). A stream function ψ inside a sphere is found now from a linear equation

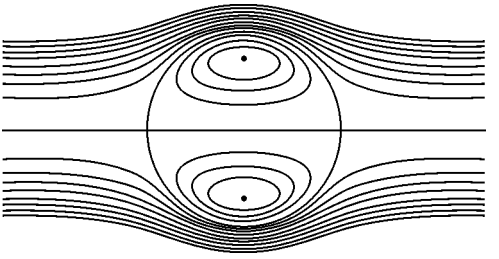

Fig. 1.9. Streamline pattern of a Hill's spherical vortex, from Lamb (1932)

$\frac{\partial^2\psi}{\partial z^2}+\frac{\partial^2\psi}{\partial r^2}-\frac{1}{r}\frac{\partial\psi}{\partial r}=-r^2A.$ Solution to this equation inside the sphere which satisfies the condition $\psi=0$ at the surface of the sphere is $\psi=(1/10)Ar^2(a^2-z^2-r^2).$ The flow inside the sphere is continuously matched with the external flow corresponding to a potential flow past a solid sphere of radius a by a uniform stream of speed u_0 in the direction of the negative z-axis at infinity. The stream function of the external flow (for $r^2+z^2>a^2$) has the form $\psi=-u_0r^2[1-a^3(r^2+z^2)^{-3/2}]/2.$ Match of the tangential components of velocity at the surface of the sphere for inner and outer flows yields the constant $A=15u_0/2a^2$. Hence, the stream function and the vorticity distribution inside the sphere are represented by the formulas $\psi=(3/4)u_0r^2a^{-2}(a^2-z^2-r^2)$ and $\omega=rA=(15/2)u_0a^{-2}r,$ respectively. The streamline pattern of a Hill's vortex for equidistant values of ψ is shown in Fig. 1.9. From the obtained stream function one can find the components of the flow velocity inside the sphere

$$u=\frac{3}{2}u_0\left(1-\frac{2r^2+z^2}{a^2}\right),\quad v=\frac{3}{2}u_0\frac{zr}{a^2}$$

and outside the sphere

$$u=u_0\left[\left(\frac{a^2}{z^2+r^2}\right)^{5/2}\frac{2z^2-r^2}{2a^2}-1\right],\quad v=\frac{3}{2}u_0\frac{zr}{a^2}\left(\frac{a^2}{z^2+r^2}\right)^{5/2}.$$

The presented solution allows us to determine integral parameters of Hill's vortex: circulation $\Gamma=5au_0$, impulse $P=2\pi\rho a^3u_0$ and energy $T=(10/7)\pi\rho a^3u_0^2$. It is natural to define a radius R of Hill's vortex as a coordinate r of the point inside the sphere in the $z=0$ plane, where $u=0$. This condition gives $R^2=a^2/2$.

1.8 Family of Steady Vortex Rings

Hill's vortex is a particular example of steady vortex rings. One may suggest that in general there exists a family of steady vortex rings. Clearly, the motion can be steady only in a reference frame translating with the vortex ring, in which the vortex ring is at rest and subject to a uniform flow of speed u_0 equal to the translational speed of a vortex ring in a fluid at rest at infinity. With $\psi_0(z,r)$ denoting a

stream function in this coordinate frame, the problem of constructing steady models of a vortex ring is reduced to determining u_0 and region A in a meridional cross-section of the ring, in which according to the condition of flow steadiness (1.8), equation $\omega/\sigma = f(\psi_0)$ must be valid, and at the boundary ∂A of the region $\psi_0 = \text{const}$, i.e. the boundary of the region is a streamline. Approximate analytical solution of this problem for thin-cored vortex rings with an arbitrary function $f(\psi_0)$ was derived by Fraenkel (1970, 1972). Earlier, Lichtenstein (1925) calculated the shape of vortex ring cross-section for $\omega = \text{const}$, but this case does not meet the condition of steadiness of axisymmetric vortex flows. Expressions for the shape of a ring cross-section in case $\omega/r = \text{const}$ were obtained earlier also by Dyson (1893) in his calculation of a gravitational potential of toroidal bodies.

Solution to the problem posed here is based on the expression for a stream function

$$\psi_0(z,r) = -\frac{u_0 r^2}{2} + \psi(z,r), \tag{1.30}$$

where $\psi(z,r)$ is a stream function of a vortex ring moving with velocity u_0 in a fluid at rest. The function ψ according to (1.12) and to condition of steadiness $\omega = \sigma f(\psi_0)$ has the form

$$\psi(z,r) = \frac{1}{2\pi}\iint_A G(z-\zeta, r, \sigma) f(\psi_0)\, d\zeta\, d\sigma, \tag{1.31}$$

where $G = (r\sigma^3)^{1/2}\left[\left(2/k - k\right)K(k) - 2E(k)/k\right]$ is the kernel of the integral, K and E are the complete elliptic integrals of the first and second kind with the modulus $k = (4r\sigma/[(z-\zeta)^2 + (r+\sigma)^2])^{1/2}$ and ζ and σ are the coordinates in the region A, over which the integration is performed. Obviously, G corresponds to the stream function of a circular line vortex passing through the point (ζ, σ) of a meridional cross-section of the vortex. Using, as previously, the asymptotic expressions of the elliptic integrals in the region within a cross-section of the ring, where $k \to 1$, we have

$$\left(\frac{2}{k} - k\right)K - \frac{2}{k}E \approx \ln\frac{4}{k'} - 2 + O(k'^2 \ln k'), \quad \text{where } k' = \left(1 - k^2\right)^{1/2}.$$

Substituting (1.31) into (1.30) yields an integral equation for ψ_0, A, and u_0:

$$\psi_0 = -\frac{u_0 r^2}{2} + \frac{1}{2\pi}\iint_A G(z-\zeta, r, \sigma) f(\psi_0) d\zeta\, d\sigma. \tag{1.32}$$

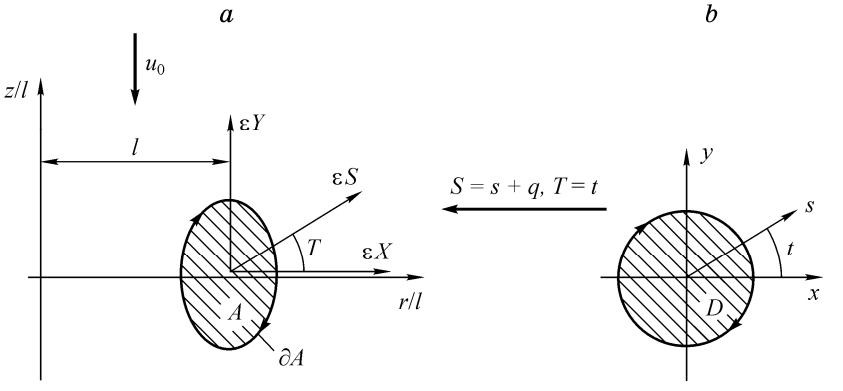

Fig. 1.10. Mapping of a vortex ring cross-section on a plane vortex (following Fraenkel 1972) (*a*) cross-section of a vortex ring, (*b*) circular cross-section of a cylindrical vortex

Denote by l the position $(z = 0,\ r = l)$ of stagnation point ($\mathbf{u} = 0$) in the area A, and by ε the small cross-section parameter defined on ∂A as $(r-l)^2 + z^2 \approx \varepsilon^2 l^2$ as $\varepsilon \to 0$. Thereafter we introduce dimensionless coordinates (S,T) and (X,Y) (Fig. 1.10*a*):

$$r/l - 1 = \varepsilon X = \varepsilon S \sin T, \quad z/l = \varepsilon l = \varepsilon S \cos T$$

$$\sigma/l - 1 = \varepsilon X' = \varepsilon S' \sin T', \quad \zeta/l = \varepsilon Y' = \varepsilon S' \cos T'.$$

Now the kernel $G(z-\zeta,\ r,\sigma) = l^2 G_1(S, S_1, \varepsilon)$ may be approximated by the stream function of a plane flow induced by a straight vortex line normal to the chosen meridional plane and intersecting it at the point (ζ,σ). $G_1(\mathbf{S},\mathbf{S}',\varepsilon) = (\ln(1/\varepsilon|\mathbf{S}-\mathbf{S}'|) - 2)(1 + O(\varepsilon S + \varepsilon S'))$, where $|\mathbf{S}-\mathbf{S}'| = \left(S^2 + S'^2 - 2SS'\cos(T-T')\right)^{1/2}$ is the distance between the ends of the radius vectors $\mathbf{S}$ and $\mathbf{S}'$. It means that we may treat an analogous problem for the plane flow. Let (s,t) be polar, and $x = s\cos t$, $y = s\sin t$ Cartesian coordinates in this plane as above (Fig. 1.10*b*) with the origin at the center of the unit circle D: $s < 1$, $0 < t < 2\pi$. Let $\Omega(s)$ be the vorticity in the circle D. The plane-flow stream function induced by a vortex cylinder of cross-section D, has the form

$$\psi_1 = \frac{1}{2\pi} \iint_D \ln \frac{s'}{|\mathbf{s}-\mathbf{s}'|} \Omega(s') s' ds' dt', \tag{1.33}$$

where $|\mathbf{s}-\mathbf{s}'|$ is defined like $|\mathbf{S}-\mathbf{S}'|$.

Returning to the axisymmetric problem (1.32), assume that the vorticity $\omega/r = f(\psi_0)$ is prescribed parametrically:

$$\begin{aligned} \omega/r &= (U/\varepsilon^2 l^2)\,\Omega(s) \\ \psi_0 &= U l^2[\psi_1(s) + B(\varepsilon)] \end{aligned} \qquad (0 \le s \le 1), \tag{1.34}$$

where U is a certain velocity characterizing the intensity of vorticity, Ω and ψ_1 are the same quantities as in (1.33), and B is the constant equal to ψ_0/Ul^2 at the image of the point $s = 0$ in the (z, r) plane and must be found in the course of solution. Let us seek a mapping $S = s + q(s,t,\varepsilon)$, $T = t$ of the closed cross-section D of the vortex cylinder on the closed cross-section A of a steady vortex ring (see Fig. 1.10). The function q is to be such that the integral equation (1.32) is satisfied. Let us demand that $q \approx O(s)$ for $s \to 0$. Thus the stagnation point $s = 0$ in the (x, y) plane is mapped at the stagnation point $S = 0$ $(z = 0,\ r = l)$ and the streamlines in A are described by (1.33) with $s = 1$ on ∂A. Substituting (1.33) and (1.34) into (1.32) yields the equation for the function $q(s,t,\varepsilon)$ and the constants $U(\varepsilon)$, $B(\varepsilon)$

$$\psi_1(s) + B = -\frac{1}{2}W(1+\varepsilon(s+q)\cos t)^2 + \\ + \frac{1}{2\pi}\iint_D G_1(s+q, s'+q', \varepsilon)\left(1+\frac{q'}{s'}\right)\left(1+\frac{\partial q'}{\partial s'}\right)\Omega' s'\,ds'\,dt'$$

$(0 \le s \le 1)$, where $W = u_0/U$, $q' = q(s', t')$, $\Omega' = \Omega(s')$.

Expanding G_1 in power series in ε, Fraenkel obtained the solution to the problem in the form of power series in ε. Using additional notation $\delta = \varepsilon \ln(8/\varepsilon)$ the basic parameters specifying the vortex ring are represented by the flowing expressions:

cross-sectional area of the ring $\quad |A| = \iint_A dr\,dz = \pi\varepsilon^2 l^2(1 + O(\delta^2))$,

circulation $\quad \Gamma = \iint_A \omega\,dz\,dr = \pi\,Ul(1 + O(\delta^2))$,

translational speed $\quad u_0 = \frac{1}{4}U\left[\ln\frac{8}{\varepsilon} - \frac{1}{2} + 4\int_0^1 V^2(s)s\,ds\right](1 + O(\delta^2))$,

impulse $\quad P = \pi\rho\iint_A \omega r^2\,dz\,dr = U\pi^2\rho l^3(1 + O(\delta^2))$,

kinetic energy $\quad T = \pi\rho\iint_A \left(\psi_0 + \frac{1}{2}U_0 r^2\right)\omega\,dz\,dr =$

$$= U^2\pi^2\rho l^3\left[\frac{1}{2}\ln\frac{8}{\varepsilon} - 1 + 2\int_0^1 V^2(s)s\,ds\right](1 + O(\delta^2)),$$

stream function $\psi_0(0,l) = Ul^2 B =$

$$= Ul^2 \left[\frac{3}{8} \ln \frac{8}{\varepsilon} - \frac{15}{16} - \psi_1(1) - \frac{1}{2} \int_0^1 V^2(s) s \, ds \right] (1 + O(\delta^2)),$$

where V is the linear velocity of fluid rotation around the axis of the straight vortex of circular cross-section. The formula for u_0 implies that if $\Omega = 1$, and $V = s\Omega/2$, then $\int_0^1 V^2 s \, ds = 1/16$, and one obtains Kelvin's formula (1.26) for the translational speed. When $\Omega = 0$, it implies the result

$$u_0 = \frac{1}{4} U \left[\ln \frac{8}{\varepsilon} - \frac{1}{2} \right] \tag{1.35}$$

which was obtained by Hicks (1884) for the speed of translation of a hollow vortex ring. Vortex rings with hollow cores are quite real physical objects and are frequently observed in experiments in liquids when cavitation occurs due to a pressure fall in a vortex core and a toroidal cavity is produced. A vortex ring in water with the cavitating hollow core is shown in the photograph (Fig. 1.11). Approximate description of the structure of hollow vortex rings was given by Hicks (1884, 1885), Vladimirov (1973), and Vladimirov and Rybak (1976).

Of special interest is the model of a vortex ring with the simplest vorticity distribution $\omega/r = \text{const}$; an example is Hill's spherical vortex. Such vorticity distribution is commonly called uniform. In this case, the relevant vortex cylinder is described by $\Omega = 1$, $V = s/2$, $\psi_1 = -s^2/4$. One might expect in advance that the shape of the vortex ring cross-section in general would be different from a circle, as exemplified by Hill's vortex whose meridional cross-section is a half-disk. The parameter ε can no longer be considered as a ratio of a vortex core radius to the vortex ring radius. Therefore Fraenkel (1970, 1972) and Norbury (1973) suggested another definition of the parameter of smallness of the core cross-section $\varepsilon_* = (A/\pi R_*^2)^{1/2}$, where A is the cross-sectional area of the ring, R_* is the radius of the ring, which is defined as half the sum of the smaller and larger distances from the symmetry axis to the core boundaries: $R_* = (r_{\min} + r_{\max})/2$. These new parameters are advantageous,

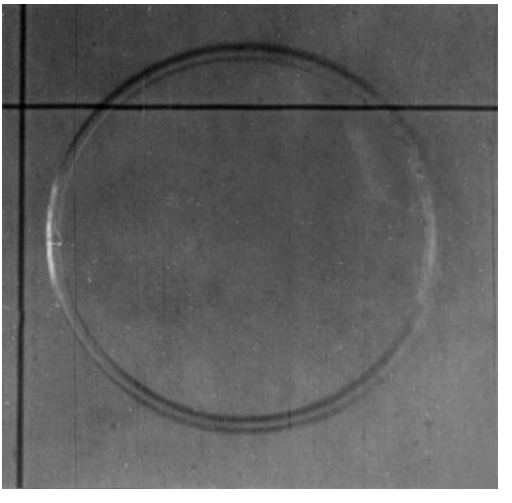

Fig. 1.11. A vortex ring in water with a cavitating hollow core

since they are related more simply to the circulation Γ and to the cross-sectional area A of the ring. This notation also simplifies the equation of the shape of the core boundary, and ε_* is readily obtained from experiments and is known for Hill's vortex, whereas the value of ε is not. Fraenkel established relationship between the parameters ε_*, R_* and the quantities ε and l introduced earlier: $R_*/l = 1 - 5\varepsilon/8 + O(\delta^4)$, $\varepsilon_*/\varepsilon = 1 + 141\varepsilon^2/123 + O(\delta^4)$, and defined a new reference velocity U_* instead of U. In this notation we have $\omega/r = U_*/\varepsilon_*^2 R_*^2$, $U_*/U = 1 + 61\varepsilon^2/64 + O(\delta^4)$, and parameters of a vortex ring with uniform vorticity are:

$$|A| = \pi\varepsilon_*^2 R_*^2,$$

$$\Gamma = U_* R_* \pi (1 + O(\delta_*^4)),$$

$$u_0 = \frac{U_*}{4}\left[\ln\frac{8}{\varepsilon_*} - \frac{1}{4} + \varepsilon_*^2\left(-\frac{3}{8}\ln\frac{8}{\varepsilon_*} + \frac{15}{32}\right) + O(\delta_*^4)\right],$$

$$P = U_* R_*^2 \pi^2 \rho\left[1 + \frac{3}{4}\varepsilon_*^2 + O(\delta_*^4)\right],$$

$$T = U_* R_*^3 \pi^2 \rho\left[\frac{1}{2}\ln\frac{8}{\varepsilon} - \frac{7}{8} + \frac{3}{16}\varepsilon_*^2 \ln\frac{8}{\varepsilon_*} + O(\delta_*^4)\right],$$

where $\delta_* = \varepsilon_* \ln(8/\varepsilon_*)$.

Fraenkel points out that although this theory is constructed under the assumption that $\varepsilon_* \to 0$, some of the resulting formulas are also suitable for rather substantial dimensions of the vortex cross-section. For instance, the formula for the speed of translation u_0 has an error less that 6% even for $\varepsilon_* = \sqrt{2}$, which corresponds to Hill's spherical vortex.

The equation of the vortex core boundary ∂A in polar coordinates (s, θ), defined by the equations $r - R_* = s\sin\theta$, $z = s\cos\theta$, is

$$s = \varepsilon_* R_*\left[1 + \varepsilon_*^2\left(\frac{3}{8}\ln\frac{8}{\varepsilon_*} - \frac{17}{32}\right)\cos 2\theta - \varepsilon_*^3\left(\frac{21}{128}\ln\frac{8}{\varepsilon_*} - \frac{273}{1024}\right)(\sin 3\theta + \sin\theta) + O(\delta_*^4)\right].$$

The shape of the core boundary and the streamline $\psi_0 = 0$ bounding the vortex atmosphere are shown in Fig. 1.12 for three values of ε_*.

The Fraenkel theory gives a single-parameter (ε_*) family of steady thin-cored vortex rings. The value $\varepsilon_* = 0$ obviously corresponds to a circular line vortex of zero cross-section, discussed in Section 1.5. In accordance with the definition of

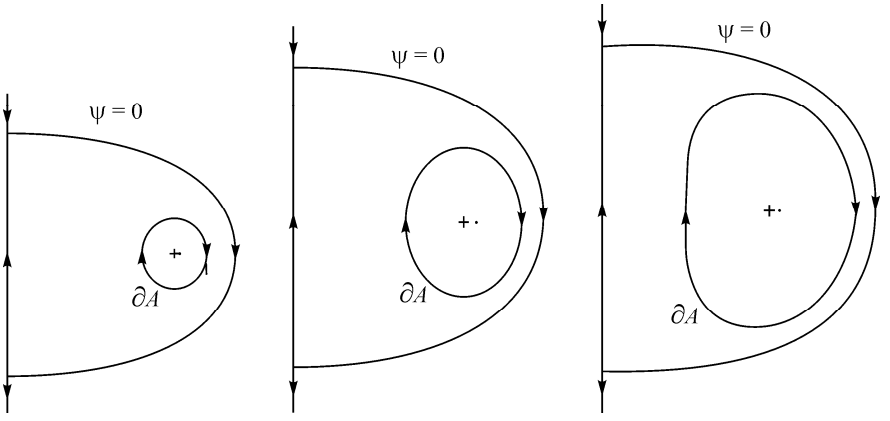

Fig. 1.12. The core boundary ∂A of a vortex ring and the dividing streamline $\psi = 0$. From left to right: $\varepsilon_* = 0.2, 0.4, 0.6$ (Fraenkel 1972).

Hill's spherical vortex, $A = \pi a^2/2$, $R = a/2$, where a is the radius of the sphere, and hence, $\varepsilon_* = \sqrt{2}$. It is generally believed that the whole one-parameter family (with the parameter ε_*) of steady vortex rings is located in the range $0 \le \varepsilon_* \le \sqrt{2}$, that is on one end of this family is a circular line vortex of zero cross-section and on the other end there is Hill's spherical vortex. This notion appears to be somewhat conventional, because theory does not impose any restrictions on expanding this family towards greater values of ε_*, which would give vortex ring models extended along the axis of symmetry. However, in experiments such elongated vortex rings with $\varepsilon_* > \sqrt{2}$ are not observed, and in a way it substantiates the conjecture that the parameter ε_* ranges from 0 to $\sqrt{2}$.

It is difficult to analytically model vortex rings for $\varepsilon_* \sim \sqrt{2}$. Thus Norbury (1973) numerically calculated the structure of vortex rings over the whole range $0 \le \varepsilon_* \le \sqrt{2}$ of the parameter ε_* solving equation (1.32) in the particular case $\omega/r = \Omega = \text{const}$. The shape of a vortex ring found numerically for several values of ε_*, is shown in Fig. 1.13. Figure 1.14 gives the streamline $\psi_0 = 0$ dividing the vortex ring atmosphere with the internal flow with circulation from the external potential flow, for various values of ε_*. The dimensionless circulation $\overline{\Gamma} = \Gamma/UR_*$, translational velocity $\overline{u_0} = u_0/U$, impulse $\overline{P} = P/(\rho U R_*^3)$, and kinetic energy $\overline{T} = T/(\rho U^2 R_*^3)$ versus ε_* are shown in Fig. 1.15. The quantities u_0, P, T were made dimensionless (see Fig. 1.15) using the density of the medium ρ, ring radius R_* defined as a half the sum of the minimum and maximum distances from the axis of symmetry to the vortex core boundary, and by the parameter $U = \Omega R_* \varepsilon_*^2$

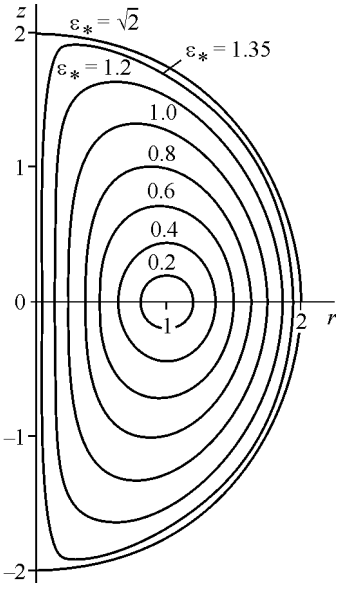

Fig. 1.13. Cross-sectional shapes of a vortex ring (Norbury 1973)

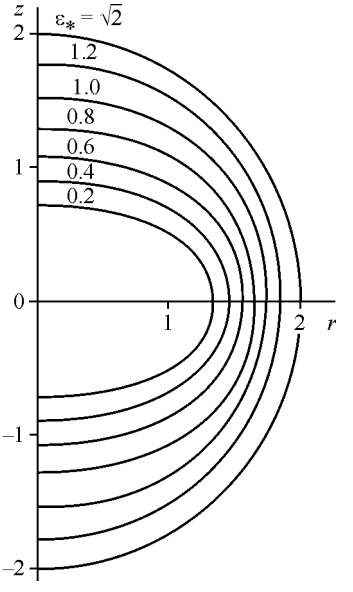

Fig. 1.14. The shape of the vortex atmosphere (streamlines ψ = 0) (Norbury 1973)

with the dimension of velocity. Numerical values of some quantities corresponding to a circular line vortex ($\varepsilon_* = 0$) and Hill's spherical vortex ($\varepsilon_* = \sqrt{2}$) are also shown on the axis of ordinates. Thus, this section reports theoretical models of a family of steady vortex rings obtained for an ideal fluid.

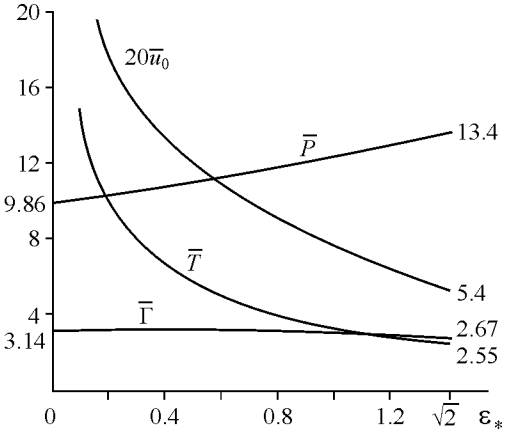

Fig. 1.15. The propagation velocity, circulation, impulse, and kinetic energy versus the parameter ε_* (from Norbury 1973)

1.9 Translational Velocity of a Vortex Ring

Calculation of the speed of translation u_0, one of the major characteristics of a vortex ring, is a nontrivial problem. One could see it when Lamb's model of a vortex ring was discussed in Section 1.6. Starting from Lamb's ideas, Saffman (1992) obtained a more universal formula for the propagation speed of thin-cored vortex rings which is also appropriate in case of arbitrary vorticity distribution. It is worthy to outline derivation of this formula.

Consider a thin vortex ring moving in a medium at rest. Let us write the velocity field of the ring as follows

$$\mathbf{u} = \mathbf{u}_0 + \tilde{\mathbf{u}}, \tag{1.36}$$

where $\mathbf{u}_0$ is the translational velocity of the ring, and $\tilde{\mathbf{u}}(\tilde{u}, \tilde{v})$ is the velocity vector in a reference frame traveling with the vortex ring. Substituting (1.36) into the formula (1.20) for the kinetic energy T, and accounting for the impulse definition (1.16) yields

$$T = \rho \mathbf{u}_0 \int (\mathbf{r} \times \boldsymbol{\omega})\, dV + \rho \int \tilde{\mathbf{u}} \cdot (\mathbf{r} \times \boldsymbol{\omega})\, dV = 2u_0 P + \rho \int \tilde{\mathbf{u}} \cdot (\mathbf{r} \times \boldsymbol{\omega})\, dV, \tag{1.37}$$

where

$$P = \pi\rho \iint_{\Sigma} \omega(z,r) r^2\, d\Sigma \approx \pi\rho R^2 \Gamma. \tag{1.38}$$

Here $\Gamma = \iint_{\Sigma} \omega(z,r)\, d\Sigma$ is the circulation, R is the radius of the ring, Σ is the cross-sectional area of the ring. The velocity u_0 can be found from (1.37), provided that T and the second integral term in the right-hand side of this expression are known. The kinetic energy T can be calculated using the formula (1.19): $T = \pi\rho \iint_{\Sigma} \psi\omega\, dz dr$, where ψ is the stream function. According to (1.14) the stream function $\psi = (2\pi)^{-1} \int_{\Sigma} (r_2 + r_1)\ [K(\lambda) - E(\lambda)] \omega(\zeta, \sigma)\, d\zeta\, d\sigma$, where r_1, r_2, λ are defined by relations (1.13). As far as ring cross-section dimensions are small compared to the radius of the ring, in the core $r_1 \ll r_2$, $r_2 \approx 2R$, $\lambda \approx 1$. Thus approximately $E(\lambda) \approx 1$, $K(\lambda) \approx 2^{-1} \ln 16 / \lambda'^2$, where $\lambda'^2 = 1 - \lambda^2 = 4 r_1 r_2 / (r_1 + r_2)^2 \approx 2 r_1 / R$ and hence $\psi \approx (R/2\pi) \int_{\Sigma} (\ln 8R / r_1 - 2) \omega(\zeta, \sigma)\, d\zeta\, d\sigma$. Assume to a first approximation that the cross-section of the thin ring is circular with radius a, and trajectories of fluid particles are circles about the center at $z = 0$, $r = R$, where R is the ring radius. Introduce polar coordinates (s, θ) with the origin at this point (see Fig. 1.6). In these coordinates $r_1^2 = s^2 + s'^2 - 2ss' \cos(\theta - \theta')$, $\omega(\zeta, \sigma) \approx \omega(s)$, $d\Sigma = s' ds' d\theta'$ and

$$\psi(s) \approx (R/2\pi) \int_0^a \int_0^{2\pi} \left[\ln 8R - \ln(s^2 + s'^2 - 2ss' \cos(\theta - \theta'))^{1/2} - 2 \right] \omega(s')\, d\theta' s' ds'.$$

Integrating this expression over the angle θ', as in Section 1.6, we obtain

$$\psi = R\left[(\ln 8R - 2)\int_0^a \omega(s')s'ds' - \left(\ln s\int_0^s \omega(s')s'ds' + \int_s^a \omega(s')\ln s's'ds'\right)\right].$$

Let us define $\gamma(s) = 2\pi\int_0^s \omega(s')s'ds'$ (clearly, $\gamma(a) = \Gamma$). Then the stream function becomes $\psi(s) = (R\Gamma/2\pi)\left[\ln 8R/a - 2 + \Gamma^{-1}\int_s^a (\gamma(s')/s')\,ds'\right]$. Substituting ψ in (1.19), we find the kinetic energy

$$T = \pi\rho\iint_\Sigma \psi\omega d\Sigma = \pi\rho\int_0^a\int_0^{2\pi} \psi(s)\omega(s)s\,ds\,d\theta = \frac{\rho R\Gamma^2}{2}\left[\ln\frac{8R}{a} - 2 + \frac{1}{\Gamma^2}\int_0^a \frac{\gamma^2(s)}{s}ds\right]. \quad (1.39)$$

Let us now determine the last term in equation (1.37):

$$\int \tilde{\mathbf{u}}\cdot(\mathbf{r}\times\boldsymbol{\omega})\,dV = 2\pi\iint r\omega(r\tilde{u} - z\tilde{v})\,dz\,dr. \quad (1.40)$$

Suppose that the fluid motion about the vortex ring is steady. In this case the equations of motion (1.4) and (1.5) imply the identity $r^2\tilde{u}\omega - rz\tilde{v}\omega = -3rz\tilde{v}\omega + \partial(zr^2\tilde{u}\omega)/\partial z + \partial(zr^2\tilde{v}\omega)/\partial r$. Substitution of this identity in (1.40) yields $2\pi\iint_\Sigma (r^2\tilde{u}\omega - rz\tilde{v}\omega)\,d\Sigma = -6\pi\iint_\Sigma zr\tilde{v}\omega\,d\Sigma$, since the terms with partial derivatives vanish upon the integration over the vortex cross-section. Assuming to leading order that $\omega \approx \omega(s)$, $\tilde{v} \approx \Gamma(s)\cos\alpha/2\pi s$, $r \approx R$, $z = s\cos\alpha$, $d\Sigma = d\alpha s ds$, we obtain

$$\int \tilde{\mathbf{u}}\cdot(\mathbf{r}\times\boldsymbol{\omega})\,dV = 2\pi\iint_\Sigma r\omega(r\tilde{u} - z\tilde{v})\,d\Sigma = -6\pi\iint_\Sigma rz\tilde{v}\omega\,d\Sigma = -\frac{3}{4}R\Gamma^2. \quad (1.41)$$

Substituting (1.41) and (1.39) into (1.37) yields

$$\frac{\rho R\Gamma^2}{2}\left[\ln\frac{8R}{a} - 2 + \frac{1}{\Gamma^2}\int_0^a \frac{\gamma^2(s)}{s}ds\right] = 2u_0\pi\rho R^2\Gamma - \frac{3}{4}\rho R\Gamma^2,$$

which implies the formula for the translational speed of a thin-cored vortex ring with an arbitrary vorticity distribution

$$u_0 = \frac{\Gamma}{4\pi R}\left[\ln\frac{8R}{a} - \frac{1}{2} + \frac{1}{\Gamma^2}\int_0^a \frac{\gamma^2(s)}{s}ds\right] = \frac{\Gamma}{4\pi R}\left[\ln\frac{8R}{a} - \frac{1}{2} + \frac{2\pi^2 a^2\overline{v_\theta^2}}{\Gamma^2}\right].$$

where $v_\theta = \gamma(s)/2\pi s$, and the overbar denotes the average over the cross-section. Obviously, for $v_\theta = \omega s/2$ it leads to Kelvin's formula (1.26), and for $v_\theta = 0$ to Hick's formula (1.35) for a hollow vortex ring.

One may also point to the representation of the propagation speed of the vortex ring in terms of its integral properties

$$u_0 = \frac{T}{2P} + \frac{3}{8}\frac{P}{\pi^2 \rho R^3},$$

which also follows from (1.37).

2 Hydrodynamic Structure of a Vortex Ring

Theoretical models of vortex rings obtained in the framework of the ideal fluid theory apparently give only a qualitative idea of a structure and characteristics of vortex rings that form and exist in a real viscous fluid. Until recently, direct experimental studies of the hydrodynamic structure of real vortex rings have been lacking, and thus it has not been clear how realistically theoretical models of vortex rings reflect the actual phenomenon. The lack of reliable experimental data on the structure of a vortex ring and on the structure of concentrated vortices in general, with the latter being one of the basic types of fluid and gas motion in natural conditions and in technical devices, is mostly explained by complexity and unsteady character of vortex motion in a fluid, and by imperfection of suitable scientific instrumentation. There are only experimental investigations by Timme (1957) and Kirde (1962), who studied the structure and evolution of one of the types of concentrated vortices forming in a crossflow past a cylindrical body and representing the so-called Karman vortex street (Karman and Rubach 1912; Schlichting 1969). In the experiments these vortices appeared on the water surface during the horizontal motion of a vertically set cylinder which was partly extended above the surface. A flow field of these vortices was studied by observing and registering tracks of small particles on the free surface of the liquid. However, it is clear that each of the vortices constituting the Karman street is not a completely isolated vortex structure in an unbounded medium, because it experiences the influence of the closely located body that is flowed past and the whole chain of the Karman vortices. These investigations give only an indirect idea of the structure of single concentrated vortices. The difficulties in performing direct measurements of a velocity field of vortices developing in actual conditions, such as whirlwinds, tornados, and hurricanes, are quite obvious.

This chapter reports results of the first experimental investigation of the hydrodynamic structure of a real air vortex ring carried out by Akhmetov and Kisarov (1966) by measuring a velocity flow field using hot-wire anemometers. Results of similar studies of the vortex ring structure made later by other researchers are also reported.

2.1 Experimental Procedure

A vortex ring in the experiments was generated by impulsive ejection of a submerged air jet from an open end of a cylindrical tube 75 mm in diameter by a

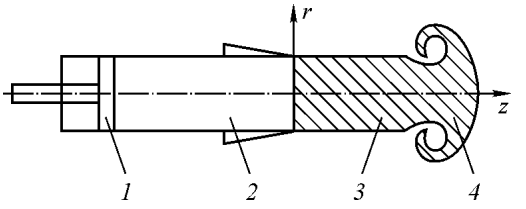

Fig. 2.1. A scheme of a vortex ring generator. (*1*) piston; (*2*) cylinder; (*3*) jet; (*4*) forming vortex ring

piston moving inside the tube. Figures 2.1 and 2.2 show the layout and appearance of the experimental setup for investigation of the vortex ring structure. The piston was driven by a special mechanical gear which provided strict repeatability of the piston motion program in recurrent runs. The specific type of the motion program was of little importance for these studies. But repeatability of the piston motion was of critical importance for generating identical vortex rings in recurrent runs, since in each start of a vortex ring, velocity components were registered only along a single line parallel to the tube axis, and on lines located at other distances from the axis velocities were measured in repeated vortex ring starts. Thus, the whole velocity flow field could be studied only through multiple starts of equal vortex rings. It is obvious that in this measurement procedure vortex rings generated in repeated runs must be identical. The experimental device provided required repeatability of the piston motion program and generation of equal vortex rings. The piston motion was controlled by a photoelectric sensor from the motion of a comb rack connected with the piston. Piston translation S and velocity V (and thus the velocity of the jet flowing out of the tube) as functions of time t realized experimentally are qualitatively shown in Fig. 2.3.

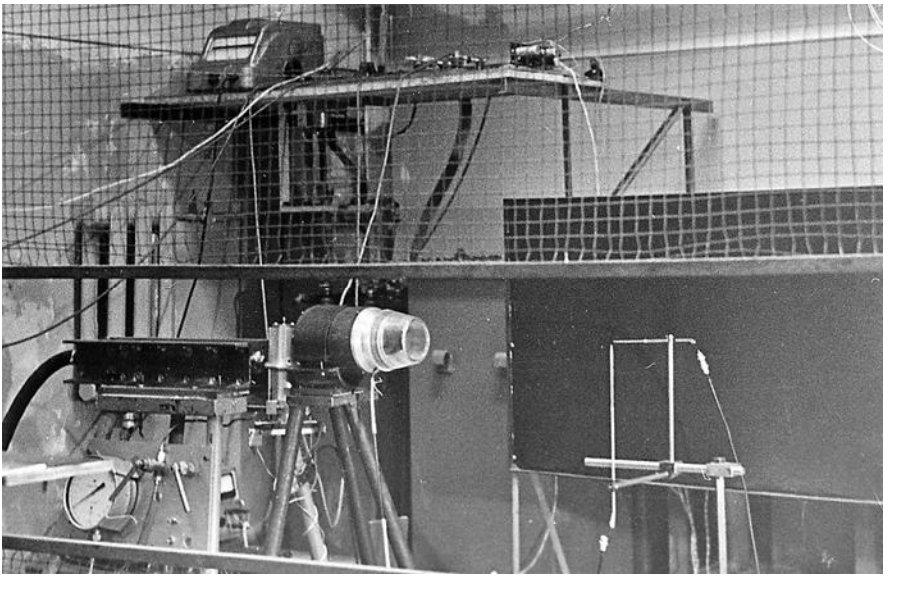

Fig. 2.2. Layout of the experimental device

In principle, one can imagine a layout for simultaneous measurement of the whole velocity field of one and the same vortex ring, using a large number of probes placed at various distances from the axis of symmetry. However, insertion of a large number of probes (even miniature in size) into a vortex ring may result in perturbation of the flow under investigation, therefore this procedure of probe measurements of the vortex ring structure appears to be inapplicable.

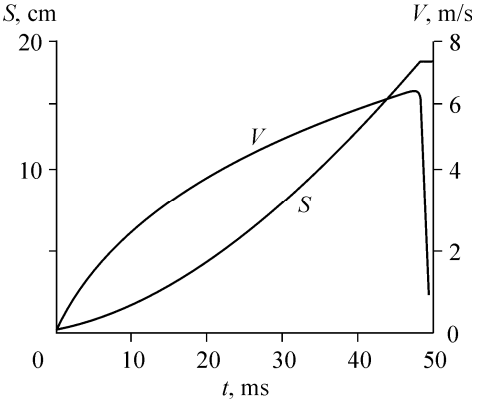

Fig. 2.3. Piston stroke and velocity versus time

On jet ejection a vortex ring forms near the open end of the tube, which then moves in an open space along the tube axis away from the exit cross-section. It follows from the experiments that vortex ring formation is completed at a distance of a few diameters of the tube opening. By this time the translational velocity of a vortex becomes virtually constant. One can assume that further the vortex moves in an unbounded medium independently of the vortex-generating device. It is interesting to determine vortex ring characteristics at the instant when the formation process is completed, because they can be used as initial conditions to solve the problem of motion of the vortex formed in an unbounded medium. In line with this reasoning, the velocity field of a vortex ring was determined by two hot-wire anemometers positioned on a vortex path at a distance of 5.45 tube diameters from the tube opening, where the vortex-ring formation process may be considered as completed.

2.2 Hot-Wire Anemometry: Method for Measuring Two-Dimensional Velocity Field

Since the flow in a vortex ring is axisymmetric, two velocity components, axial and radial, were determined. Velocities were measured with hot-wire anemometers of constant temperature DISA-55A01 with the probes made of wire filaments 5 μm across and 1 mm long heated by electric current and fixed on thin wire pins projecting from a cylindrical probe holder 2 mm in diameter (Fig. 2.4). The principle of velocity determination by a hot-wire anemometer is based on measuring heat removal from the preheated cylindrical filament by an air stream flowing past it. The circuit diagram of the constant temperature anemometer is shown in Fig. 2.5. One can see that the probe whose sensitive filament *1* constitutes resistance R_x, is joined up into one of the legs of the electric measuring resistance

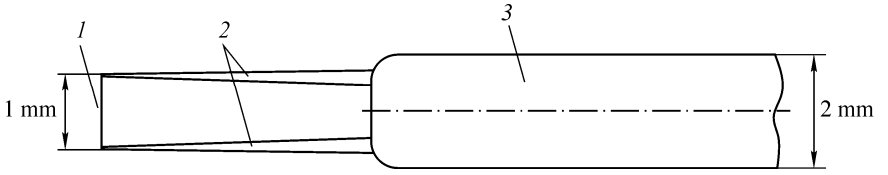

Fig. 2.4. Hot-wire anemometer probe. (*1*) sensitive wire of the probe; (*2*) current-carrying pins; (*3*) probe holder

bridge *2*, whose signal is applied to the input of an electronic amplifier *3*. The bridge is fed from the feedback line *4* by the output voltage V of the electronic amplifier *3*, i.e. the circuit represents a servo system which maintains resistance and, hence, the constant temperature of the filament. The operating temperature of the probe filament is set at ~300 °C. The use of the electronic negative-feedback circuit for feeding the measuring bridge is of fundamental importance for measuring high-frequency signals, because the response time of the probe filament itself is about 10 ms despite its small thickness. Therefore, an anemometer without the servo system is not capable of measuring variable velocity alternating at a frequency higher than 100 Hz. Owing to feeding of the bridge through the feedback line, possible variations of the probe filament resistance (and temperature) are almost instantaneously counteracted by the voltage change at the amplifier output, thus the probe filament resistance and temperature are kept constant. This makes it possible to increase the operating frequency of the anemometer hundreds of times and measure variable velocity at frequencies of up to 10^4–10^5 Hz. Design of hot-wire constant-temperature anemometers and their applications are given in more detail elsewhere (King 1914; Laurence 1953; Kovasnay 1954; Hinze 1959).

The velocity field of a vortex ring was determined in a vertical plane passing through the symmetry axis of the ring using two hot-wire anemometer probes located on the path followed by the vortex. The probe wires were located virtually at one point of the measurement plane (Fig. 2.6). The wire of probe 1 was oriented normal to this plane, hence the velocity vector was always normal to the probe wire and this probe measured the absolute value (magnitude) of the velocity. The wire of probe 2 designed to determine the direction of the velocity vector was placed in the measurement plane at a given angle θ_0 to the axis of symmetry z. When using the probe methods, it is important to eliminate a

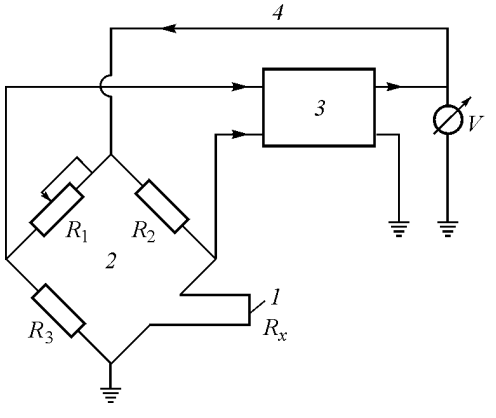

Fig. 2.5. Hot-wire anemometer circuit diagram (*1*) probe wire; (*2*) measuring resistance bridge R_1– R_3, R_x; (*3*) electronic amplifier; (*4*) feedback line; V is the output voltage of the amplifier

possibility of disturbing the flow under study by the probes inserted into the stream. Two options of spatial orientation of the probes were used in measurements of the velocity field of a vortex ring (Fig. 2.7). The holder of probe 2 was always positioned normal to measuring plane, hence did not belong to this plane and practically did not disturb the flow in it. The holder of probe 1 designed for measuring the absolute value of velocity was positioned in the measuring plane and was oriented perpendicular (Fig. 2.7*a*) or parallel (Fig. 2.7*b*) to the *z*-axis of symmetry depending on the cross-section of the vortex ring where the velocity distribution was measured. In some cross-sections the velocity distribution was measured twice with different orientations of the probe 1 holder which allowed control of the absence of flow disturbances by the measuring probes.

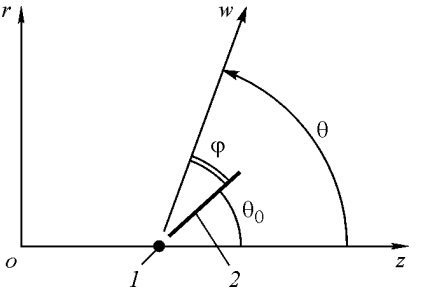

Fig. 2.6. Orientation of probe wires and the velocity vector ***w.*** (*1*) probe 1 wire (normal to the *z*0*r*-plane); (*2*) probe 2 wire (lies in the *z*0*r*-plane)

The principle of velocity measurement by a hot-wire anemometer can be understood by comparing the rate of heat removal from the heated probe filament by the flow with the electric power supplied to the filament in order to maintain its constant resistance and temperature. From the theory of temperature boundary layers

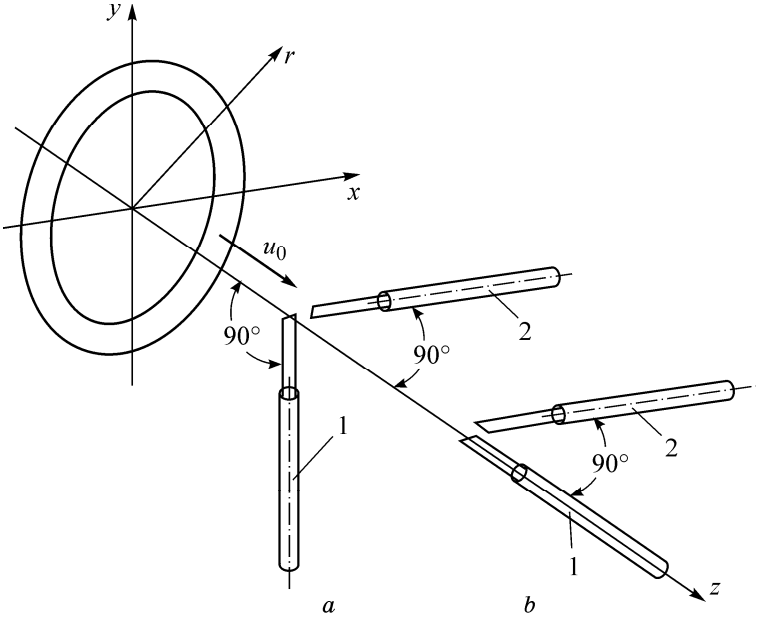

Fig. 2.7. Two options of probe orientation in measurements of the velocity field of a vortex ring

(Schlichting 1968) it is known that the crossflow past a cylinder (probe filament) carries away from the cylinder surface the heat flux q, which is determined by the dimensionless heat-transfer coefficient referred to as Nusselt number Nu and by the temperature difference ΔT between the heated cylinder and the fluid: $q = a\,\mathrm{Nu}\,\Delta T$, where a is a proportionality factor. The Nusselt number is a function of the Reynolds number $\mathrm{Re} = wd/\nu$, based on the flow velocity w, cylinder diameter d, and coefficient of kinematic viscosity of the medium ν. At small Reynolds numbers corresponding to the flow past a thin probe filament at moderate velocities, the flow can be considered laminar. In this case the Nusselt number is related to the Reynolds number by $\mathrm{Nu} = \alpha + \beta\,\mathrm{Re}^{1/2}$, where α and β are constants (Schlichting 1968). The electric current power N supplied to the filament in order to compensate for the heat removal q is determined via the voltage V at the probe and probe filament resistance R as $N = V^2/R$. As far as the electric resistance R of the probe and, hence, the filament temperature are maintained constant, then assuming $\Delta T = \mathrm{const}$ and equating N and q, we obtain King's law known in hot-wire anemometry

$$V^2 = V_0^2 + k\sqrt{w}, \tag{2.1}$$

which determines dependence of the measured output voltage V of a hot-wire anemometer on the value of the stream velocity w (King 1914). Evidently, the value V_0 corresponds to the voltage needed for setting the operating temperature of the filament at zero velocity. Thus using a probe with a filament oriented perpendicular to the velocity vector, it is possible to measure the velocity magnitude. The coefficient k in King's law is a function of the angle φ between the probe filament and direction of the velocity vector. This dependence allows determination of the angle φ using the second probe whose filament is positioned perpendicular to that of the first probe at a certain given angle θ_0 to the z-axis (see Fig. 2.6). Thus the angle θ between the velocity vector and coordinate axis z is determined. The nature of the dependence of the hot-wire anemometer signal on the angle φ between the probe filament and velocity vector can be determined if one assumes that the case $\varphi = 0$ corresponds to the longitudinal flow around the external surface of the filament, which is equivalent to the longitudinal flow around a plane plate of width $b = \pi d$ and length l representing the developed external surface of the filament. In the flow past a plate the heat-transfer coefficient Nu also linearly depends on $\mathrm{Re}^{1/2}$ (Schlichting 1968). Therefore, one may consider that the total amount of heat removed from the filament per unit time by a flow with the velocity component $w\sin\varphi$ normal to the wire and $w\cos\varphi$ parallel to the wire, should be $q = q_1 + q_2$, where $q_1 = \alpha_1 + a_1\Delta T\sqrt{w\sin\varphi}$ and $q_2 = \alpha_2 + b_2\Delta T\sqrt{w\cos\varphi}$. Equating the total heat flux q carried away from the filament by the flow and the

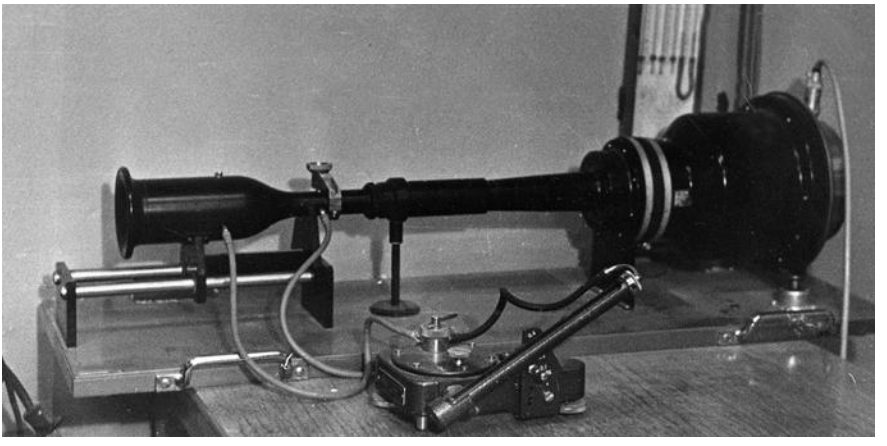

Fig. 2.8. Wind tunnel for probe calibration

power of the electric current U^2/R supplied to the probe to keep the constant filament temperature gives the formula

$$U^2 = U_0^2 + c(\varphi)\sqrt{w} = U_0^2 + \left(a\sqrt{\sin\varphi} + b\sqrt{\cos\varphi}\right)\sqrt{w}, \qquad (2.2)$$

which determines the dependence of the output voltage U of the second hot-wire anemometer on the velocity magnitude w and angle φ between the probe filament and velocity vector. This dependence allows determination of the angle φ and direction of the velocity vector θ provided the measured values of w and U (see Fig. 2.6). However the analytical forms of anemometer signals (2.1) and (2.2) were used only for estimating the accuracy of w and φ. For measurement of the velocity field of a vortex ring the dependence of V on w for the first probe and dependence of U on φ and w for the second probe were obtained by means of direct calibration of the probes in a special small-scale low-turbulent wind tunnel (Fig. 2.8). The calibration curve of probe 1 for measuring the absolute value of the velocity is shown graphically in Fig. 2.9, where the value $V - V_0$ in arbitrary units is plotted as a function of w. The second probe designed for measuring the direction of the velocity vector was calibrated as a function of the angle φ between the probe filament and direction of the velocity vector at fixed values of the velocity. Under calibration this probe was inserted into the wind tunnel through a small hole in the side

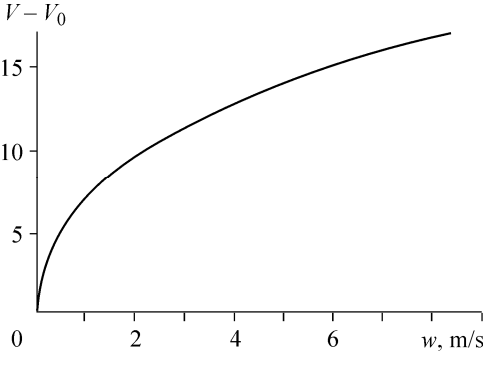

Fig. 2.9. Calibration curve of probe 1

wall of the tunnel in its working cross-section. The desired values of the orientation angle φ were set by rotating the probe around the axis of its holder. The calibration curves for this probe are shown in Fig. 2.10, where the quantity proportional to the difference $U - U_0$ is plotted as a function of the angle φ. The coefficient $c(\varphi) = a\sqrt{\sin\varphi} + b\sqrt{\cos\varphi}$ from equation (2.2) is also plotted as a function of the angle φ for coefficient values a = 490 and b = 20 obtained from the probe calibration curves (Fig. 2.11). The solid line in the plot represents calculation using this formula, and empty circles correspond to the measured data on probe calibration. Evidently the calculated values of $c(\varphi)$ differ from the experimental data only in a small neighborhood of the point $\varphi = 0$, which is probably due to the flow disturbance at zero angle φ by a relatively thick current carrying probe pin supporting its thin filament.

As stated above, during the study of the vortex ring structure we supposed that the flow is axisymmetric. Accordingly the hot-wire probes were placed on the path of a vortex ring in the vertical plane passing through the *z*-axis. The filament of the probe measuring the velocity magnitude was oriented normal to this plane, and the filament of the probe for measuring the direction of the velocity vector was oriented in this plane at a certain fixed angle θ_0 to the *z*-axis (see Fig. 2.6).

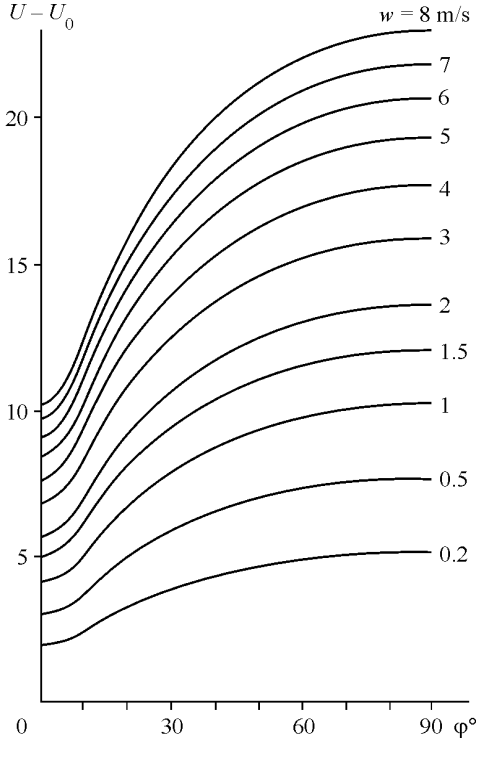

Fig. 2.10. Calibration curves of probe 2

Such probe arrangement made it possible to measure both the absolute value and direction of the velocity vector as functions of time along one line parallel to the *z*-axis, at each vortex startup. In measurements the vortex structure was assumed to be unchanged during its propagation through the measuring point, as evidenced by the constancy of the vortex ring velocity u_0. The transition from time dependence of the velocity components to dependence on the space coordinates z, r was performed via the transform $z = u_0 t$, where u_0 is the translational velocity of a vortex ring (directed along the *z*-axis) and t is the current time. Thus, at each passage of a vortex ring through the probes, distributions of both the radial v and axial u velocity components could be measured along a single line $r = \text{const}$ parallel to the *z*-axis. With the probes consecutively shifted along the

r-axis by 10 mm intervals, the whole flow pattern was determined by repeated vortex runs. The experiment was repeated five times for each of the sections, so that it was possible to check the stability of the results and use averaged data in the analysis. The measurements were carried out at eight values of *r*.

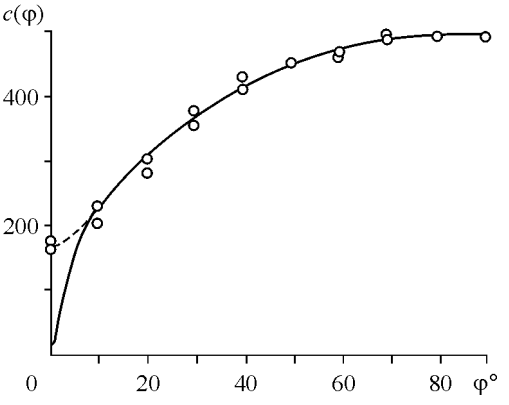

Fig. 2.11. Coefficient $c(\varphi)$ in Eq. (2.2) as a function of angle φ

It should be mentioned that the measured hot-wire anemometer signals allowed direct determination of the magnitudes of the velocity components only (except for sign), because the hot-wire anemometer technique of velocity measurement based on the thermal effect, gives no way to deduce signs of the velocity components. However, owing to the knowledge of the qualitative flow pattern and streamline configuration of a vortex ring (see Fig. 1.2), the sign of each velocity component and changes of signs of the velocity projections to the opposite ones can be unambiguously determined from the expected streamline shape. Thus this measuring procedure enables us to identify the complete pattern of velocity component distribution in the vortex ring.

The translational velocity of the vortex ring was determined by photographing the vortex motion as a function of time. The vortex ring was simultaneously visualized with the use of smoke supplied into the vortex-generator nozzle. The vortex motion was recorded through a narrow slot diaphragm aligned parallel to the vortex motion onto a film moving uniformly perpendicular to the slot. In such a manner, the film shows the law of the vortex motion in time, which allows its translational velocity to be determined. One of such pictures of the vortex motion shown in Fig. 2.12 represents the distance traveled by the vortex ring

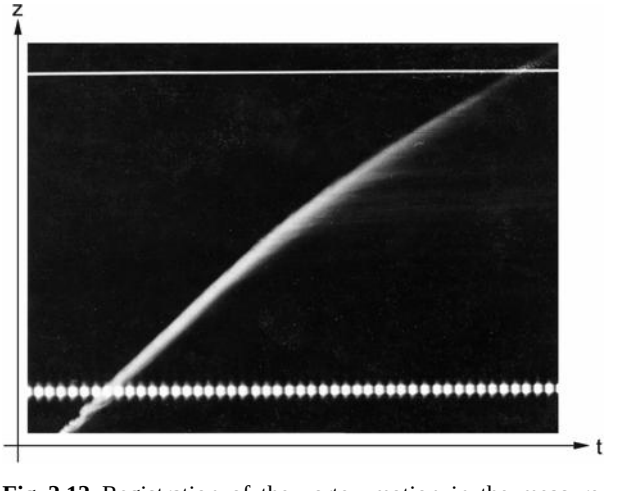

Fig. 2.12. Registration of the vortex motion in the measurement region (near the probes)

versus time. Analysis shows that the translational velocity of the examined vortex ring is $u_0 = 1.75 \pm 0.05$ m/s. Variation of the translational velocity of the vortex during its pass through the hot-wire probes did not exceed 1.5%. Besides the anemometer signals the time-resolved path of the piston, time marks and synchronization pulses that could be used to establish a time correspondence between the anemometer signals and the motion-picture were also recorded. The apparatus and the measuring system were controlled from a common switchboard.

2.3 Estimations of Measurement Accuracy of Two-Dimensional Velocity Field with Hot-Wire Probes

Thus, the absolute value of the velocity w and the angle θ between the velocity vector and symmetry axis z in cylindrical coordinates are the directly measured quantities (see Fig. 2.6). From these data one can deduce the velocity projections u, v on the coordinate axes z and r, respectively

$$u = w\cos\theta, \quad v = w\sin\theta. \tag{2.3}$$

It should be noted once more that measurements by hot-wire anemometers provide only magnitudes of the velocity components except for sign. The signs or the directions of velocity projections can be obtained with relative ease from a qualitative streamline pattern which is known from theoretical models of vortex rings as well as from the continuity condition for the space derivatives of the velocity projections in the vicinity of the points where the velocity components change sign. Obviously, to determine the absolute values of the velocity projections u and v, it is sufficient to know the absolute value of the velocity w and values of the angle θ in the range $0 \le \theta \le \pi/2$. Since the velocity components u and v are determined from the measured quantities w and θ, errors in u, v are also specified by the measuring errors Δw, $\Delta\theta$ of the velocity magnitude w and angle θ. As it was shown above (see Fig. 2.6), $\theta = \theta_0 + \varphi$, where θ_0 is the positioning angle of the probe 2 filament with respect to the z-axis when the velocity field is measured, and φ is the angle between the probe filament and velocity vector. In experiments, the errors in the positioning angle θ_0 of the probe 2 filament were negligibly small compared with the measuring errors of the angle φ, hence one could assume that $\Delta\theta = \Delta\varphi$, i.e. the error in determining the angle θ was equal to the measuring error of the angle φ.

The procedure for estimating the errors of the velocity projections u and v can be exemplified by determining the error Δu of the axial velocity component u. The error Δu can be found using the known rules for calculating errors of a function that are due to the measurement errors of the function arguments (Squires 1968).

Within the measurement accuracy the quantity $u(w,\theta)$ can be approximately considered a linear function of its arguments. Then

$$\Delta u = \Delta u_w + \Delta u_\theta = \frac{\partial u}{\partial w}\Delta w + \frac{\partial u}{\partial \theta}\Delta\theta, \tag{2.4}$$

where $\Delta u_w = (\partial u/\partial w)\Delta w$ and $\Delta u_\theta = (\partial u/\partial\theta)\Delta\theta$ are the errors of determination of the velocity component *u* due to the measurement errors in *w* and θ. Partial derivatives are defined by (2.3): $\partial u/\partial w = \cos\theta$, $\partial u/\partial\theta = -w\sin\theta$. Thus, we have $(\Delta u)^2 = (\Delta u_w)^2 + (\Delta u_\theta)^2 + 2\Delta u_w \Delta u_\theta$. Since *w* and θ are independent quantities, on averaging of this equation over pairs of *w* and θ from their distributions, the last term in the right-hand side vanishes and the formula for the root-mean-square error Δu of the magnitude of the axial velocity component takes the form

$$\Delta u = \left[\Delta w^2 \cos^2\theta + \Delta\theta^2 w^2 \sin^2\theta\right]^{1/2}. \tag{2.5}$$

The rms error Δv of the magnitude of the radial velocity component is obtained in the same manner

$$\Delta v = \left[\Delta w^2 \sin^2\theta + \Delta\theta^2 w^2 \cos^2\theta\right]^{1/2}. \tag{2.6}$$

It follows from (2.5) and (2.6) that in order to estimate the errors of velocity components, one needs to know the measurement errors Δw and $\Delta\theta$. As stated above, $\Delta\theta = \Delta\varphi$, i.e. the problem of determining $\Delta\theta$ reduces to determining the error $\Delta\varphi$ of measurement of the angle φ between the filament of probe 2 and velocity vector.

Measurements on probe calibration

Since in measurements of the velocity field of a vortex ring the velocity magnitude *w* and angle φ are determined from calibration curves of hot-wire anemometer probes, it is necessary to know the errors of measurement of the hot-wire anemometer signals *V* and *U* during probe calibration. The hot-wire anemometer probes were calibrated in a special low-turbulence wind tunnel (see Fig. 2.8). The magnitude of the flow velocity in the tunnel *w* was determined from the measurement of the pressure difference Δp between two cylindrical sections of the tunnel with considerably different diameters by means of an inclined-tube fluid micromanometer. The velocity *w* and pressure difference Δp are related by Bernoulli's

formula $\Delta p = \rho w^2/2$, where ρ is the air density. Hence the relative accuracy of velocity determination during probe calibration is $\delta w/w = \delta(\Delta p)/2\Delta p$, where $\delta(\Delta p)$ is the error of the pressure difference measurement. For $w \geq 4$ m/sec the value of the relative error $\delta(\Delta p)/\Delta p$ of measurement of the pressure difference by the manometer in use was within 0.025, thus $\delta w/w \leq 0.0125$. At smaller velocities the errors of measurement of the pressure difference rise steeply. However, it is at small velocities that King's law (2.1) is most accurate, i.e. V^2 linearly depends on $\sqrt{w}$. Plotting this function from the measured values of V at $w = 0$ and $w \geq 4$ m/s, we may obtain dependence of the output voltage of a hot-wire anemometer V on w with sufficient accuracy for small velocities as well. Hence, the relative error of velocity measurement during probe calibration can be considered $\delta w/w \leq 0.0125$ in the whole velocity w range. The performed estimations demonstrate that the influence of such error of velocity measurement on the accuracy of plotting of the probe calibration curves is inessential. The errors in the signal of the second hot-wire anemometer caused by inaccuracy in the positioning angle φ when probe 2 was calibrated, also occurred to be negligibly small. It is necessary to account only for the measurement error of the anemometer signal itself which was $\Delta V \approx 0.005 V_0$. The output voltage of the second anemometer was measured with the same accuracy $\Delta U \approx 0.005 U_0$.

Errors in measurement of velocity magnitude

The velocity magnitude w is determined from the measured anemometer signal V using the calibration curve of probe 1 (see Fig. 2.8), hence the error in the velocity magnitude Δw depends on the error in the measured signal V. The procedure used here suggests that Δw caused by the error ΔT of signal measurement from anemometer 1 can be estimated as $\Delta w = (dw/dV)\Delta V$. Substitution of the derivative dw/dV obtained from King's law (2.1) yields the measuring error for w as a function of the measurement error of the output signal of the hot-wire anemometer

$$\Delta w = \frac{\partial w}{\partial V}\Delta V = \frac{4\sqrt{w}}{k}\left(V_0^2 + k\sqrt{w}\right)^{1/2}\Delta V. \qquad (2.7)$$

As pointed out above, the measurement errors of signals of both hot-wire anemometers were practically constant. However, this error appears twice. First it appears during probe calibration, and second, when the velocity field of a vortex ring was measured. Thus, the net measurement error of the anemometer signal should be doubled and taken equal to $\Delta V \approx 0.01 V_0$. Substitution of this value in (2.7) gives the error of determination of the velocity magnitude Δw. Figure 2.13 shows

Δw as a function of the velocity magnitude w. It follows from (2.7) that the relative error $\Delta w/w$ of the velocity magnitude increases as w decreases.

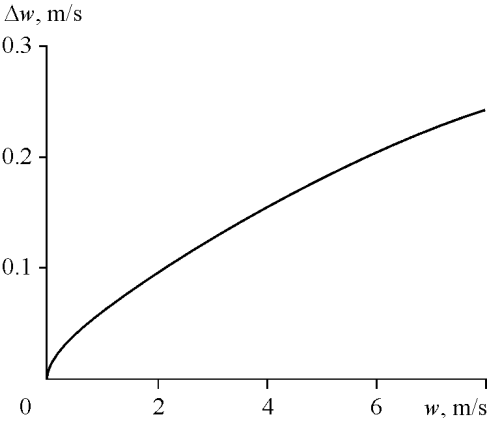

Fig. 2.13. Measurement errors of the absolute velocity

Errors in measurement of velocity projections

To find the velocity projections from (2.3), one needs to estimate the accuracy of measuring the angle θ between the velocity vector and coordinate axis z (see Fig. 2.6). Since $\theta = \theta_0 + \varphi$ and errors in the positioning angle θ_0 of the probe 2 filament relative to the z-axis are negligibly small, $\Delta\theta = \Delta\varphi$ and determination of the error $\Delta\theta$ of the angle θ reduces to evaluating the accuracy of measurement of the angle φ between the probe 2 filament and velocity vector. When φ approaches zero or $\pi/2$, the accuracy of determination of the angle φ from the anemometer signal U falls sharply (see Fig. 2.10). Therefore, in order to eliminate large errors in determining the angle φ, the velocity field of a vortex ring was measured twice: at the positioning angles of the filament of probe 2 equal to $\theta_0 = 0$ and $\theta_0 = \pi/2$. In processing of the measuring results we used the data which corresponded to the angle range $0 \le \varphi \le \pi/4$, where the curves of U as functions of φ have larger slope (see Fig. 2.10), and φ can be determined to a higher accuracy. Thus, for the positioning angle of the probe filament $\theta_0 = 0$, the angle θ in the range $0 \le \theta \le 45^\circ$ was defined as $\theta = \pm\varphi$ and values of the angle in the range $45^\circ \le \theta \le 90^\circ$ were at first roughly estimated using the measured data for $\theta_0 = 0$ and then were determined more precisely using the formula $\theta = \pm(\pi/2 + \varphi)$, provided the measured angle φ for $\theta_0 = \pi/2$. This procedure allowed us to reduce the errors of determination of the angle θ. The measurement errors of the angle φ can be found from (2.2), but we used a simpler approximate form of the analytical dependence of the signal U of probe 2 on the angle φ and velocity magnitude w

$$U^2 \approx U_0^2 + a\sqrt{\sin\varphi}\,\sqrt{w}, \tag{2.8}$$

which provides a quite accurate approximation of (2.2) in the angle range $10^\circ \le \varphi \le 45^\circ$ of practical importance given the coefficient a = 515.

As in estimating the errors of measurement of the velocity magnitude, we assume that within the measured values the angle φ can be considered a linear function of its arguments U and w. Then the error $\Delta\varphi$ in the magnitude of φ can be represented as a sum $\Delta\varphi = \Delta\varphi_U + \Delta\varphi_w$, where $\Delta\varphi_U = (\partial\varphi/\partial U)\Delta U$ is the error in the angle φ due to the error ΔU of measurement of the signal U of hot-wire anemometer 2, and $\Delta\varphi_w = (\partial\varphi/\partial w)\Delta w$ is the error in the angle φ, due to the error Δw of determination of the velocity magnitude w. Calculating partial derivatives of φ from (2.8) yields

$$\Delta\varphi_U = \frac{4\sqrt{\sin\varphi}\,U\Delta U}{a\sqrt{w}\cos\varphi} = \frac{4\sqrt{\sin\varphi}\left(U_0^2 + a\sqrt{\sin\varphi}\sqrt{w}\right)^{1/2}}{a\sqrt{w}\cos\varphi}\Delta U, \qquad (2.9)$$

$$\Delta\varphi_w = -\operatorname{tg}\varphi\frac{\Delta w}{w}. \qquad (2.10)$$

The root-mean-square error $\Delta\varphi$ in the value of φ is calculated by the formula

$$\Delta\varphi^2 = \Delta\varphi_U{}^2 + \Delta\varphi_w{}^2. \qquad (2.11)$$

The quantity Δw in (2.10) has been already defined in the previous subsection. The net error ΔU of measurement of the output signal of probe 2 in (2.9) being the sum of errors of U measurements during probe calibration and study of the velocity field of a vortex, is $\Delta U \approx 0.01U_0$, as for probe 1. The measurement errors for the angle φ are determined by substituting Δw and ΔU into (2.9) and (2.10). As it was mentioned above, the error of determination of the angle φ is also large in the

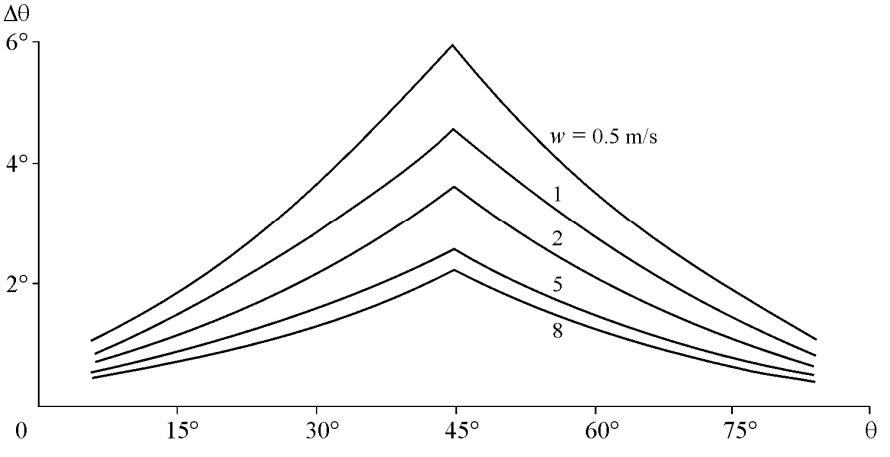

Fig. 2.14. Measurement errors of the orientation angle of the velocity vector

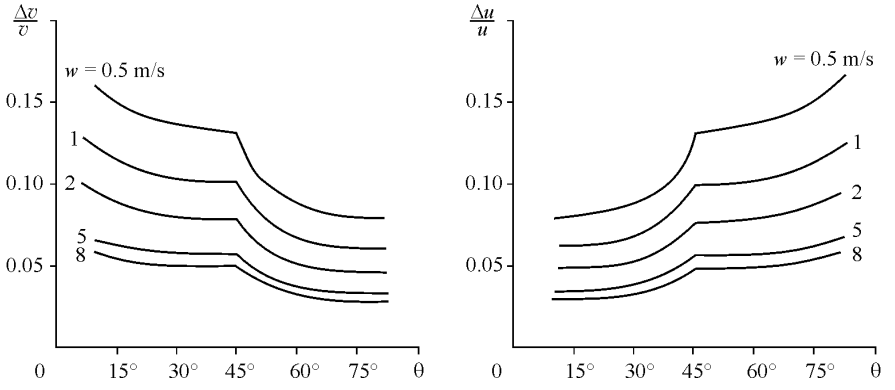

Fig. 2.15. Relative errors of velocity components determination

neighborhood of $\varphi = 0$. However, when $\varphi = 0$, one of the velocity components (for instance, u) equals w, hence the error of determination of this velocity component is also Δw. Another velocity component (v) in the neighborhood of the angle $\varphi = 0$ is an odd function. Thus, the magnitude of this velocity component in the point corresponding to $\varphi = 0$ can be found with sufficient accuracy by point interpolation for the values corresponding to $\varphi > 0$. The calculated errors $\Delta\theta = \Delta\varphi$ as functions of the angle magnitude θ at various velocity magnitudes w are shown in Fig. 2.14. The increase in errors of determination of θ at small w is due to increased $\Delta w/w$ in (2.9).

The errors in determination of the velocity projections in a vortex ring are estimated from the values of Δw and $\Delta\theta$ obtained above from (2.5) and (2.6). Clearly, the errors Δu, Δv of the magnitudes of the velocity components u and v as well as u and v themselves are functions of the parameters w and θ, which are directly measured in experiments. The relative errors $\Delta u/u = \sqrt{(\Delta w/w)^2 + \mathrm{tg}^2\theta\,\Delta\theta^2}$, $\Delta v/v = \sqrt{(\Delta w/w)^2 + \mathrm{ctg}^2\theta\,\Delta\theta^2}$ of determination of the velocity components versus the parameters w and θ are plotted in Fig. 2.15. Note that the increase in the relative error $\Delta u/u$ of determination of the axial velocity component for $\theta > 45°$ and relative error $\Delta v/v$ of determination of the radial velocity component for $\theta < 45°$ in Fig. 2.15 is explained not by an increase in the measuring errors of the velocity components, but by a decrease in the very velocity components (2.3) in the corresponding ranges of the angle θ, whereas the absolute errors Δu and Δv over the whole range of θ do not exceed their values at $\theta = 45°$, which is evident from (2.5), (2.6) and Fig. 2.14. Since the quantities $\Delta\theta$, $\Delta u/u$ and $\Delta v/v$ for $0 \le \theta \le 45^\circ$ and for $45^\circ \le \theta \le 90^\circ$ correspond to different positioning angles of the probe filament θ_0, their curves as functions of the angle θ have a break at $\theta = 45°$.

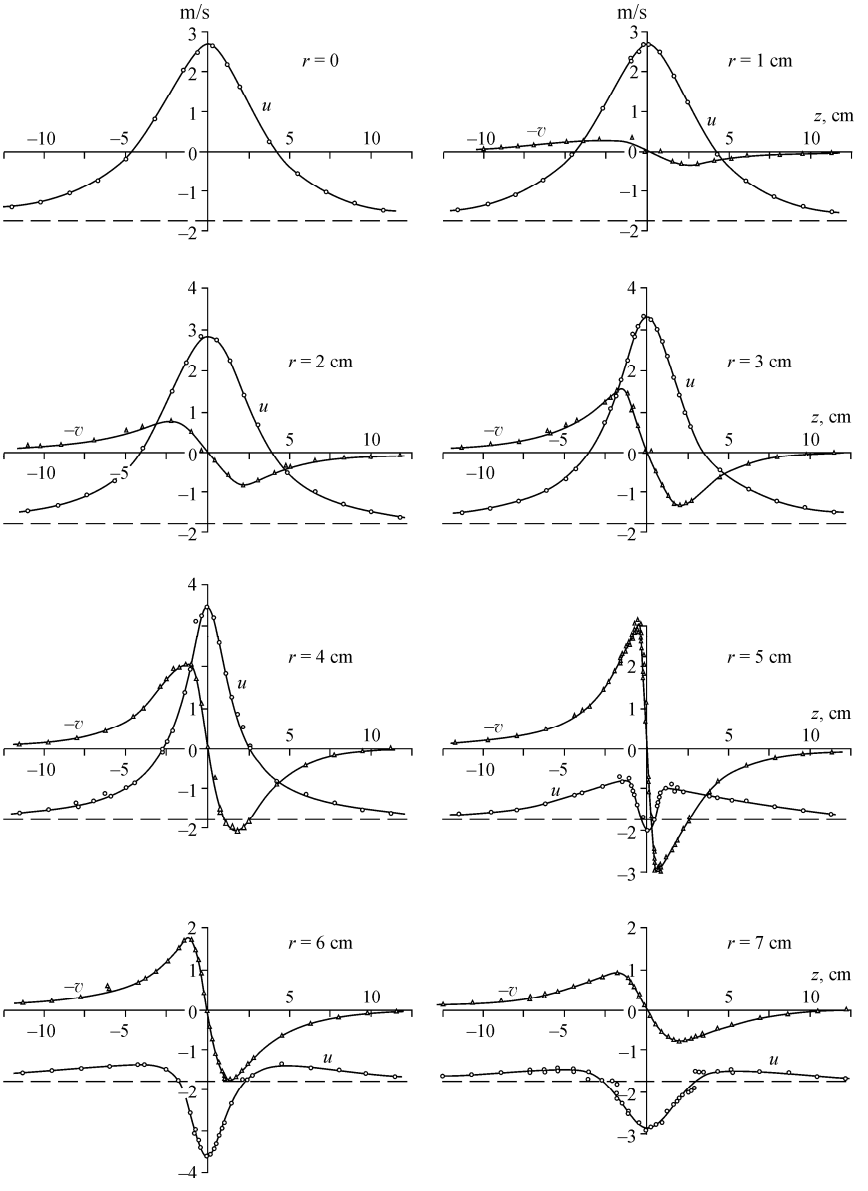

Fig. 2.16. Velocity field of a vortex ring

2.4 Velocity Field of Vortex Ring

Distributions of the velocity components obtained by identification of the oscillograms of the signals from hot-wire anemometers are shown in Fig. 2.16, where u and v denote the axial and radial velocity components, respectively. The curves were drawn using interpolation of discrete values of u and v by cubic splines (Ahlberg et al. 1967; Vershinin 1981; Vershinin et al. 1988).

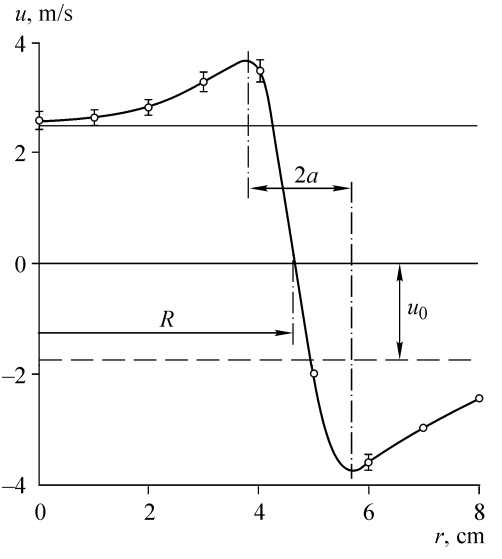

Fig. 2.17. Velocity distribution in the plane $z = 0$

Velocity distributions on the plots are presented in the frame moving with the vortex ring. The dashed line parallel to the abscissa axis in each of the plots corresponds to the value of the translational velocity u_0 of the vortex ring. When this dashed line is considered to be the z-axis, distributions of the axial velocity component u would appear in a fixed laboratory frame. Distribution of the radial velocity component v is invariant to such transformation of coordinates.

Of interest is the distribution of the axial velocity component u along the r-axis in the plane $z = 0$, where the radial velocity component is zero, $v = 0$ (Fig. 2.17). The distance along the r-axis from the origin to the point of intersection of the curve $u(0, r)$ with the abscissa axis determines the radius of the vortex ring, $R = 46.5$ mm. The velocity distribution in the neighborhood of the point $r \approx R$ has an almost linear character. The linear segment of the curve corresponds to the vortex core, and the distance $2a$ along the r-axis between the extreme points at the ends of the linear segment of the curve can be taken as the vortex-core diameter. The dashed straight line parallel to the r-axis corresponds to the translational velocity of the vortex ring (see Fig. 2.17). The Reynolds number of the vortex ring, determined on the basis of the ring radius R and velocity u_0 for a

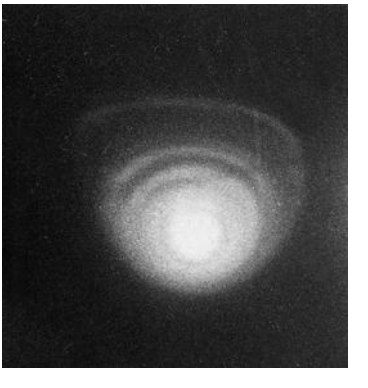

Fig. 2.18. Visualization of the vortex core cross-section

kinematic viscosity $\nu = 1.49 \cdot 10^{-5}$ m^2/s (Schlichting 1968; Kikoin 1976) corresponding to the experimental conditions (T = 293 K) is $\mathrm{Re} = u_0 R/\nu = 4.54 \cdot 10^3$. Note that the hot-wire probe signals are smooth curves without pulsations. Thus, the vortex ring under study can be assumed laminar. This is substantiated also by the smoke-visualization of the meridional cross-section of the ring near the vortex core, where the smoke is distributed in layers, i.e. the flow is laminar (see the photograph in Fig. 2.18).

2.5 Stream Function and Structure of Stream Lines

An important characteristic of the vortex ring structure is the streamline pattern which can be constructed using the obtained velocity field. The continuity equation for axisymmetric flows implies that the stream function is determined by the equations $u = -r^{-1}\partial\psi/\partial r$ and $v = r^{-1}\partial\psi/\partial z$. Hence, $\psi = \int_L r(udr - vdz)$, where the contour integral is taken in the axial plane along a curve L connecting a certain starting point, where $\psi = 0$ with the point (z, r). Taking into account that on the z-axis (i.e. at $r = 0$) $\psi = 0$, one can calculate the values of ψ over the whole plane of interest using the measured velocity field u, v. Distributions of ψ versus r at various z are shown in Fig. 2.19. These data corresponding to the values of ψ in the vortex-fixed frame can be used for plotting the streamline pattern. Streamlines of the vortex ring plotted for equally spaced values of ψ with a step $\Delta\psi = 4 \cdot 10^{-4}$ m^3/s are shown in Fig. 2.20. In complete conformity with Reynolds' viewpoint (Reynolds 1876), the zero streamline ($\psi = 0$), which consists of the

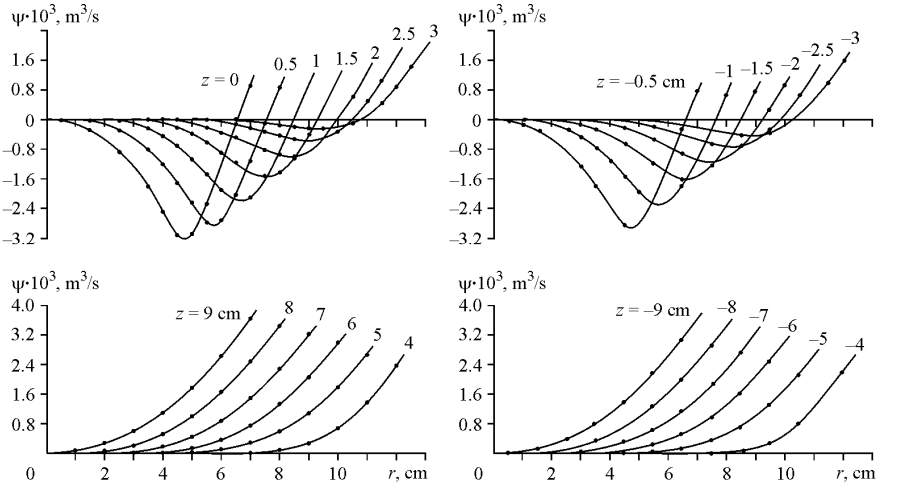

Fig. 2.19. Stream function ψ for various values of z

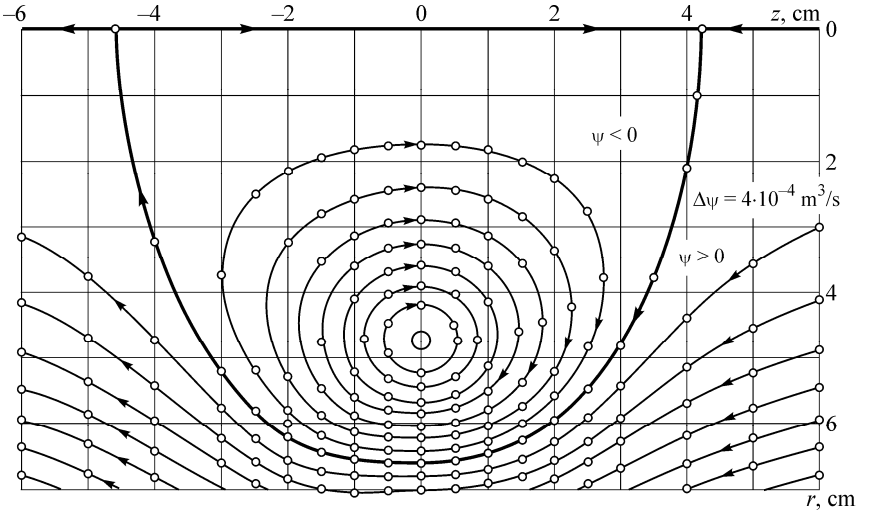

Fig. 2.20. Streamline pattern

z-axis and a certain closed curve, divides the flow domain into two subdomains. For $\psi < 0$ all streamlines are closed, and the fluid circulates around the vortex core. For $\psi > 0,$ the streamlines are non-closed curves corresponding to the flow without separation past a solid body bounded by the surface $\psi = 0.$ As $|\psi|$ increases, the shape of the closed streamlines approaches the shape of circle with the center at $r = R$, $z = 0$ and when $|r - R| \le 0.5$ cm the streamlines are almost circular. A certain asymmetry of the streamlines with respect to the plane $z = 0$ is observed. The closed streamline $\psi = 0$ cuts off segments on the *z*-axis whose lengths differ approximately by 10%. The asymmetry of the vortex in the direction of motion can probably be attributed to the influence of medium viscosity. The shape of the surface of revolution formed by the closed streamline $\psi = 0$ is close to the shape of a flattened ellipsoid of revolution with a semiaxes ratio $h/l \approx 1.5.$ This liquid ellipsoid is the atmosphere of the vortex ring and propagates together with the latter.

2.6 Vorticity Distribution. Vortex Core. Circulation

With a knowledge of the velocity field, it is possible to determine the distribution of vorticity $\omega = |\mathrm{rot}\mathbf{u}| = \partial v/\partial z - \partial u/\partial r$ in a vortex ring. To find ω and energy properties of a vortex ring, one needs to calculate space derivatives of the velocity components. It is known that direct differentiation of experimental dependences

which are obtained with a spread of the measured values, leads to large errors. Therefore, all obtained velocity distributions were interpolated using smoothing splines (Ahlberg et al. 1967; Vershinin et al. 1988), and derivatives of u and v were found as derivatives of these interpolating splines which allowed reduction of their errors to the values comparable to the measurement errors of the velocity components themselves. Figure 2.21 shows the calculated distributions of ω along the radial coordinate r in the plane $z = 0$ and along the axial coordinate z at $r = R$. One can see that the vorticity is concentrated in the form of a sharp peak in the neighborhood of the point $z = 0$, $r = R$, and reaches its maximum of $\omega_{\max} \approx 1600\ \text{s}^{-1}$ at this point.

The experimental vorticity distribution is closely approximated by the following empirical formula:

$$\omega = \omega_{\max}\, \bar{r}\, \text{ch}^{-1}\left[11.7\left(\bar{z}^2 + (\bar{r}-1)^2\right)^{1/2}\right], \text{ where } \bar{r} = r/R \text{ and } \bar{z} = z/R.$$

The region of vorticity concentration corresponds to the core of the vortex ring. Such concentrated vorticity distribution in a real ring may provide some substantiation for the theoretical models of vortex rings, which assume that vorticity is completely localized within a toroidal region. Although in a real vortex ring the vorticity distribution is smooth and does not have a sharp boundary, the width of the vorticity distribution in some sense characterizes the effective size d of the cross-section of the vortex core. For example, if the transverse size of the vortex core d is defined as a width of the vorticity distribution at the level $\omega = \omega_{\max}/2$ one obtains $d \approx 21-22$ mm. This approach is used in particular in optical studies

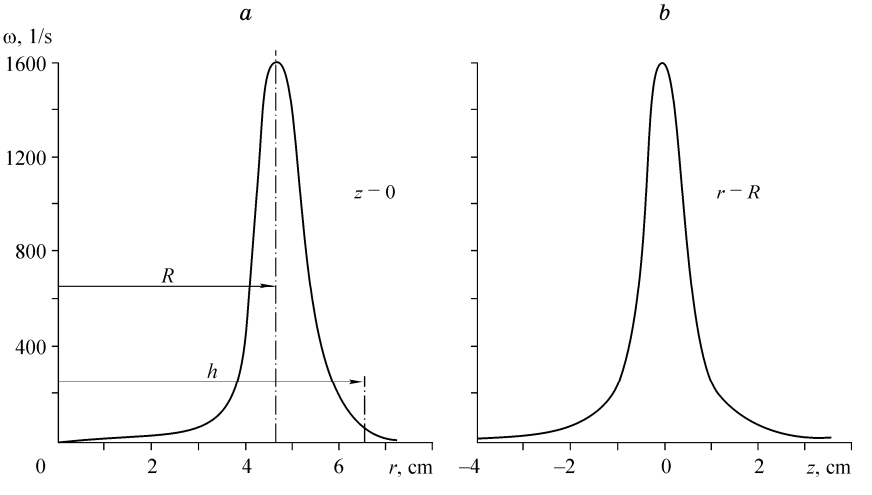

Fig. 2.21. Vorticity distribution: (*a*) along the *r*-axis in the plane $z = 0$; (*b*) along the *z*-axis at $r = R$

for estimating the width of spectral lines. However from the experimental point of view the cross-section size of thin-cored vortex rings is more readily evaluated from the plot of the axial velocity distribution along the *r*-axis in the plane $z = 0$ (see Fig. 2.17), because in this case one does not need to determine the vorticity. According to Fig. 2.17 the distance along the radial coordinate *r* between the extremum points of the curve $u = u(z = 0,\ r)$ on both sides from the point $r = R$ can be taken as the vortex-core diameter. The linear size of the vortex core determined in this manner is 18.8 mm. Since the shape of the core cross-section is close to a circle, it is possible to introduce the notion of the radius of the vortex core *a*, which in this case is equal to 9.4 mm. Of greater interest is the dimensionless ratio of the vortex core radius to the radius of the vortex ring $\varepsilon = a/R \approx 0.202$, assumed in theoretical models as a parameter of smallness of the core size. The values of *a* and velocity $u_{\max}$ at the core boundary allow one to determine the circulation around the core $\gamma = \oint \mathbf{u} \cdot d\mathbf{l} = 2\pi a u_{\max}$. According to Fig. 2.17, $u_{\max} \approx 3.65$ m/s, which implies $\gamma \approx 0.216$ m^2/s. The velocity distribution provided the values of circulation around the closed streamlines inside the vortex atmosphere as well. Dependence of the circulation on the value of the stream function is plotted in Fig. 2.22. It implies that the total vorticity flux (the total value of the vortex ring circulation $\Gamma = \iint_\Sigma \omega\, d\Sigma$) through the area Σ of the meridional cross-section of the vortex ring surrounded by the streamline $\psi = 0$ is equal to $\Gamma = 0.385$ m^2/s. Hence $\gamma/\Gamma \approx 0.56$, that is about half the total vorticity flux is concentrated in the core. Of interest is estimation of the translational speed of the vortex ring from the values *R*, Γ, *a*. In Chapter 1 we showed that the theoretical models of a vortex ring give the translational velocity of the ring in the form $u_0 = (\Gamma/4\pi R) f(\varepsilon)$, where *f* is a function of the parameter $\varepsilon = a/R$. Such dependence of u_0 on Γ and *R* obviously follows from dimensional considerations. The model of a thin-cored vortex ring in an ideal fluid gives $f \approx \ln 8/\varepsilon - 1/4$, which corresponds to Kelvin's formula (1.26). It should be borne in mind that the vortex ring models discussed in Chapter 1 were derived under the assumption that the whole vorticity is concentrated in the vortex core, whereas a real vortex ring is characterized by continuous vorticity distribution over the whole volume of the vortex atmosphere. Thus the formulas for the translational velocity obtained in the framework of the models of a vortex ring in an ideal fluid can serve only for rough estimations of the vortex

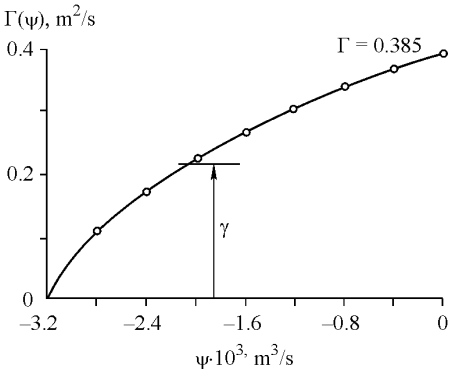

Fig. 2.22. Velocity circulation around the closed streamlines in the vortex atmosphere

ring velocity. In particular, it is not clear which value of circulation must be inserted in Kelvin's formula in order to get the value of the translational velocity of the vortex ring studied in this chapter. If the total circulation $\Gamma = 0.385\ \mathrm{m^2/s}$ is substituted into Kelvin's formula, then we obtain $u_0 \approx 2.29\ \mathrm{m/s}$ and if Γ is considered to be the circulation around the vortex core $\gamma \approx 0.216\ \mathrm{m^2/s}$, then $u_0 \approx 1.27\ \mathrm{m/s}$. Both of these calculated values of u_0 do not agree with the ring velocity of 1.75 m/s measured in the experiment. It should be noted that calculations of u_0 using the theoretical formulas of Chapter 1 fit better to the experimental data, when instead of the total circulation of the vortex ring Γ one takes the value of the circulation equal to $(\Gamma + \gamma)/2$ or $\sim 0.75\Gamma$.

Equation (1.8) of Chapter 1 states that axisymmetric vortex flows are stationary provided that $\omega/r = f(\psi)$, where f is an arbitrary function of ψ. It is of interest to find out the appearance of this function for the vortex ring under study. The variation of ω/r with ψ in the cross-section $z = 0$ obtained from the experimental data is depicted graphically in Fig. 2.23. Arrows on the plot indicate increasing r. It can be seen that the dependence of ω/r on ψ is ambiguous, as for the same value of ψ, the quantity ω/r has different values for $r < R$ and for $r > R$. Thus we may infer that the vortex ring under investigation is not a stationary configuration. However, when ω/r is plotted versus ψ using the measured ω for various values of z, the experimental points fill with a random spread the whole inner region of the hysteresis loop of the two branches of the curve (see Fig. 2.23). This dependence plotted over a great number of ω/r values that correspond to the range $-4.6 < z < 4.2$ is shown in Fig. 2.24. The experimental data are approximated on the average by an empirical formula $(\omega/r)_* \approx 0.683 \exp(4.77\psi_*)$, where $(\omega/r)_* = (\omega/r)(R^2/u_0)$ and $\psi_* = \psi/u_0 R^2$ are the dimensionless quantities. These results imply that the majority of the theoretical models of a vortex ring presented in Chapter 1 constructed under the simplest assumption $\omega/r = \mathrm{const}$ differ drastically from the real vortex ring studied here. It is evident that on substitution of the dependence of ω/r on ψ obtained from the experiment into the

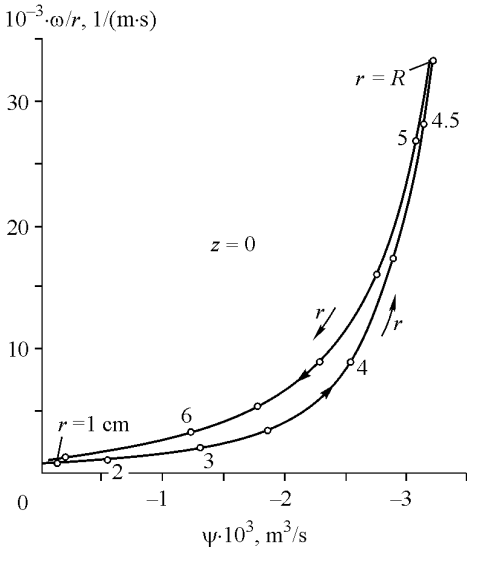

Fig. 2.23. Condition of vortex ring steadiness

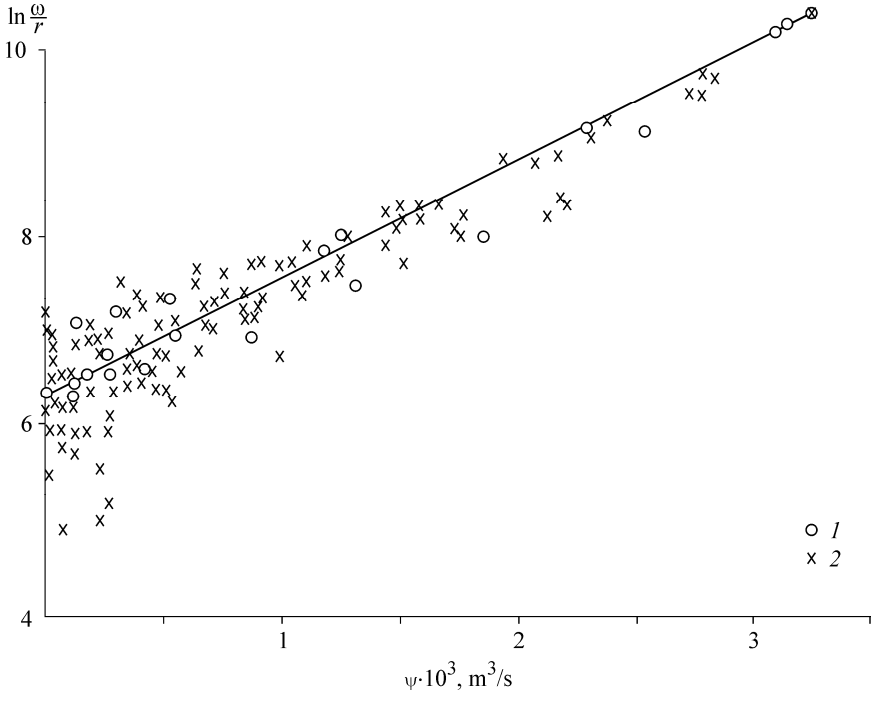

Fig. 2.24. Dependence of ω/r on ψ from measurement of ω over the whole cross-section of the vortex ring ($-4.4 < z < 4.2$). Experimental points: (*1*) $r < R$; (*2*) $r > R$

right-hand side of equation (1.29) instead of the function $f(\psi)$, which remains unknown in the framework of an ideal fluid model, equation (1.29) becomes completely defined and can provide a basis for theoretical studies of the structure of real vortex rings.

2.7 Dynamic Characteristics of a Vortex Ring

The distributions of velocity, stream function and vorticity obtained above allow evaluation of the main dynamic properties of the vortex ring as well. It follows from the presented streamline pattern (see Fig. 2.20) that the volume of the fluid moving along with the vortex ring and localized within the stream surface $\psi = 0$ has the shape close to that of ellipsoid of revolution flattened in the direction of motion (along the *z*-axis). This closed fluid volume is called vortex atmosphere. The vortex atmosphere has the volume $V = 0.846 \cdot 10^{-3}$ m^3. The corresponding ellipsoid of revolution whose volume is equal to the volume of the vortex atmosphere has semiaxes $h = 6.78$ cm along the *r*-axis and $l \approx 4.4$ cm along the *z*-axis.

The coefficient of virtual mass of such an ellipsoid in the direction of motion is $\mu \approx 0.83$ (Kochin et al. 1964).

Momentum and energy of a vortex ring

To evaluate the impulse of the vortex ring, we use formula (1.18) obtained by Vladimirov (1977, 1979), which implies that the impulse of a vortex ring can be represented as a sum of momenta of the fluid inside the vortex atmosphere and of the virtual mass of a corresponding solid body. Assuming that the volume of the vortex atmosphere is $V = 0.846 \cdot 10^{-3}$ m^3, and the density of the medium is $\rho = 1.21$ kg/m^3, we obtain the impulse of the vortex ring $P = (1+\mu)\,\rho V u_0 \approx 3.3 \cdot 10^{-3}$ N·s.

The energy of the vortex ring is the sum of the energies of the fluid inside and outside of the vortex atmosphere. These components are determined separately. The energy of the vortex atmosphere T_a is determined by direct integration of the velocity distribution over the volume V of the velocity distribution

$$T_a = \rho \int_V \frac{(u+u_0)^2 + v^2}{2} dV = 4.54 \cdot 10^{-3} \text{ J}.$$

The energy of the fluid outside the vortex atmosphere is estimated on the basis of the coefficient of virtual mass μ of the vortex atmosphere $T_f = \mu \rho u_0^2 V/2 = 1.3 \cdot 10^{-3}$ J. Hence, the total energy of the vortex ring $T = T_a + T_f = 5.84 \cdot 10^{-3}$ J. Note that $T_f/T_a = 0.22$, i.e. the kinetic energy of the fluid flowing past the vortex ring atmosphere comprises only a fifth of the energy of fluid motion in the vortex atmosphere.

It is also instructive to compare the energy in the vortex ring atmosphere with the energy T_f of a solid body of the same mass moving in an empty space with the velocity of the vortex ring u_0. Calculations give $T_t = \rho u_0^2 V/2 = 1.55 \cdot 10^{-3}$ J and $T_a/T_f = 2.93$, hence the energy of the fluid in the vortex atmosphere is approximately three times the energy of the corresponding solid.

Dissipation of vortex ring energy

Evaluation of the energy dissipation $F = \partial T/\partial t$ of a vortex ring caused by viscosity of the medium is also of interest. It is known (Lamb 1932; Serrin 1959) that the viscous dissipation of energy per unit volume of the fluid is determined as $\Phi = 2\mu D : D$, where μ is the dynamic viscosity coefficient and $D : D$ is the product of the strain tensor $D_{ij} = (\partial V_i/\partial x_i + \partial V_j/\partial x_i)/2$. Thus,

$$D:D=\left(\frac{\partial v}{\partial r}\right)^2+\left(\frac{\partial u}{\partial z}\right)^2+\frac{1}{2}\left(\frac{\partial v}{\partial z}+\frac{\partial u}{\partial r}\right)^2.$$

The distribution of energy dissipation Φ in the vortex ring along the r-axis in the plane $z = 0$ is plotted in Fig. 2.25. As it could be expected, the energy dissipation reaches the maximum value in the zone of high gradients of velocity near the vortex-core boundary and the minimum value inside the core, where the fluid motion is close to rotation of a solid. The energy dissipation in the fluid volume V is determined (Lamb 1932; Serrin 1959) by the formula

$$F=\frac{\partial T}{\partial t}=\iiint\limits_V \Phi\, dV=\mu\left[\iiint\limits_V \omega^2 dV+\iint\limits_\Sigma \frac{\partial q^2}{\partial n}d\Sigma-2\iint\limits_\Sigma [\mathbf{u}\times\boldsymbol{\omega}]d\boldsymbol{\Sigma}\right],$$

where Σ is the area of the surface bounding the volume V, q is the absolute value of the velocity, $\mathbf{n}$ is the outward normal to the surface Σ. The energy dissipation is calculated separately inside the vortex atmosphere and in the fluid surrounding the vortex atmosphere. Assuming that $\mu = 17.9\cdot10^{-6}$ kg·m^{-1}·s^{-1} at $T = 293$ K (Schlichting 1968; Kikoin 1976), we find the energy dissipation in the vortex atmosphere $F_a = 17.9\cdot10^{-6}(57.3-6.92-2\cdot2.24) = 0.82\cdot10^{-3}$ W. The energy dissipation F_f outside the vortex atmosphere is determined in a similar manner. The volume integral over V vanishes, as $\omega \approx 0$ outside the vortex atmosphere. The calculations yield $F_f = 0.204\cdot10^{-3}$ W. Thus, the total energy dissipation of the vortex ring is $F = F_a + F_f = 1.02\cdot10^{-3}$ W. Based on this value of F, we can estimate the energy loss δT during the time $\delta t = 2R/u_0$ of vortex ring propagation to

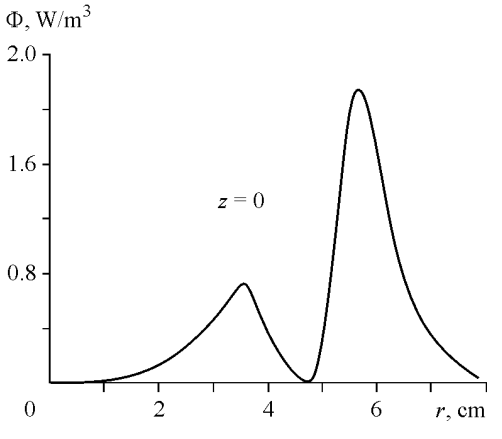

Fig. 2.25. Distribution of the energy dissipation Φ along the r-axis in the plane $z = 0$

a distance equal to its diameter 2*R*. As $\delta t = 0.054$ s and $F = \partial T/\partial t$, then $\delta T = F\delta t = 1.02 \cdot 10^{-3} \cdot 0.054 = 0.055 \cdot 10^{-3}$ J. Hence, $\delta E/E \approx 0.01$, i.e. the vortex ring loses approximately 1% of its energy during the time δ*t*.

Comparison of vortex ring energy dissipation and power required for motion of a streamlined body in a viscous fluid

Lavrent'ev and Shabat (1973) put forward an idea that it is possible to reduce the drag of solids in a viscous fluid by organizing a flow similar to a flow in a vortex ring. This idea is validated by the following simple experiments. If a mass of air contained in a child's balloon is ejected with an initial velocity of 5–10 m/s, the balloon will move to a distance equal to 1.5–2.0 m; if the same mass of air is ejected from a circular orifice with the radius equal to the balloon radius, a vortex ring is formed, which moves to a distance greater by a factor of 10 to 15. An impression is created that the motion of the fluid mass in the form of a vortex ring occurs with substantially lower energy dissipation.

This problem attracted the attention of many researchers. Lugovtsov and Lugovtsov (1971) theoretically determined the energy dissipation in a flow with two hollow straight-line vortices of the opposite signs, and Sennitskii (1981) measured the drag of two parallel solid cylinders rotating in the opposite directions. The drag of the rotating cylinders was found to be lower than that of non-rotating cylinders, but not to the extent estimated theoretically. Each of these flows is a plane analog of a vortex ring. It seems of interest to directly determine the energy dissipation during the motion of a vortex ring and to compare it with the power necessary for the motion in a viscous medium of a streamlined solid body whose volume is equal to the volume *V* of the vortex ring atmosphere, and velocity is equal to the propagation speed of the ring u_0. The values of the energy and power loss of the vortex ring obtained above allow for such comparison (Akhmetov 2008a).

Numerous experiments show that the minimum drag is observed in non-separated flows around axisymmetric spindle-shaped solids with aspect ratios (ratio of the body length *l* to its transverse size *d*) $k = l/d = 5–6$ (Goldstein 1965). As the drag of the body in a non-separated flow is determined by skin friction only, it is necessary to know the area of the body surface. The area of the surface of a streamlined body can be approximately estimated as the area of the surface of an extended ellipsoid of revolution with a semiaxes ratio $k = 6$ and with a volume equal to the volume *V* of the vortex-ring atmosphere. The length of such an ellipsoid is $L = (6k^2/\pi)^{1/3} V^{1/3}$ and the area of its surface is $S = (9\pi/2k^2) AV^{2/3}$. Here $A = 1 + (k^2/(k^2-1)^{1/2})\arcsin((k^2-1)^{1/2}/k)$. Substituting the values $V = 0.846 \cdot 10^{-3}$ m^3 and $k = 6$, we obtain $L \approx 0.387$ m, and $S \approx 0.0625$ m^2. The Reynolds number for this body moving with the vortex-ring

velocity $u_0 = 1.75$ m/s is $\mathrm{Re} = u_0 L/\nu = 4.52 \cdot 10^4$. The hydrodynamic drag Q of the body can be determined as the drag of a flat plate with a wetted surface area S. Thus, $Q = c_f \rho u_0^2 S/2$, where c_f is the skin friction coefficient of a flat plate wetted on one side. As the flow is laminar for $\mathrm{Re} < 5 \cdot 10^5 – 10^6$ (Goldstein 1965; Schlichting 1968), the value of c_f can be determined from the Blasius formula: $c_f = 1.328\,\mathrm{Re}^{-1/2} = 0.625 \cdot 10^{-2}$ (Schlichting 1968). The drag force of the body is $Q \approx 0.723 \cdot 10^{-3}$ N, and the power W necessary for this body to move is $W = Qu_0 \approx 1.265 \cdot 10^{-3}$ W. A comparison of the power W and the energy dissipation of the vortex ring $F = 1.02 \cdot 10^{-3}$ W shows that the energy spent during the vortex-ring motion is only slightly lower than the corresponding value for a streamlined solid of an identical volume. It should be noted that the energy loss during the actual motion of a solid can be somewhat higher than the value obtained here, because the motion of all solids at these Reynolds numbers is accompanied by flow separation and by formation of a co-current wake behind the body, which increases the drag force. The ratio of W to the energy dissipation F_f outside the vortex atmosphere is $W/F_f \approx 6.2$, i.e., the energy loss in the case of motion of a body similar in shape and volume to the vortex atmosphere with a corresponding moving boundary is much lower than the power necessary for a streamlined solid to move. Clearly, this gain in energy expenses can be utilized in practice only for a body similar to the vortex-ring atmosphere with a corresponding moving boundary, and creating such a body is a challenge for engineers. Some experiments on flow past cylindrical bodies with a moving boundary are described by Prandtl and Tietjens (Prandtl 1949; Prandtl and Tietjens 1934).

Based on the energy estimates obtained, we can try to give some qualitative explanations for the experimental results described above. Obviously, two factors are responsible for the greater path of the vortex ring, as compared with the path covered by the sphere-shaped solid body. First, the vortex-ring atmosphere is a body with a moving boundary, which ensures a non-separated flow with a lower drag force. Second, the total energy of the vortex ring consists not only of the energy of translational motion, but also of the energy of circulation motion of the fluid in the vortex atmosphere. As shown above, the energy of the fluid in the vortex-ring atmosphere is approximately three times the energy of the solid of the same mass. Clearly, the mobility of the vortex-atmosphere surface is ensured by the circulation motion of the fluid in the vortex atmosphere. Obviously, all energy of the vortex ring is spent for its motion. These two factors (higher value of the initial energy of the vortex ring and mobility of the surface bounding the vortex atmosphere) offer a qualitative explanation for the fact that the vortex ring covers a greater distance than a solid body of an identical mass, which is particularly true for a spherical body (balloon) with flow separation.

2.8 Other Investigations of Vortex Ring Structure

The above results of the experimental investigation of a vortex ring obtained by Akhmetov and Kisarov (1966), were the first to give sufficiently comprehensive idea of the structure and parameters of a real vortex ring. Later, similar experimental studies of structure of particular realizations of vortex rings were also carried out by other authors (Maxworthy 1972, 1977; Sullivan et al. 1973; Weigand and Gharib 1997). The main difference of these works from the study presented above is in the procedure of measuring the velocity field of a vortex ring, because the velocity field was determined not by hot-wire anemometer apparatus, but Laser Doppler Velocimeter (LDV, also known as Laser Doppler anemometer (LDA)) (Yeh and Cummins 1964; Durst et al. 1976; Koronkevich et al. 1983) or PIV-method (Particle Image Velocimetry) (Willert and Gharib 1991) of identification of the velocity field in a plane cross-section of the flow. The most extensive data on the structure of two particular realizations of air vortex rings were obtained by Sullivan et al. (1973). This work presented the study of the structure of the two laminar vortex rings: ring 1 whose radius and velocity were $R \approx 2.77$ cm, $u_0 \approx 0.731$ m/s (Reynolds number of the vortex ring $\mathrm{Re} = Ru_0/\nu \sim 1.35 \cdot 10^3$), and ring 2 with $R \approx 3.39$ cm, $u_0 \approx 4.12$ m/s ($\mathrm{Re} \sim 9.3 \cdot 10^3$). The vortex rings in this study were produced by ejecting a slug of air from an orifice in a special chamber by periodic pulses of an acoustic loudspeaker built-in at the opposite wall of the chamber. Accordingly, vortex rings were produced in a periodic manner, and velocity field of vortex rings traveling through the measurement point was determined at a certain distance from the orifice by a single-component LDV via consecutive scanning of the flow field. That is, the method of determining the velocity field of a vortex was virtually analogous in detail to the procedure described in Section 2.2. Quantitative comparison of the results of this work with the above presented study of the vortex ring structure is not quite correct, because different realizations of vortex rings were investigated. However, some data obtained by the authors are instructive for qualitative comparison. Figure 2.26 presents velocity distributions along the r-axis for $z = 0$ for both rings studied in this work. Obviously, these plots are analogous to the plot in Fig. 2.17 that was used to determine the radius of the vortex ring and the cross-section size

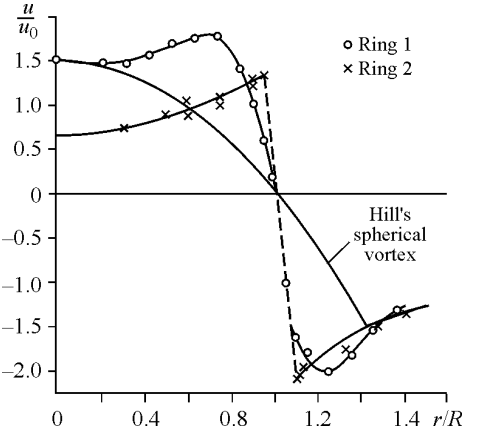

Fig. 2.26. Velocity distribution in the plane $z = 0$ (Sullivan et al. 1973)

of the vortex core. It can be seen that in the velocity distribution of vortex ring 2, which has a larger propagation speed, the experimental points are absent from the vortex core, which is probably due to the limitations of the measuring method used there, which will be discussed below in remarks on the methods of measurement of the velocity field. Figure 2.27 shows the superimposed streamline patterns constructed from the measured velocity field and visualized structure of the vortex 1. Vorticity distribution in the ring 1 is shown in Fig. 2.28, together with the vorticity distributions in Hill's spherical vortex and in theoretical models of thin-cored vortex rings based on the assumption that $\omega/r = \text{const}$. The plot $\omega/r = f(\psi)$ obtained experimentally and shown in Fig. 2.29 is similar to Fig. 2.23. It is noted that the assumption $\omega/r = \text{const}$ used in a number of theoretical studies is not realized in actual conditions.

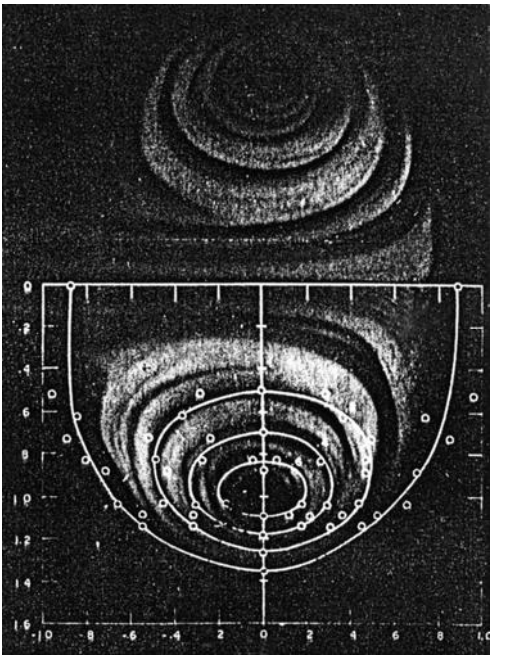

Fig. 2.27. Cross-section visualization and vortex ring streamlines (Sullivan et al. 1973)

Maxworthy (1972) used LDV and presented the measured velocity distribution in the plane $z = 0$ of a vortex ring, whose Reynolds number was $\mathrm{Re} = Ru_0/\nu = 0.885 \cdot 10^4$ and vorticity distributions in a vortex ring with $\mathrm{Re} = Ru_0/\nu = 1.05 \cdot 10^4$.

Weigand and Gharib (1997) carried out the experimental investigation of the structure of six realizations of laminar vortex rings in water using LDV and PIV methods and obtained the corresponding velocity and

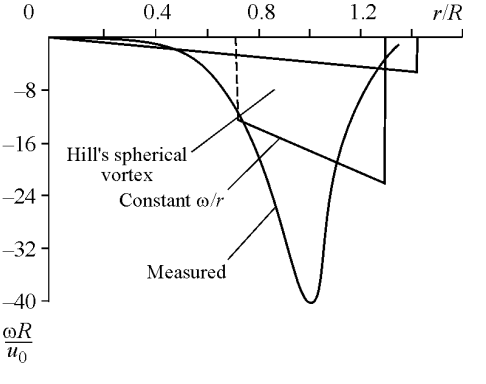

Fig. 2.28. Vorticity distribution along the *r*-axis in the plane $z = 0$ (Sullivan et al. 1973)

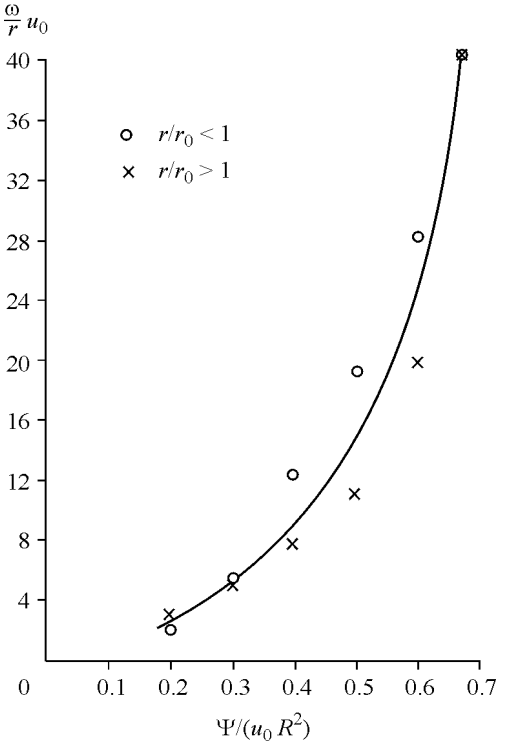

Fig. 2.29. Dependence of ω/r on ψ (Sullivan et al. 1973)

vorticity distributions. Vortex rings were produced by a piston pushing water from a circular nozzle. Vortex rings with Reynolds numbers in the range $830 \le \mathrm{Re} \le 1650$ were studied (Reynolds number is defined here as a ratio of the circulation of a vortex ring to the kinematic viscosity coefficient). Circulation values and core radii a of these vortices were determined. It was demonstrated that the radial vorticity distributions presented as a dependence of the ratio of ω to its maximum value ω_0 on the dimensionless distance $\bar{y}_1 = (r - R)/a$ from the center of the core can be squeezed into a practically one experimental dependence for all the vortex rings studied in that work (Fig. 2.30). This experimental plot is approximated well by the Gaussian curve $\omega/\omega_0 = \exp(-\eta^2 \bar{y}_1^2)$ with some parameter η. The authors also noted that approximation formulas for the vorticity distribution in the neighborhood of the core of a vortex ring suggested by other researchers (Maxworthy 1972; Gleser and Coles 1990) give a broader pattern of the vorticity distribution compared with the experiment. Of interest is the experimental plot of evolution of the vortex ring diameter D in the course of its formation and motion near the exit hole of the nozzle (Fig. 2.31). This plot implies that the change of the vortex ring diameter (and, hence, the formation of the vortex ring) does not cease at the time when the piston stops but continues for some time after the piston has stopped and the jet discharge has ceased.

Thus, the experimental data obtained by other measurement methods (Maxworthy 1972, 1977; Sullivan et al. 1973; Weigand and Gharib 1997) qualitatively substantiate the above results of investigation of the vortex ring structure (Akhmetov and Kisarov 1966) by means of hot-wire anemometer probes.

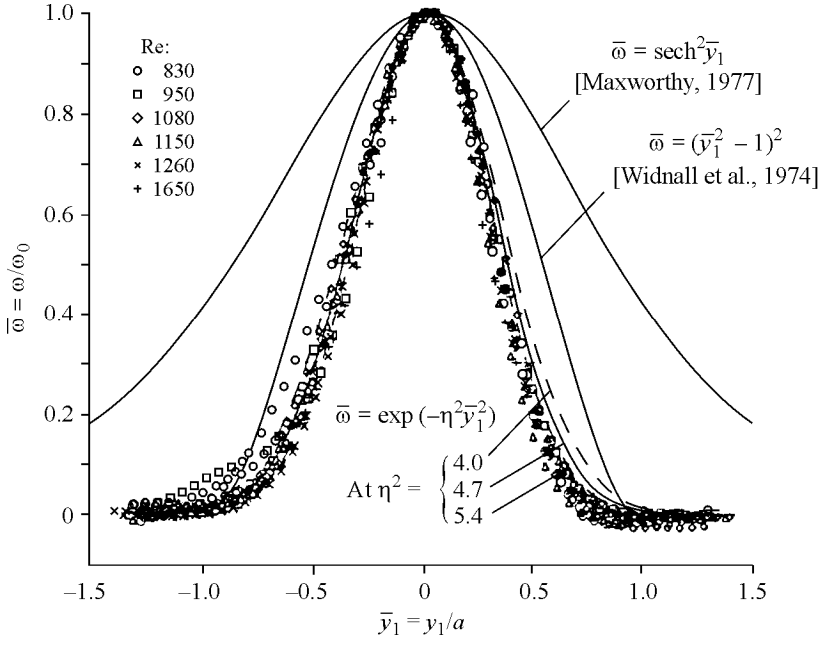

Fig. 2.30. Vorticity distribution in vortex rings (Weigand and Gharib 1997)

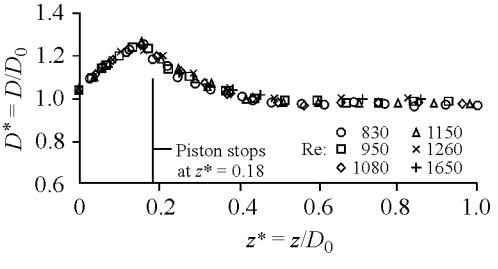

Fig. 2.31. Variation of the diameter D of vortex ring 1 during its formation. D_0 is the diameter of the nozzle, z is the distance from the nozzle exit, $\mathrm{Re} = \Gamma/\nu$ is the Reynolds number of the ring (Weigand and Gharib 1997).

2.9 Comments on Experimental Methods of Studying Velocity Flow Field

As evident from the above, various methods are used to determine velocity field of vortex rings: hot-wire anemometry (HWA), laser Doppler velocimetry (LDV), and particle image velocimetry (PIV). It is instructive to note the main advantages and drawbacks of these methods.

The hot-wire anemometer (HWA) method has the following advantages: flow velocity is a directly measured quantity; hot-wire apparatus is stable in operation, does not require additional tuning and adjustment during measurements, and allows for measuring sufficiently high-frequency signals. The drawbacks of this technique are as follows: possible disturbance of the studied flow by hot-wire probes, which is especially undesirable when a flow with closed streamlines is investigated; the need to calibrate each HWA probe; dependence of a HWA signal on variations of medium temperature; nonlinear response of an output HWA signal to the measured velocity which substantially complicates determination of a magnitude and sign of separate velocity components even in two-dimensional flows with a qualitatively known pattern. Hot-wire anemometry methods are most efficient for studying turbulent characteristics of flows, since in this case small pulsations about some average value are measured, and a calibration curve, linearized in the vicinity of this average velocity value, enables one to determine not only the magnitudes but also the signs of turbulent pulsations of velocity.

In contrast to a hot-wire anemometer, LDV is a remote technique of velocity measurement without the need to insert of any measuring probes into flow of interest. The point of velocity measurement in the flow is formed as a focusing point of light beams which practically do not disturb the flow, and the region of the beam focusing has minimum dimensions. Analyzing the spectrum of light scattered by the particles in the region of beam focusing, one can determine particle velocities in fluid. This method suggests that particles are carried by the fluid, and their velocities coincide with the fluid velocity. The LDV technique does not require preliminary calibration of a device, since the output signal is proportional to the measured velocity component with a numerical factor known in advance. Modern two-component LDV systems can simultaneously measure the magnitude and direction of both velocity components at a given point.

However, along with the mentioned merits, LDV also has fundamental disadvantages. The main one is that LDV measures velocities of microscopic particles suspended in the fluid and entrained with it rather than the fluid velocity itself. It is obvious that particle velocities are not necessarily equal to the fluid velocity. Such equality is possible only when particle and fluid densities are identical. This is virtually unattainable for air flows and other gas media, since densities of solid or liquid particles are commonly about 1000 times greater than the density of the embedding gas medium. As a result, LDV velocity measurements of gas flows become unreliable in regions with large local accelerations, because in such regions particle motion is governed not only by the fluid velocity, but also by temporal and spatial accelerations of the fluid. Concentrated vortices with streamlines of large curvature and with large velocity gradients in their cores are examples of such flows with large local accelerations. In particular, the velocity field of vortex rings in the laboratory frame is unsteady. It is also evident that while measuring high-frequency variations of the flow velocity, one needs to provide sufficiently high concentration of particles in the fluid volume of interest, but this is not always possible, since heavy particles are swept away from the flow regions with large streamline curvature, which are characterized by great local accelerations. The absence of the experimental points from the velocity distribution in the core

of more intense vortex ring 2 (see Fig. 2.26) which represents measurement results by Sullivan et al. (1973) might be explained by small concentration or no particles in the core of this ring due to sweeping-off action of centrifugal forces. When flows in water or other liquids are investigated, there exists a possibility to select particles whose density would match the fluid density. Sometimes there is no need to introduce artificial particles into the fluid, since the particles originally present in tap water may suffice. However, when structure of intense vortices is studied in liquids, other limitations arise. It is known that in the cores of vortices of high intensity the pressure drops sharply, hence leading in liquids to cavitation in the vortex core. Thus, investigation of fluid flow pattern with induced cavities by means of light beams becomes virtually unfeasible. In contrast to this, hot-wire anemometry is used to measure velocity fields in gas media, which does not impose any limitations on maximum flow velocities like those discussed above. Moreover, since the particles remain in the region of the laser beam focus for a short time only, real-time processing of LDV signals becomes complicated, and capabilities for measuring velocity alternating at high frequency, and particularly turbulent properties of fluid and gas flows are restrained. These drawbacks may be the reason why there are almost no experimental studies of turbulence by means of LDV that would be as good in quality as the classical investigations using hot-wire anemometry apparatus (Hinze 1959). Laser Doppler methods of measuring velocity flow field, despite their considerable advantages, have not yet become a complete substitute to hot-wire anemometry technique of studying velocity field of fluid and gas flows.

Measurement of the velocity flow field by the PIV technique, as measurement using LDV, is also based on determining velocities of particles suspended in fluid. This method implies registration of two or several particle distribution pictures in a certain plane cross-section of the flow at short time intervals. On computer processing the picture obtained is divided into small cells as on graph paper, and then the motion and velocity of a group of particles in each cell are determined. This procedure being applied to all cells of the registered flow picture provides determination of virtually instantaneous velocity field over the whole plane, which is a substantial advantage of this method and is specifically attractive in investigation of velocity field of nonstationary and complex flows like vortex rings. However, the PIV technique in essence also measures velocities of particles suspended in fluid, hence the drawbacks of the LDV technique are also inherent in the PIV method. Thus, the hot-wire anemometer technique and optical methods of studying velocity flow field should be considered complementary measurement techniques.

3 Structure and Parameters of a Family of Vortex Rings Formed on Outflow of a Submerged Jet

Experimental results on the vortex ring structure presented in Chapter 2 for the first time provided a deep insight into the structure and properties of real vortex rings. However, the structure was revealed only for several randomly chosen vortex rings. At the same time, of considerable scientific and practical interest is determination of the structure and properties of a broad family of pulsed vortex rings which form when some finite volume of a fluid is given a certain momentum in an unbounded space filled with the fluid. Formation of vortex rings on discharge of a finite-length submerged jet from an orifice or outlet of a cylindrical tube is the main method of generating most intense rings. The problem is to determine the properties and parameters of the whole class of vortex rings in accordance with the criteria that specify generation conditions. Such data can provide the initial conditions in the statement of the problem of motion of a formed vortex ring in an unbounded viscous medium and can be also useful for practical applications of vortex rings. There are numerous studies of dependence of vortex ring properties on its formation conditions. The most essential results were obtained by Tarasov (1973) and Maxworthy (1977). Tarasov used visualized flow patterns to measure the diameter and translational speed of a vortex ring as functions of the length and Reynolds number of the jet. Information on the core size and vortex ring circulation obtained in the same manner as functions of the parameters controlling the generation process, seems not to be accurate enough and can be considered only as some rough estimates of these quantities. Maxworthy (1977) used direct measurement of the velocity distribution in a vortex ring be means of a laser Doppler anemometer and determined the number of important parameters of the vortex ring, namely its diameter and total circulation, core diameter and circulation around the core. Particularly, it was shown that the vortex core contains ~50% of the total circulation of the vortex ring, which is consistent with the data presented in Chapter 2. However, the results of this investigation are insufficient to get a comprehensive idea of the structure of the considered family of vortex rings, because the dependence of the vortex ring properties on the geometric and kinematic parameters that control its generation were studied within a relatively narrow range of these parameters. More comprehensive and systematic investigation of the structure and parameters of a large family of vortex rings generated by impulsive discharge of a submerged air jet from a circular cylindrical nozzle was presented in a recent study by Akhmetov (2001). The main criteria that specify the process of vortex ring formation are established, and vortex ring properties and parameters as functions of these criteria varying in a wide range are determined.

The obtained results are not only of scientific interest, but can be used for practical purposes to obtain vortex rings with the required properties.

3.1 Experimental Procedure

The purpose of the present investigation is to determine the structure and parameters of a whole family of vortex rings formed during discharge of a submerged jet of finite length and to recognize dependence of vortex ring parameters on criteria that determine the process of their generation.

Detailed experimental studies of vortex ring structure presented in Chapter 2 demonstrate that a vortex ring can be characterized, to a first approximation, by a finite number of parameters which provide quite sufficient notion about its structure. The technique used to determine the vortex ring parameters in this series of studies is generally similar to that used in the studies of the structure of a laminar vortex ring (see Chapter 2). We determined the velocity field of a vortex ring in the same manner using hot-wire anemometers. However, in the present studies detailed velocity field patterns or vorticity distributions in vortex rings were not of interest in their own right, and measurements of velocity field served only as a means for determining a finite set of kinematic and geometric parameters of a vortex ring which characterize its structure. In some cases we also applied methods utilized by many authors (Maxworthy 1977; Gleser and Coles 1990; Weigand and Gharib 1997), which simplify determination of certain parameters. For example, it is easier to find the total circulation of a vortex ring by integrating the velocity distribution $\Gamma = \oint_{ABCDA} \mathbf{u}(z,r)\cdot d\mathbf{l}$ along the closed rectangular contour *ABCDA* (Fig. 3.1) of large dimensions, whose side *AB* lies on the axis of symmetry. When dimensions of the rectangle *ABCDA* are large enough, it is obvious that the integrals along the sides *BC* and *DA*, which are perpendicular to the flow velocity at infinity, vanish, and one has to integrate only the velocity distribution along the symmetry axis (line *AB*) and along *CD*, where the flow velocity is constant and equal to u_0. It is also evident that by setting a velocity probe far from the discharge outlet of the nozzle at the point *B* on the symmetry axis of the flow along which the vortex ring propagates, one can measure the velocity distribution as a function of time, $u(t)$, along the line *AB*. Assuming that the translational velocity of the vortex ring u_0 remains constant as it moves through the probe, one may change variables $z = z_B - u_0 t$, $u(z) = u(t) - u_0$ and switch from integration along the lines *AB* and *CD* to integration over time. It can be shown that in so

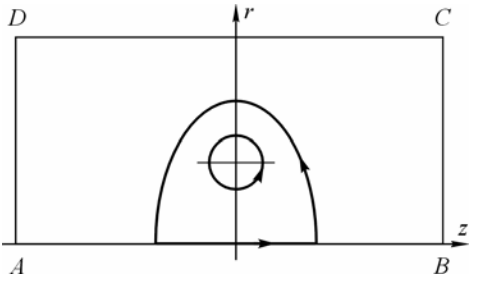

Fig. 3.1. Contour of integration for determining the total circulation of a vortex ring

doing the circulation is Determined from the measured velocity distribution on the symmetry axis $u(t)$ by the expression

$$\Gamma = \int\limits_{ABCDA} \mathbf{u}(z,r)\cdot d\mathbf{l} = \int\limits_{AB} \mathbf{u}(z,0)\cdot d\mathbf{l} - \int\limits_{CD} u_0 dz = u_0 \int\limits_0^{t_A} u(t)dt,$$

where $t_A \to \infty$.

The advantage of this procedure is obvious, since in order to find the total circulation of a vortex ring, it is sufficient to measure the velocity distribution $u(t)$ on the symmetry axis in a single run of a vortex ring, without comprehensive study of the velocity or vorticity distributions over the whole flow field.

Experimental Setup

The present investigations require the precise setting of the parameters specifying the process of vortex ring formation and possibility to vary these parameters in a sufficiently wide range. For this reason, another experimental facility was used to generate vortex rings. The number of determining parameters can be reduced if a vortex ring is generated on discharge of a jet at constant velocity V_0 during a given interval T. In the majority of experimental studies (Tarasov 1973; Maxworthy 1977; Gleser and Coles 1990; Weigand and Gharib 1997; Gharib et al. 1998) such a jet is created by expelling a fluid from a cylindrical tube using a piston actuated by some mechanical device. The jet velocity and discharge duration are determined from the velocity and duration of the piston motion. However, this procedure has a number of drawbacks. One of them is that the piston and the fluid expelled from the tube cannot be instantaneously accelerated and stopped at a given point of time. Hence, the velocity will be a function of time, since it will have regions of acceleration and deceleration. If experiments are carried out in water, then at the instant of a sudden piston stop, the liquid jet moving at a large speed, may separate from the piston surface and continue its inertial motion in an uncontrolled manner, i.e. the actual length of the jet may differ from the total piston stroke. Because of these shortcomings, the jet parameters and, hence, the conditions of vortex ring formation appear to be dependent on the law of motion of the piston. Therefore, in this study we used another method of creating a jet of finite length. This technique provides discharge of an air jet at constant velocity V_0 during the whole specified time interval T.

Vortex rings were generated by an experimental setup (Fig. 3.2*a*) which consisted of receiver *1* with compressed air, bypass valve *2*, and expansion chamber *3* with an outlet nozzle *4*. The shaped channel of the nozzle, which consists of an inlet confuser part and an outlet cylindrical part of length l_c and outlet radius $R_0 = 37.5$ mm, ensures discharge of the submerged air jet from the chamber with a uniform velocity profile at the nozzle exit. The external surface of the nozzle is conical with the angle of taper θ, and the cone generator is 200 mm long. The expansion chamber is connected to receiver *1* with compressed air through

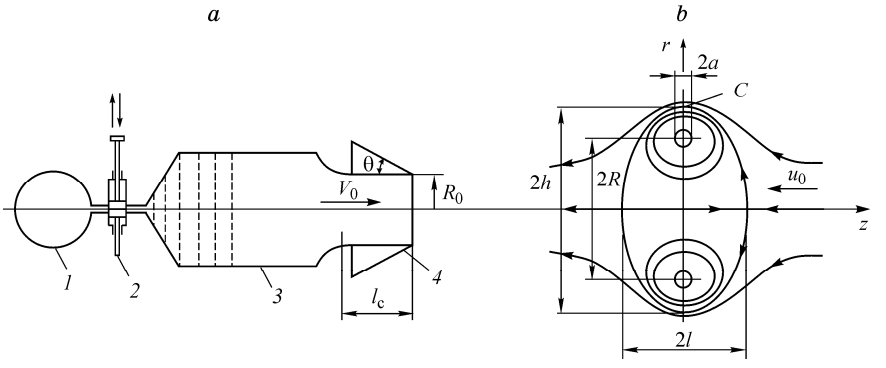

Fig. 3.2. Schematic layout of vortex ring generator (*a*) and a formed vortex ring (*b*)

quick-opening electromagnetic valve *2*. When the valve opens, the compressed air passes from the receiver to the chamber and pushes the air inside to the nozzle. The large swirls and pulsations of air in the chamber produced by the opening of the valve are damped by a screen and by a system of fine-meshed grids. After a certain time T (in the range 1–1000 ms) the valve closes and the jet from the nozzle is interrupted. The initial pressure p in the receiver and its volume were chosen to be sufficiently large (5 MPa) that the pressure did not change notably during the discharge time T and ensured constant critical (Ovsyannikov 1981; Liepmann and Roshko 1966) velocity of discharge and gas flow rate through the calibrated orifice of the valve. This ensures constancy of the gas flow rate in time and discharge velocity V_0 of the air jet from the nozzle. The desired value of the jet velocity V_0 is specified by mere change of diameter of the exit orifice of the valve. The length and volume of chamber *3* were sufficiently large that the jet ejected from the nozzle was formed from the unperturbed air contained in the chamber before the valve opening and the gas leaving the receiver was not able to reach the nozzle exit. However, an excessive increase in chamber dimensions occurred to be counter-productive, since the expansion chamber and the nozzle formed a Helmholtz resonator where intense low-frequency acoustic oscillations were excited, resulting in pulsations of the discharge velocity of the jet at the nozzle. It was revealed that discharge of a pulsating jet produces not a single vortex ring, but a chain of several vortices. In order to restrict the pulsation level to an acceptable value, small damping holes were drilled on the lateral surface of the chamber and wrapped with a rubber tape on the exterior, which allowed us to significantly reduce the quality factor of the resonator and provided constant jet speed. The experimental setup ensured identical parameters of the jet and vortex rings produced in jet discharge in repeated runs. The magnitude and profile uniformity of the jet velocity at the nozzle exit cross-section was controlled by hot-wire anemometer

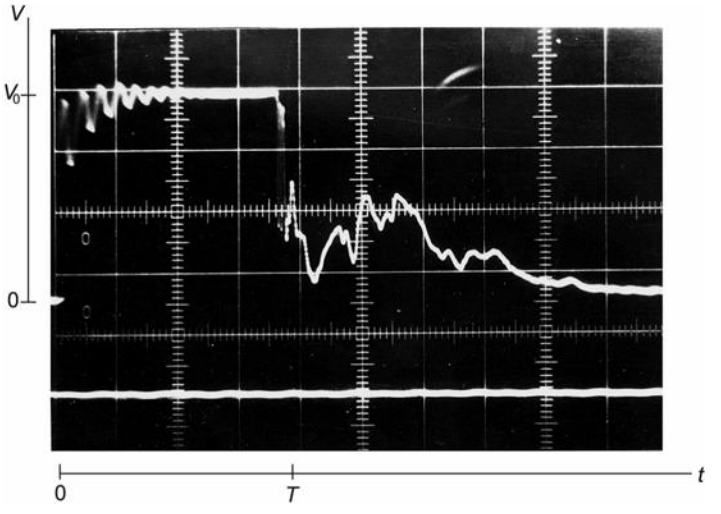

Fig. 3.3. Registration of the jet velocity at the nozzle exit

measurements. A typical oscillogram of the hot-wire anemometer signal representing the jet velocity at the nozzle exit as a function of time T is shown in Fig. 3.3.

3.2 Criteria Determining Vortex Ring Formation Process

From the description of the experimental setup and its operation principle it follows that the formation of a vortex ring during pulsed discharge of a submerged air jet from a cylindrical circular nozzle is determined by the following set of dimensional parameters

$$R_0,\ l_c,\ \theta,\ V_0,\ T,\ \rho,\ \mu,$$

which denote the nozzle radius, the length of the cylindrical portion of the nozzle, the cone angle of the outer surface of the nozzle, the jet velocity, time of jet discharge, the density and dynamic viscosity coefficient of the medium, respectively. The current time is not included in this set of parameters, because the purpose of this study is to determine the parameters of the vortex ring at the characteristic time, when vortex ring formation is completed, and its further propagation can be treated as a motion in an unbounded fluid which does not depend on the formation dynamics. According to the dimension theory (Sedov 1959; Barenblatt 1996), one may choose R_0, V_0, ρ as quantities with independent dimensions and compose four dimensionless combinations from the parameters listed above that determine the formation of the vortex ring:

$$L_* = V_0 T / R_0, \quad \mathrm{Re} = V_0 R_0 / \nu, \quad \theta, \quad l_c / R_0, \tag{3.1}$$

where $\nu = \mu/\rho$ is the kinematic viscosity coefficient (in experiments $\nu = 15 \cdot 10^{-6}$ m^2/s).

The experiments were carried out at fixed length of the cylindrical portion of the nozzle $l_c/R_0 = 2$, the vortex ring parameters were determined with variation of the three dimensionless quantities L_*, Re, θ, which specify the dimensionless length of the ejected jet (or duration of the discharge), the Reynolds number of the jet, and the cone angle of the external surface of the nozzle, respectively.

3.3 Basic Properties of Vortex Rings

To make a list of the desired parameters of a vortex ring, we can use results of the experimental studies of the vortex ring structure presented in Chapter 2 and conclusions from existing theoretical models of vortex rings. According to these data, a formed vortex ring can be imagined as a closed volume of vortical liquid with a shape close to an "oblate" ellipsoid of revolution which moves in the surrounding fluid with translational speed along the minor axis of the ellipsoid (see Fig. 3.2*b*). This closed volume of the fluid is called vortex atmosphere. The motion of the medium around the vortex atmosphere is similar in pattern to a potential flow without separation past the corresponding solid body. Inside the vortex atmosphere, the fluid circulates along closed streamlines that encompass the toroidal vortex core consisting of circular vortex lines. The vorticity distribution in the meridional section of the vortex ring has the form of a bell-shaped curve (see Fig. 2.21) with the maximum at the center of the core. About half the total vorticity flux (velocity circulation flux) is concentrated within the core, which, in most cases, occupies only 3–5% of the cross-sectional area of the vortex atmosphere. The main properties of a vortex ring with the specified structure are characterized in a simplified form by the following finite set of parameters (see Fig. 3.2*b*):

R, radius of the vortex ring (or the radius of the circular axis of the vortex);
A, radius of the vortex core;
h and l, lengths of the semiaxes of the vortex atmosphere;
u_0, translational velocity of the vortex ring;
Γ, total circulation of velocity of the vortex ring (along the outer closed streamline C encompassing the vortex atmosphere;
γ, velocity circulation around the vortex core;
V, volume of the vortex atmosphere;
P, impulse of the vortex ring.

Using the quantities R_0, V_0, ρ, we can write the parameters of the vortex ring in dimensionless form

$$R_* = \frac{R}{R_0}; \quad a_* = \frac{a}{R_0}; \quad u_0^* = \frac{u_0}{V_0}; \quad \Gamma_* = \frac{\Gamma}{V_0 R_0}; \quad \gamma_* = \frac{\gamma}{V_0 R_0};$$

$$V_* = \frac{V}{\pi R_0^3}; \quad \frac{h}{R_0}; \quad \frac{l}{R_0}; \quad P_* = \frac{P}{\pi\rho R_0^3 V_0}. \tag{3.2}$$

Some relative quantities, h/l, γ/Γ, and $\varepsilon = a/R$, are also convenient to characterize the structure of the vortex ring in discussion of the experimental results. As noted earlier, the vortex ring parameters were determined from the velocity field measured by two hot-wire anemometer probes. The probes were placed on the vortex ring path at a distance $z = 12R_0$ from the nozzle exit. The distance was chosen such that in all experiments by the time the vortex arrived at the probes the formation of a vortex ring had been completed. The principles of measuring the velocity field, speed of translation and determining of some integral properties of a vortex ring are practically the same as those used to study the structure of a laminar vortex ring. These techniques as well as details of determination of some parameters of vortex rings are described in Chapter 2. The experimental results obtained in the present investigation are presented graphically below as dependence of the dimensionless parameters and properties of a vortex ring (3.2) on dimensionless criteria (3.1) which determine conditions of ring formation.

3.4 Vortex Ring Parameters as Functions of Jet Length

The influence of the jet length or discharge duration $L_* = V_0 T / R_0$ on the properties of a vortex ring was studied at a fixed jet velocity $V_0 = 7.3$ m/s, which corresponds to the Reynolds number of the jet $\mathrm{Re} = 1.825 \cdot 10^4$ (for $R_0 = 0.0375$ m). The nozzle cone angle was $\theta = 13.13°$. The jet length was varied by changing the time of jet discharge *T*. The studies of vortex rings were performed for five values of the jet length: $L = V_0 T = 70,\ 142,\ 286,\ 420,\ 695$ mm $(1.87 \le L_* \le 18.53)$. Experimental characteristics of the vortex rings that form with these jet parameters are shown in Fig. 3.4 as functions of the dimensionless jet length L_*. One can see that the main dimensionless parameters of the vortex ring increase rapidly with an increase in L_* while $L_* \le 6$–8. With a further increase in jet length, the rate of growth of all parameters slows down, and the translational velocity u_0^*, ε and γ/Γ virtually do not change (see Fig. 3.4). Only the radii of the vortex R_* and of the core a_*, and the velocity circulation Γ_* continue to increase notably. The volume of the vortex atmosphere V_* and the impulse of the ring P_* at large L_* depend almost linearly on the length of the jet ejected from the nozzle.

Circulation of a vortex ring as a function of L_* was also measured by other authors (Didden 1979; Gharib et al. 1998). The work by Gharib et al. (1998) deserves special consideration. They found that the circulation of a vortex ring increases with the jet length L_* only until $L_* \le 8$–10, and subsequently remains constant, despite

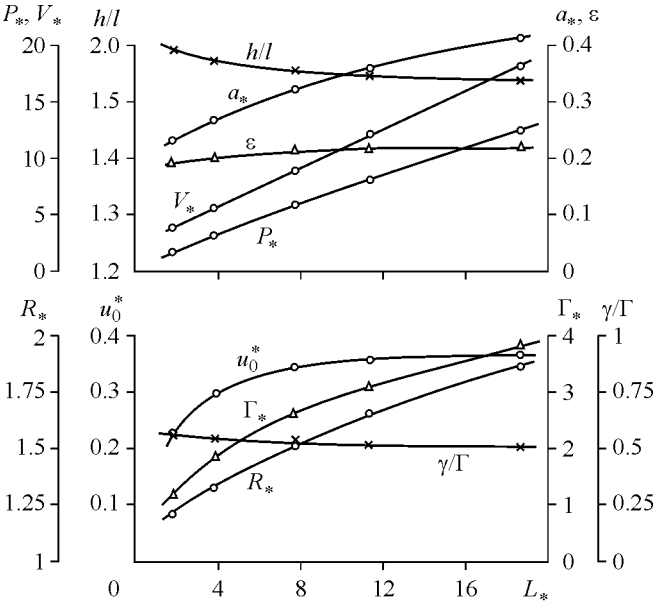

Fig. 3.4. Vortex ring parameters versus the jet length L_*

the continuing ejection of the jet. Evidently, this conclusion contradicts the result of the experimental study (Akhmetov 2001) presented in Fig. 3.4, which implies that the circulation of a vortex ring increases monotonically with the jet length at least up to $L_* \approx 20$, and no crisis events in circulation growth are observed at smaller values of L_*. Since the outlined discrepancy between dependences of the circulation of a vortex ring on the jet length is of fundamental nature, let us consider in more detail the layout and conduction of experiments in that study

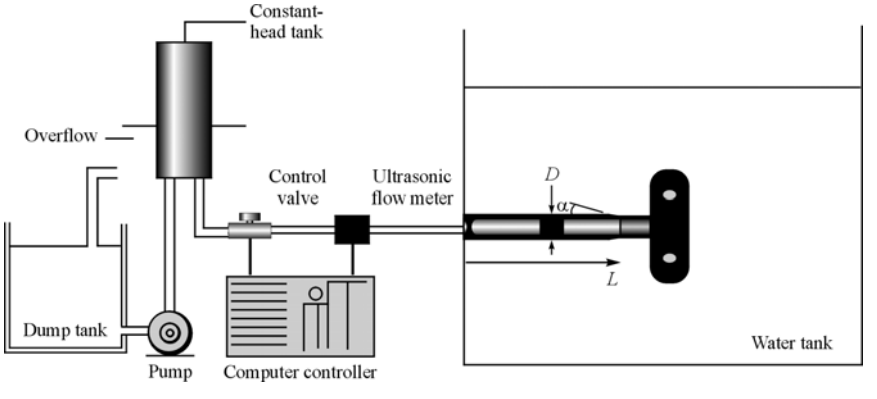

Fig. 3.5. General scheme of vortex ring generator (Gharib et al. 1998)

(Gharib et al. 1998). A vortex ring was generated by a piston pushing a water jet from a cylindrical tube with the inner diameter $D = 2R_0 = 25.4$ mm and length ~15*D*. The experimental facility consists of the two water tanks mounted at different heights (Fig. 3.5). A horizontal open-end tube with a movable piston inside it was inserted into the lower tank. It is this tank where observations and studies of vortex rings formed on expelling a water jet from the tank are carried out. The upper tank with a constant water level is connected with the tube space behind the piston by a water conduit. When the valve in the conduit is opened, the water head in the upper tank drives the piston which pushes the fluid filling the tube out of its open end. A computer-controlled valve allowed one to obtain various velocity programs of the piston and various durations of jet discharge. In the experiments the velocity of the jet flowing out of the tube U_p was determined indirectly, by measuring the average velocity in the conduit which supplies water from the upper tank to the tube space behind the piston, rather than by the direct measurement of the piston velocity or velocity profile of the jet in the exit outlet of the nozzle. The two basic series of experiments were performed at jet velocities of 7.5 and 15 cm/s. The piston stroke *L* and hence the length of the jet flowing out from the tube were determined by integrating the velocity U_p over time, $L = \int_0^t U_p dt$. The velocity flow field in the lower tank arising due to jet discharge from the tube measured using the PIV (Particle Image Velocimetry) technique (Willert and Gharib 1991) allows determination of the vorticity in the plane passing through the tube axis. This vorticity distribution enables calculation of the circulation in a vortex ring being formed during the jet discharge. The circulation of the vortex ring is compared with the value of the total circulation that appears in the fluid on jet discharge, whose current value was estimated at $\Gamma(t) = (1/2)\int_0^t U_p^2 dt$. A typical plot of the total circulation $\Gamma(t)$ in the fluid and circulation of the forming vortex ring as functions of dimensionless discharge time $U_p t/D$ is shown in Fig. 3.6. This plot implies that at $U_p t/D \approx 4$–5 (which corresponds to the dimensionless jet length $L_* = L/R_0 = 8$–10 with the notation adopted in the beginning of this chapter) a crisis occurs, namely the circulation of the vortex ring ceases to grow further and subsequently the circulation of the ring remains the same, despite the continuing jet discharge and growth of the total circulation in the fluid. The authors believe that the obtained time value $U_p t/D \approx 4$–5 can be called universal time scale of vortex ring formation, which is a threshold

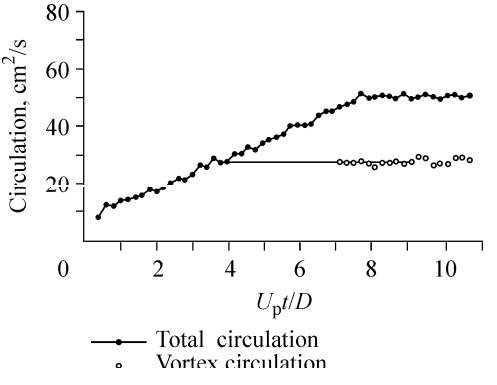

Fig. 3.6. Dependence of circulation on duration of jet discharge (Gharib et al. 1998)

for the circulation of the vortex ring when it reaches its limiting value equal to the total circulation in the fluid at this instant of time. However, according to the data (Akhmetov 2001) presented above in Fig. 3.4, the circulation of the vortex ring continues to increase monotonically with the jet length at $L_* = L/R_0 > 8–10$ (i.e. at $U_p t/D > 4–5$) up to the maximum value of $L_* \sim 20$ achieved in the experiments, and no crisis events at smaller jet lengths are observed. In order to explain the observed saturation of the growth of the vortex ring circulation, Gharib et al. (1998) refer to the visualized patterns of the process of vortex ring formation at various jet lengths (Fig. 3.7). The pictures are taken at a distance $z/D = 9$ from the tube outlet section. The two upper pictures in Fig. 3.7 correspond to the relative jet lengths $L/D = 2$ and $L/D = 3.8$, and give evidence that formation of these rings has been almost completed by the time when the pictures are taken. The lower picture corresponds to $L/D = 8$; here the jet is still being ejected, and behind the main vortex ring that forms in the head portion of the jet, a few more secondary vortex

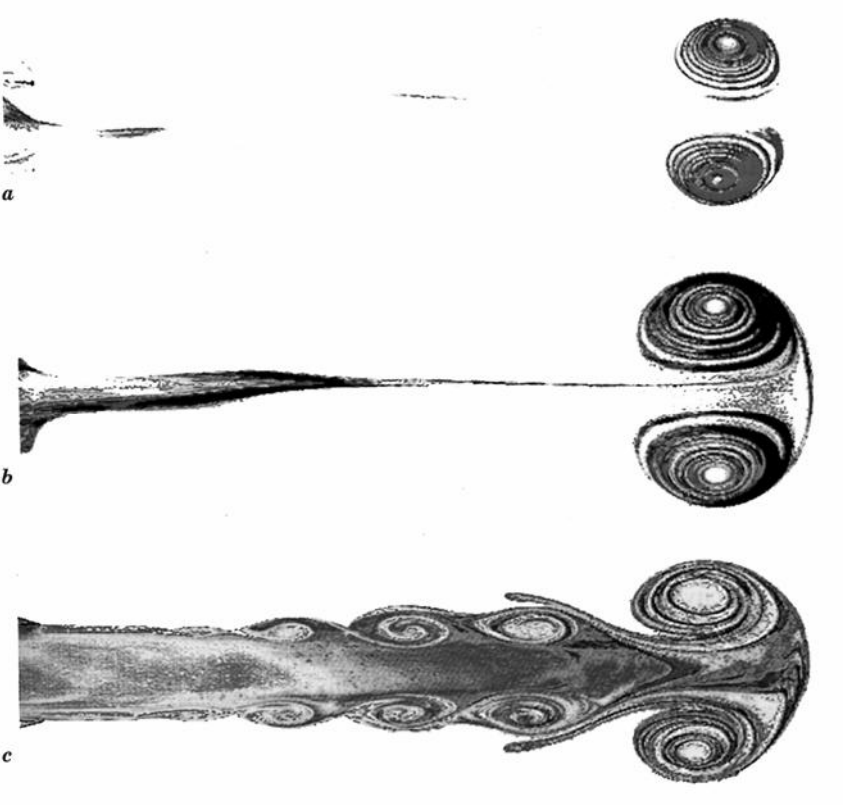

Fig. 3.7. Visualization of vortex ring formation for different durations of jet discharge (Gharib et al. 1998). (*a*) $U_p t/D = 2$; (*b*) $U_p t/D = 3.8$; (*c*) $U_p t/D = 8$

objects are observed. Since the secondary vortices entrain a portion of vorticity of the vortex sheet flowing off the tube edge, it is evident that further growth of the circulation of the leading vortex ring would be limited by the circulation value that has existed by the moment when the secondary vortices start to emerge. This mechanism reasonably explains the effect of limitation of vortex ring circulation discovered in that work and shown in Fig. 3.5. However, it is controversial to state that a dimensionless time of jet discharge equal exactly to $U_p t/D \approx 4–5$ is some universal time scale which characterizes the phenomenon of limitation of the growth of circulation of the vortex ring. In the initial stage of the experiments by Akhmetov (2001), the formation of secondary vortices in the trailing region of the jet was also observed, but it was clarified that origination of the secondary vortices was due to pulsations of the jet velocity. Obviously, pulsations of the jet velocity lead to periodic variations in intensity of the cylindrical vortex sheet flowing off the nozzle edge; as a result, the sheet loses stability and rolls up into secondary vortices. In these experiments pulsations of the jet velocity appeared owing to the excitation of intense acoustic oscillations in the system consisting of an expansion chamber and a nozzle (see Fig. 3.2), which constituted a Helmholtz resonator with a high quality factor. When the resonator quality factor was reduced, the intensity of pulsations of the jet velocity decreased drastically, and the formation of secondary vortices ceased. It follows that as long as the jet length was below $L_* \approx 20$ (i.e. for $L/D \le 10$), the secondary vortices appeared as a consequence of pulsations of the jet velocity, rather than owing to a natural instability of the vortex sheet. After the pulsations of the jet velocity had eliminated, the formation of secondary vortices ceased. Monotonic growth of the vortex ring circulation in Fig. 3.4 with an increase in the jet length up to $L_* \sim 20$ directly confirms that only a one-head vortex ring forms. It is difficult to point to a specific mechanism which might be responsible for the early development of instability of the mixing layer of the jet flowing out of the tube and for the origination of secondary vortices in the study considered (Gharib et al. 1998). We can only suggest that the secondary vortices in these experiments appeared either due to a stick-slip motion of the piston inside the tube, or due to transverse oscillations of the exit end of a rather long cantilever fitted tube as the piston moved inside. Of course, one cannot argue that it would be possible to prevent loss of vortex sheet stability and formation of secondary vortices at any duration of jet discharge. At the same time one cannot accept, following Gharib et al. (1998), that the time value $U_p t/D \approx 4–5$ is really some universal time scale characterizing the process of vortex ring formation. To determine the maximum possible duration of jet discharge above which a system of vortices forms instead of a single vortex ring even without any noticeable external perturbations of the jet, but rather due to a natural instability of a vortex sheet, further more subtle investigations are needed. It is only clear that this threshold value of L_* exceeds 20 and is probably a function of the Reynolds number of the jet.

3.5 Dependence of Vortex Ring Parameters on the Jet Reynolds Number

The effect of the jet Reynolds number $\mathrm{Re} = V_0 R_0 / \nu$ on the vortex ring structure was studied at constant values of the jet length $L_* = V_0 T / R_0 = 2.5$ and angle $\theta = 13.13^\circ$. The Reynolds number was varied by changing the jet velocity V_0 due to the change of the passage section of quick-response valve *2* (see Fig. 3.2). To keep the jet length $L = V_0 T$ constant, the time of jet discharge *T* was varied to follow the variation of jet velocity. The most thorough studies of the vortex ring structure were performed at jet velocities V_0 = 7.5, 11.5, 20, 29 m/s, i.e. for the jet Reynolds number ranging from $1.875 \cdot 10^4$ to $7.2 \cdot 10^4$. Some properties of a vortex ring were also determined at significantly lower Reynolds numbers, as small as $\mathrm{Re} \sim 20$.

Laminar and turbulent vortex rings

Observation of visualized flow pattern in a vortex ring imply that depending on the jet Reynolds number two different types of vortex rings form. For $\mathrm{Re} \le (1–2) \cdot 10^4$, laminar vortices form with a layered spiral structure, which is retained as the vortex moves further. A smoke visualization photograph of a laminar vortex ring taken shortly before the end of formation process is shown in Fig. 3.8. Turbulent vortex rings that form at large Re numbers are not layered. The flow in their atmosphere is turbulent. However, smoke visualization reveals well-cut toroidal vortex core (Figs. 3.9, 3.10, 1.1). Illumination of the vortices by a sheet light beam in the meridional plane provided photographs of vortex cross-sections shown in Figs. 3.8 and 3.9. Figure 3.10 shows the front view of a turbulent vortex ring. It is worth noting that along the toroidal core the smoke is distributed not uniformly, but in periodical bunches, and the core itself consists of seemingly separate cells bounded by the torus surface and meridional planes (see Fig. 3.10). The number of cells in this photograph is 26. Additional studies showed that the cellular smoke structure exists outside the vortex core, and inside the core the smoke is distributed uniformly. Comparison of this pattern with the other known phenomena of periodic distribution of fine particles in fluids (for example,

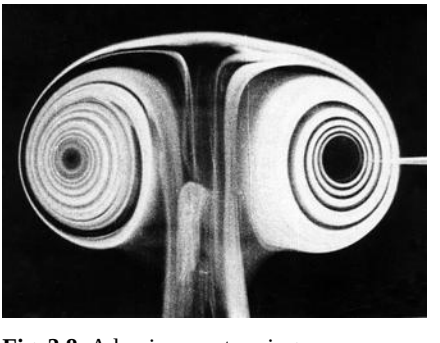

Fig. 3.8. A laminar vortex ring

Fig. 3.9. A turbulent vortex ring

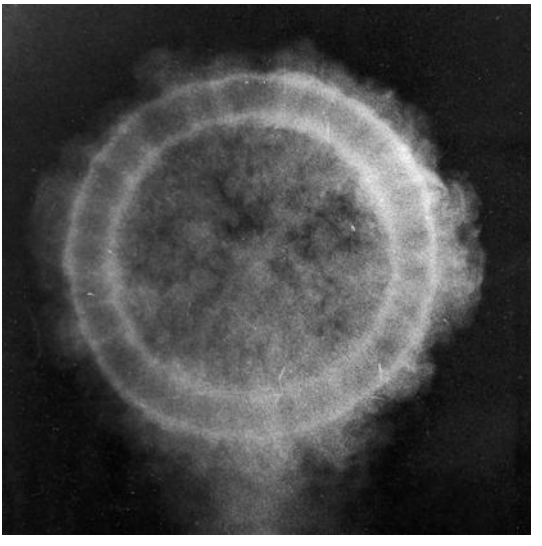

Fig. 3.10. The core of a turbulent vortex ring

aggregation of dust in nodes of standing sound waves in a tube or Taylor vortices between rotational coaxial cylinders) suggests that for certain Re numbers, there exists a secondary nonaxisymmetric flow near the core. One possible type of such secondary flow may be represented by radial fluid motions directed from the core near certain cell boundaries and to the core near the neighboring boundaries. Obviously, the number of cells at the torus in this case should be even.

Results of measurements of vortex ring parameters as functions of Reynolds number are presented in Fig. 3.11. It can be seen that the strongest dependence of vortex ring parameters on Re is observed for $\mathrm{Re} \le 10^4$, i.e. for laminar vortex rings. The plots imply that for $\mathrm{Re} > (1\text{–}2)\cdot 10^4$, i.e. when a vortex ring is turbulent, the dimensionless values of the radius R_* and circulation Γ_* of the vortex rings are virtually independent of Re. Variations in the translational velocity u_0^* for $\mathrm{Re} > 10^4$ are also negligible. It is established that circulation around the core γ_* is virtually constant, $\gamma_* \approx 0.565\text{–}0.575$. At large Reynolds numbers the cross-section of the vortex core has almost circular shape, and the core radius a_* decreases with an increase in Re. It means that vorticity in the core becomes more concentrated as the Reynolds number increases. Analysis of the vorticity distribution showed that the vortical region of the laminar vortices which can be

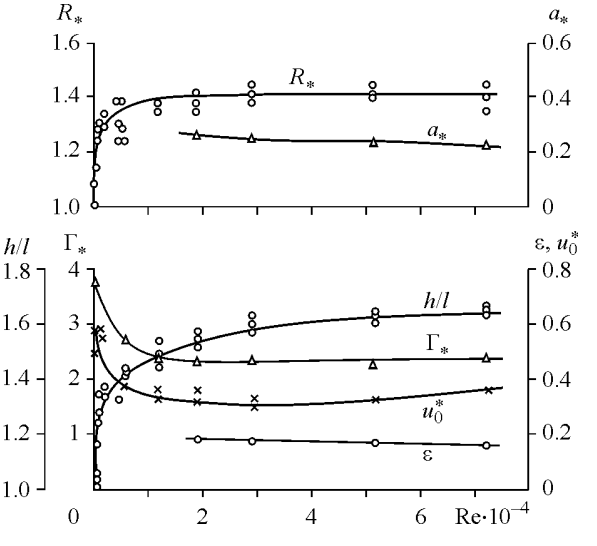

Fig. 3.11. Experimental dependence of vortex ring properties on the jet Reynolds number

also called the vortex core, occupies a considerable area of the meridional section of the vortex atmosphere, and the core section is out-of-circle in shape. Therefore, for small Re, the parameter $\varepsilon = a/R$ was determined as $\varepsilon = (s/\pi R^2)^{1/2}$, where s is the cross-sectional area of the vortex core. Configuration and dimensions of the vortex atmosphere are of interest. It is experimentally established that the transverse semiaxis of the vortex atmosphere h seems not at all to depend on Re, and the longitudinal semiaxis l increases rapidly as Re decreases. As a result, with decreasing Re, the ratio of the semiaxes h/l tends to unity, i.e., the vortex atmosphere becomes near-spherical. The photographs of the vortex ring produced at Re = 20 are shown in Fig. 3.12. This vortex ring was generated by jet ejection from a 1 cm diameter nozzle by a piston, and the working media were high viscosity solutions of glycerin in water. Although the axis of the nozzle of the vortex generator was oriented horizontally, which complicated homogeneous coloring of the whole volume of the vortex, one can see that the vortex atmosphere is near-spherical (see Fig. 3.12). Apparently, such laminar vortex rings are similar in structure to a theoretical model of a spherical Hill's vortex discussed in Chapter 1.

Note that high-speed turbulent vortex rings are characterized by considerable angular velocities of the fluid in the core. The mean angular velocity in the core $\tilde{\omega}$ can be estimated as the ratio of the linear velocity u_c on the boundary of the core to the core radius a, $\tilde{\omega} \sim u_c/a$. According to measurement results, for $\mathrm{Re} \geq 10^4$ the mean linear velocity u_c on the core boundary of high-velocity vortex rings can be estimated at $u_c \approx (3\text{–}5)u_0$, hence the following estimate is valid $\tilde{\omega} \sim (3\text{–}5)u_0/a$. The data given in Fig. 3.11 implies that for $\mathrm{Re} = 7.25 \cdot 10^4$ the vortex ring is characterized by the values $u_0 \approx 11$ m/s, $\varepsilon = a/R \approx 0.154$, $R_* = R/R_0 \approx 1.42$. Substituting these values of a and u_0 into the expression for the angular velocity yields $\tilde{\omega} \approx (20\text{–}33)u_0/R$ and hence, the angular velocity in the core of this vortex ring is $\tilde{\omega} \sim (4.2\text{–}7) \cdot 10^3$ s^{-1}. In several experiments vortex rings were generated by means of a shock tube, and such vortex rings had a speed of translation of $u_0 \geq 100$ m/s (in particular, we achieved $u_0 = 99$ m/s, $R = 33$ mm) at $V_0 = 198$ m/s and $R_0 = 25$ mm. Estimating the angular velocity in this case from the above formula,

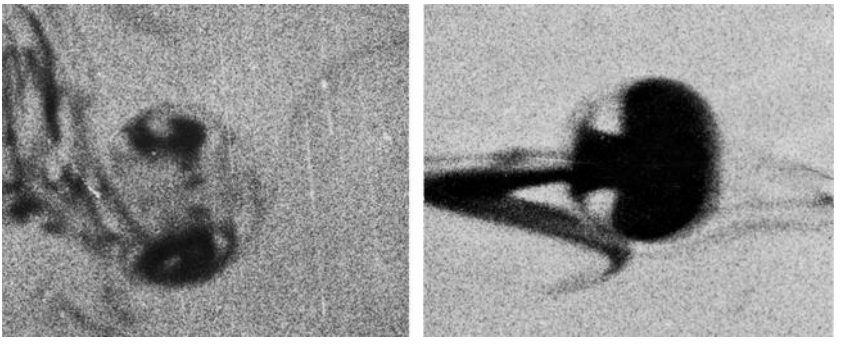

Fig. 3.12. A spherical vortex ring

we obtain for this high-speed vortex ring $\tilde{\omega} \approx 10^5$ s^{-1} (i.e. $n \approx 10^6$ rev/min). One might expect that at such values of the angular velocity the gas (air) pressure and density in the vortex core substantially drop, and the effects of compressibility of a medium may emerge. Some experimental results on high-speed vortex rings generated by shock tubes and also on plasma vortex rings can be found in literature (Elder and Haas 1952; Yusupaliev 2005).

Turbulence in the vortex ring

A special feature of the plots presented in Fig. 3.11 is that all parameters of the vortex ring vary smoothly as its structure changes from laminar to turbulent (at $\mathrm{Re} \sim 10^4$), without any jumps and hysteresis effects which are characteristic of the transition from laminar to turbulent regime in shear flows. Of great interest is the structure of turbulence in a vortex ring, since peculiarities of turbulence in vortex rings may be typical of other types of concentrated vortices as well. At present, no sufficiently complete systematic studies of turbulence in concentrated vortices are available. Some idea of turbulence in a vortex ring can be inferred from registration of turbulent velocity fluctuations. Figure 3.13 shows velocity oscillograms in a turbulent vortex ring measured by hot-wire anemometers along the line parallel to the *z*-axis and intersecting the vortex core. These signals were obtained for $L_* = 2.5$ and $\mathrm{Re} = 7.5 \cdot 10^4$ (R = 51.5 mm, u_0 = 11 m/s). The minimum values of the signals at the center of the frame correspond to the center of the vortex core, and the maximum values on both sides from the core correspond to the core boundary. This implies that inside and far from the core velocity fluctuations are few to absent. Near the core boundary fluctuation amplitudes become as large as mean velocity values in this region (this is evident, as the value of the measured velocity is approximately proportional to the fourth power of the hot-wire probe signal). It may be noted that the velocity fluctuations are not stochastic as in boundary layers, but are quasi-periodic in nature. We may state from the distribution of velocity fluctuations that the flow in the core of a turbulent vortex ring is laminar and turbulence exists only outside the core. This conclusion is substantiated by a visualized flow pattern. Being formed of air homogeneously colored with smoke, the turbulent vortex ring attains the shape of a torus with distinct boundaries, although the vortex atmosphere around the ring moves together with it (see Fig. 3.9, 3.10). It means that, because of turbulent diffusion, the smoke particles soon escape from the vortex atmosphere and remain only inside the core and close to its boundary. Vladimirov and Tarasov (1979b) and Vladimirov et al. (1980) demonstrated that on passage of a vortex ring through a colored fluid cloud, the whole vortex atmosphere becomes colored except for the

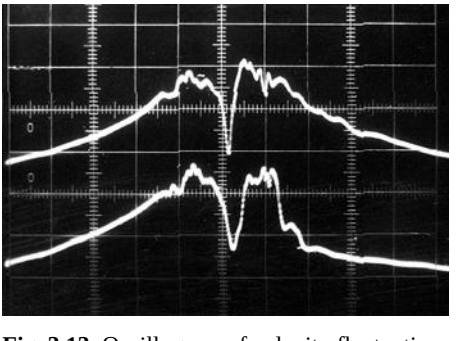

Fig. 3.13. Oscillogram of velocity fluctuations near the boundary of the vortex core

vortex core, where there is no dye. These experiments suggest that turbulent mixing occurs only in the vortex ring atmosphere, whereas the vortex core remains laminar. The discovered phenomenon that concentrated vortices, which are in general turbulent, have laminar cores, is called suppression of turbulence in the cores of concentrated vortices (Vladimirov and Tarasov 1979b; Vladimirov et al. 1980) and is explained by the elasticity effects of rotating flows (Greenspan 1968).

In order to interpret the nature of velocity fluctuations near the core boundary, one can address the results of the special study of the vortex core structure (Akhmetov and Tarasov 1986). This work reports a detailed investigation of the flow between two coaxial disks rotating with a constant angular velocity in the same direction. On the axis of symmetry between the disks there appears a vortex whose core is distinctly visualized with smoke (Fig. 3.14). The measurements of the velocity of this flow in the fluid using a laser Doppler anemometer give radial distributions of the azimuthal velocity component u and vorticity ω between the disks (Fig. 3.15), which show that a linear vortex with a rigidly rotating core emerges between the disks. By making the flow pattern visible, it was established that the vortex core cross-section loses its circular symmetry when a certain critical Reynolds number $\mathrm{Re} = R^2 n/\nu$ (composed of the radius R and angular velocity n of the disks) is exceeded and, depending on Re, takes on the shape of an oval, triangle, quadrangle, etc. (Fig. 3.16). The polygonal shape of the vortex cross-section is virtually independent of the axial coordinate in the entire flow region, except for thin boundary layers at the disks, and hence the vortex core is a polygonal prism rotating about the disk axis at some angular velocity. Obviously, the observed picture of the core cross-section represents an azimuthal wave running over the surface of the core, which is perceived by an eye and recording equipment as a polygon. The results of the measurements are in qualitative agreement with the conclusions of theoretical studies of the structure and wave perturbations

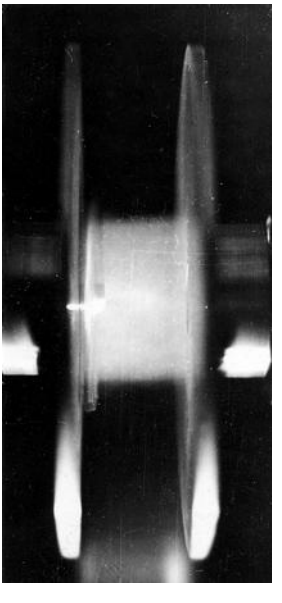

Fig. 3.14. A linear air vortex between rotating disks. Smoke visualization. Disk axis is horizontal

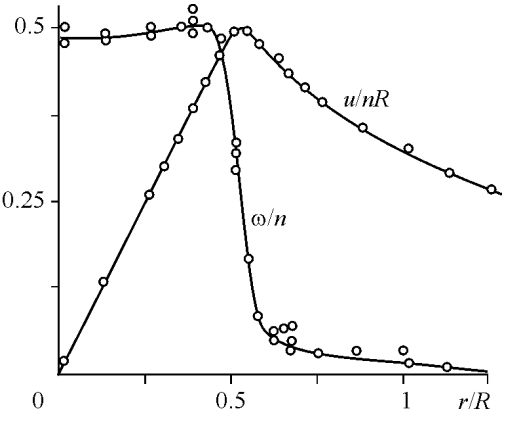

Fig. 3.15. Distribution of the azimuthal velocity component and vorticity in the vortex core between the disks. $\mathrm{Re} = 2 \cdot 10^5$

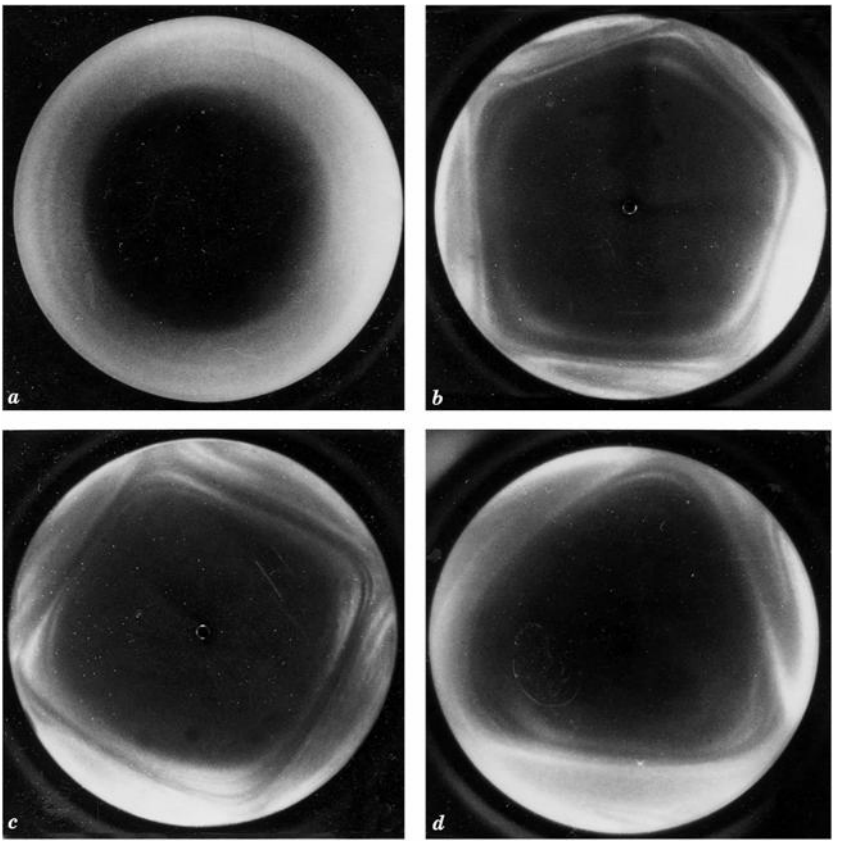

Fig. 3.16. Polygonal shapes of the vortex core cross-section. (*a*) Re < 10^3; (*b*) Re = 10^3; (*c*) Re = $1.5 \cdot 10^3$; (*d*) Re = $2 \cdot 10$

of vortex cores in plane flows (Abrashkin and Yakubovich 1987; Abrashkin and Zenkovich 1997; Abrashkin 1999).

For sufficiently large Reynolds numbers, when the flow becomes turbulent, a system of smaller secondary vortices appears in the vortex core (Fig. 3.17). These secondary vortices have somewhat larger vorticity than its average value over the core cross-section. The core is being deformed in a continuous way to take the form of polygons with the number of corners changing at different instants of time. When the core cross-section shape experience abrupt transformations, the vortex core ejects vortical fluid masses from the polygon corners to the surrounding flow. This ejected fluid propagates radially in the form of spiral arms (Fig. 3.18). Non-vortical fluid from the surrounding medium is captured into the ring along the inner surface of the spiral arms.

Thus, diffusion of vorticity from the vortex core is neither axisymmetric nor continuous, but rather occurs through ejection of discrete jets of the vortical fluid in the form of spiral arms. Similar phenomena are essential for other types of

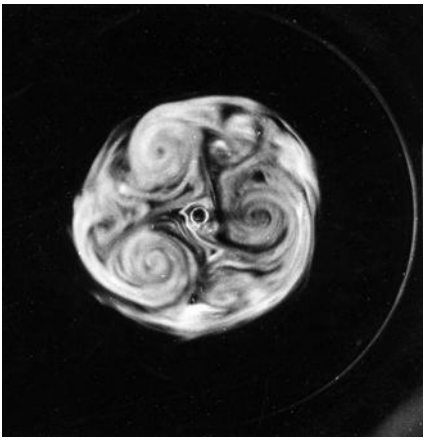

Fig. 3.17. A system of secondary vortices in the core of the primary vortex. $Re = 4.9 \cdot 10^4$

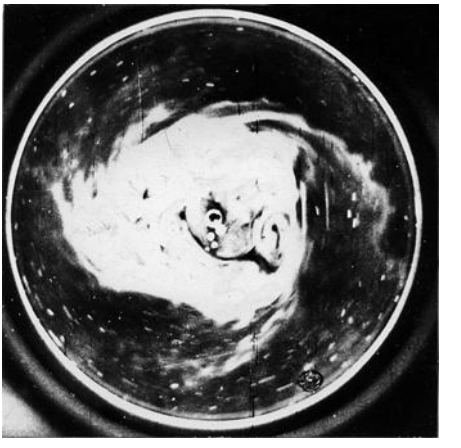

Fig. 3.18. Ejection of the vortical fluid from the core in the form of spiral arms. $Re = 4.9 \cdot 10^4$

concentrated vortices as well and in particular can be observed in the cores of vortex rings (Fig. 3.19).

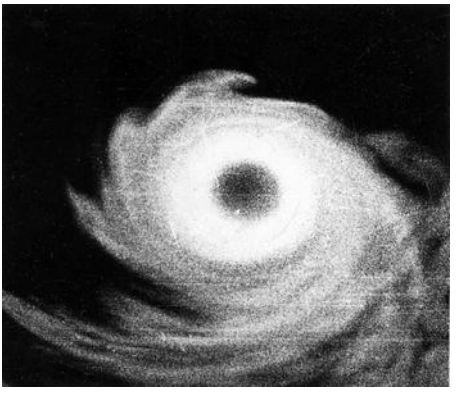

Fig. 3.19. Spiral jets on the surface of a turbulent vortex ring

These experiments suggest that the velocity fluctuations observed on crossing of the vortex core by the measuring probes (see Fig. 3.13) can be caused by deformations (wavy perturbations of the surface) of the cross-section of the core of the vortex ring and by ejection of jets of vortical fluid in the form of spiral arms. Thus more thorough experimental and theoretical investigations of oscillations and stability of con centrated vortices are required. Such studies were pioneered by Kelvin (1880). The subsequent works (Krutzsch 1939; Maxworthy 1977; Widnall et al. 1974; Saffman 1978) showed that a vortex ring can be unstable also with respect to bending perturbations of the core. The modern status of research on oscillations, stability and transition to turbulence of vortex rings is presented in a fundamental review by Kop'ev and Chernyshev (2000). The authors determined the main types of vortex ring oscillations and established that a vortex ring with monotonically decreasing vorticity outside the core is also unstable with respect to small perturbations. Shear instability is due to interaction between oscillations of the vortex core and a flow outside the core with the decreasing vorticity, where a system of critical layers with intensification of vorticity field emerges. This review also

presents reasonable speculations on how the nonlinear stage of instability development may lead to turbulence in the vortex atmosphere. Thus, the results of the works discussed here demonstrate that turbulence most likely occurs in the atmosphere of a vortex ring, but does not penetrate into the vortex core, so that the flow in the core remains laminar.

3.6 Dependence of Vortex Ring Parameters on the Nozzle Angle of Taper

The influence of the taper angle θ of the outer surface of the nozzle (see Fig. 3.2) on vortex ring parameters was studied at $\mathrm{Re} = 4.05 \cdot 10^4$, $L_* = 3.07$ for the four values of the angle θ: 13.13, 39, 65, and 90°. We used the nozzles with quite sharp edges, and the generator of the outer cone surface was 200 mm long in all experiments. The most essential results of this series of experiments are presented in Fig. 3.20, which shows that the vortex ring parameters depend weakly on θ.

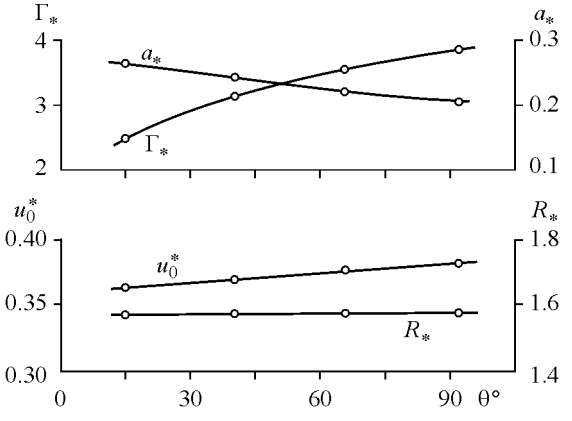

Fig. 3.20. Influence of the nozzle angle of taper on vortex ring parameters

3.7 Comparison between Some Conclusions from Theoretical Models of Vortex Rings and Experiment

The experimental data obtained above can be used to compare some conclusions of the existing theoretical models of vortex rings with the actually observed structure of vortex rings. Of course, such a comparison is somewhat conventional in nature, since the majority of the existing models have been derived ignoring medium viscosity and based on the assumption that vorticity is concentrated only within the toroidal vortex core, outside of which the flow is non-vortical. Under these assumptions, the cross-section of the vortex core has sharp boundaries and the core dimensions are well defined. The notion of a vortex core is a conventional characteristic of real vortex rings, since the vorticity distribution in the meridional cross-section

of the vortex ring is represented by a continuous bell-shaped function that smoothly decays to zero with distance from the point of maximum vorticity. Thus, there is no physical boundary separating the vortex core from the flow outside the core. Nevertheless, the notion of a vortex core occurs to be appropriate for approximate description of the structure of real vortex rings by a finite number of parameters. In this case the vortex core is defined either as a region of the meridional cross-section of the vortex ring, where vorticity exceeds half its maximum value, or by other means (for example, from distribution of the rotational velocity component in the vicinity of the point of maximum vorticity) considered in Chapter 2. It is clear that because different definitions exist, the area and dimensions of the core section of a real vortex ring are not uniquely and exactly measured parameters.

The theoretical models imply that the geometric dimensions and kinematic parameters of a vortex ring depend heavily on the dimensionless parameter ε, the ratio of the effective transverse size of the core section to the radius of the ring itself, $\varepsilon = (s/\pi R^2)^{1/2}$, where s is the cross-sectional area of the core and R is the ring's radius. For thin vortex rings whose core section is a circle of radius a, obviously, $\varepsilon = a/R$. The parameter ε is characteristic of vorticity concentration and, hence, of vortex ring structure.

It is known that a moving vortex ring carries along a certain volume of fluid called vortex atmosphere. The vortex atmosphere commonly has the shape close to an ellipsoid of revolution oblate in the direction of motion. According to the results of Sections 1.6, 1,8, the ratio h/l of the transverse semiaxis h of the vortex atmosphere to the longitudinal semiaxis l is determined by the parameter ε. Dependence of h/l on ε based on the experimental and theoretical data is shown in Fig. 3.21. The solid curve represents the theoretical dependence, symbols denote the experimental points obtained by various authors and the point corresponding to the numerical calculation by Lugovtsov (1979) of the self-similar structure of a vortex ring as the turbulent viscosity coefficient tends to zero. As seen from the plot, the experimental points lie slightly below the theoretical curve, but the

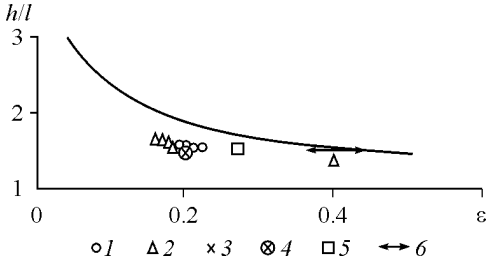

Fig. 3.21. Dependence of the semiaxes of the vortex ring atmosphere on the parameter ε. Solid line represents theoretical calculation from Sect. 1.6 and numerical calculation by Norbury (1973). Experimental points: (*1*) experiments from Sect. 3.5; (*2*) experiments from Sect. 3.6; (*3*) experiments from Sect. 3.7; (*4*) experiments from Chapter 2; (*5*) experiments by Sullivan et al. (1973); (*6*) model of a turbulent vortex ring (calculation) by Lugovtsov (1979)

qualitative character of the theoretical dependence of the parameter h/l on ε is consistent with the experimental data (see Fig. 3.21).

It is interesting to compare the theoretical values of the vortex ring impulse and speed of translation with the experiment. Theoretical studies (see Chapter 1) suggest that for small values of ε, the impulse P and the translational velocity u_0 are related to the radius R and the circulation Γ through the expressions of the form $P = \pi\rho R^2\Gamma\, f_1(\varepsilon)$ and $u_0 = (\Gamma/4\pi R)\, f_2(\varepsilon)$, where f_1 and f_2 are functions of ε. It is also known that $f_1(\varepsilon) = P/\pi\rho R^2\Gamma \approx 1$ as $\varepsilon \to 0$, which is accurate to ε^2, and f_2 depends on ε logarithmically, $f_2 \approx \ln(8/\varepsilon) - 1/4$. The values of f_1 and f_2, found from the experimental values of R, Γ, P, u_0 and calculated as functions of ε are given in Figs. 3.22 and 3.23. Figure 3.22 shows that the experimental values of the function f_1 are close to unity over a sufficiently wide range of values ε, which allows (1.23) to be used for estimating the vortex ring impulse. The theoretical function $f_2(\varepsilon)$ (solid curve in Fig. 3.23) also qualitatively agree with the experimental data, but the quantitative agreement between theory and experiment is worse in this case. This discrepancy may be due to both imperfection of the theoretical models of a vortex ring and insufficiently correct determination of the parameter ε from the experimental vorticity distribution.

It may be noted that calculations of the translational velocity u_0 from the theoretical formulas obtained in Chapter 1 and from the experimental values R, Γ, ε virtually always give overestimated values for u_0, which apparently indicates that these formulas are inappropriate for quantitative evaluation of the translational speed of real vortex rings with wide smooth vorticity distribution.

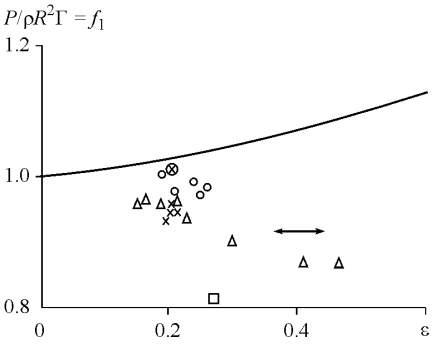

Fig. 3.22. Impulse versus the parameter ε. Solid line represents calculation by Norbury (1973). See the legend in Fig. 3.21

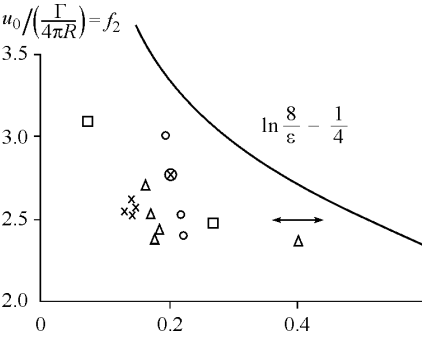

Fig. 3.23. Translational velocity as a function of the parameter ε. Solid line represents calculation by Eq. (1.26). See the legend in Fig. 3.21

4 Vortex Ring Formation

The results of the experimental investigations of the vortex ring structure presented in Chapter 3 show how its parameters depend on the formation conditions and can be used to generate vortex rings with prescribed properties. However, the very mechanism of vortex ring formation has not been addressed yet, though it is evident that the laws of formation are interesting to be revealed not only from the physical point of view, but also in the context of theoretical estimations of the vortex ring parameters as functions of the initial conditions which determine its formation process.

4.1 Vortex Ring Generation by Impulsive Motion of a Circular Disc

Vortex rings can be generated by various methods, and in all cases it is important to determine the ring parameters that depend on its formation conditions. One method implies that a flat circular disk of radius c submerged into a fluid is suddenly moved forward with velocity U along the axis of symmetry; after that, the disk is immediately removed from the fluid. Vortex rings of this kind (more exactly, half-rings) can be observed, for instance, on the surface of coffee poured into a cup, which is rapidly stirred by a small spoon half-submerged into the cup (Klein 1910; Anton 1939; Betz 1950). Through simple and clear considerations, Taylor (1953) derived formulas for estimating the parameters of the vortex ring formed owing to the disk motion.

In the beginning of the disk motion when separation of flow from the disk edge has not yet developed, the flow generated by the disk may be assumed to be potential. Calculation of this potential flow is presented in many textbooks on hydrodynamics (Lamb 1932; Kochin et al. 1964; Batchelor 1967). In particular, the velocity potential on the disk is determined in cylindrical coordinates z, r, θ by the expression $\varphi = \mp 2U\pi^{-1}(c^2 - r^2)^{1/2}$ for $z = \pm 0, \quad r < c,$ and the radial velocity on the surface of the disk is $\pm(2Ur/\pi c)(1 - r^2/c^2)^{-1/2}$. The upper sign in these formulas correspond to the side towards which the disk is moving. If now the disk were suddenly removed from the fluid, there would be a plane disk-like vortex sheet consisting of concentric vortex lines with the center at the disk axis. The strength of the vortices γ and vorticity ω of the vortex sheet are determined by

$$\gamma(r) = \frac{4U}{\pi} \frac{r}{\sqrt{c^2 - r^2}}, \qquad \omega = \gamma(r)\,\delta(z),$$

where $\delta(z)$ is the Dirac delta function. Owing to axial symmetry, the vortex impulse of the sheet is directed along the z-axis and according to the impulse definition (1.16), (1.17) it has the value

$$P = \frac{1}{2}\rho\left|\int_V (\mathbf{r}\times\boldsymbol{\omega})\,dV\right| = \frac{1}{2}\rho\iint_\Sigma \omega r^2 d\Sigma = \frac{1}{2}\rho\int_0^c 2\pi\gamma r^2 dr = \frac{8}{3}Uc^3. \tag{4.1}$$

The kinetic energy of the potential flow is

$$T = \frac{\rho}{2}\iint \varphi\frac{\partial\varphi}{\partial n}d\Sigma = -\frac{\rho U}{2}\int_0^c 2\pi r(\varphi_- - \varphi_+)dr = 4\rho U^2\int_0^c r\sqrt{c^2-r^2}\,dr = \frac{4}{3}\rho U^2 c^3, \tag{4.2}$$

since at the disk $\partial\varphi/\partial n = -U$. The velocity circulation around a contour that starts and ends in the center of the disk is

$$\Gamma = \int_0^c \gamma\,dr = \frac{4Uc}{\pi}. \tag{4.3}$$

The vortex sheet remaining after removal of the disk, subsequently rolls up into a toroidal spiral and finally transforms into a vortex ring of radius R. No other vortical structures, apart from the ring, appear in the fluid. Thus one may assume that it takes the same values of circulation, impulse and energy that were calculated for the disk motion. Considering Lamb's model described in Section 1.6 as the simplest model of a vortex ring, we obtain the following expressions for the impulse, energy and translational velocity of the ring

$$P' \approx \pi\rho R^2\Gamma, \tag{4.4}$$

$$T' = \frac{\rho R\Gamma^2}{2}\left(\ln\frac{8R}{a} - \frac{7}{4}\right), \tag{4.5}$$

$$u_0 \approx \frac{\Gamma}{4\pi R}\left(\ln\frac{8R}{a} - \frac{1}{4}\right), \tag{4.6}$$

where a is the radius of the core of the vortex ring.

From the equality $P' = P$ we have $8\rho c^3 U/3 = \pi\rho R^2\Gamma$. Along with (4.3) it implies that

$$R = \sqrt{2/3}\,c. \tag{4.7}$$

From $T' = T$ and (4.2), (4.5) we have

$$\ln\frac{8R}{a} = \frac{7}{4} + \frac{2}{\rho R\Gamma^2}\frac{4}{3}\rho U^2 c^3 = \frac{7}{4} + \frac{8}{3}\frac{c^3U^2}{R\Gamma^2}.$$

Using (4.3) and (4.7) we obtain $\ln 8R/a = 7/4 + \pi^2 c/6R \approx 3.76$, so that $R/a = 5.37$ and $a/c = 0.152$. Substituting the obtained quantities into (4.6), we find the translational velocity of the vortex ring

$$u_0 = \frac{Uc}{\pi^2 R}(3.76 - 0.25) = 0.436U .$$

Thus, the fundamental characteristics of the vortex ring generated by impulsive motion of the disk are completely determined in terms of the two parameters, namely the radius c and the velocity U of the disk. However, such a method of vortex ring generation, despite its elegance and simplicity, can be considered as a rather speculative experiment or as a method for production of vortex rings for qualitative research only, because it is hardly possible in real experiments to ensure controlled motion and subsequent removal of the disk from the fluid without disturbing the resultant flow.

4.2 Vortex Ring Formation on Outflow of a Submerged Jet

Impulsive vortex rings are mainly generated by exhaustion of a finite-length submerged jet from a circular orifice or from an open end of a cylindrical tube. It was just this very method used for generating the rings which were thoroughly studied in Chapters 2 and 3. Using this technique, it is easy to determine and control the condition of vortex ring formation. Here also emerges the problem of obtaining analytical estimations of the properties of the vortex ring being formed depending on the parameters of the jet and experimental facility. This problem attracted the attention of many researchers (Wedemeier 1961; Bardotti and Bertotti 1964; Saffman 1975; Didden 1979; Pullin 1979; Vladimirov and Tarasov 1980; Nitzsche 1996; Sullivan et al. 2008). Saffman (1975) considered the model of vortex ring formation from a finite-length cylindrical vortex sheet in an unbounded fluid. The energy, impulse and circulation of the vortex sheet are equated to the energy, impulse and circulation of the vortex ring, hence providing the estimation of the vortex ring parameters. Obviously, such problem statement is analogous to the problem of estimating the parameters of the vortex ring generated by disk motion considered above. In fact, the same technique was also used by Sullivan et al. (2008) to estimate the vortex ring parameters. This model, however, is inconsistent with the real pattern of vortex ring formation, because the cylindrical sheet does not form during jet exhaustion: the vortex sheet immediately starts to roll up into a toroidal spiral, and a vortex ring forms. Vladimirov and Tarasov (1980) proposed a physically more grounded model of vortex ring formation. Based on the laws of conservation of impulse and energy and additional assumptions on the distribution of circulation in the vortex core, Vladimirov and Tarasov (1980) determined the changes in some parameters of the vortex ring in the course of jet exhaustion. Their model provides a qualitatively correct idea about the dynamics of vortex ring formation and the evolution of some characteristics of the vortex ring during jet exhaustion. In deriving the formulas, however, they used the law of

energy conservation with no allowance for dissipation of some part of the jet energy in the course of vortex formation. The fact that the jet impulse is not completely transformed to the vortex ring impulse is also ignored. Therefore, the available formulas do not allow exact quantification of the parameters of the vortex ring formed.

A model of formation of the vortex ring during exhaustion of a submerged jet is presented below. The model is based on a more correct application of conservation laws. Formulas for almost all characteristics of the vortex ring are derived and found to be in agreement with experimental data (Akhmetov 2001, 2008b).

Vortex ring formation process

To elucidate the physical meaning of the experimental regularities presented in Chapter 3 and obtain analytical formulas for the main parameters of a vortex ring depending on its formation conditions, we need to have a notion about the dynamics of vortex ring formation during discharge of a submerged jet from a cylindrical tube. Consider the formation process of the ring being produced on discharge of a submerged air jet with a constant velocity V_0 during the time T from an open end of the cylindrical tube of radius R_0. In Fig. 4.1, several frames from the film are presented that illustrate the most characteristic stages of vortex ring formation near the open end of the tube. The flow was visualized by smoke supplied to the tube before the start of the jet discharge. The asymmetry of the pattern about the axis of the tube on the first frames in Fig. 4.1 is caused by the nonuniform initial distribution of the smoke density in the tube. The jet flows from the tube from left to right, and the generators of the tube are denoted by horizontal lines. Rolling-up of the vortex sheet into a toroidal spiral begins immediately as the leading front of the jet emerges from the hole (frame 1). This toroidal spiral forms a seed for the core of the vortex ring. The pattern of the spiral rolling-up of the vortex sheet during the jet exhaust from the tube is shown also in Fig. 4.2. As the jet moves, the vortex recedes from the edge of the hole. The leading edge of the mushroom-like head of the vortex in Fig. 4.1 is the boundary of the fluid which has been in the tube prior to the startup of the process. It follows from results of experiments that during most of the jet discharge time (except for the initial stage, when $t \ll R_0/V_0$) the velocity of motion of the leading edge of the jet is equal to $V_0/2$, i.e. half the jet velocity. The jet feeding the vortex retains the cylindrical shape when leaving the hole, and only at the entrance to the vortex, its cross section slightly decreases (frames 2–5 in Fig. 4.1). The core of the vortex ring forms from the mixing layer of the lateral boundary of the jet which rolls up into a spiral surface on the entrance to the vortex. Some amount of the surrounding fluid along the jet boundary is also entrained in the vortex. The jet discharge ceases between frames 5 and 6. By this time, the trailing edge of the jet coincides with the exit section of the tube. After the jet discharge has stopped, the vortex is being further filled with the fluid from the jet tail which is between the tube exit and the vortex. It should be noted that the jet tail produces roll-up of a secondary vortex ring, which moves behind the main vortex ring for some time and dissipates soon. In the last frame in Fig. 4.1, the formation of the vortex ring is practically completed.

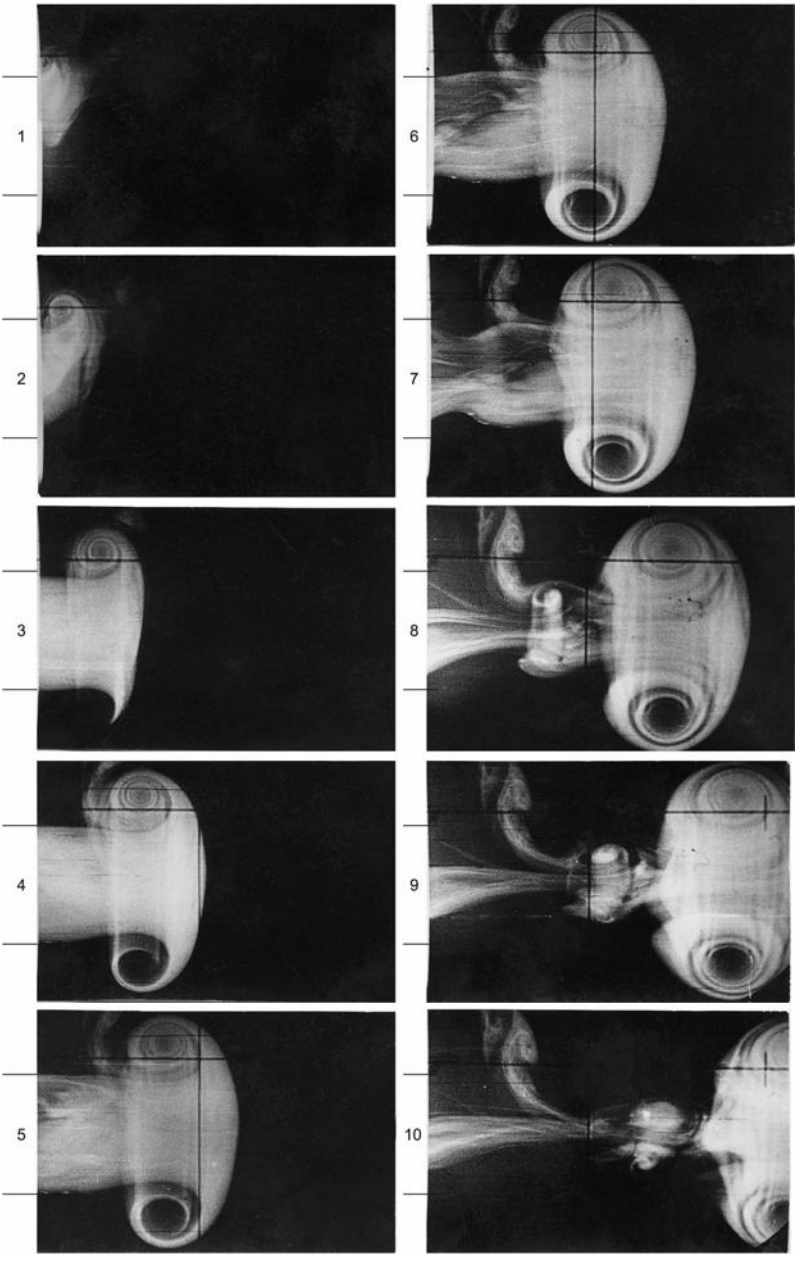

Fig. 4.1. Vortex ring formation process. *1–10* are the frame numbers

It follows from the presented film frames that a substantial portion of the volume of the ejected jet is entrained in the atmosphere of the vortex ring and a relatively small amount of the surrounding fluid is entrained in the vortex (dark coils of the

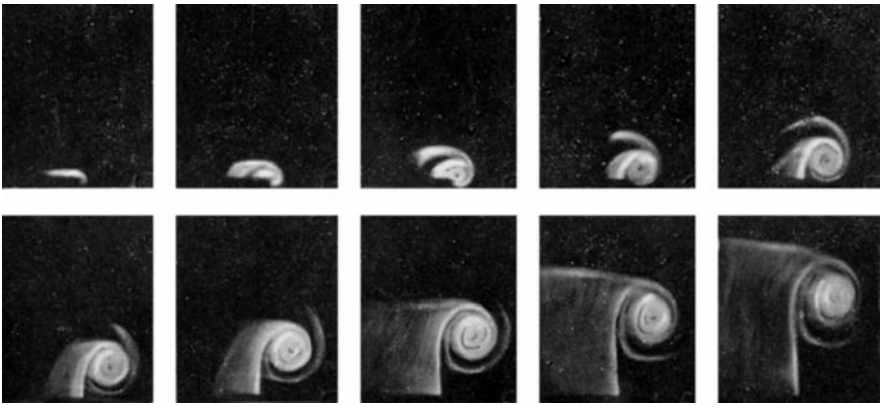

Fig. 4.2. Vortex sheet rolling-up into a spiral surface

spiral). This explains the linear increase in the volume V_* of the vortex ring atmosphere with increased jet length (see Fig. 3.4).

Model of vortex ring formation

A pattern of vortex ring formation during exhaustion of a submerged jet, which is consistent with experimental observations, is schematically shown in Fig. 4.3. Vortex ring formation is considered in cylindrical coordinates (z, r). According to Fig. 4.3, the forming vortex has passed a distance s from the tube exit and is fed by the cylindrical jet flowing from the tube with the velocity V_0. At a distance λ from the tube exit, the jet is almost undisturbed and represents a cylindrical body. The portion of the jet to the right of the cross-section $z = \lambda$ can be considered to have been already entrained in the vortex. According to Fig. 4.3, on the basis of the laws of conservation of impulse and circulation and involving some kinematic considerations, we can derive formulas for determining almost all parameters characterizing the structure of the vortex ring formed as functions of the jet length and Reynolds number of the jet. The forming vortex ring was assumed to be thin in calculations, which corresponds to high values of the jet Reynolds number ($\mathrm{Re} = R_0 V_0 / \nu \geq 10^4$). It is also assumed that the relations between the ring parameters are determined by the formulas of theoretical models for the vortex ring in an ideal fluid presented in Chapter 1.

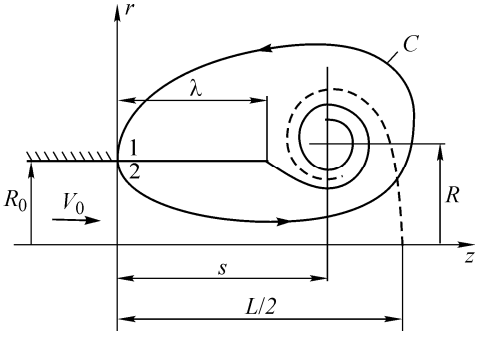

Fig. 4.3. Sketch of vortex ring formation

Vortex impulse. The impulse of the vortex ring can be determined by estimating the change of the vortex impulse in the fluid during jet exhaustion. The vortex impulse **P** is known to be determined by the integral

$$\mathbf{P} = \frac{1}{2}\rho\int_{\tau}(\mathbf{r}\times\boldsymbol{\omega})d\tau,$$

where ρ is the medium density, $\boldsymbol{\omega}$ is the vorticity vector (curl of the velocity), **r** is the radius vector, τ is the still volume of integration corresponding to the ambient fluid outside the tube. Hence, the rate of change of the vortex impulse in a still volume τ is determined by

$$\frac{\partial\mathbf{P}}{\partial t} = \frac{1}{2}\rho\int_{\tau}\left(\mathbf{r}\times\frac{\partial\boldsymbol{\omega}}{\partial t}\right)d\tau,$$

the right side of this expression being brought with the use of the Helmholtz equation $\partial\boldsymbol{\omega}/\partial t = \mathrm{rot}(\mathbf{u}\times\boldsymbol{\omega})$ to an integral over the surface Σ bounding the fluid outside the tube:

$$\frac{\partial\mathbf{P}}{\partial t} = \frac{1}{2}\rho\iint_{\Sigma}\{\mathbf{n}[\mathbf{r}\cdot(\mathbf{u}\times\boldsymbol{\omega})] - (\mathbf{n}\cdot\mathbf{r})(\mathbf{u}\times\boldsymbol{\omega}) + \mathbf{n}q^2 - 2(\mathbf{n}\cdot\mathbf{u})\mathbf{u}\}d\Sigma. \qquad (4.8)$$

Here $q = |\mathbf{u}|$ is the absolute value of velocity and **n** is the outward normal to the surface Σ. The surface Σ consists of the tube exit section, the outer surface of the tube, and the surface located at an infinite distance from the tube exit, which includes the entire space filled with the fluid outside the tube. In calculations, we can assume that $\mathbf{u} = \boldsymbol{\omega} = 0$ on the outer surface of the tube. Then, the integral over the tube surface vanishes. The integral over the surface infinitely distant from the tube exit is also equal to zero, since $\boldsymbol{\omega} = 0$ at infinity and the velocity **u** has an asymptotic behavior of a source (i.e., $|\mathbf{u}| \sim |\mathbf{r}|^{-2}$ as $|\mathbf{r}| \to \infty$). There remains only the integral over the tube exit cross section, which has two characteristic zones: zone of exhaustion of the central core of the jet with $\mathbf{u} = \mathbf{V}_0$, $\boldsymbol{\omega} = 0$ and ring-shaped zone of exhaustion of the boundary layer of thickness δ from the inner wall of the tube. Taking into account that $\delta/R_0 \ll 1$, we can assume that $\mathbf{u} = \mathbf{k}V_0/2$ and $\boldsymbol{\omega} = \mathbf{e}\mathrm{V}_0/\delta$ on the average over the entire cross section of the boundary layer (**k** is the unit vector along the *z*-axis and **e** is the unit vector directed along the azimuthal coordinate). During integration, the terms of order δ/R_0 and higher are dropped as being negligibly small. It follows from calculations that the vector $\partial\mathbf{P}/\partial t$ directed along the *z*-axis has the value $\partial P_z/\partial t = \pi\rho R_0^2 V_0^2$, hence, the impulse in the fluid at the time *T* is

$$P_z = \int_0^T \frac{\partial P_z}{\partial t}dt = \pi\rho R_0^2 V_0^2 T. \qquad (4.9)$$

According to Fig. 4.3, there are two vortex structures in the fluid at the time $t = T$: the forming vortex ring and the rear part of the cylindrical vortex sheet of length λ whose impulse equals $P_\lambda = \pi\rho R_0^2 \lambda V_0$. It follows from experiments that the rear part of the vortex sheet at $t > T$ transforms into a small secondary vortex ring with an impulse P_1 on the rear front of the jet, which soon dissipates. Approximately, we can assume that $P_1 = \alpha P_\lambda$, where α is the proportionality coefficient of about unity. Thus, for $t > T$, the impulse of the fluid P_z is a sum of the impulses of the main vortex ring P and the secondary vortex structure P_1 on the rear front of the jet, i.e. $P_z = P + \delta P_1$. Hence, the impulse of the vortex ring is $P = P_z - P_1 = \pi\rho R_0^2 V_0^2 T - \alpha\pi\rho R_0^2 \lambda V_0$. Theoretical models of the vortex ring (see Chapter 1) predict that the impulse of a thin-cored vortex ring is related to the circulation Γ and the ring radius R by the formula $P \approx \pi\rho R^2 \Gamma$. Substituting this formula into the above expression yields the relation of R and Γ to the jet parameters V_0, T, λ

$$R^2\Gamma = R_0^2 V_0^2 T - \alpha R_0^3 V_0 \lambda . \tag{4.10}$$

Circulation. The vortex ring circulation can be determined as a function of the jet parameters by estimating the total velocity circulation Γ_C arising as the jet escapes from the tube into the ambient space. In estimating the velocity circulation Γ_C one should take into account that the jet velocity near the nozzle exit during a small initial period $t_0 \ll R_0/V_0$ is not equal to V_0, because the intensity γ of the vortex sheet formed on the inner wall of the tube is not constant along the tube generatrix (at $t = 0$). The calculations of the potential flow arising at the initial time (Bardotti and Bertotti 1964; Pullin 1979) imply that the distribution of γ_0 near the tube edge (at $t = 0$) has the form $\gamma_0 = A/\sqrt{z}$, where A is a constant and z is the distance from the exit cross section inward the tube. At this stage, the flow near the tube edge is self-similar and is determined only by the coefficient A. The self-similar stage of vortex sheet roll-up was considered in several works (Didden 1979; Pullin 1979; Nitzsche 1996).

Nevertheless, the velocity circulation Γ_C arising in the fluid at large times of jet exhaustion $(T \gg t_0)$ can be estimated without analyzing the initial stage of vortex sheet evolution in detail. The effect of the self-similar stage of vortex sheet roll-up on circulation in the fluid can be estimated by assuming that the velocity circulation Γ_C at the time $t = 0$ already acquires a certain finite value γ, and the further growth of circulation in the fluid proceeds with a constant velocity of jet exhaustion. The quantity γ can be considered an empirical constant whose value at $T \geq R_0/V_0$ is small as compared with Γ_C.

Figure 4.3 shows that the only vortical region in the fluid is the vortex sheet displaying spiral roll-up. If we make a cut along the vortex sheet and along the tube generatrix, the flow in the entire space bounded by the cut surfaces can be assumed to be irrotational and to have a velocity potential φ. Let us calculate the velocity circulation over the motionless contour C, which covers the spiral end of the vortex sheet with the ends at points 1 and 2 on different sides of the cut on the

orifice edge, by moving from point 2 to point 1 and taking into account the initial value of the circulation

$$\Gamma_C = \gamma + \oint_C \mathbf{u} \cdot d\mathbf{l} = \gamma + \oint_C \frac{\partial \varphi}{\partial l} dl = \gamma + (\varphi_1 - \varphi_2).$$

The potential difference $\varphi_1 - \varphi_2$ can be found from the Cauchy's integral (Kochin et al. 1964) of the equations of motion of an ideal fluid

$$\frac{\partial \varphi_1}{\partial t} + \frac{V_1^2}{2} + \frac{p_1}{\rho} = \frac{\partial \varphi_2}{\partial t} + \frac{V_2^2}{2} + \frac{p_2}{\rho},$$

where $V_1 = 0$, $V_2 = V_0$. As the jet boundary is a straight line near the tube edge, we have $p_1 = p_2$ (otherwise, the vortex sheet at the tube exit would deflect in the radial direction). Thus, we obtain

$$\varphi_1 - \varphi_2 = \int_0^T \left(\frac{\partial \varphi_1}{\partial t} - \frac{\partial \varphi_2}{\partial t} \right) dt = \frac{1}{2} \int_0^T (V_2^2 - V_1^2)\, dt = \frac{V_0^2 T}{2} = \frac{V_0 L}{2}.$$

Then, the velocity circulation in the fluid (at the time $t = T$) is

$$\Gamma_C = \gamma + (\varphi_1 - \varphi_2) = \gamma + V_0 L/2.$$

According to Fig. 4.3, the total velocity circulation in the fluid Γ_C at $t = T$ is a sum of the circulation Γ of the vortex ring and the circulation Γ_λ of the rear part of the vortex sheet of length λ, i.e. $\Gamma_C = \Gamma + \Gamma_\lambda$. It may be demonstrated that $\Gamma_\lambda = \lambda V_0$. As the rear part of the vortex sheet at $t > T$ remains outside the vortex ring and dissipates, the vortex ring circulation is determined by the expression

$$\Gamma = \Gamma_C - \Gamma_\lambda = \gamma + V_0 (L/2 - \lambda). \tag{4.11}$$

Geometric condition. To determine R and Γ as functions of L, we need one more equation. The condition of energy conservation cannot be applied in this case, because it is difficult to estimate what part of the jet energy passes to the vortex ring and what part dissipates. An approximate geometric relation that follows from Figs. 4.1 and 4.3 can be used as such an equation. It was found in experiments that the velocity of propagation of the fore front of the jet is $V_0/2$; hence, the distance between the fore front of the jet and the rear part of the jet outside the vortex ring is $L/2 - \lambda$ (see Fig. 4.3); in addition, this segment and the transverse size $d \sim 2(R - R_0)$ of the spiral structure inside the vortex ring are commensurable in magnitude (see Fig. 4.3). Hence, we obtain

$$L/2 - \lambda \approx k\, 2(R - R_0), \tag{4.12}$$

where k is the dimensionless proportionality coefficient of about unity.

Radius, circulation and impulse of a vortex ring. In the dimensionless variables $R_* = R/R_0$, $\Gamma_* = \Gamma/R_0 V_0$, $L_* = L/R_0$, $\lambda_* = \lambda/R_0$ and $\gamma_* = \gamma/R_0 V_0$ the set of equations (4.10)–(4.12) takes the form

$$\begin{cases} R_*^2\Gamma_* = L_* - \alpha\lambda_*, \\ \Gamma_* = \gamma_* + (L_*/2 - \lambda_*), \\ L_*/2 - \lambda_* = 2k(R_* - 1). \end{cases} \tag{4.13}$$

This system yields a cubic equation for determining the radius R_* as a function of the jet length L_*

$$R_*^3 - \left(1 - \frac{\gamma_*}{2k}\right)R_*^2 - \alpha R_* - \frac{1-\alpha/2}{2k}L_* + \alpha = 0.$$

By solving this equation, we can determine the circulation $\Gamma_* = \gamma_* + 2k(R_* - 1)$, the impulse $P_* = R_*^2\Gamma_*$, and the parameter $\lambda_* = L_*/2 - 2k(R_* - 1)$. The best agreement between the solutions of the above-given equations and the experimental data in Fig. 3.4 is observed for the values of the constants $\alpha = 0.85$, $\gamma_* = 0.4$, $k \approx 2$. The dependences of R_*, Γ_*, P_* on L_* obtained by the numerical solution of these equations are plotted as solid curves in Fig. 4.4. The points represent the experimental values of R_*, Γ_*, P_* shown in Fig. 3.4; the measurement error is also indicated. It should be noted that Eqs. (4.10)–(4.12) were derived under the assumption that $L_* \gg 1$ and cannot be used for $L_* \to 1$. As it follows from Fig. 3.4, however, the calculations of the vortex ring parameters in the range $1.87 \le L_* \le 18.53$ are in agreement with the experimental data. For approximate estimates, the dependences of R_*, Γ_*, P_* on the jet length L_* can be presented explicitly by approximating the dependence $\lambda_*(L_*)$ in the experimentally studied range $1.87 \le L_* \le 18.53$ by some appropriate function. For instance, the dependence $\lambda_*(L_*)$ obtained numerically is adequately approximated by a function of the form $\lambda_*(L_*) = a\ln(\mathrm{ch}(cL_*))$ with coefficients $a \approx 2.424$ and $c \approx 0.1696$. With

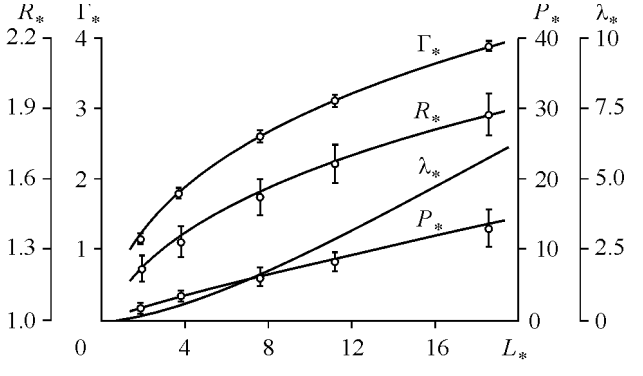

Fig. 4.4. Comparison of theoretically calculated vortex ring properties with experimental data

such an approximation of λ_* the vortex ring parameters R_*, Γ_*, P_* as functions of the jet length L_* can be calculated from simple formulas

$$R_* \approx 1+[L_*/2-\lambda_*(L_*)]/4,$$

$$\Gamma_* \approx 0.4+[L_*/2-\lambda_*(L_*)],$$

$$P_* \approx L_* - 0.85\lambda_*(L_*).$$

Thus, for $\mathrm{Re} \geq 10^3$, the radius, circulation, and impulse of the vortex ring are determined only by the dimensionless duration of jet exhaustion L_* (or jet length) and do not depend on the jet Reynolds number Re, which is supported by the experimental data (Akhmetov 2001) (see also Figs. 3.4, 3.11).

Radius of a vortex ring core. In terms of the model proposed, we can derive formulas for determining one more important structural parameter of the vortex ring, vortex core radius a, as a function of L_* and Re. Obviously, comprehensive calculation of vortex core formation requires solving a rather complicated problem of rolling up of the mixing layer of the jet into the vortex core with allowance for viscosity of the medium. Nevertheless, the character of the dependence of the vortex core radius a_* on L_* and Re can be determined without studying the process of vortex layer roll-up in detail but estimating only the volume of the fluid entering the vortex core during vortex core formation. As seen from Fig. 4.5, the fluid enters the vortex core during its formation through two channels: along the mixing layer of the jet (hatched region), which is a continuation of the boundary layer flowing off the inner surface of the nozzle, and along the branch of the spiral from the ambient space and the vortex atmosphere (non-hatched region).

Let us first estimate the volume q_1 of the fluid entrained into the vortex core from the mixing layer of the jet. Obviously, the velocity of the fluid inflow from the mixing layer into the vortex V_λ equals the difference between the mean velocity $\tilde{V}$ in the mixing layer and the velocity $u_\lambda = d\lambda/dt$ of axial motion of the point $z = \lambda$: $V_\lambda \approx \tilde{V} - u_\lambda$. The mean velocity averaged over the mixing layer thickness can be approximately taken as $\tilde{V} \approx V_0/2$; hence, the velocity of fluid inflow from the mixing layer of the jet into the vortex core is $V_\lambda \approx \tilde{V} - u_\lambda = V_0/2 - d\lambda/dt$. In studying the exhaustion of free jets, the flow in the mixing layer of the jet at moderate distances from the nozzle exit (within several nozzle radii) was found to be laminar (Abramovich 1960; Bai Shiyi 1954). Therefore, the mixing layer thickness δ_1 at the vortex entrance can be

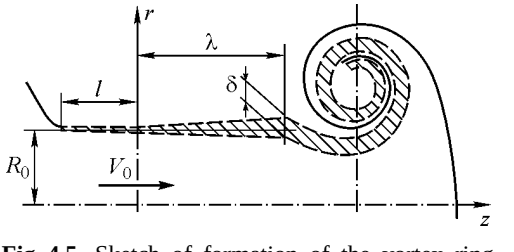

Fig. 4.5. Sketch of formation of the vortex ring core

estimated by the relation $\delta_1 \sim b\sqrt{\nu t_1}$ (Schlichting 1968), where b is the dimensionless proportionality coefficient and $t_1 \sim (l+\lambda)/V_0$ is the time of displacement of the fluid particles to a distance $l+\lambda$. Thus, we obtain $\delta_1 \sim b\sqrt{\nu(l+\lambda)/V_0} = b\sqrt{R_0(l+\lambda)}\,\mathrm{Re}^{-1/2}$. The coefficient b can be found from the velocity distribution in the mixing layer of the jet (Bai Shiyi 1954; Schlichting 1968). Approximating the velocity distribution in the mixing layer of the jets (Bai Shiyi 1954; Schlichting 1968) by a linear function, we can find the value $b \approx 5.22$. Hence, the volume q_1 of the fluid inflowing during the time T from the mixing layer into the vortex core is described by the expression

$$q_1 \approx \int_0^T 2\pi R_0 \delta V_\lambda dt = \pi b R_0\,\mathrm{Re}^{-1/2} \int_0^T \sqrt{R_0(l+\lambda)}\left(V_0 - 2\frac{d\lambda}{dt}\right)dt =$$

$$= \pi b R_0\,\mathrm{Re}^{-1/2} \int_0^L \sqrt{R_0(l+\lambda)}\left(1 - 2\frac{d\lambda}{dz}\right)dz,$$

where $z = V_0 t$ and $L = V_0 T$.

As noted above, in addition to the volume q_1, a flow of a non-vortical fluid also enters the vortex core (non-hatched branch of the spiral in Fig. 4.5). It is difficult to determine the volume q_2 of this flow without calculating the process of rolling up of the mixing layer of the jet into a toroidal spiral surface. Based on Fig. 4.5, however, we can assume that the thickness of both branches of the spiral (hatched and non-hatched regions) is approximately identical; moreover, the velocities of fluid inflow along both branches of the spiral are also identical. Therefore, to a first approximation, the volume q_2 of the fluid entering the vortex core (non-hatched branch of the spiral in Fig. 4.5) is proportional to q_1, i.e., $q_2 \sim \beta q_1$ (β is an empirical coefficient). Thus, the total volume of the fluid entering the vortex core is determined by $q \approx (1+\beta)q_1$ By equating the volume q of the fluid entering the vortex core to the volume of the toroidal core of the vortex ring $q_c = 2\pi R \pi a^2$ we obtain the following expression for the core radius of the vortex ring

$$a \sim \left(\frac{(1+\beta)b}{2\pi R}\right)^{1/2} \mathrm{Re}^{-1/2}\left[R_0 \int_0^L \sqrt{R_0(l+\lambda)}\left(1 - 2\frac{d\lambda}{dz}\right)dz\right]^{1/2}.$$

Using the dimensionless parameters $a_* = a/R_0$, $R_* = R/R_0$, $l_* = l/R_0$, $\lambda_* = \lambda/R_0$, $z_* = z/R_0$, $L_* = L/R_0$, and $b \approx 5.22$, we can write the formula for determining the vortex radius a_* in the form

$$a_* = \frac{a}{R_0} \approx \mathrm{Re}^{-1/4}\left(\frac{1+\beta}{2\pi R_*}\right)^{1/2}\left\{\int_0^{L_*} \sqrt{l_* + \lambda_*}\; dL_* - \frac{4}{3}\left[(l_* + \lambda_*)^{3/2} - l_*^{3/2}\right]\right\}^{1/2}. \quad (4.14)$$

In equation (4.14), the functions $R_*(L_*)$ and $\lambda_*(L_*)$ for $L_* \geq 1.87$ were determined above. In integrating (4.14), we assumed that $\lambda_*(0) = 0$, since the length of the rear part of the jet equals zero for a zero length of the jet, as it follows from Fig. 4.4. Therefore, we can assume that the form of the function $\lambda_*(L_*)$ for $L_* < 1.87$ does not exert any significant influence on the values of a_* calculated for $L_* \geq 2$ if the values of λ_* are sufficiently high. Clearly, the vortex core radii a_* calculated by (4.14) are only applicable in the range $1.87 \leq L_* \leq 18.53$, where equations (4.13) are valid (see Fig. 4.4). In this range, the best matching between the values of a_* calculated by (4.14) and the experimental data (Akhmetov 2001) is reached for $\beta \approx 3.234$. This means that the volume of the fluid entering the vortex core along the branch of the spiral that is not hatched in Fig. 4.5 is approximately three times the volume of the fluid entering from the mixing layer of the jet. The power-law dependence of a_* on the Reynolds number Re is in agreement with the dependence of $\ln a_*$ on $\ln \mathrm{Re}$ plotted on the basis of the experimental data (Akhmetov 2001) (Fig. 4.6). The tangent of the angle of the straight line plotted through the experimental points in Fig. 4.6 is $-1/4$, which completely agrees with (4.14). It was also noted (Tarasov 1973; Maxworthy 1977) that the measured results predicted the dependence of the form $a \sim \mathrm{Re}^{-1/4}$. The dependence of a_* on the jet length L_* (for $\mathrm{Re} = 1.825 \cdot 10^4$ and $l_* = 2$) is plotted in Fig. 4.7 by the solid curve; the points are the experimental data (Akhmetov 2001). Equation (4.14) also determines the character of the dependence of a_* on the length λ_* of the cylindrical segment of the nozzle, though no experimental data are available for this case. In using Eq.(4.14) for calculations, one should take into account that the formula was derived under the assumption of a small thickness of the mixing layer of the jet δ_1 as compared with the jet radius

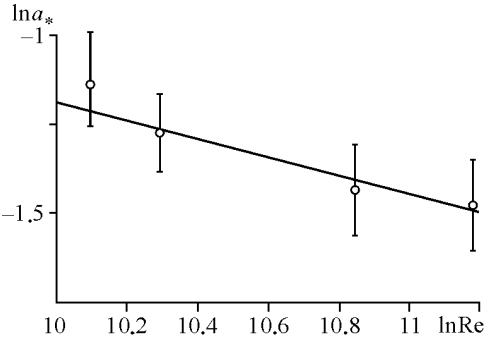

Fig. 4.6. Experimental dependence of the vortex core radius a_* on the jet Reynolds number

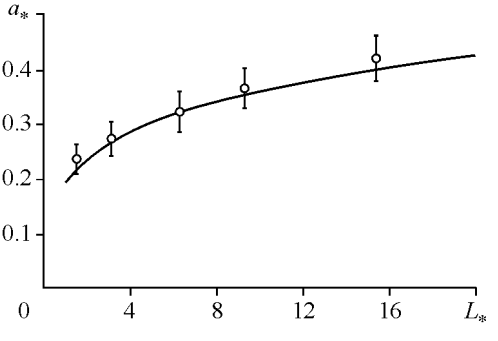

Fig. 4.7. Dependence of the vortex core radius a_* on the jet length. Solid line represents calculation by Eq. (4.17) and experimental points represent the data of Fig. 3.4

R_0, hence, the formula is applicable for $\delta/R_0 \sim ((l_* + L_*)/\mathrm{Re})^{1/2} \ll 1$, which corresponds to conditions of formation of turbulent thin-cored vortex rings at sufficiently high Reynolds numbers of the jet.

Translational velocity of a vortex ring. The results obtained above allow us to calculate the translational velocity of the vortex ring u_0 using known theoretical formulas (Lamb 1932; Saffman 1992), for instance, the Kelvin formula

$$u_0 = \frac{\Gamma}{4\pi R}\left(\ln\frac{8R}{a} - \frac{1}{4}\right).$$

As the vortex core radius a in this formula is a function of the jet length L_* and Reynolds number Re, the velocity of the vortex ring also depends on these parameters. It is clear that u_0 is scarcely affected by Re, and it is only the dependence of u_0 on the jet length L_* that is important. Having obtained expressions for calculating all parameters in this formula, we can find the translational velocity of the vortex as a function of L_*. The calculated dependence of $u_0^* = u_0/V_0$ on L_* is plotted by the solid curve in Fig. 4.8; the points correspond to the experimental values of u_0^* borrowed from (Akhmetov 2001). It is seen that the Kelvin formula overestimates u_0^* even though the values of all parameters used in this formula (R, Γ, a) are consistent with the experiment. This fact suggests that the formulas for the translational velocity of the vortex ring, derived within the framework of an ideal fluid under the assumption that the vorticity is focused in the vortex core only, cannot provide accurate quantitative estimates for the velocity of real vortex rings with a smooth bell-shaped distribution of vorticity extended outside the vortex core as well. In general, the very notion of the vortex core is not defined clearly enough for real vortex cores with smooth distributions of vorticity. This notion is used only to characterize the width of the peak in the vorticity distribution and to describe the vortex ring structure by a finite number of parameters. Obviously, a more detailed theory is needed to calculate the translational velocity of real vortex rings. It should be noted, however, that the agreement between the values of u_0^* calculated by the Kelvin formula and the experimental data can be improved through a correction $\alpha \approx 0.75$ in this formula. The dependence of u_0^* on the jet length L_* calculated with the use of this correction is plotted by the dashed curve in Fig. 4.8.

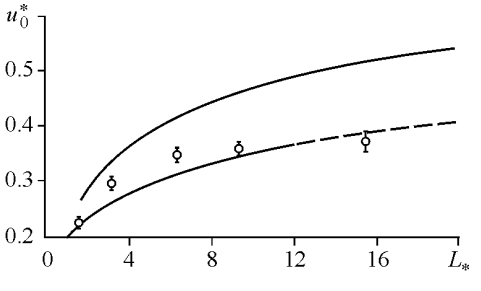

Fig. 4.8. Translational velocity of the vortex ring versus the jet length. Calculation (solid line) and experimental data of Fig. 3.4 (circles)

Vortex ring energy. Available theoretical models of the vortex ring (Lamb 1932) predict that the energy T of a thin-cored vortex ring is determined as a function of the parameters R, Γ, and a

$$T = \frac{\rho R \Gamma^2}{2}\left(\ln\frac{8R}{a} - \frac{7}{4}\right).$$

Obviously, the dimensionless value of the energy $T_* = T/\rho\pi R_0^3 V_0^2$, like the vortex ring velocity u_0^*, depends little on the Reynolds number of the jet. Analysis of the calculated dependence of T_* on the jet length L_* (Fig. 4.9) shows that T_* changes almost proportionally to L_*. We may assume that the calculated dependence of T_* describes the qualitative behavior of the vortex ring energy as a function of the jet length. It is difficult, however, to check the quantitative correctness of the calculation, because no experimental data on the dependence of T_* on the jet length L_* are available.

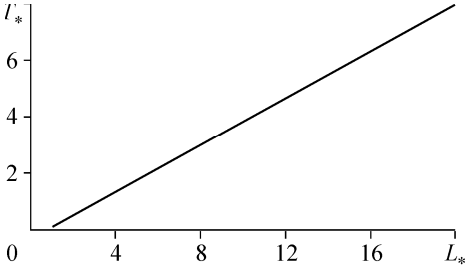

Fig. 4.9. Dependence of vortex ring energy on jet length

Thus, the proposed model of vortex ring formation, which was constructed with the use of only one empirical constant for each functional dependence to be determined, allows one to calculate almost all characteristics of the vortex ring formed in the case of pulsed discharge of a submerged jet and to predict the vortex ring structure.

5 Motion of Turbulent Vortex Rings

Produced in one way or another, vortex rings subsequently move away from the vortex-generating apparatus and propagate in a virtually unbounded medium. The motion of a formed vortex ring in an unbounded medium is the main stage of its existence in terms of both duration and distance traveled by the ring until it decays owing to the viscosity of the medium. Determination of the laws of motion and evolution of a formed ring is a fundamental problem of vortex ring dynamics. This problem is rather complicated since viscosity must be taken into account, and until recently it has not had a theoretical solution. Lugovtsov was the first to give the original formulation and solution of the problem of motion of turbulent vortex rings (Lugovtsov et al. 1969; Lugovtsov 1970, 1974, 1976a,b, 1979; Lugovtsov and Lugovtsov 1971). Experimental verification of the theoretical results was obtained mainly by Tarasov (Lugovtsov et al. 1969; Tarasov 1973, 1975b).

Following Lugovtsov, we consider some facts that characterize the motion of a formed vortex ring. Experiments imply that at small values of the initial Reynolds number ($\mathrm{Re} \le 10^3$) defined by the radius R and propagation velocity of the ring u_0, the vortex ring is laminar and has a stable spiral structure, clearly revealed by flow visualization (see Fig. 3.8). At larger Reynolds numbers the spiral structure becomes unstable, and the vortex ring starts oscillating in a wavy manner and deforming. However, we cannot consider such a perturbed ring motion to be the real turbulence, because wavy phenomena most commonly occur at medium range Reynolds numbers corresponding to the transition from laminar to turbulent motion. Experimental and theoretical data on the motion of laminar vortex rings, wave formation phenomena and stability are reported elsewhere (Krutzsch 1939; Widnall et al. 1974; Kambe and Oshima 1975; Maxworthy 1977; Moffat and Moore 1978; Saffman 1970, 1978; Kaltaev 1982; Berezovski and Kaplanski 1987; Gleser and Coles 1990). At Reynolds numbers $\mathrm{Re} > 10^3$ the motion drastically changes in nature as it becomes turbulent. The spiral structure emerging in the initial stage of formation diffuses in a short time and visualization shows only a clear-cut toroidal core of the vortex (see Figs. 3.9 and 3.10), and as follows from experiments, the structure of a turbulent vortex depends little on details of initial and boundary conditions. Soon after the vortex ring formation, a certain vorticity distribution develops, being independent of the vortex generation procedure. Averaged motion in a turbulent vortex is determined by vortex dimensions and velocity only. The results of the experimental studies of turbulent vortex ring motion for Reynolds numbers in the range 10^4–10^7 can be found in (Lugovtsov et al. 1969; Lugovtsov 1970, 1974, 1976a,b, 1979; Tarasov 1973, 1975b). It follows from the experiments that in this range of Reynolds numbers the radius of the vortex ring linearly increases with the traveled distance, that is the ring radius depends on the

distance as $R(t) = R_0 + \alpha L(t)$, where $L(t)$ is the distance traveled by the vortex measured from the point where the vortex has finally formed, R_0 is the initial radius of the ring, and α is a coefficient of order 10^{-2}–10^{-3}. We may suppose that the value of α is determined by conditions of vortex ring formation. It remains constant in the subsequent motion. Thus, by the moment when the formation of a turbulent vortex ring is completed, a certain universal vorticity distribution is developed, characterized by a single parameter α whose value may depend on specific conditions of ring formation. These physical considerations suggest that distributions of vorticity and other quantities in a turbulent vortex ring are self-similar. The same can also be formally inferred from the dimensional analysis of the parameters that govern the motion of a turbulent vortex ring.

5.1 Statement of the Problem

The motion of a vortex ring in an unbounded viscous medium is an initial value problem, with the vortex ring parameters at the moment of completion of its formation being the initial values. According to the results of investigations of vortex ring structure reported in Chapters 2 and 3, the initial radius of the ring R_0, the linear size of the core cross-section (core radius) a_0, which characterizes the degree of vorticity concentration in the vortex ring, the translational velocity u_0, and the vortex ring circulation Γ_0 are parameters that determine the structure of the completely formed vortex ring. The impulse **P** is the most fundamental characteristic of the vortex ring, because the vortex impulse is an integral of motion which is conserved not only in an ideal fluid, but in a viscous medium as well. Since we consider time evolution of the vortex, the current time t and medium properties, namely its density ρ and dynamic viscosity coefficient μ, must be added to the set of parameters governing the vortex motion. From this point it is more convenient to replace the dynamic quantities, $P = |\mathbf{P}|$ and μ, by the kinematic impulse $J = P/\rho$ and kinematic viscosity coefficient $\nu = \mu/\rho$. Thus, we have seven dimensional kinematic parameters

$$R_0, a_0, u_0, \Gamma_0, J, \nu, \text{ and } t. \tag{5.1}$$

If we choose J and ν as dimensionally independent variables, then according to the dimensional analysis (Sedov 1959; Barenblatt 1996), one can obtain from (5.1) five dimensionless parameters governing the motion of the vortex ring

$$\Pi_1 = t(\nu^2/J),\ \Pi_2 = R_0(\nu/J)^{1/2},\ \Pi_3 = a_0(\nu/J)^{1/2},\ \Pi_4 = \Gamma_0/\nu,\ \Pi_5 = u_0(J/\nu^3)^{1/2}.$$

The fundamental theorem of the dimensional analysis theory (Sedov 1959; Barenblatt 1996) implies that any of the unknown characteristics Φ_i of the vortex ring made dimensionless by means of J and ν, must be a function of these five dimensionless characteristic parameters, i.e. $\Phi_i = \Phi_i(\Pi_1, \Pi_2, \Pi_3, \Pi_4, \Pi_5)$. The physical meaning of the constant parameters $\Pi_1 - \Pi_5$, being the arguments of the

functions Φ_i can be revealed by estimating their magnitudes. Since by the order of magnitude $\Gamma_0 \sim R_0 u_0$ and $J \sim R_0^3 u_0$, we have the following estimates

$$\Pi_1 = \nu^2 t/J, \quad \Pi_2 \sim \mathrm{Re}^{-1/2}, \quad \Pi_3 \sim (a_0/R_0)\,\mathrm{Re}^{-1/2}, \quad \Pi_4 \sim \mathrm{Re}, \quad \Pi_5 \sim \mathrm{Re}^{3/2}, \quad (5.2)$$

where $\mathrm{Re} = R_0 u_0/\nu \sim J/\nu R_0^2$ is the Reynolds number of the vortex ring composed of the initial values of radius and translational velocity of the vortex ring. Obviously, determination of the vortex ring motion as a function of five parameters $\Pi_1 - \Pi_5$, where Π_1 is the current time, is a rather complex problem. It can be simplified if we consider only turbulent vortex rings which are characterized by large Reynolds numbers. Experiments imply that a vortex ring can be assumed to be turbulent at $\mathrm{Re} > 10^4$. According to estimations (5.2), as $\mathrm{Re} \to \infty$, the parameters behave as $\Pi_2 \to 0$, $\Pi_3 \to 0$ and $\Pi_4 \to \infty$, $\Pi_5 \to \infty$, that is the parameters Π_2 and Π_3, which govern the motion of the turbulent vortex ring are very small, while Π_4 and Π_5 are large, and only the parameter $\Pi_1 \sim (u_0 t/R_0)\,\mathrm{Re}^{-2}$ varies in a wide range. Supposedly, the parameters $\Pi_2 - \Pi_5$, which are too small or too large compared with unity, are inessential for characterization of the motion of the turbulent vortex ring. Such a hypothesis occurs to be feasible in many cases (see, for example, Golitsyn (1973) and Barenblatt (1996)). Following this hypothesis, we may assume that at large values of the initial Reynolds number (at large values of the impulse *J*) the motion of the turbulent vortex ring is determined by the dimensionless parameter Π_1 alone. Apart from Π_1, the ratio $\Pi_3/\Pi_2 = a_0/R_0 = \varepsilon$, being in general of about unity, can also serve as a characteristic parameter. However, when the motion of a specific vortex ring realization corresponding to a fixed value $\varepsilon = \mathrm{const}$ is regarded, the structure and properties of the vortex ring (i.e. all functions Φ_i) are determined by the single parameter $\Pi_1 = \nu^2 t/J$. Hence, provided a time-dependent scale $r_*(t)$ of spatial variables and a scale $v_*(t)$ of any property of the vortex ring $v(t)$, the distribution of $v(t)$ at various moments of time can be represented in the form $v(t)/v_*(t) = f[r/r_*(t)]$. Thus, distributions of all properties of the vortex ring at various times are similar and can be obtained from one another through the similarity transformation, i.e. the structure of the turbulent vortex ring is self-similar. To solve this problem, we also need to specify the form of the turbulent viscosity coefficient. Lugovtsov suggests the effective viscosity coefficient ν_e as a sum of the molecular viscosity ν and the turbulent viscosity, $\nu_e = \nu_t + \nu$. Then a hypothesis is introduced that the turbulent viscosity ν_t is a function of time only and does not depend on space coordinates (Lugovtsov et al. 1969; Lugovtsov 1970, 1974, 1976a,b, 1979). Hence, the turbulent viscosity is determined by characteristic scales of motion being the radius $R(t)$ and the velocity $u(t)$ of the vortex ring

$$\nu_t = \gamma R(t) u(t), \quad (5.3)$$

where γ is a constant whose value may be determined by comparing theoretical results with experiment. The form of the time dependence of the turbulent viscosity can be derived from the dimensional analysis of the characteristic parameters (5.1)

$$\nu_t = \lambda J^{1/2} t^{-1/2}, \tag{5.4}$$

where $\lambda = \text{const}$ is the dimensionless coefficient to be determined from experiment. Since the motion of turbulent vortex rings corresponds to large values of *J*, the ratio $\nu/\nu_t = \nu/(\lambda J^{1/2} t^{-1/2})$ is negligibly small. Then the effective viscosity can be approximated in the form $\nu_e = \nu_t(1+\nu/\nu_t) \approx \nu_t = \lambda J^{1/2} t^{-1/2}$. Substituting this value of ν_e in Π_1 instead of the molecular viscosity ν yields $\Pi_1 = \lambda^2$. Hence, the dimensionless characteristics of a vortex ring Π_i are determined by functions of the form $\Pi_i = \Phi_i(\varepsilon, \lambda^2)$. Evidently, the hypothesis that ν_t is independent of space coordinates is a rather strong assumption, since there is no turbulence at large distances from the vortex ring where the fluid is at rest. Molecular viscosity of the medium plays a dominant role there. Nevertheless, assuming that viscosity actually manifests itself in flow regions with large velocity gradients located inside and near the vortex ring and with distance from the ring the velocity gradients and, hence, the influence of viscosity diminish, the accepted hypothesis might be a reasonable model of turbulence.

5.2 Laws of Motion of a Turbulent Vortex Ring

Consider a particular realization of a turbulent vortex ring for a certain value $\varepsilon = \text{const}$. Then $\Phi_i = \Phi_i(\Pi_1) = \Phi_i(\lambda^2) = \text{const}$, i.e. all dimensionless characteristics of the vortex ring Φ_i depend only on the constant λ. This result allows us to find out directly from dimensional considerations how some parameters of the turbulent vortex ring interesting for comparison with experiment vary with time. Let us introduce the time-dependent scale of space coordinates $r_*(t) = J^{1/4} t^{1/4}$. Linear quantities along the *z*- and *r*-axes made dimensionless using r_* are written as $\Phi_z = z/J^{1/4}t^{1/4} = \Phi_z(\lambda) = \text{const}$, $\Phi_r = r/J^{1/4}t^{1/4} = \Phi_r(\lambda) = \text{const}$, i.e., distances along the *z*-axis vary with time as $z = J^{1/4}t^{1/4}\Phi_z$ and the radius of the vortex ring varies as $R = J^{1/4}t^{1/4}\Phi_r$. We assume then that by the moment $t = t_0$ the vortex ring has the radius R_0 and the translational velocity u_0. Measuring time from this instant $(\tau = t - t_0)$, we obtain the distance *L* traveled by the ring during the time τ as $L(\tau) = z(t_0+\tau) - z(t_0) = J^{1/4}[(t_0+\tau)^{1/4} - t_0^{1/4}]\,\Phi_z$, and the ring radius $R(\tau) = J^{1/4}(t_0+\tau)^{1/4}\Phi_r$. The speed of translation can be found by differentiating $L(\tau)$ with respect to time, $u(\tau) = J^{1/4}(t_0+\tau)^{-3/4}\Phi_z/4$. The obtained expressions can be reduced to the form more convenient for comparison with experiment.

Assuming that $R = R_0$, $u = u_0$ at $\tau = 0$ and using the notation $\Phi_r/\Phi_z = \alpha(\varepsilon, \lambda^2)$, we exclude $t_0 = R_0/4\alpha u_0$ from the preceding formulas and obtain

$$L(\tau) = \frac{R_0}{\alpha}\left[\left(1+\frac{4\alpha u_0}{R_0}\tau\right)^{1/4} - 1\right], \tag{5.5}$$

$$R(\tau) = R_0\left(1+\frac{4\alpha u_0}{R_0}\tau\right)^{1/4}, \tag{5.6}$$

$$u(\tau) = u_0\left(1+\frac{4\alpha u_0}{R_0}\tau\right)^{-1/4}. \tag{5.7}$$

Expressions (5.5) and (5.6) immediately show that $R(\tau) = R_0 + \alpha L(\tau)$. Thus, directly from the dimensional analysis we have established the remarkable fact that a turbulent vortex ring expands linearly with the distance traveled. This fact was first discovered experimentally and stimulated development of the theoretical model describing the motion of turbulent vortex rings. Vortex ring properties as functions of time described by Eqs. (5.5)–(5.7) are quite easily and reliably determined from experiment. The dimensionless coefficient $\alpha(\varepsilon, \lambda)$ characterizing the angle of expansion of a vortex ring can be found by comparing the derived formulas with experiment. Numerous experiments of this kind were carried out by Tarasov (Lugovtsov et al. 1969; Tarasov 1973, 1975b). The experiments established that the values of α occurred to be very small, about 10^{-3}–10^{-2}. Figure 5.1 shows the plot of the distance traveled by the ring with the initial parameters $R_0 = 0.1$ m, $u_0 = 4.3$ m/s and $\alpha = 6\cdot 10^{-3}$ as a function of time. The circles represent the experimental data, and the solid line was calculated from (5.5). It is seen that the theoretical dependence agrees well with the experiment, although some deviation of the theoretical curve from the experimental data can be observed at large times. Expression (5.5) has the essential disadvantage that the distance traveled by the vortex ring L is infinite as $\tau \to \infty$, which certainly contradicts the experimental facts. Probably, L experiences the unbounded growth as $\tau \to \infty$, because according to (5.4) the turbulent viscosity decreases with time and at some instant equals the molecular viscosity, after which the molecular viscosity cannot be ignored. The validity of this assumption may be directly verified. Indeed, two characteristic time scales can be composed of the two characteristic parameters (5.1)

$$T_1 = \frac{R_0^4}{J} \sim \frac{R_0}{u_0} \quad \text{and} \quad T_2 = \frac{J}{\nu^2} = \frac{1}{\Pi_2^4} T_1 \sim \frac{R_0^2 u_0^2}{\nu^2}\frac{R_0}{u_0} = \mathrm{Re}^2 \frac{R_0}{u_0} \sim \mathrm{Re}^2 T_1.$$

The scale T_1 obviously corresponds to the time it takes for the ring to travel a distance of the order of R_0. It is clear that in a time T_1 the vortex ring is still insufficiently far from the vortex-generating apparatus and its motion for $t < T_1$ cannot

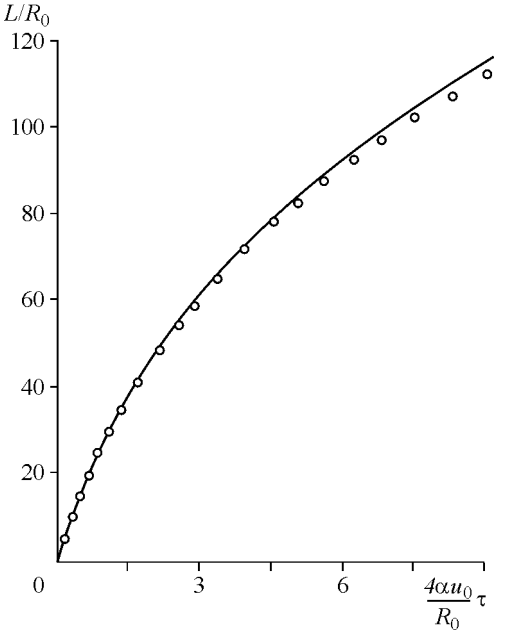

Fig. 5.1. Distance traveled by the vortex ring as a function of time. Calculation by Eq. (5.5) (solid line) and experimental data (points) (Lugovtsov et al. 1969)

be regarded as turbulent and occurring in an unbounded medium. The time scale $T_2 \sim \mathrm{Re}^2 T_1$ is large at large Re and is the upper time limit of the range where the accepted model of turbulence and formulas (5.5)–(5.7) still can be used. The inequality $\nu/\nu_t = \nu/(\lambda J^{1/2} t^{-1/2}) \ll 1$ implies that $t < \lambda^2 J/\nu^2 = \lambda^2 T_2 \sim \mathrm{Re}^2 R_0/u_0$, i.e. for $t > T_2$ the hypothesis of the prevailing role of the turbulent viscosity becomes invalid. We may suppose that the time scales T_1 and T_2 determine the time range $(T_1 < t < T_2)$ within which the accepted model of turbulence remains valid, and the motion of the vortex ring is described by formulas (5.5)–(5.7).

Equation (5.5) allows determination of the distance $L_{\max}$ traveled by a turbulent vortex ring by the moment $t = T_2$. Assuming that $\alpha \mathrm{Re}^2 \gg 1$ as $\mathrm{Re} \to \infty$, we have

$$\frac{L_{\max}}{R_0} = \frac{L(T_2)}{R_0} = \frac{1}{\alpha}\left[\left(1 + \frac{4\alpha u_0}{R_0} T_2\right)^{1/4} - 1\right] \sim \frac{(1 + 4\alpha \mathrm{Re}^2)^{1/4} - 1}{\alpha} \sim \sqrt{2}\,\alpha^{-3/4}\,\mathrm{Re}^{1/2}. \quad (5.8)$$

Clearly, this formula is only an estimate. More reliable data on the total distance traveled by the vortex ring until it decays can be found experimentally. Using a large number of measurements in the range $10^3 < \mathrm{Re}_0 < 10^6$, Tarasov (1975b) plotted $L_{\max}/R_0$ versus Re_0 (Fig. 5.2) and obtained an empirical formula

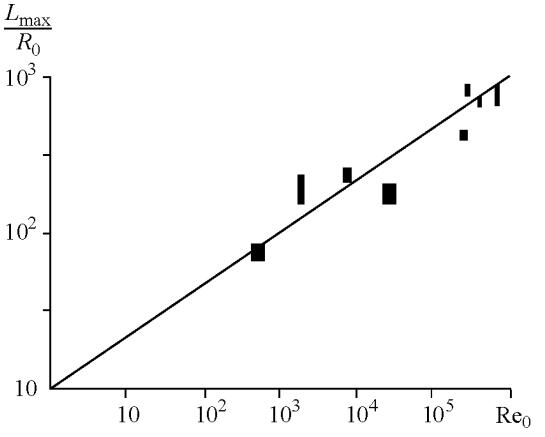

Fig. 5.2. Maximum distance traveled by a vortex ring as a function of the Reynolds number of the vortex ring (Tarasov 1975b)

for estimating the maximum distance traveled by the vortex ring in the form $L_{max}/R_0 = 10\,\mathrm{Re}_0^{1/3}$. Thus, the experimental data also imply that the maximum distance traveled by the vortex ring depends on the Reynolds number according to the power law, though with a different power than in the estimate (5.8). It is not improbable that the discrepancy between the powers of the Reynolds number in Tarasov's empirical formula and theoretical estimate (5.8) is not of fundamental importance and is only due to inaccurate approximation of the experimental data characterized by large scatter.

As noted above, the dimensionless coefficient of expansion of a vortex ring α can be a function of the two dimensionless parameters λ and ε. Dependence of α on the parameter ε being the characteristic of the initial structure of vortex rings can be revealed from experimental data. In his work Tarasov (1973) demonstrated the results of measurements of the coefficient α for vortex rings as a function of the initial Reynolds number $\mathrm{Re}_0 = u_0 R/\nu$ of the vortex ring (Fig. 5.3). It is seen that α rapidly decreases with

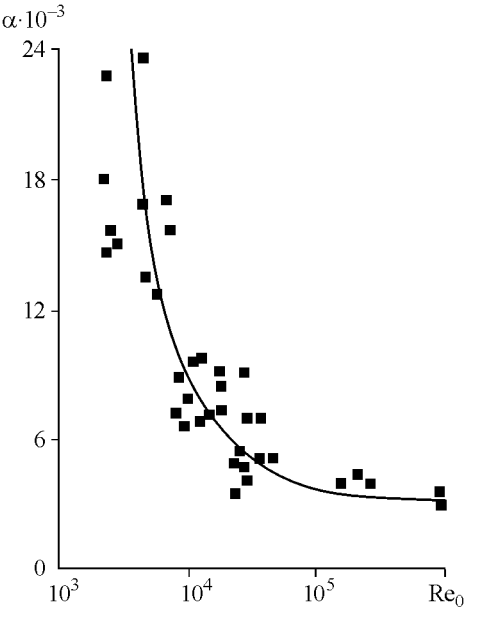

Fig. 5.3. Coefficient of vortex ring expansion α as a function of the initial Reynolds number Re_0 of the vortex ring (Tarasov 1973)

an increase in the Reynolds number. On the other hand, Fig. 3.11 shows the experimental dependences of the parameter ε, the radius R, and the translational velocity u_0 of the vortex ring on the jet Reynolds number. Therefore, using the data of Fig. 3.11, one may plot the parameter ε as a function of the Reynolds number Re_0 of the vortex ring (Fig. 5.4). Comparing the data of Fig. 5.3 and Fig. 5.4 for equal Reynolds numbers Re_0, we will obtain the dependence of the expansion coefficient of the vortex ring α on the parameter ε (Fig. 5.5). It follows from Fig. 5.5 that the expansion coefficient of the vortex ring α is uniquely related to the parameter ε. Since the parameter ε, to some extent, characterizes the initial structure of the vortex ring, then apparently each specific realization of a turbulent vortex ring with a certain value of the coefficient α should be characterized by its individual self-similar structure corresponding to the specific value of ε determined by the conditions of vortex ring formation.

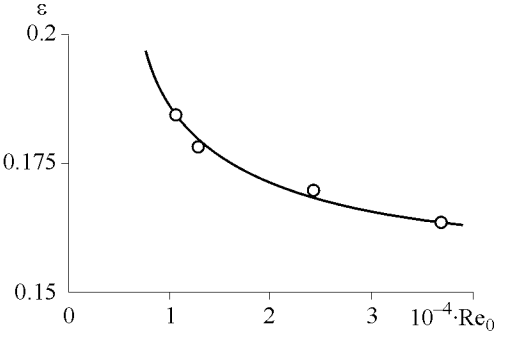

Fig. 5.4. Parameter ε as a function of the vortex ring Reynolds number Re_0. From the data of Fig. 3.11.

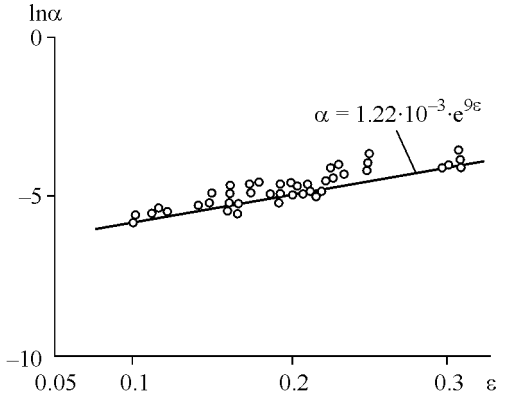

Fig. 5.5. Coefficient of vortex ring expansion α as a function of the parameter ε. From the data of Figs. 5.3 and 5.4.

5.3 Structure of a Turbulent Vortex Ring

The above formulas (5.5)–(5.7) describe the evolution of only some external characteristics of a turbulent vortex ring. The whole structure of the vortex ring can be determined on the basis of a solution of the equations of motion of a viscous fluid (Navier-Stokes equations (Lamb 1932; Kochin et al. 1964; Batchelor 1967)). Suppose that the fluid is incompressible and body forces acting on the fluid are potential. Applying the curl operator (rot) to the vector Navier-Stokes equation, we obtain the following set of equations for calculating the motion of a turbulent vortex ring.

$$\frac{\partial \mathbf{\Omega}}{\partial t} = \operatorname{rot}[\mathbf{u}\times\mathbf{\Omega}] - \nu_t(t)\operatorname{rot}\operatorname{rot}\mathbf{\Omega}, \quad \mathbf{\Omega} = \operatorname{rot}\mathbf{u}, \quad \operatorname{div}\mathbf{u} = 0. \tag{5.9}$$

Here we have used the turbulent viscosity $\nu_t(t)$ introduced above. Assume that the fluid is at rest at infinity and that the averaged velocity field **u** and vorticity distribution $\mathbf{\Omega}$ are determined by a self-similar solution of set (5.9). The following initial conditions are prescribed for set (5.9). At $t = 0$, $\mathbf{\Omega} = 0$ everywhere in the unbounded space, apart from the origin of coordinates where is located a vortex ring of infinitesimal radius and infinitely large intensity, but with finite vortex impulse $\mathbf{J} = (1/2)\int[\mathbf{r}\times\mathbf{\Omega}]dV$. That is at $t = 0$

$$\mathbf{\Omega}(0,\mathbf{r}) = -\mathbf{J}\times\nabla\delta(\mathbf{r}),$$

where **r** is the radius vector, **J** is the vortex impulse, and $\delta(\mathbf{r})$ is the Dirac delta function.

In such statement the problem occurs to be self-similar (Lugovtsov et al. 1969; Lugovtsov 1970, 1974, 1976a,b, 1979). The problem is considered in cylindrical coordinates *z*, *r*. The vorticity $\mathbf{\Omega}$ and the stream function Ψ are chosen to be the unknown functions. Let us introduce the dimensionless self-similar variables x, y, ω, ψ

$$x = \frac{z}{(Jt)^{1/4}}, \quad y = \frac{r}{(Jt)^{1/4}}, \quad \omega(x,y) = \Omega t, \quad \psi(x,y) = \Psi\frac{t^{1/4}}{J^{3/4}}. \tag{5.10}$$

The turbulent viscosity is taken, as earlier in (5.4), in the form $\nu_t(t) = \lambda J^{1/2}t^{-1/2}$. The constant λ is related to the coefficient α by the expression

$$\alpha = \frac{y_0(\lambda)}{x_0(\lambda)}, \tag{5.11}$$

where $x_0(\lambda)$ and $y_0(\lambda)$ are the coordinates of the point where $\omega(x, y)$ reaches maximum. In the self-similar variables (5.10) the set of equations (5.9) is reduced to the form

$$\lambda\left(\omega_{xx} + \omega_{yy} + \frac{1}{y}\omega_y - \frac{1}{y^2}\omega\right) + \frac{1}{4}(x\omega_x + y\omega_y) + \omega = \frac{1}{y}\left(\psi_y\omega_x - \psi_x\omega_y + \frac{1}{y}\psi_x\omega\right), \tag{5.12}$$

$$\psi_{xx} + \psi_{yy} - \frac{1}{y}\psi_y = -y\omega. \tag{5.13}$$

Here x is the distance along the axis of symmetry and y is the distance from the axis of symmetry.

We seek a solution of this problem subject to the conditions

$$\omega \to 0,\ \psi \to 0 \text{ as } x^2 + y^2 \to \infty;\ \ \omega = 0,\ \psi = 0 \text{ at } y = 0 \text{ and} \tag{5.14}$$

$$\pi \int_{-\infty}^{\infty} \int_{0}^{\infty} \omega y^2 dx dy = 1. \tag{5.15}$$

The normalization condition (5.15) follows from conservation of the vortex impulse **J** in the original set (5.9).

It should be noted that this problem has a plane analog corresponding to the motion of a pair of linear vortices of opposite signs. Pukhnachev (1971) proved the existence of a self-similar solution to the plane problem and showed that the problem could be reduced to an integral equation whose nontrivial solution could be written in terms of the Legendre polynomials. Polishchuk, while being a student of Novosibirsk State University, in his degree thesis in 1972, proved solvability of the axisymmetric problem and obtained a numerical solution for small *J*.

Model problem

To solve the problem outlined above we have to apply numerical methods. However, before starting numerical calculations, it is useful to have some preliminary idea about the solution nature, which can be inferred from consideration of a simplified model problem. Lugovtsov (1974) considered the following set of equations as such a model problem

$$\lambda\left(\omega_{xx} + \omega_{yy} + \frac{1}{y}\omega_y - \frac{1}{y^2}\omega\right) + \frac{1}{4}(x\omega_x + y\omega_y) + \omega = \frac{1}{y_0}\psi_y(x_0, y_0)\omega_x, \tag{5.16}$$

$$\psi_{xx} + \psi_{yy} - \frac{1}{y}\psi_y = -y\,\omega \tag{5.17}$$

with the same boundary conditions and normalization as in the exact statement (5.11)–(5.15). Here x_0 and y_0 are the coordinates of the point where $\omega(x, y)$ is maximum. Equation (5.12) has been reduced to the form (5.16) provided that at the point x_0, y_0, where ω reaches maximum, $\psi_x(x_0, y_0) \sim \alpha\psi_y(x_0, y_0)$ and $\alpha \ll 1$. We may expect that solution of the model problem will allow the estimation of the point position $x_0(\lambda)$, $y_0(\lambda)$ and vorticity maximum $\omega(x, y)$ at least, within an order of magnitude. The model problem has an exact solution

$$\omega = \frac{y}{64\pi\sqrt{2\pi}\,\lambda^{5/2}} \exp\left[-\frac{(x - x_0)^2 + y^2}{8\lambda}\right],$$

$$\psi = \frac{y^2}{4\pi(8\lambda)^{3/2} s^3}\left[\Phi(s) - \frac{2}{\sqrt{\pi}} s \exp\left(-s^2\right)\right],$$

where

$$s^2 \equiv ((x - x_0)^2 + y^2)/8\lambda, \quad x_0 = \frac{1}{2\pi\sqrt{2\pi \mathrm{e}}}\left[1 - \left(\frac{\pi \mathrm{e}}{8}\right)^{1/2} \Phi\left(\frac{1}{\sqrt{2}}\right)\right] \lambda^{-3/2},$$

$$y_0 = 2\lambda^{1/2}, \quad \alpha = \frac{4\pi\sqrt{2\pi \mathrm{e}}}{1 - \left(\frac{\pi \mathrm{e}}{8}\right)^{1/2} \Phi\left(\frac{1}{\sqrt{2}}\right)} \lambda^2, \quad \Phi(z) = \frac{2}{\sqrt{\pi}} \int_0^z \exp\left(-\tau^2\right) d\tau.$$

This solution of the approximate problem shows that the parameter λ, like the coefficient α, is rather small, which complicates numerical solution of the problem (5.11)–(5.15).

Structure of a turbulent vortex ring in the limit of vanishing viscosity

Faced with the difficulty of solving the exact problem, it is of interest to study the limiting case $\lambda \to 0$ corresponding to vanishing viscosity (Lugovtsov 1976). This limiting solution may serve as a basis for solving the problem numerically at finite values of λ. To solve the problem at $\lambda \to 0$, we change variables

$$\xi = \frac{1}{\lambda^{1/2}}\left(x - \frac{1}{\lambda^{3/2}} \xi_0\right), \quad \eta = \frac{1}{\lambda^{1/2}} y, \quad \mu = \frac{1}{\lambda^2}, \tag{5.18}$$

$$\omega = \frac{1}{\lambda^2} \bar{\omega}(\xi, \eta), \quad \psi = \frac{1}{\lambda^{1/2}}\left(\Psi + \frac{1}{8} \xi_0 \eta^2\right).$$

This change represents stretching and transition to the reference frame related with the vortex ring. Equation (5.12) in new variables takes the form

$$\bar{\omega}_{\xi\xi} + \bar{\omega}_{\eta\eta} + \frac{1}{\eta}\bar{\omega}_\eta - \frac{1}{\eta^2}\bar{\omega} + \frac{1}{4}(\xi\bar{\omega}_\xi + \eta\bar{\omega}_\eta) + \bar{\omega} = \mu\left[\Psi_\eta \frac{\partial}{\partial\xi}\left(\frac{\bar{\omega}}{\eta}\right) - \Psi_\xi \frac{\partial}{\partial\eta}\left(\frac{\bar{\omega}}{\eta}\right)\right], \tag{5.19}$$

and Eq. (5.13) and normalization (5.15) retain their form with the replacement $x \to \xi$ and $y \to \eta$. The boundary conditions for $\bar{\omega}$ remain as before, and for Ψ we have $\Psi_\eta/\eta \to -\xi_0/4$, $\Psi_\xi/\eta \to 0$ as $\xi^2 + \eta^2 \to \infty$, and $\Psi = 0$ at $\eta = 0$. The value ξ_0 is determined from the condition that the maximum $\bar{\omega}$ lies in the plane $\xi = 0$. Based on the approximate solutions to the problem in hand (Lugovtsov 1970, 1974), one may suppose that in new variables the solution tends to a certain bounded limiting solution as $\lambda \to \infty$ (respectively, $\mu \to \infty$). Then it follows from (5.19) that as $\mu \to \infty$, the expression $\bar{\omega}/\eta = \Omega = \Omega(\Psi)$ is true, though $\Omega(\Psi)$ remains undetermined. In the desired solution, the streamline $\Psi = 0$ divides the

flow into two regions, namely the outer region where streamlines go from infinity to infinity, and the inner region being the vortex atmosphere where streamlines are closed curves. Due to the boundary condition for $\bar{\omega}$, definition of Ω implies that in the outer region $\Omega = 0$ and $\Omega(\Psi)$ in the inner region is to be determined. A similar problem for steady flows of a viscous fluid with closed streamlines in the case when the Reynolds number tends to infinity was considered by Batchelor (1956). Following the ideas of Batchelor's work, we integrate Eq. (5.19) over the region being bounded by some closed streamline to obtain the equality

$$\oint \eta \nabla\Omega \cdot \mathbf{n} dl + 2\oint \Omega n_\eta dl + \frac{1}{4}\oint \xi\eta\Omega n_\xi dl + \frac{1}{4}\oint \eta^2 \Omega n_\eta dl + \frac{1}{2}\iint \eta\Omega \, d\xi d\eta = 0, \quad (5.20)$$

where dl is the streamline element and $\mathbf{n}$ is the unit normal to the streamline. Equation (5.20) is valid for arbitrary μ, since the right hand side of (5.19) vanishes upon integration. Lugovtsov (1976, 1979) demonstrated that passing to the limit $\mu \to \infty$ and keeping in mind that $\Omega \to \Omega(\Psi)$, Eq. (5.20) is cast into an ordinary differential equation

$$P(\Psi)\frac{d\Omega}{d\Psi} = \frac{1}{2}\Gamma(\Psi) + \frac{3}{4}S(\Psi)\,\Omega(\Psi), \quad (5.21)$$

where $P(\Psi) = \iint \eta^3 \Omega \, d\xi d\eta$, $S(\Psi) = \iint \eta \, d\xi d\eta$, and $\Gamma(\Psi) = \iint \eta\Omega \, d\xi d\eta$ is the velocity circulation. Integration is carried out over the region bounded by a closed streamline. The assumption that the limiting solution is bounded implies its continuity. So, the condition $\Omega(0) = 0$ must also be satisfied.

Thus, the problem of determining the structure of a turbulent vortex ring in the limiting case $\mu \to \infty$ reduces to solving the problem of matching (Lavrent'ev and Shabat 1973) the potential (in the outer region where $\Psi < 0$) and vortical (in the inner region where $\Psi > 0$) flows of the inviscid fluid provided that Ψ and $\nabla\Psi$ are continuous at the boundary being determined by the streamline $\Psi = 0$. The form of the function $\Omega(\Psi) = \omega/\eta$ in the inner region is governed by (5.21).

A solution to this limiting problem was found. Calculations show that the velocity, the value of the vortex impulse and kinetic energy of the vortex ring are defined by the expressions $U = k_1 \Gamma/R$, $J = k_2 \Gamma R^2$, $E = k_3 \Gamma^2 R$, respectively, with $k_1 = 0.1978$, $k_2 = 2.8773$, $k_3 = 0.5081$. The quantity α determined experimentally is asymptotically related at large μ to the calculated quantities by the expression

$$\alpha = \frac{\eta_0}{\mu \xi_0} = \frac{3834}{\mu}, \quad (5.22)$$

where $\xi_0 = 0.001486$, $\eta_0 = 5.698$. Using the experimental data (Tarasov 1973, 1975b) which imply that for large Reynolds numbers $\alpha \approx 0.003$, we may evaluate from (5.22) the value of the parameter $\mu \sim 10^6$. From definitions of the turbulent viscosity (5.3) and parameter α (5.11), and assuming change of variables (5.18),

we obtain that the coefficient γ is related to α by $\gamma = 4\alpha/\eta_0^2 \approx 0.1\alpha$. Substituting the above value of α yields $\gamma \approx 0.0003$, which is two orders of magnitude smaller than an analogous coefficient relating the radius and velocity of a jet to the turbulent viscosity in the theory of turbulent jets (Abramovich 1960; Bai Shiyi 1954; Schlichting 1968). The smallness of γ apparently explains why vortex rings have longer distance of travel than turbulent jets of comparable parameters. The neglect of the molecular viscosity is justified if $\nu_t/\nu \gg 1$, which gives according to (5.3), $\mathrm{Re} \gg 10^4$.

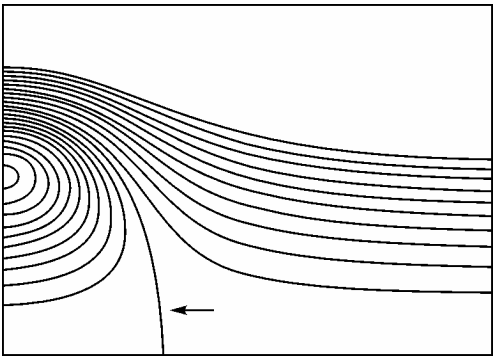

Fig. 5.6. Streamline pattern of a turbulent vortex ring (Lugovtsov 1979)

Calculation results

Some results of numerical calculations are presented in Fig. 5.6–5.9. Figure 5.6 shows the streamline pattern which yields the ratio of the semiaxes of the vortex atmosphere bounded by the closed streamline $\Psi = 0$, $h/l \approx 1.57$. The calculated distributions of the dimensionless velocity u/U, stream function Ψ/UR^2 and vorticity $\omega R/U$ along the radial coordinate r/R in the plane $z = 0$ are shown by solid lines in Figs. 5.7, 5.8, and 5.9, respectively. Here R is the radius and U is the translational velocity of the vortex ring. Figures 5.7–5.9 also represent the experimental data by Akhmetov and Kisarov (1966) and Sullivan et al. (1973). These plots imply that the theoretical distributions of u, Ψ, ω substantially differ from the experimental measurements. In particular, it is seen from Fig. 5.9 that the calculated vorticity distribution in a turbulent vortex ring is more diffuse and less concentrated than even in the experimentally studied laminar vortex rings. Of course, comparison of the self-similar structure of a turbulent vortex ring with the experimental data (Akhmetov and Kisarov 1966; Sullivan et al. 1973) is not quite correct, as these works present the results of investigation of the structure of

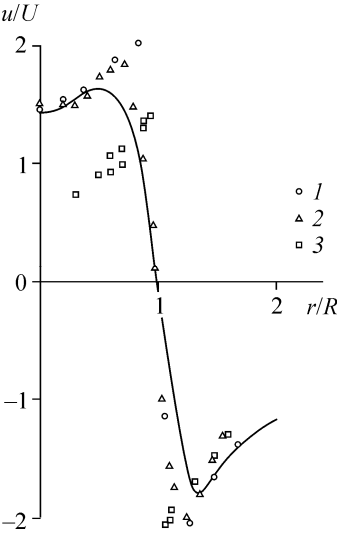

Fig. 5.7. Velocity distribution along the r-axis in the plane $z = 0$ (Lugovtsov 1979). The solid line represents calculation. Experimental data: (*1*) by Akhmetov, Kisarov (1966); (*2*), (*3*) by Sullivan et al. (1973)

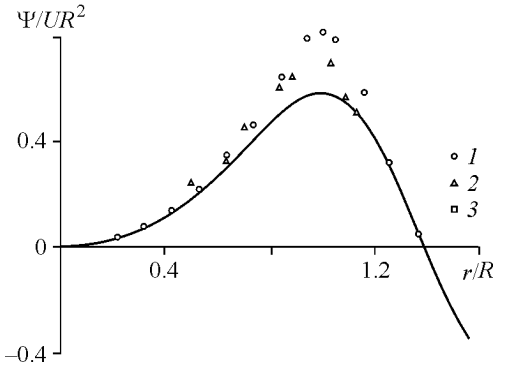

Fig. 5.8. Stream function in the plane $z = 0$ (Lugovtsov 1979). See the legend in Fig. 5.7.

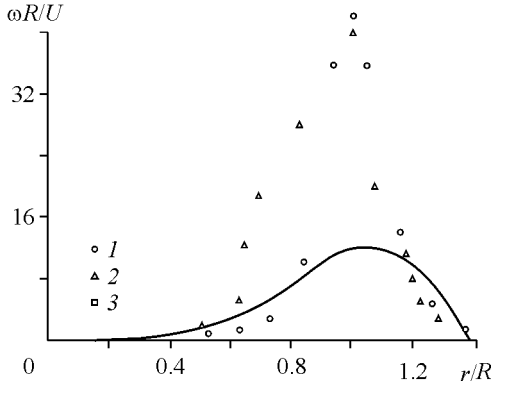

Fig. 5.9. Vorticity distribution in the plane $z = 0$ (Lugovtsov 1979). See the legend in Fig. 5.7.

laminar vortex rings corresponding to the Reynolds numbers $\mathrm{Re} \sim 10^3$. The experimental results on the structure of vortex rings as function of the Reynolds number presented in Chapter 3 imply that the vorticity distribution in a turbulent vortex ring should be more concentrated than in laminar vortex rings. This can be verified by analyzing the experimental data from Section 3.5, which demonstrate that in turbulent vortex rings about half the total vorticity of a vortex ring is concentrated in the core. Since the radius a of the vortex core and the parameter $\varepsilon = a/R$ decrease with an increase of the Reynolds number (see Fig. 5.4), the vorticity distribution in real vortex rings becomes more concentrated as the Reynolds number increases.

Discussion

Possible reasons why the calculated vorticity distribution derived within the theoretical model of a turbulent vortex ring is of diffuse nature was discussed in detail by Lugovtsov (1979) and Vladimirov et al. (1980). In particular, they noted that a

more concentrated vorticity distribution following from experimental data is probably due to the fact that a velocity field of vortex rings was measured at a moderate distance from experimental apparatus, where the structures of the velocity field and of the vorticity possibly had not yet achieved the self-similar regime. It is however more likely that the main theoretical assumption that the turbulent viscosity is independent of space coordinates needs correction, because there are experimental pieces of evidence and theoretical considerations indicating that the turbulent viscosity is actually not constant over the entire volume of a vortex, but rather decreases towards the core of the vortex ring.

This is supposed from the distribution of a passive additive carried by a vortex ring. As seen from Figs. 3.9 and 3.10, the turbulent vortex ring formed by air uniformly colored with smoke, acquires the shape of a torus with well-defined boundaries, although the atmosphere enclosing the vortex moves along with the ring. This implies that smoke particles are scattered in a short time from the atmosphere owing to turbulent diffusion and remain only in the vortex core. Vladimirov and Tarasov (1979b) and Vladimirov et al. (1980) established that when a vortex ring passes through a colored cloud of fluid, the whole vortex atmosphere becomes colored, apart from the toroidal core where the dye does not reach. These experiments point to the absence or sharp decrease in turbulent diffusion and turbulent viscosity in the vortex core. The authors coined the term "suppression of turbulence in the cores of concentrated vortices" for the existence of a laminar core in the turbulent vortex ring. The oscillograms of the velocity distribution along the line passing through the core of the vortex ring shown in Fig. 3.13, also indicate that there are no turbulent pulsations of velocity in the vortex core, as they are present only outside the vortex core in its atmosphere. Theoretical investigations of oscillations and stability of vortex rings (Kop'ev and Chernyshev 2000) established that the flow in the atmosphere of a vortex ring is unstable with respect to small perturbations, which suggests that turbulence in a vortex ring is generated in its atmosphere. Thus, the existing factors imply that turbulence in a vortex ring is not homogeneous, and against the background of a turbulent atmosphere the flow in the core of the vortex ring remains laminar.

It is quite possible that when developing theoretical models the abovementioned experimental facts taken into account will provide more concentrated vorticity distribution in turbulent vortex rings consistent with the experimental data. Dependence of the turbulent viscosity on coordinates does not contradict the assumption of self-similarity of the structure of turbulent vortex rings. Lugovtsov (1979) and Vladimirov et al. (1980) presented some approaches to modeling turbulent stresses in a vortex ring accounting for the experimental facts and ways of improving the theory of motion of turbulent vortex rings described above. It should be noted again that at present there are no sufficiently complete experimental data and theoretical speculations which would allow us to determine the spatial structure of the turbulent viscosity in flows with concentrated vortices. Therefore, further experimental investigations of turbulent vortex rings and concentrated vortices in general are of current interest for elucidating the mechanisms of generation and structure of turbulence and for developing models of turbulence applied to flows with concentrated vortices, consistent with experiment.

6 Practical Implementation of Vortex Rings: Extinction of Fires at Gushing Gas and Oil Wells

For a long time the problem of vortex rings was merely speculative. There were no real examples of their use in practice. Only recently a fundamentally new method of extinguishing fires on spouting gas and oil wells by means of air vortex rings has been developed on the basis of systematic experimental and theoretical studies of the formation, structure and motion of vortex rings carried out in Lavrent'ev Institute of Hydrodynamics (Akhmetov et al. 1980a,b; Akhmetov et al. 1996; Akhmetov and Tarasov 1983; Akhmetov et al. 1998; Akhmetov and Lugovtsov 2002). The proposed technique has been found to be highly efficient and applicable for extinguishing gas and oil fires of virtually arbitrary intensity.

6.1 Origination and Characteristics of Powerful Gas and Oil Gushers

High-power gas and oil gushers occur as a result of accidents during well drilling. Deep wells are drilled using a core drill equipped with a core bit and a core barrel. The core drill is driven by a turbine which is rotated by the pressure of water or dense clay mud supplied to the tube. During drilling a casing string extends progressively deeper to prevent the drilled section from caving. In the process the casing string is filled with water or dense clay mud. A head of liquid in the hole creates a pressure to prevent the outburst of oil or gas to the surface. During drilling the casing lowers below the producing bed containing oil or gas, hence oil and gas cannot move upwards through the open lower end of the pipe of large diameter. To provide production of valuable fluids, the wall of the casing of the drilled hole is perforated at the level of the producing bed by specially shaped explosive charges. The diameter and number of perforated holes are determined depending on the reservoir pressure, thus providing the required controlled flow rate of oil or gas from the well. Emergency spouting occurs when, because of procedural violations, the ground surface end of the well appears to be open at the time when the open bottom end of the casing has not extended yet below the producing bed. In this case high reservoir pressure pushes out the column of liquid filling the hole during drilling, and uncontrolled outflow of oil or gas through the large diameter

string pipe begins. In most cases the drill pipe and the core bit are also thrown up with the fluid. At the ground surface such outflow appears as an intense gusher. A spouting gas cloud is usually electrified and if a spark discharge occurs between this cloud and surrounding metal structures, the spout catches fire. Flow rates of the most high-power gushers reaches 10–20 million m^3 of gas or 10 thousand tons of oil per day, and when such a gusher catches fire, there originates a plume up to 80–100 m high with the thermal power about 4–5 GW. Various types of fires at spouting wells are shown in Fig. 6.1.

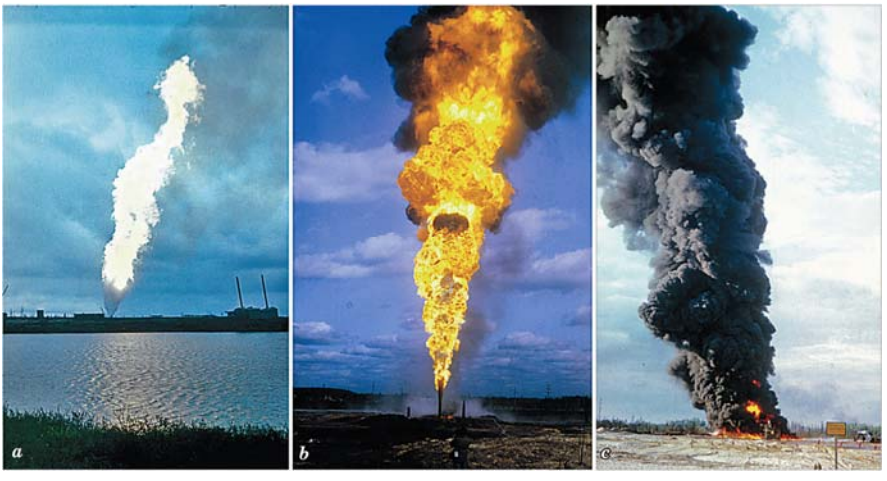

Fig. 6.1. Types of fires at emergency spouting wells. (*a*) gas gusher with the flow rate ~$16 \cdot 10^6$ m^3/day; (*b*), (*c*) oil gushers with flow rates ~$(5–6) \cdot 10^3$ tons/day

Traditional methods of extinguishing fires on gas and oil wells

Until present several ways of extinguishing gas and oil spout fires have existed: by means of powerful water jets and by jets of special fire-extinguishing powders; by gas-water jets created by aircraft turbojet engines or by explosion of a powerful concentrated charge near the well mouth. These methods are suitable for quenching fires on gusher with gas flow rates up to 3–5 million m^3/day and oil flow rates up to 3–5 thousand tons per day, however, they become of little efficiency in quenching more powerful burning gushers. Therefore, the fire extinguishing on high-power gas and oil gushers requires a large number of skilled specialists and technical means. Elimination of such an emergency takes many weeks and months, which leads to considerable economic waste and environmental damage. Thus, development of highly efficient and simple methods of extinguishing fires on spouting gas and oil wells is a topical problem.

6.2 Combustion of Gas and Oil Gushers. Conditions of Stabilization and Flame-Out

Characteristic features of combustion of gas and oil spouts are well illustrated by the example of gas jets. Precisely gas and mixed gas and oil spouts are the most intense type of spouts arising on emergencies at wells. In actual conditions such jets are turbulent. When a gas jet discharging from the well ignites, a so-called diffuse plume forms, which has an axisymmetric cigar shape in a calm atmosphere (Lewis and von Elbe 1961; Vulis and Yarin 1978). The gas in the plume is burnt off in a thin superficial layer, which to a first approximation may be regarded as a surface where the fuel and oxidizer concentrations vanish, and turbulent diffusion transport of the fuel from the jet and of the oxidizer from the atmosphere directed to this surface are in stoichiometric proportion. This diffusive combustion front has no propagation velocity, therefore it cannot stay on its own on the jet flowing upwards. Stabilization of the flame takes place in the lower portion of the plume where the combustion mechanism is somewhat different. When the gas flows from the opening, a turbulent mixing layer of the gas and ambient air forms on the initial portion of the jet surface, which is not burning. The gas concentration in this layer smoothly decreases in the radial direction, as the oxidizer (air) concentration increases. In a certain middle part of the mixing layer a homogeneous fuel-oxidizer mixture occurs with a stoichiometric proportion. When such a mixture prepared for combustion ignites, the flame front can propagate in the mixing layer with a finite velocity even upstream if the turbulent burning velocity w_t exceeds the local jet speed. But since the jet velocity increases as the outlet opening is approached, the local jet velocity u_f equals the turbulent burning velocity w_t at some height, and the flame becomes stabilized. That is the equality $u_f = w_t$ is the condition of flame stabilization. It appears impossible to calculate exactly the turbulent burning velocity w_t. However, estimates show that the value of w_t is roughly equal to the pulsation velocities of the jet. Maximum route-mean-square pulsations of the axial jet velocity are $\sim 0.2u_{\max}$, where $u_{\max}$ is the velocity on the jet axis (Abramovich 1960). Taking this value as an estimate for the burning velocity, we may assume that the maximum speed of flame propagation upstream the gas jet spouting at ~300–450 m/s will be of about 50 m/s. The above analysis of the mechanism of flame stabilization on the jet implies that extinguishing a burning jet requires the inequality $u_f > u_{\max}$ to be valid. Then the condition of flame stabilization at a given height breaks, and the flame is carried upwards by the flow and finally torn off the jet. It is clear that the above inequality can be satisfied either by increasing the local flow velocity u_f in the region of flame stabilization, or by reducing the turbulent burning velocity w_t.

6.3 Determination of Flow Rate of Burning Underexpanded Gas Gushers

When extinguishing fires on powerful gas gushers it is necessary to evaluate the flow rate of the burning gusher, since the gas flow rate is one of the main parameters

determining the extent of the efforts and the material and technical resources required for emergency elimination. However, it is often impossible to directly measure the flow rate of a burning gusher, and there are no efficient remote techniques for determining the jet flow rate. It follows from observations that the flow rate of high-power gas gushers and the height of a plume being formed on their ignition are related. This suggests that remote measurement of the plume height allows an estimation of the gas flow rate (Akhmetov 1994).

Depending on the discharge velocity at the outlet opening gas jets are divided into two types: normally expanded jets whose discharge velocity is smaller than the sound velocity, and underexpanded jet flowing out from the opening at the sound velocity. In the first case the pressure in the exit cross-section of the jet and over the whole jet flow field is constant and equal to the pressure in the ambient atmosphere. Therefore, such jets may be called isobaric. If the gas pressure in the outlet cross-section of the jet exceeds the ambient pressure, such jets are called underexpanded. The discharge velocity of underexpanded jets is equal to the sound velocity in the flow (critical velocity) (Ovsyannikov 1981; Liepmann and Roshko 1966). The excess pressure forces the gas to expand after leaving the opening, and the flow becomes supersonic. Note that due to high discharge velocity and large scales the gas jets are turbulent in both cases.

Plume height on combustion of a normally expanded isobaric gas jet

Let us determine first, following Baev et al. (1977), the plume height of burning isobaric jets. It is known from the theory of submerged turbulent jets (Abramovich 1960; Bai Shiyi 1954; Schlichting 1968) that the diameter D of a turbulent jet linearly increases with distance x from the initial cross-section of the jet, i.e. $D = d_0 + cx,$ where d_0 is the initial jet diameter and c is the coefficient determining the angle of expansion of the jet. Taking x to be the plume height H and accounting for $H \gg d_0,$ we readily obtain that the plume height H and jet diameter at this height are approximately related by

$$D \approx cH. \tag{6.1}$$

We may assume that at the level of the plume top the gas in the jet completely burns out. Conservation of the following quantities can be written for two sections of the jet — at the outlet and at the maximum plume height

flow rate $$(1+L)\rho_0 u_0 F_0 = \rho u F, \tag{6.2}$$

momentum flux $$\rho_0 u_0^2 F_0 = \rho u^2 F, \tag{6.3}$$

energy $$c_{p0} T_0 + L c_{pa} T_a + W = (1+L) c_p T, \tag{6.4}$$

where $\rho, u, F = \pi D^2/4$ are the density, velocity and cross-section area of the jet, respectively, L is the stoichiometric coefficient being the characteristic of the ratio of masses of the oxidizer (in this particular case, of the air) and the gas, needed for complete gas combustion, W is the calorific value of gas, and c_{p0}, c_{pa}, c_p are the

specific heat of the gas, atmospheric air, and combustion products, respectively. The quantities ρ, u, F with the subscripts 0 in (6.2), (6.3) correspond to the outlet cross-section of the jet with the diameter d_0 and the same quantities without subscripts correspond to the jet section at the plume height. It follows from (6.2) and (6.3) that $D^2/d_0^2 = (1+L)^2\,\rho/\rho_0$, where $\rho/\rho_0 = \mu_0 T/\mu T_0$ according to the equation of state, μ and μ_0 are the molecular weights of the gases in the respective jet sections. The temperature ratio can be found from the energy conservation equation (6.4)

$$\frac{T}{T_0} = \frac{W}{(1+L)c_p T_0}\left(1 + \frac{c_{p0}T_0 + Lc_{pa}T_a}{W}\right).$$

For the gases with high calorific value (say, for hydrocarbons) the second term in parenthesis is negligibly small compared to unity, hence approximately $T/T_0 \approx W/((1+L)c_p T_0)$, and therefore $D/d_0 = ((1+L)W\mu_0/c_p T_0\,\mu)^{1/2}$. With (6.1) taken into account, this yields the formula for determining the plume height during combustion of isobaric gas jets

$$H = \frac{kd_0}{\sqrt{T_0}}, \tag{6.5}$$

where $k \approx c^{-1}((1+L)W\mu_0/c_p\mu)^{1/2}$ and c is the dimensionless empirical coefficient characterizing the expansion angle of a turbulent jet and depending generally on the ratio of the gas and air densities (Abramovich 1960). As seen from (6.5), the height of a diffuse plume being formed during combustion of normally expanded turbulent gas jets depends only on the initial jet diameter, temperature and thermophysical properties of a gas and is not related to the flow rate of the gas jet.

The reason why the plume height does not depend on the gas flow rate is qualitatively explained as follows. A change in gas flow rate causes a respective change of the jet speed and intensity of turbulent velocity fluctuations, thus resulting in a change of turbulent diffusion of gases to the plume surface. Intensification of gas mixing at the plume surface with increasing jet flow rate provides burning out of the gas at constant surface area and geometric dimensions of the plume irrespective of the jet velocity. It should be noted that during extinguishing fires of normally expanded gas gushers the need to estimate the gas flow rate does not commonly emerge at all, because, owing to moderate intensity of such gushers, elimination of the fire and emergency at the well is achieved by relatively simple tools.

Combustion of an underexpanded gas jet

The most high-power gas gushers are underexpanded, i.e. the gas pressure p_* at the opening exit exceeds the pressure p in the ambient atmosphere. The gas discharge velocity in the exit cross-section of the well is equal to the velocity of sound u_* in the stream (critical velocity). After flowing out of the hole the gas expands, and the flow in the jet becomes supersonic. In the initial segment of the jet there arises a system of rarefaction and compression waves, which make the pressure in the jet equate gradually with the atmospheric pressure with distance from

Fig. 6.2. Discharge of an underexpanded gas gusher from the well with formation of a barrel-shaped system of shock waves

the exit section, and after that the flow is practically the same as in normally expanded jets. The discharge of an underexpanded gas gusher from the well with formation of a barrel-shaped system of shock waves is shown in Fig. 6.2. Shock-wave structure is naturally visualized due to condensation of heavier gas fractions (for instance, propane, butane, water vapor) upon expansion of a methane jet at the well outlet and virtually instantaneous evaporation of condensed droplets at the shock-wave front emerging on deceleration of the supersonic flow. Observations of discharge and combustion of underexpanded gas jets show that the length of the initial underexpanded segment of the jet is small as compared with the plume height, and the flame is often elevated even above the initial jet segment, which provides good reasons for thinking that combustion takes place only on the isobaric segment of the jet, whose length is dominant (Fig. 6.3).

This implies that combustion of an underexpanded gusher can be considered as combustion of a normally expanded jet whose initial diameter is equal to the diameter of the transition cross-section of the underexpanded jet where the pressure in the jet first equals the atmospheric pressure. Therefore, the plume height H measured from this cross-section can be found from (6.5), taking the initial diameter d_0 and temperature of the jet to be equal to the diameter D and temperature T, respectively, in the transition cross-section of the underexpanded jet. It can be shown that the diameter D of the transition cross-section of the underexpanded jet is determined by the jet discharge velocity from the opening and by the flow rate. The suggested model of combustion of an underexpanded gas jet allows us to find the relation between the jet flow rate and the plume height (Akhmetov 1994).

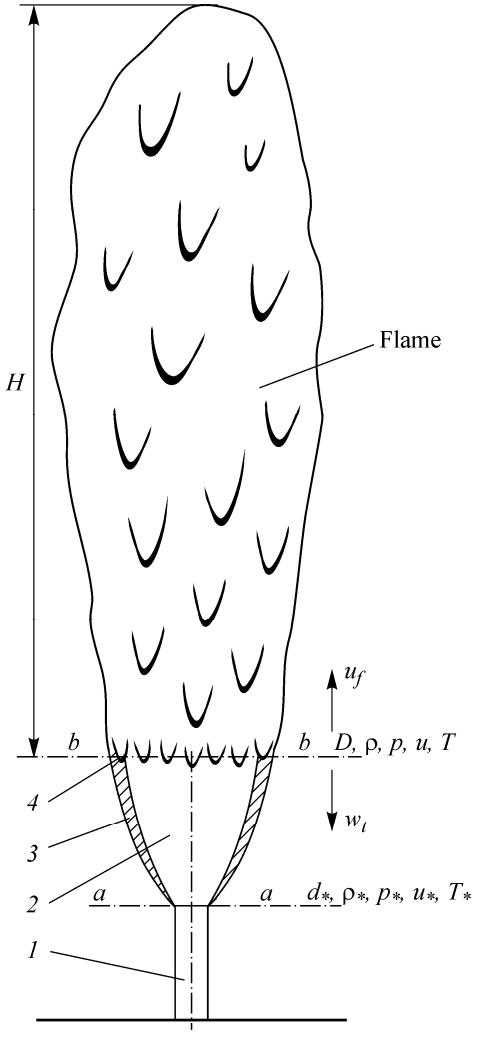

Fig. 6.3. Scheme of discharge and combustion of an underexpanded gas jet. (*1*) outlet pipe, (*2*) underexpanded segment of the jet, (*3*) turbulent mixing layer of the jet, (*4*) flame stabilization zone; d_*, ρ_*, p_*, u_*, T_* are the jet diameter, gas density, pressure, velocity, and temperature, respectively, at the exit cross-section ($a - a$) of the jet; d, ρ, p, u, T are the same quantities in the isobaric cross-section ($b - b$) of the jet; u_f is the jet velocity in the zone of flame stabilization; w_t is the turbulent burning velocity.

Dependence of plume height on flow rate of an underexpanded gas jet

Suppose that the flow in the jet is one-dimensional and the amount of air entrained in the jet at its relatively short initial segment can be neglected. To evaluate the mass flow rate q, we use (6.5) and conditions of mass and momentum conservation

in two cross-sections (see Fig. 6.3) of the underexpanded jet, namely at the exit from the opening and in the transition cross-section

$$q = \rho_* u_* S_* = \rho u S\,, \tag{6.6}$$

$$\rho u^2 S - \rho_* u_*^2 S_* = (p_* - p) S_*\,, \tag{6.7}$$

where ρ_*, u_*, p_*, S_* are the density, velocity gas pressure, and cross-sectional area at the exit, and ρ, u, p, S are the same quantities in the transition, isobaric cross-section of the jet. The gas discharges from the opening with the critical velocity

$$u_* = \sqrt{\gamma R T_*}\,, \tag{6.8}$$

where γ is the adiabatic index and R is the universal gas constant. Using also the equations of state for a gas in the considered cross-sections of the jet

$$p_* = \rho_* R T_*\,, \tag{6.9}$$

$$p = \rho R T\,, \tag{6.10}$$

we obtain the set of equations (6.5)–(6.10) which reduces after transformations to the single quadratic equation for mass flow rate q of the underexpanded gas jet as a function of the plume height H

$$\frac{4k^2 R}{\pi p H^2} q^2 - \left(\frac{2(\gamma+1)}{\gamma} R T_0 \right)^{1/2} q + \frac{\pi p d_*^2}{4} = 0. \tag{6.11}$$

Solution to this equation gives the dependence of q on the plume height. In oil and gas industry gas flow rate is evaluated not in mass but in volumetric units corresponding to the gas density ρ_N under normal atmospheric conditions $p = p_N = 10^5$ Pa, $T = T_N = 288$ K. Hence, it is more convenient to write the solution to (6.11) as a dependence of the volumetric flow rate of a gas gusher $Q = q/\rho_N = q/(p_N/RT_N)$ on the plume height H

$$Q = \alpha \left(1 + \sqrt{1 - \beta / H^2} \right) H^2\,, \tag{6.12}$$

where $\alpha = [\pi(2(\gamma+1)\gamma R T_0)^{1/2}/8\gamma] T_N p / k^2 p_N$, $\beta = (2\gamma/(\gamma+1)) k^2 d_*^2 / T_0$, d_* is the diameter of the well opening, and $T_0 = T_*(\gamma+1)/2$ is the gas stagnation temperature. As follows from (6.12), in order to determine the gas flow rate, one needs to know also the gas stagnation temperature T_0 in the exit cross-section of the well. It is not always possible to measure the gas temperature before extinguishing the fire. However, since the dependence of Q on T_0 is relatively weak, and the gas temperature varies only a little between various gushers, the gas flow rate can be estimated with an accuracy sufficient for practical purposes using some average value T_0. The value of the coefficient k which enters (6.5) and the subsequent formulas for estimating the flow-rate of underexpanded jets can be found numerically. However,

k depends on the parameter c which characterizes the jet expansion angle and is not clearly defined, therefore k is more reliably evaluated from (6.12) using estimations of Q and H at fixed values of α and β. Such experimental data imply that for methane (CH_4) gas jets, among which there are also gas gushers on wells, $k \approx 2.48 \cdot 10^3$ K$^{1/2}$.

It may be shown that the condition of the gusher underexpansion $p_*/p > 1$, which is necessary for applying the flow-rate calculation formula (6.12), is reduced to the inequality $H > ((\gamma+1)/2)^{1/2} k d_* T_0^{-1/2}$, which can be easily verified at fire extinguishing. Provided this condition is true, (6.12) can be used to estimate the flow rate of burning gas gushers for any degree of the jet underexpansion. The flow rate of highly underexpanded gushers (when $p_*/p \gg 1$) can be estimated by the simpler approximate formula

$$Q \approx \frac{\pi\sqrt{2(\gamma+1)\gamma R T_0}}{4\gamma} \frac{p T_N}{k^2 p_N} H^2, \qquad (6.13)$$

which follows from (6.12) for $\beta/H^2 \ll 1$. Assuming that $T_0 \sim 293$ K, $p = p_N = 10^5$ Pa and $T = T_N = 288$ K, we obtain that for highly underexpanded methane gushers $Q \approx 2.33 \cdot 10^3 H^2$, where H is measured in meters and Q in m^3/day. Figure 6.4 compares this approximate dependence with the existing measurement results. Calculation using approximate formula (6.13) underestimates the plume height at small flow rates, but calculated values of the plume height obtained from exact formula (6.12) are in agreement with the measurement results over the whole range of flow-rate measurements. Thus, the intensity of high-power gas gushers can be characterized by such a simple and conveniently measured parameter as diffusive plume height H.

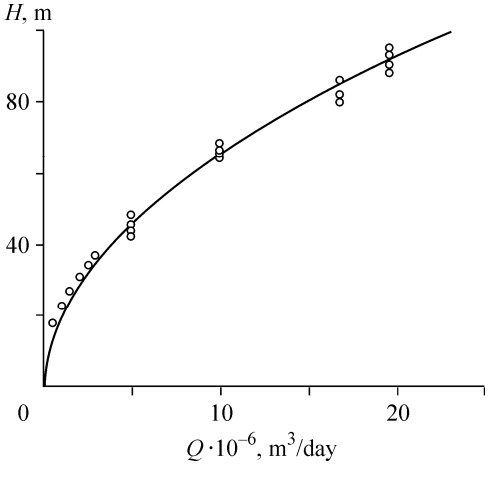

Fig. 6.4. Plume height at combustion of underexpanded gas jets as a function of the gas flow rate. Calculation by the approximate formula (6.13) (solid line), direct measurements of the flow rate after fire extinction (points).

From the physical point of view, dependence of the height of a diffusive plume being formed on combustion of underexpanded gas jets on the gas flow rate is explained as follows. The cross-section diameter D of an underexpanded jet at the height where the jet flow becomes isobaric and combustion of a gas jet begins, is a

function of the gas flow rate, i.e. $D = D(q)$ and the plume height H in combustion of isobaric jets, according to (6.5), is proportional to its initial diameter, which in this case coincides with D, so $H \sim D(q)$. Hence, this implies the existence of the functional dependence between the gas jet flow rate and the plume height in combustion of the underexpanded jet.

6.4 Physical Grounds for Extinguishing of a Diffusion Plume by an Air Vortex Ring

As noted above, in combustion of a gas and oil jet the lower edge of the flame is stabilized at some height where the local flow velocity u_f on the jet surface is equal to the turbulent burning velocity w_t at this point. That is the flame is stabilized on the jet under the condition

$$u_f \approx w_t . \tag{6.14}$$

If the flow velocity u_f in the zone of flame stabilization is somehow increased externally, the stabilization condition will break and the lower edge of the flame will be carried upwards by the flow, and finally torn off the jet. A similar situation takes place when the velocity of flame propagation w_t decreases. Thus, in order to tear the flame off the jet, one needs either to increase the flow velocity near the lower edge of the plume or to diminish the turbulent burning velocity. Experimental results show that an air vortex ring moving upwards along the axis of a burning jet can be an efficient tool for extinguishing the plume. Two vortex ring properties are the most essential factors for fire extinguishing.

The first property is the distribution of the axial velocity component u. Qualitative pictures of the u velocity distribution in the plane of a vortex ring of radius R

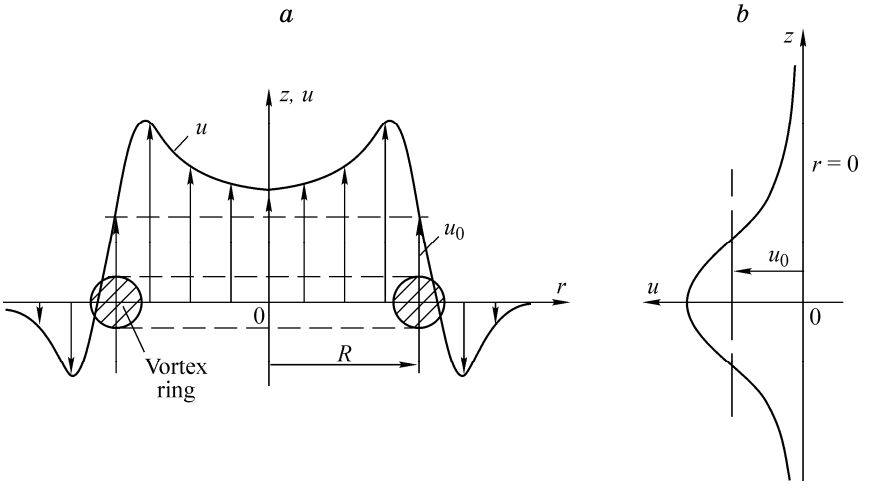

Fig. 6.5. Velocity distribution in a vortex ring, in the ring plane (*a*) and along the *z*-axis (at $r = 0$) (*b*)

(at $r = 0$) and on the symmetry axis z (at $r = 0$) in the axisymmetric coordinate system z, r are shown in Fig. 6.5. These plots make evident that the axial velocity component inside the ring (for $r < R$, $z \approx 0$) is everywhere greater than the translational velocity of the vortex ring u_0 and has the same direction. Obviously, the velocity field of a vortex ring moving along the axis of a jet of smaller radius than the ring radius is superimposed on the velocity field of the jet and increases the velocity over the whole cross-section of the jet being passed by the vortex ring, whence the flame is carried upwards and is torn off the jet.

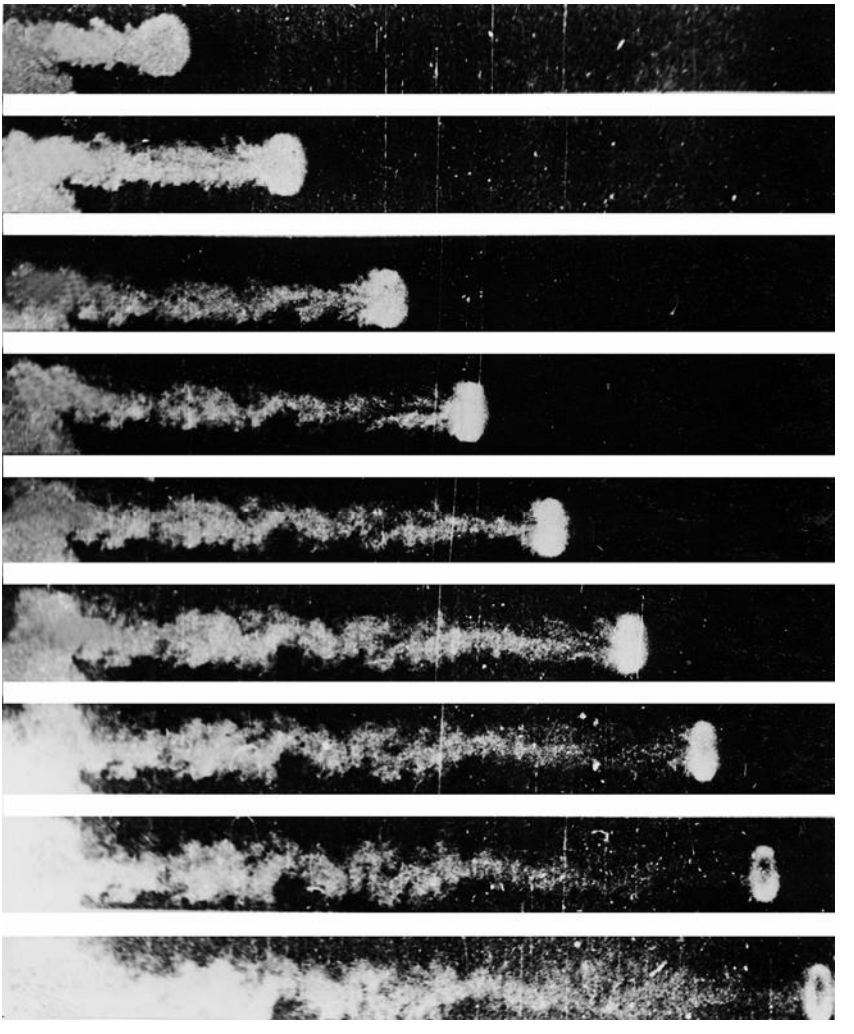

Fig. 6.6. Sequential pictures illustrating the transfer of a dispersed admixture by a vortex ring

The second property of the vortex ring which is favorable for plume extinguishing is that a certain volume of fluid, the so-called vortex atmosphere, moves together with the vortex ring. The vortex atmosphere is shaped like an ellipsoid of rotation oblate in the direction of motion. In a frame of reference moving with the vortex, the motion of the ambient medium coincides with the flow without separation past a solid body corresponding to the vortex atmosphere, and inside the vortex atmosphere the fluid circulates along closed streamlines (see Fig. 2.20). The existence of a flow region with closed streamlines is favorable for containing fine particles within this region, therefore the vortex ring can transfer dispersed powder introduced into its atmosphere during vortex formation. Mechanisms of transfer of a dispersed admixture by a vortex ring were studied theoretically and experimentally in the works (Lugovtsov 1970; Buzukov 1971; Tarasov and Yakushev 1974). The motion of an air vortex ring filled with dispersed matter is illustrated in Fig. 6.6.

In the initial stage of motion, the dispersed matter is efficiently confined and transferred in the vortex atmosphere and then gradually spreads forming a wake (see Fig. 6.6). For extinguishing gas and oil plumes by vortex rings, it is most feasible to use dispersed admixtures of special fine fire extinguishing agents intended for extinguishing fires of gaseous and liquid hydrocarbon fuels (Shriber and Porst 1975). When a cloud of fire extinguishing agent with a large total surface area of particles is introduced into the flame, the powder rapidly absorbs the heat to diminish the temperature and turbulent burning velocity w_t. As the vortex ring filled with the dispersed fire extinguishing agent moves along the jet axis, the combined effect of these two factors, namely the increased local jet velocity u_f and reduced turbulent burning velocity w_t, violates the flame stabilization condition (6.14) on the jet. As a result, the flame rapidly moves upwards and tears off the jet.

The possibility of extinguishing plumes by means of vortex rings was established in elementary tests of extinguishing the flame on an asbestos wick 3–4 mm in diameter and ~0.5 m long, wetted with gasoline or kerosene. The wick was suspended vertically, and a vortex ring ~10–12 cm across moved along the wick upwards with an initial velocity of ~4–6 m/s. The plume was quenched virtually in all trials. Successful results of the tests of extinguishing such a makeshift plume demonstrated that an air vortex ring moving along the axis of a burning jet can also be used in extinguishing flame on gas-liquid fuel jets.

Experiments on flame extinguishing of gas gushers

In order to perform experimental check of the above physical considerations, we carried out laboratory-scale tests of extinguishing a gas plume produced during spouting of condensed propane from an opening ranging from 1 to 5 mm in diameter. By weighing the propane cylinder before and after the tests the gas flow rate was estimated to vary from 0.013 to 0.65 kg/s. Interaction of jets with a vortex ring is not sufficiently studied. Obviously, a jet passing through a vortex ring expedites its destruction. However, it was established that the initial stage of vortex ring motion along the jet, when the ring is most resistant to disturbances, is especially important for the upward flame shifting and blowing it off the burning jet. Figure 6.7 illustrates the sequential phases of vortex ring motion along the

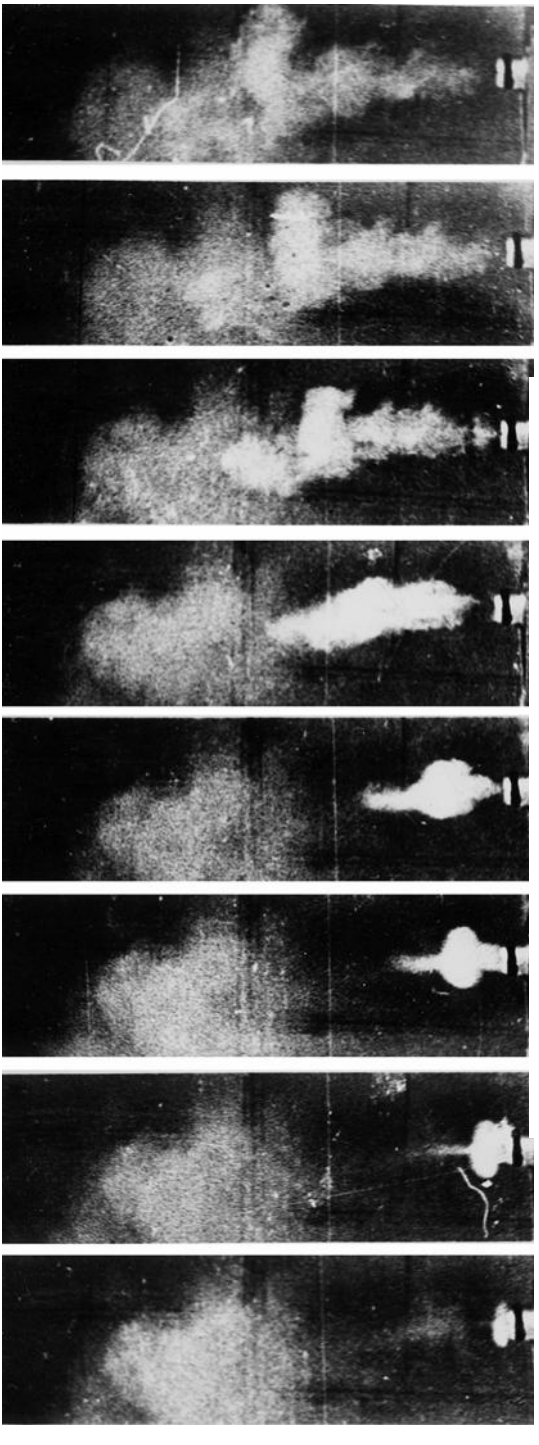

Fig. 6.7. Vortex ring motion along the gaseous propane jet

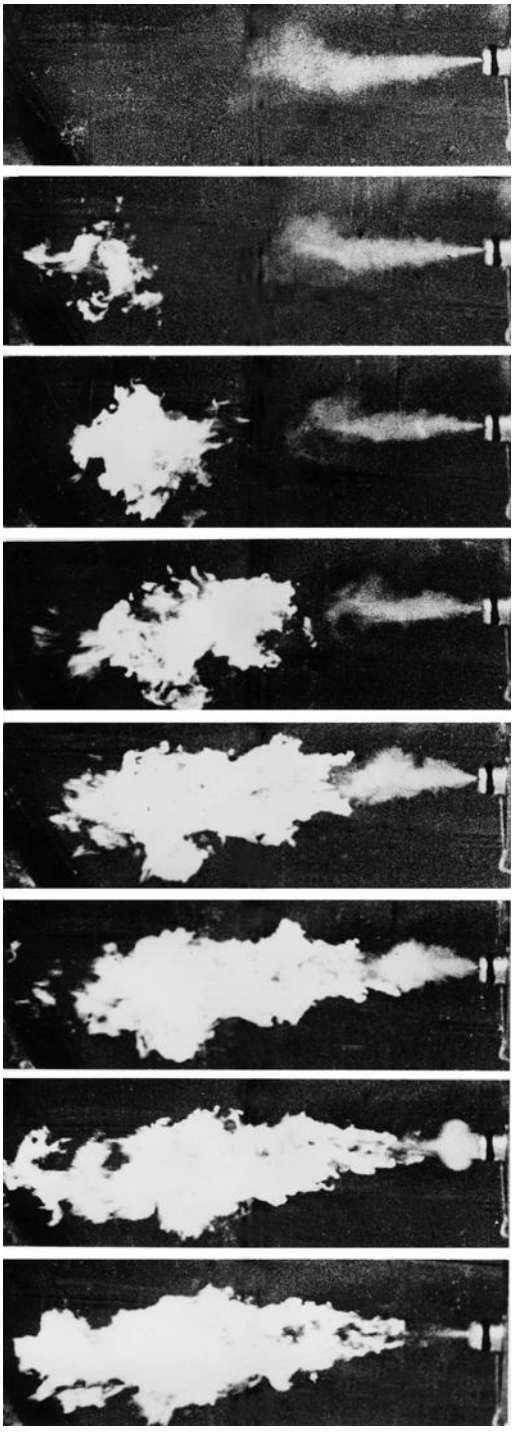

Fig. 6.8. The process of extinguishing a plume by a vortex ring

propane jet that is not burning. One can see that at the starting motion stage the gas jet having larger initial velocity than the vortex ring flows through the ring. But as the vortex ring travels a distance about several diameters of the ring, flowing of the jet through the ring becomes impossible, since the jet velocity rapidly falls in comparison with the translational velocity of the vortex ring. When this jet is ignited, there arises a plume 2–2.5 m high with the maximum diameter ~0.3 m. The extinguishing process using an air vortex ring is shown in Fig. 6.8. The first frames clearly illustrate the vortex ring visualized with smoke moving upwards along the spout axis. The whole process of the plume extinguishing lasts for ~0.2 s; during the first half of this period the flame is blown off the lower segment of the jet, and during the remaining time the fuel cloud above the vortex ring is burning out.

Later the principle of pressing the fuel out by the propane pressure was used also in constructing a large-scale field experimental apparatus for producing spouts with a fuel flow rate of up to 5.2 kg/s (Fig. 6.9). The device consists of a cylindrical tank *1* with capacity of 1 m^3 (the tank is 2 m high and 0.8 m in diameter) with fuel *2*. The main pipeline *3* attached to the tank has a vertical outlet *4* which ends with changeable nozzles *5*. For safety reasons, the tank and the main pipeline are buried in the ground. Devices *6* and *7* for fuel filling, manometer *8* and tank fuel level unit *9* are mounted into the upper tank cap. The electromagnetic valve *10*

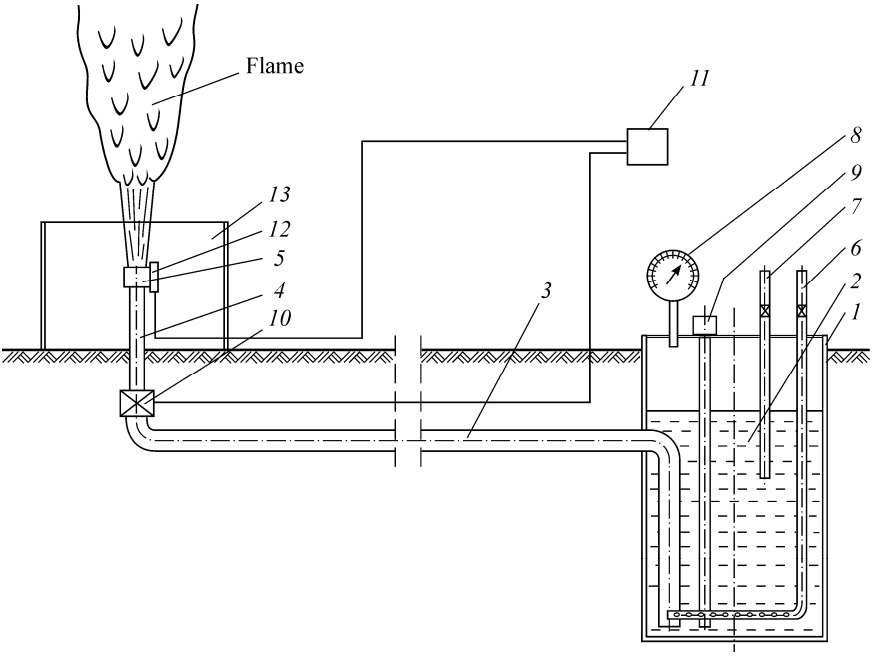

Fig. 6.9. Layout of the experimental apparatus for producing spouts with flow rate to 5.2 kg/s for testing of extinguishing of this spout. See the legend in the text.

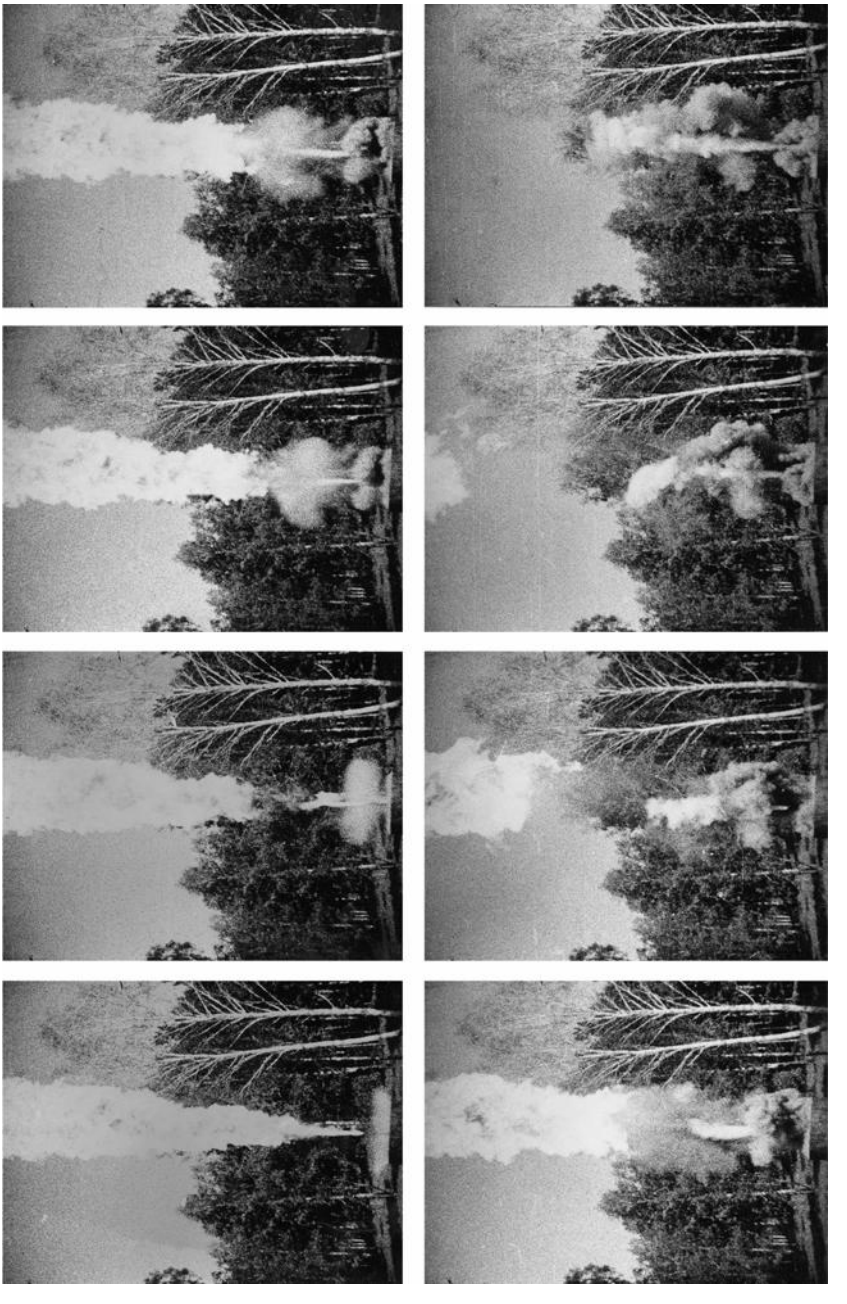

Fig. 6.10. Extinguishing of the propane jet plume with a flow rate of ~5.2 kg/s by a high-speed air vortex ring

controlled from the remote console *11* is built in the main pipeline 80 mm in diameter. The spouting fuel jet is fired by the powder-charge igniter *12* with an electric primer. The design of the experimental apparatus allowed us to produce not only propane, but also kerosene jets and jets consisting of mixture of propane and kerosene. The maximum plume height attained by such jets in combustion was 30 m. In the first series of experiments plume extinguishing was accomplished by a purely air vortex ring without the use of any fire extinguishing agents, i.e. the flame was torn off the jet only due to the action of the velocity field of the vortex ring on the plume.

The vortex ring was produced by explosion of a small ring charge placed on the bottom of the cylindrical tube *13* of large diameter mounted on the ground surface coaxially to the spouting jet. Figure 6.10 demonstrates film frames showing separate stages of extinguishing plume ~30 m high by an air vortex ring. The vortex ring was colored with smoke to visualize the process. We can see the rise of the vortex ring along the jet axis and gradual upward shifting of the flame. In the last film frame the plume has already been extinguished, and one can see the discharge of the propane jet which is not burning any more. The experiments showed that fire extinguishing of high-speed gas spouts can be carried out by an air vortex ring with an initial velocity of about 50–100 m/s. However, vortex rings with such initial velocities can be obtained at discharge of a high-speed air jet from a tube of large diameter. It is obvious that the necessity to bring bulky structures to an emergency well and to mount them near the well mouth would substantially complicate the use of this method. Therefore, it has become clear that it is preferable to use relatively low-speed vortex rings to extinguish real fires on wells, since they can be produced easier, without any devices and structures. However, in this case the intensity of the velocity field of a low-speed vortex ring might occur to be insufficient for flame blow-off, and then it is necessary to diminish the turbulent burning velocity w_t in the mixing layer of the jet. To solve this problem, it was suggested to use the ability of a vortex ring to carry a dispersed admixture, for instance, fire extinguishing powders. It was mentioned above that introduction of dispersed fire xtinguishing powder into the flame abruptly diminishes the reaction rates of combustion and flame propagation. In this case extinguishing of a burning plume by an air vortex ring carrying dispersed fire

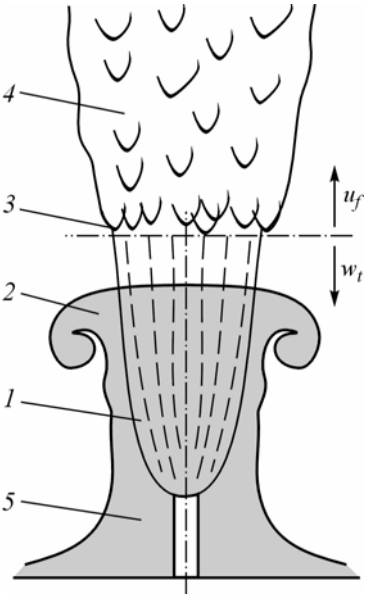

Fig. 6.11. Scheme of plume extinguishing by a vortex ring filled with a dispersed fire-extinguishing powder. (*1*) jet, (*2*) vortex ring, (*3*) lower edge of the flame, (*4*) plume, (*5*) cloud of fire-extinguishing powder in the trail of the vortex ring.

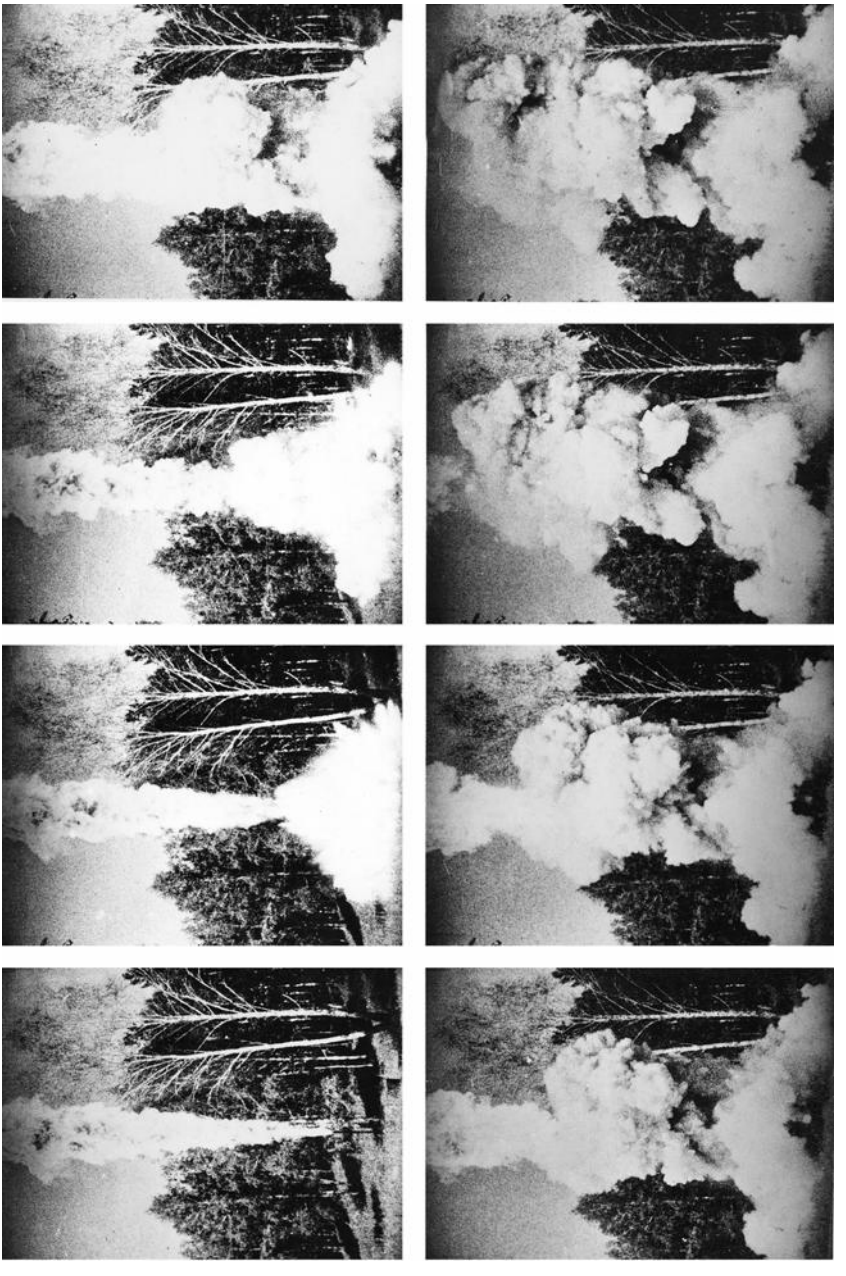

Fig. 6.12. Plume extinguishing by a vortex ring filled with a dispersed fire-extinguishing powder

extinguishing powder in its atmosphere is accomplished by a combined effect of two factors. First, as a vortex ring moves along the spout axis, the velocity field induced by the vortex ring is added to the velocity of a spouting jet (see Fig. 6.5), thus increasing the local jet velocity u_f in the region of flame stabilization. Second, the dispersed powder cloud transferred in the vortex atmosphere enters the flame and sharply diminishes the turbulent burning velocity w_t. The combined effect of these two factors breaks the condition of flame stabilization (6.14) on the jet, whence the flame is rapidly moved upwards and torn off the jet. The extinguishing efficiency is also enhanced by the blowout of a part of the dispersed powder from the vortex ring into its trail, which embraces the lower extinguished part of the plume with the powder cloud and hence eliminates the possibility of its repeated ignition. The vortex ring filled with dispersed fire extinguishing powder is produced by explosion of a small linear charge placed on the ground surface around a well and overlain with a layer of extinguishing powder. When this charge explodes, there arises a pulse gas-powder upward-moving jet, which soon transforms into a mushroom-like vortex ring containing the dispersed powder and moving along the spout axis (Fig. 6.11). The process of extinguishing of a ~30 m high plume by a vortex ring filled with dispersed fire extinguishing powder is shown in Fig. 6.12.

6.5 Principles of Scale Modeling and Calculation of Amount of Fire Extinguishing Agents

With the purpose of establishing the principles of modeling and calculation of agents required for extinguishing fires of arbitrary scale gas and oil spouts by a vortex ring, we carried out a series of experimental studies on extinguishing burning methane, propane, kerosene, and oil spouts. Flow rates of the test spout varied in a wide range from 0.01 to 70 kg/s. The plume height in these tests varied from 2 to 50 m and the maximum diameter of the plume varied from 0.3 to 8 m. The experiments on extinguishing high-power full-scale oil gushers with flow rate to

Fig. 6.13. Stages of fire extinguishing at an experimental oil spout with a flow rate of 6100 tons/day

6100 tons per day were carried out at a specially equipped testing ground near the Samotlor oil field in the Tyumen region of Russia (Fig. 6.13). The experiments show that the vortex-powder method is efficient for extinguishing gas and liquid plumes of virtually any intensity. It was established that the diameter of a vortex ring D_V needed for extinguishing the plume must be approximately equal to the maximum diameter of the plume D_F. The experimental dependence of D_V on D_F is presented in Fig. 6.14. The proportionality between D_V and D_F implies that the volume of a vortex ring (the volume of the vortex atmosphere) and the mass of dispersed fire extinguishing powder (given its concentration) contained in this volume must be proportional to D_F^3. It is known from investigations of combustion of gas jets (Lewis and von Elbe 1961; Vulis and Yarin 1978) that turbulent diffusion plumes are geometrically similar, and the ratio of the plume height H to its maximum diameter D_F is nearly constant, hence we take the plume height H as a basis for calculation of the amount of fire extinguishing agents, since it can be easier determined under conditions of a well fire and is uniquely related to the gusher flow rate. These considerations and results of experimental studies allowed us to obtain formulas for calculating the mass of a fire extinguishing powder M and the mass of the explosive m required for extinguishing plumes of height H: $M = k_1 H^3$, $m = k_2 H^3$, where k_1, k_2 are constant coefficients. As a result of experiments, the optimum procedures and practical techniques of bringing and placing fire extinguishing agents near a well mouth under fire conditions were also elaborated. The established principles of calculation and modeling, as well as the practical procedures for implementation of the method guarantee fire extinguishing of compact (i.e. spouting in the form of a single jet) gas and oil gushers of virtually any intensity.

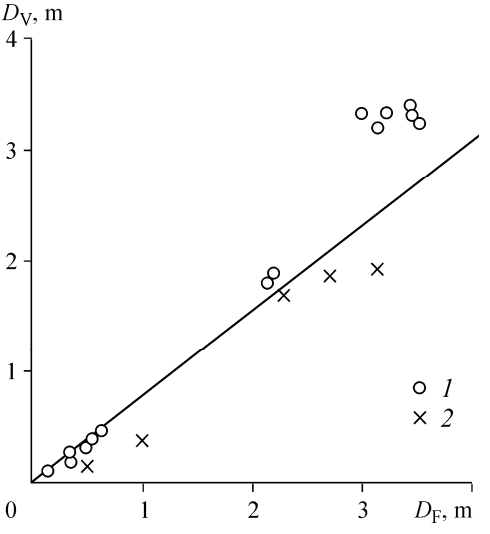

Fig. 6.14. Vortex ring diameter D_V required for plume extinguishing as a function of the maximum plume diameter D_F. (*1*) the plume was extinguished, (*2*) the plume was not extinguished

6.6 Extinguishing of Real Well Fires by a Vortex Ring

The proposed method was used for extinguishing a number of large fires on emergency spouting wells on the territory of the former USSR. The fire on a high-power gas condensate gusher in Uzbekistan was the first one extinguished by this method (Akhmetov and Tarasov 1983; Kasymov 1983). The open spouting and the well fire

occurred during exploration drilling at a new gas field in a desert arid region. The gusher flow rate peaked to 20 million cubic meters of gas per day at a plume height of 90–95 m. Powerful pumping stations, units with aircraft turbojet engines used for extinguishing such fires, and other complicated fire fighting equipment were brought to the emergency location. The fire extinguishing was complicated by the absence of water in the region of the well location. Water was stored in specially made basins with a net capacity of ~5000 m^3, which were filled through metal pipes laid at a distance of more than 20 km. More than 400 persons took part in eliminating the emergency. During a month there were eight attempts to extinguish the fire using traditional methods. However, all attempts had failed. Then for the first time it was decided to use the vortex-powder extinguishing method. Preparation to extinguishing by this method took several hours, and the fire was extinguished at the first try. Figure 6.15 shows the photograph of one of the final stages of extinguishing, when the flame had been almost torn off the plume.

Thus, vortex rings came into practice for the first time. The developed high-performance vortex-powder method allows extinguishing fires on high-power gas and oil gushers arising at emergencies on wells. To extinguish a fire using this method, an air vortex ring filled with dispersed fire extinguishing powder acts on a plume in a pulsed way. The vortex ring is produced by explosion of a small

Fig. 6.15. Extinguishing of the fire at the gas well in Uzbekistan. Gusher flow rate ~$20 \cdot 10^6$ m^3/day, plume height ~90 m

distributed charge. The advantages of the method are revealed to the maximum extent in extinguishing fires on extremely high-power gas and oil gushers, when traditional methods appear to be inefficient. The method allows a drastic reduction of time needed to extinguish a fire. A fire of any possible intensity can be extinguished by several skilled specialists during one day using a minimum amount of fire extinguishing materials. Application of the method does not require bulky and expensive equipment and machinery to be transported to the emergency site and to be used there. The method is well suited for use in arid desert regions and in winter conditions, because water is not needed for flame extinguishing. By now the vortex-powder method has been successfully used to extinguish a number of large fires on gas and oil gushers in Uzbekistan and West Siberia.

References

Abramovich, G.N.: Theory of Turbulent Jets (in Russian). Fizmatgiz, Moscow (1960)

Abrashkin, A.A.: Vortex waves and vortices in an ideal incompressible fluid. Synopsis of Doctor Thesis in phys. and math. sciences, Inst. of Applied Mechanics of the RAS, Moscow (1999)

Abrashkin, A.A., Yakubovich, E.I.: Two-dimensional vortices in an ideal fluid. In: Nonlinear waves. Structures and bifurcation (in Russian), Nauka, Moscow, pp. 147–159 (1987)

Abrashkin, A.A., Zenkovich, D.A.: Nonlinear Kelvin waves on the boundary of a cylindrical vortex. Fluid Dynamics 32(5), 664–671 (1997)

Ahlberg, J.H., Nilson, E.N., Walsh, J.L.: The theory of splines and their applications. Academic Press, London (1967)

Alekseenko, S.V., Kuibin, P.A., Okulov, V.L.: Theory of Concentrated Vortices: An Introduction. Springer, Heidelberg (2007)

Akhmetov, D.G.: Burning gusher flowrate evaluation based on diffusive plume height. Combustion, Explosion, and Shock Waves 30(6), 746–749 (1994)

Akhmetov, D.G.: Formation and basic parameters of vortex rings. J. Appl. Mech. Tech. Phys. 42(5), 794–805 (2001)

Akhmetov, D.G.: Vortex rings (in Russian: Vikhrevye kol'tsa). Academic Publishing House GEO, Novosibirsk (2007)

Akhmetov, D.G.: Loss of energy during the motion of a vortex ring. J. Appl. Mech. Tech. Phys. 49(1), 18–22 (2008a)

Akhmetov, D.G.: Model of vortex ring formation. J. Appl. Mech. Tech. Phys. 49(6), 909–918 (2008b)

Akhmetov, D.G., Kisarov, O.P.: Hydrodynamic structure of a vortex ring. J. Appl. Mech. Tech. Phys. 7(4), 87–90 (1966)

Akhmetov, D.G., Lugovtsov, B.A.: Vortex-powder method of fire extinguishing on gushing oil and gas wells (in Russian). In: Proceedings of a school-seminar Physics of an oil bed, Novosibirsk, pp. 7–13 (2002)

Akhmetov, D.G., Lugovtsov, B.A., Maletin, V.A.: Vortex powder method for extinguishing fire on spouting gas-oil wells. Prevention of hazardous fires and explosions. In: Proc. of Advanced research workshop NATO SC/SB RAS, Novosibirsk, May 12–15, 1998, pp. 319–328. Kluwer Acad. Publ., Dordrecht (1999)

Akhmetov, D.G., Lugovtsov, B.A., Maletin, V.A., Mironov, B.A., Tarasov, V.F., Chernukhin, N.E.: Novel methods of fire extinguishing on oil and gas wells under conditions of emergency gushing. In: Problems of development of oil and gas complex of Siberia (Collected reports), Inst. of Geology and Geophysics. SB RAS, Novosibirsk, vol. 2, pp. 180–185 (1980a)

Akhmetov, D.G., Lugovtsov, B.A., Maletin, V.A., Tarasov, V.F., Chernukhin, N.E.: Inventor's certificate No.895174 of the USSR dated by 09.01.1981 (in Russian). Bulletin of Inventions 4, 272 (1996)

Akhmetov, D.G., Lugovtsov, B.A., Tarasov, V.F.: Extinguishing gas and oil well fires by means of vortex rings. Fiz. Goreniya Vzryva 5, 8–14 (1980b)

Akhmetov, D.G., Tarasov, V.F.: Extinguishing fire of a powerful gas gusher. In: Dynamics of Continuous Media (collected scientific papers) (in Russian), vol. 62, pp. 3–10. Institute of Hydrodynamics, Novosibirsk (1983)

Akhmetov, D.G., Tarasov, V.F.: Structure and evolution of vortex cores. J. Appl. Mech. Tech. Phys. 27(5), 690–694 (1986)

Akhmetov, D.G., Vladimirov, V.A., Il'in, K.I., Makarenko, B.G., Nikulin, V.V., Tarasov, V.F.: Hydrodynamics of vortical flows (bibliographical index). In: Lavrentiev Inst. Hydrodynamics. Siberian Division Acad. Sci.USSR, Novosibirsk (1988)

Anton, L.: Ausbildung eines Wirbels an der Kante einer Platte. Ing. Arch. 10, 411–427 (1939)

Baev, V.K., Ktalkherman, M.G., Yasakov, V.A.: Study of Gaseous Fuel Combustion (in Russian). pp.21–51, ITPM SO AN SSSR (1977)

Shiyi, B.: Fluid Dynamics of Jets. Van Nostrand (1954)

Banerji, S.K., Barave, R.V.: On Oberbecks Vortices, Phil. Mag 11, 105 (1931)

Bardotti, G., Bertotti, B.: Magnetic configuration of a cylinder with infinite conductivity. J. Math. Phys. 5, 1387–1390 (1964)

Barenblatt, G.I.: Scaling, self-similarity, and intermediate asymptotics. Cambridge University Press, Cambridge (1996)

Batchelor, G.K.: On steady laminar flow with closed streamlines at large Reynolds number. J. Fluid Mech. 1(1), 177–190 (1956)

Batchelor, G.K.: An introduction to fluid mechanics. Cambridge University Press, Cambridge (1967)

Berezovski, A.A., Kaplanski, F.B.: Diffusion of a Ring Vortex. Fluid Dynamics 22, 832–836 (1988);Translation of: Izv. Akad. Nauk SSSR, Mekh. Zhidk. Gaza 6, 10–15 (1987)

Betz, A.: Wie ensteht ein Wirbel in einer wenig zähen Flüssigkeit. Die Naturwissenschaften 9, 193–196 (1950)

Buzukov, A.A.: Properties of the formation and motion of vortex rings in water. J. Appl. Mech. Tech. Phys. 12(2), 318–325 (1971)

Didden, N.: On the formation of vortex rings: Rolling-up and production of circulation. Z. Angew. Math. Phys. 30, 101–116 (1979)

Durst, F., Melling, A., Whitelaw, J.H.: Principles and practices of laser-Doppler anemometry. Academ. Press, N.Y (1976)

Dwight, H.B.: Tables of integrals and other mathematical data. Macmillan Co., New York (1961)

Dyson, F.W.: The potential of an anchor ring. Part II. Phil. Trans. R. Soc. London. Ser A184, 1041–1106 (1893)

Elder, F.K., de Haas, N.: Experimental study of the formation of a vortex ring at the open end of a cylindrical shock tube. J. Appl. Phys. 23(10), 1065–1069 (1952)

Feynman, R.P., Leighton, R.B., Sands, M.: The Feynman Lectures On Physics. In: Mainly Electromagnetism and Matter, vol. 2. Addison-Wesley, Reading (1964)

Fraenkel, L.E.: On steady vortex rings of small cross-section in ideal fluid. Proc. R. Soc. London. Ser A316, 29–62 (1970)

Fraenkel, L.E.: Examples of steady vortex rings of small cross-section in an ideal fluid. J. Fluid Mech. 51, 119–135 (1972)

Gharib, M., Rambod, E., Shariff, K.: A universal time scale for vortex ring formation. J. Fluid Mech. 360, 121–140 (1998)

Gleser, A., Coles, D.: An experimental study of a turbulent vortex ring. J. Fluid Mech. 211, 243–283 (1990)
Goldstein, S.: Modern Developments in Fluid Dynamics. Dover (1965)
Golitsyn, G.S.: Vvedenie v Dinamiku Planetarnykh Atmosfer (in Russian). In: Introduction to the Dynamics of Planetary Atmospheres. Gidrometizdat, Leningrad (1973)
Gostintsev, Y.A., Lazarev, V.V., Solodovnik, A.F., Shatskikh, Y.V.: Turbulent thermal in a stratified atmosphere. Fluid Dynamics 21(6), 965–976 (1986);Translation of: Izv. Akad. Nauk SSSR. Mekh. Zhidk. Gaza 21(6), 141–153 (1986)
Gradshtein, I.S., Ryzhik, I.M.: Tables of integrals, series and products. Academic Press, New York (1965)
Greenspan, H.P.: The Theory of Rotating Fluids. Cambridge Univ. Press, London (1968)
Helmholtz, H.: Über Integrale der hydrodynamischen Gleichungen, welche den Wirbelbewegungen entspechen. J. Reine Angew. Math. 55, 25–55 (1858)
Hicks, W.M.: On the steady motion and small vibrations of a hollow vortex. Phil. Trans. Roy. Soc. London A175, 161–195 (1884)
Hicks, W.M.: Researches on steady vortex rings. Part II. Phil. Trans. Roy. Soc. London A176, 725–780 (1885)
Hill, M.J.M.: On a spherical vortex. Phil. Trans. Roy. Soc. London A185, 213–245 (1894)
Hinze, J.O.: Turbulence. McGraw-Hill, New York (1959)
Joukowski, N.E.: Full collection of papers. In: Kotelnikov, A.P. (ed.) Vortices, Wing Theory. Aviation (in Russian), vol. 5. Glavnaya Red. Aviats. Lit, Moscow-Leningrad (1937)
Kaltaev, A.: Study of dynamic characteristics of vortex ring motion in a viscous fluid (in Russian). In: Dynamics of continuous medium, pp. 63–70. Kazakhstan State Univ., Alma-Ata (1982)
Kambe, T., Oshima, Y.: Generation and decay of viscous vortex rings. J. Phys. Soc. Jpn. 38, 271–280 (1975)
Karman, T., Rubach, H.: Über des Mechanismus der Flüssigkeits- und Luftwiderstandes. Phys. Z. 13, 49–59 (1912)
Kasymov, B.: Battle in the Karshinskaya steppe (in Russian). Pozharnoe delo 7, 18–19 (1983)
Kelvin, L.: On vortex atoms. Phil. Mag. 34, 15–24 (1867a)
Kelvin, L., Thomson, W.: The translatory velocity of a circular vortex ring. Phil. Mag. 33, 511–512 (1867b)
Kelvin, L., Thomson, W.: Vibrations of a columnar vortex. Phil. Mag. J. Sci. 10, 155–168 (1880)
Kikoin, I.K. (ed.): Tables of Physical Values (Handbook) (in Russian). Atomizdat, Moscow (1976)
King, L.V.: On the convection of heat from small cylinders in a stream of fluids. Phil. Trans. Roy. Soc. London A214, 373 (1914)
Kirchhoff, G.: Mechanics (in Russian). Russian Acad. of Sci. Publ., Moscow (1962)
Kirde, K.: Untersuchungen über die zeitliche Weiterentwicklung eines Wirbels mit vorgegebener Anfangverteilung. Ing. Archiv. 31(6), 385–404 (1962)
Klein, F.: Über die Bildung von Wirbeln in reibungslosen Flüssigkeiten. Z. für Math. Physik. 59, 259–262 (1910)
Kochin, N.E.: Vector Calculus and Introduction to Tensor Analysis (in Russian). Nauka, Moscow (1965)
Kochin, N.E., Kibel, I.A., Roze, N.V.: Theoretical Hydromechanics. Interscience Publishers, New York (1964)
Kop'ev, V.F., Chernyshev, S.A.: Vortex ring oscillations, the development of turbulence in vortex rings and generation of sound. Physics-Uspekhi 43, 663 (2000); Translated from Russian: Uspekhi Fiz. Nauk 170(7), 713–742 (2000)

Koronkevich, V.P., Sobolev, V.S., Dubnishchev, Y.N.: Laser Interferometry (in Russian). Lazernaya Interferometriya., Novosibirsk, Nauka (1983)
Kovasnay, L.S.G.: Development of Turbulent Measuring Equipment. In: Physical Measurements in Gas Dynamics and Combustion, vol. IX. Princeton University Press, Princeton (1954)
Krutzsch, C.H.: Über eine experimentell beobachtete Erscheinung an Wirbelringen bei ihrer translatorischen Bewegung in wirklichen Flüssigkeiten. Ann. Phys. 35, 497–523 (1939)
Lamb, H.: Hydrodynamics. Cambridge University Press, Cambridge (1932)
Laurence, J.C.: Application of the constant-temperature hot-wire anemometer to the study of transient air flow phenomena. I.S.A. Journal (1953)
Lavrent'ev, M.A., Shabat, B.V.: Hydrodynamics Problems and Their Mathematical Models (in Russian), Nauka, Moscow (1973)
Lewis, B., von Elbe, G.: Combustion, Flames and Explosions of Gases. Academic Press, New York (1961)
Lichtenstein, L.: Über einige Existenzprobleme der Hydrodynamik. Math. Zeit. 23, 89–154 (1925)
Liepmann, H.W., Roshko, A.: Elements of Gas Dynamics. Wiley, New York (1966)
Lugovtsov, B.A.: On the motion of turbulent vortex ring and passive admixture transfer by it (in Russian). In: Some problems of mathematics and mechanics, Nauka, Leningrad, pp. 182–197 (1970)
Lugovtsov, B.A.: Turbulent vortex rings. Thesis synopsis for Doctor degree in phys. and math. sciences., Inst. of Hydrodynamics SB RAS, Novosibirsk (1974)
Lugovtsov, B.A.: Structure of a turbulent vortex ring in the limit of vanishing viscosity. Sov. Phys. Dokl 21, 15 (1976a)
Lugovtsov, B.A.: On the motion of a turbulent vortex ring. Archives of Mechanics 28(5-6), 759–767 (1976b)
Lugovtsov, B.A.: Turbulent vortex rings. In: Dynamics of Continuous Media (collected scientific papers) (in Russian), vol. 38, pp. 71–88. Institute of Hydrodynamics, Novosibirsk (1979)
Lugovtsov, A.A., Lugovtsov, B.A.: Example of a viscous incompressible fluid flow around a body with a moving boundary. In: Dynamics of Continuous Media (collected scientific papers) (in Russian), vol. 8, pp. 49–55. Institute of Hydrodynamics, Novosibirsk (1971)
Lugovtsov, A.A., Lugovtsov, B.A., Tarasov, V.F.: On the motion of a turbulent vortex ring. In: Dynamics of Continuous Media (collected scientific papers) (in Russian), vol. 3, pp. 50–60. Institute of Hydrodynamics, Novosibirsk (1969)
Magarvey, R.H., MacLatchy, C.S.: The formation and structure of vortex rings. Can. J. Phys. 42, 678–683 (1964)
Maxwell, J.C.: A treatise on electricity and magnetism. Dover Publications, Newyork (1954)
Maxworthy, T.: The structure and stability of vortex rings. J. Fluid Mech. 51, 15–32 (1972)
Maxworthy, T.: Some experimental studies of vortex rings. J. Fluid Mech. 81, 465–495 (1977)
Milne-Thomson, L.M.: Theoretical hydrodynamics. Macmillan and Co. Ltd, London (1938)
Moffat, H.K., Moore, D.W.: The response of Hills spherical vortex to a small axisymmetric disturbance. J. Fluid Mech. 87, 749–760 (1978)
Nitzsche, M.: Scaling properties of vortex ring formation at circular tube opening. Phys. Fluids 8(7), 1848–1855 (1996)
Norbury, J.: A family of steady vortex rings. J. Fluid Mech. 57, 417–431 (1973)
Onufriev, A.T.: Theory of the motion of a vortex ring under gravity. Rise of the cloud from a nuclear explosion. J. Appl. Mech. Tech. Phys. 8(2), 1–7 (1967)
Ovsyannikov, L.V.: Lectures on the Fundamentals of Gas Dynamics (in Russian), Nauka, Moscow (1981)

Prandtl, L.: Hydroaeromechanics (in Russian). Foreign literature Publishers, Moscow (1949)
Prandtl, L., Tietjens, O.G.: Applied Hydro- and Aeromechanics. McGraw-Hill, New York (1934); Translated from the German edition. Springer, Heidelberg (19310)
Pukhnachev, V.V.: Correctness of the plane analogue of the problem on the motion of a turbulent vortex ring. In: Dynamics of Continuous Media (collected scientific papers) (in Russian), vol. 8, pp. 85–102. Institute of Hydrodynamics, Novosibirsk (1971)
Pullin, D.I.: Vortex ring formation at tube and orifice openings. Phys. Fluids. 22, 401–403 (1979)
Reynolds, O.: On the resistance encountered by vortex rings and the relation between the vortex rings, and the streamlines of a disk. Nature 14, 477 (1876)
Saffman, P.G.: The velocity of viscous vortex rings. Stud. App. Math. 49, 371–380 (1970)
Saffman, P.G.: On the formation of vortex rings. Stud. Appl. Math. 54(3), 261–268 (1975)
Saffman, P.G.: The number of waves on unstable vortex rings. J. Fluid Mech. 84, 625–639 (1978)
Saffman, P.G.: Vortex dynamics. Cambridge University Press, Cambridge (1992)
Sallet, D.W., Widmayer, R.E.: An Experimental Investigation of Laminar and Turbulent Vortex Rings in Air. Z. Flugwiss. 22(6), 207–215 (1974)
Schlichting, G.: Boundary Layer Theory. McGraw-Hill, New York (1968)
Scorer, R.S.: Environmental aerodynamics. Wiley, New York (1978)
Sedov, L.I.: Similarity and Dimensional Methods in Mechanics. Academic Press, New York (1959)
Sennitskii, V.L.: Flow of a viscous fluid past rotating cylinders. In: Dynamics of Continuous Media (collected scientific papers) (in Russian), vol. 14, pp. 71–75. Institute of Hydrodynamics, Novosibirsk (1973)
Sennitskii, V.L.: Rotating cylinders in a viscous fluid, Part I. In: Dynamics of Continuous Media (collected scientific papers) (in Russian), vol. 21, pp. 70–83. Institute of Hydrodynamics, Novosibirsk (1975a)
Sennitskii, V.L.: Rotating cylinders in a viscous fluid, Part II. In: Dynamics of Continuous Media (collected scientific papers) (in Russian), vol. 23, pp. 169–181. Institute of Hydrodynamics, Novosibirsk (1975b)
Sennitskii, V.L.: On the motion of a pair of rotating circular cylinders in a fluid. In: Dynamics of Continuous Media (collected scientific papers) (in Russian), vol. 47, pp. 145–153. Institute of Hydrodynamics, Novosibirsk (1980)
Sennitskii, V.L.: On the drag force acting on a pair of circular cylinders in a water flow. In: Dynamics of Continuous Media (collected scientific papers) (in Russian), vol. 52, pp. 178–182. Institute of Hydrodynamics, Novosibirsk (1981)
Serrin, J.: Mathematical Principles of Classical Fluid Dynamics. Springer, Heidelberg (1959)
Shafranov, V.D.: Reviews of Plasma Physics. Leontovich, M. (ed.). vol. 3, p. 1. Consultants Bureau, New York (1967)
Shariff, K., Leonard, A.: Vortex rings. Ann. Rev. Fluid Mech. 24, 235–279 (1992)
Shriber, G., Porst, P.: Fire extinguishing agents (in Russian). Stroyizdat, Moscow (1975)
Sommerfeld, A.: Mechanics of Deformable Bodies. Academic Press, New York (1950)
Squires, G.L.: Practical physics. McGraw-Hill, London (1968)
Sullivan, J.P., Widnall, S.E., Esekiel, S.: Study of vortex rings using a laser Doppler velocimeter. AIAA J. 11(10), 1384–1389 (1973)
Sullivan, J.S., Niemela, J.J., Hershberger, R.E., Bolster, D., Donnelly, R.: Dynamics of thin vortex rings. J. Fluid Mech. 609, 319–347 (2008)
Tarasov, V.F.: Estimation of some parameters of a turbulent vortex ring. In: Dynamics of Continuous Media (collected scientific papers) (in Russian), vol. 14, pp. 120–127. Institute of Hydrodynamics, Novosibirsk (1973)

Tarasov, V.F.: On the motion of a buoyant vortex ring. In: Dynamics of Continuous Media (collected scientific papers) (in Russian), vol. 23, pp. 210–218. Institute of Hydrodynamics, Novosibirsk (1975a)
Tarasov, V.F.: Experimental investigations of turbulent vortex rings. Thesis synopsis for Candidate degree in phys. and math. sciences. Inst. of Hydrodynamics SB RAS, Novosibirsk (1975b)
Tarasov, V.F., Yakushev, V.I.: Transport in a turbulent vortex ring. J. Appl. Mech. Tech. Phys. 15(1), 106–110 (1974)
Taylor, G.I.: Formation of a vortex ring by giving an impulse to a circular disk and then dissolving it away. J. Appl. Phys. 24(1), 104 (1953)
Thomson, J.J., Newall, H.F.: On the formation of vortex rings by drops falling into liquids, and some allied phenomena. Proc. Roy. Soc. London A39, 417–436 (1885)
Timme, A.: Über die Geschwindigkeitsverteilung in Wirbeln. Ing. Archiv. 25, 205 (1957)
Turner, J.S.: Buoyant vortex rings. Proc. Roy. Soc. London A239, 61–75 (1957)
Turner, J.S.: The flow into an expanding spherical vortex. J. Fluid Mech. 18, 195–208 (1963)
Van Dyke, M.: An Album of Fluid Motion. The Parabolic Press, Stanford (1982)
Vershinin, V.V.: Derivatives of smoothing splines (in Russian), vol. 87, pp. 35–42. Vychisl. Systemy, Novosibirsk (1981)
Vershinin, V.V., Zav'yalov, Y. S., Pavlov, N.N.: Extremal Characteristics of Splines and the Problem of Smoothing (in Russian), Nauka, Novosibirsk (1988)
Villat, H.: Vortex theory (in Russian). ONTI, Moscow-Leningrad (1930)
Vladimirov, V.A.: Hollow vortex rings with small cavity cross section. In: Dynamics of Continuous Media (collected scientific papers) (in Russian), vol. 15, pp. 25–35. Institute of Hydrodynamics, Novosibirsk (1973)
Vladimirov, V.A.: Vortical momentum of flows of an incompressible liquid. J. Appl. Mech. Tech. Phys. 18(6), 791–794 (1977)
Vladimirov, V.A.: Vortical momentum of bounded ideal incompressible fluid flows. J. Appl. Mech. Tech. Phys. 20(2), 157–163 (1979)
Vladimirov, V.A., Lugovtsov, B.A., Tarasov, V.F.: Suppression of turbulence in the cores of concentrated vortices. J. Appl. Mech. Tech. Phys. 21(5), 632–637 (1980)
Vladimirov, V.A., Rybak, L.Y.: Some questions on motion of hollow vortex rings in an ideal incompressible fluid. In: Dynamics of Continuous Media (collected scientific papers) (in Russian), vol. 26, pp. 17–30. Institute of Hydrodynamics, Novosibirsk (1976)
Vladimirov, V.A., Rybak, L.Y.: Impulse and circulation of vortex rings (in Russian). Uchenye zapiski TsAGI 9(5), 111–115 (1978)
Vladimirov, V.A., Tarasov, F.F.: On vortex ring formation at high Reynolds numbers. In: Dynamics of Continuous Media (collected scientific papers) (in Russian), vol. 43, pp. 154–156. Institute of Hydrodynamics, Novosibirsk (1979a)
Vladimirov, V.A., Tarasov, F.F.: Structure of turbulence near the core of a vortex ring. Sov. Phys. Dokl. 24, 254–256 (1979b)
Vladimirov, V.A., Tarasov, V.F.: Formation of vortex rings. Izv. Sib. Otdel. Akad. Nauk SSSR, Ser. Tekh. Nauk 3(1), 3–11 (1980)
Vulis, L.A., Yarin, L.P.: Plume Aerodynamics (in Russian). Energiya, Leningrad (1978)
Wedemeier, E.: Ausbildung eines Wirbelpaares an den Kanten tiner Platte. Ing. Arch. 30, 187–200 (1961)
Weigand, A., Gharib, M.: On the evolution of laminar vortex rings. Exp. Fluids 22, 447–457 (1997)
Widnall, S.E., Bliss, D.B., Tsai, C.Y.: The instability of short waves on a vortex ring. J. Fluid Mech. 66, 35–47 (1974)
Willert, C.E., Gharib, M.: Digital particle image velocimetry. Exp. Fluids 10, 181–193 (1991)

Yeh, Y., Cummins, H.Z.: Localized fluid flow measurements with a He-Ne laser spectrometer. Appl. Phys. Lett. 4(10), 176–178 (1964)
Yusupaliev, U.: Determination of the Drag Coefficient of a Toroidal Plasma Vortex in Air. Plasma Phys. Rep. 31(6), 497–511 (2005)
Zaslavsky, B.I.: On formation and motion of buoyant vortex rings in uniform and stratified fluids (in Russian). In: Modern problems of mechanics of continuous medium, pp. 21–30. Moscow Phys. Techn. Inst., Moscow (1985)
Zaslavsky, B.I., Yur'ev, B.V.: Experimental study of transformation of a free, ball-shaped volume of a light gas into a vortex ring (in Russian). Izv. SO AN SSSR, Ser. tekhn. nauk 8(2), 40–46 (1983)

Index